UNIVERSITÀ DEGLI STUDI DI PALERMO

Dottorato in Scienze della Terra e del Mare.
Dipartimento di Scienze della Terra e del Mare.
Settore Scientifico Disciplinare GEO/08.

Gas in volcanic lakes: from dissolved gases to lake gas plumes.

IL DOTTORE
Nathalie HASSELLE

IL COORDINATORE
Prof. Alessandro AIUPPA

IL TUTOR
Prof. Alessandro AIUPPA

IL CO TUTOR
Dr. Dmitri ROUWET

CICLO XXXI
ANNO CONSEGUIMENTO TITOLO 2019

ABSTRACT

Volcanic lakes are known to dissolve or release gases coming from the underlying system (e.g. hydrothermal systems, shallow magma or mantle degassing) depending on their water chemistry and physical characteristics. CO_2 is the least soluble magmatic gas and can form a separate gaseous phase at great depth. In deep meromictic lakes, it can accumulate in the bottom layer and increase the hazard of limnic eruption. Being the dominant C specie in acidic water (pH<6.3) and the only C species at pH <3.8, CO_2 can be used to monitor the volcanic activity at acidic "wet" active volcanoes. Sulfur gases (mainly SO_2 and H_2S) are released by shallower magma and can be extensively absorbed in hydrothermal systems and volcanic lake waters. SO_2-dominant emissions are indicative of direct magmatic degassing, whereas H_2S-dominant emissions are related to reduced hydrothermal gases that have already be extensively processed by the hydrothermal system.

In this study, we assessed the potential of the seawater-designed HydroC® CO_2 probe (range 0-6000 µatm of pCO_2) to measure continuously dissolved CO_2 partial pressure at volcanic lakes. The study sites were two meromictic lakes, Barombi Mbo (Cameroun) and Averno (Italy) which are potentially able to contain large amount of dissolved CO_2 in their hypolimnions. At Barombi Mbo, we measured for the first time in March 2016 the pCO_2 from the surface (100 µatm) to 12.8m depth (6000 µatm), not deeper due to instrumental limitations. At Averno lake, we measured the pCO_2 values along vertical profiles up to the thermocline at the lake's centre in September 2016 and July 2017. A CO_2 partial pressure of 2500 µatm was measured at 12.5 m depth in 2016 and at lower depth (5 m) in 2017, likely due to the lake overturn in January 2017 that mixed CO_2-rich deep water with less concentrated upper water layers. We argued that the dissolved CO_2 did not have time to completely re-equilibrate with the atmosphere and/or that its consumption by photosynthesis was lower in the early summer (July 2017) compared to end summer measurements (September 2016). In addition, horizontal surveys were executed to study the presence of pCO_2 anomalies at shallow depth (15 m in 2016; 5 m in 2017). We found heterogeneous pCO_2 water layers (pCO_2 ranged from 2000 to 3500 µatm in 2016 and from

2000 to >6000 µatm in 2017). The highest pCO_2 spots might be related to the regional fault system (NW-SE and SW-NE), to the location of higher CO_2 flux at the bottom or to the local bathymetry. We concluded that in non-turbid lake waters, the probe can be useful to map quickly the pCO_2 and detect anomalies at large and deep lakes due to its high frequency of acquisition. Unfortunately, its measurement range is the main limitation for its application in volcanic lakes often too rich in CO_2 (above detection limit).

The second part of this work aimed at studying the degassing of acidic volcanic lakes with a Multi-GAS instrument in order to improve the assessment of the global volcanic lake gas composition, to evaluate the potential relation of lake gas with physical-chemical characteristics of lake water and to monitor the volcanic activity. Acidic lakes, by incorporating most of the heat and fluid fluxes of a volcano, can be used as a superficial "window" of the processes occurring in the underlying magmatic-hydrothermal system. Gas scrubbing by water is an important process affecting the water chemistry and the lake plume composition and changes in the lake water chemistry, temperature or diffuse/bubbling gas composition might be a precursory sign of an eruption.

At El Chichón (Mexico) and Víti (Iceland), two lakes of pH 2-3, we determined for the first time with a Multi-GAS instrument the lake gas composition and the effects of the lake water on the degassing by comparing gas ratios between fumaroles, hot pools and lake gases. We measured lower CO_2/H_2S and H_2/H_2S ratios in fumarolic gases (13-33 and 0.08-0.5, respectively) than in lake emissions (31-5685 and 0.6-35, respectively) evidencing the scrubbing of fumarolic H_2S by lake waters. At El Chichón, we estimated that only 0.2 to 5.4% of the $H_2S_{(g)}$ entering the lake bottom is not absorbed by the water and is discharged into the atmosphere. We have also found that trace levels of SO_2 (0.003-0.3 ppmv) degassed at the lake surfaces whereas it is absent in the hydrothermal system. We proposed that it is produced into the lake by the oxidation of H_2S, with sulfite as transient specie before eventually degas at the lake surfaces.

Moreover, the gas composition of Santa Ana hyperacidic crater lake (El Salvador) has been determined for the first time. During our campaigns in March and June 2017 and in April, May and

June 2018, we measured similar H_2/SO_2 (0.37-0.84) and H_2S/SO_2 (0.03-0.11) ratios. The CO_2/SO_2 ratios were higher in March 2017 (47±23) than in June 2017 and in 2018 (2.4-5.4). $CO_2(g)$ is not absorbed in hyperacidic water contrary to $SO_2(g)$, which is partially dissolved in the lake. We explained the decrease of CO_2/SO_2 gas ratios by a decrease of $SO_{2(g)}$ scrubbing due to the lower water volume and pH and the higher water temperature since June 2017 compared to March. We postulated that the gas composition measured in 2017-2018 is representative of a state of high activity lake indicated by the high surface temperature (58°C), Cl and SO_4 contents (71615 and 41206 mg/L, respectively) and acidity (-0.01) of the lake water on June 13 2017. Therefore, future gas composition evaluation needs to be cautiously interpreted. Many factors (such as the SO_2 gas scrubbing related to water volume variations due to seasonality and/or heat input, sulfur precipitation or mineral sealing) could affect the gas ratios without being linked to renewed activity, but changes in CO_2/SO_2 ratios could be indicative of a possible phreatic eruption. From the SO_2 flux measured by the DOAS station, we were able to estimate gas fluxes. In June 2017 and in 2018, the fluxes of SO_2 (41-2 31 t/day), CO_2 (117-479 t/day), H_2 (0.1-3.0 t/day), H_2O (729-6950 t/day) and H_2S (0.8-12.0 t/day) do not show significant trends.

Finally, we studied the gas composition of acidic lakes from hyperacidic to acidic geothermal lakes and their associated fumaroles worldwide. The SO_2/H_2S ratios are positively correlated with the amount of Cl+SO_4, are higher than 1 in hyperacidic lake gases and lower than 1 in emissions coming out of lakes with pH 2-6. The former are in clear correlation between the strongest magmatic input and the SO_2/H_2S ratios whereas the latter show the influence of sulfur gas (H_2S) scrubbing and SO_2 production in the lake water, likely from dissolved sulfite, in SO_2-free feeding fumaroles. This last assumption is also confirmed by the SO_2/H_2S ratios decrease and contemporaneous pH increase. H_2S and SO_2 gas scrubbing should increase as the pH increases; however lake emissions from pH 2-3 and pH 4-6 lakes have similar SO_2/H_2S ratios, which could be explained by dissolved sulfur speciation and the higher content of sulfite at higher pH, although H_2S oxidation in air cannot be excluded. A CO_2/SO_2 ratio of ~1000 appeared to distinguish between emissions from hyperacidic lakes (lower ratios) and pH 2-6 lakes (higher ratios). H_2/SO_2 (10^{-2} to 10^4) and CO_2/SO_2 are positively correlated

(r^2=0.91) between all acidic lakes gases suggesting a similar behaviour of H_2 and CO_2. If we postulated that fumaroles close to the lakes are representative of the subaquatic fumaroles feeding the lakes (as for El Chichón and Víti), the SO_2/H_2S ratios but also CO_2/S_{total} ratios are higher in lake gases compared to fumarolic gases except for both hyperacidic lakes of Yudamari (Japan; Shinohara et al., 2015) and Copahue (Argentina; Tamburello et al., 2015). Those findings highlight the necessity to constrain the kinetics of lake degassing.

ACKNOWLEDGEMENTS

CONTENTS

XI

OBJECTIVES

The two main goals of this work are to (i) study the deep CO_2 degassing behaviour into neutral to basic meromictic lakes and (ii) the outgassing of magmatic and/or hydrothermal CO_2, SO_2, H_2S and H_2 via lake plumes, e.g. after interaction of the feeding gas with acid volcanic lakes.

As for goal (i), this study aims at evaluating the CO_2 partial pressure (pCO_2) along a vertical profile through Barombi Mbo lake (Cameroun), a deep (110 m) stratified meromictic lake located in a tropical country (Chapter 3). These conditions are known to facilitate accumulation of CO_2 in the hypolimnion. Barombi Mbo has been poorly studied, but needs to be characterized because it could fit the conditions to a limnic gas burst to occur.

A second aim is to measure, for the first time in-situ and continuously, the vertical and horizontal pCO_2 structure of Averno lake (Campania, Italy) (Chapter 3). This maar lake presents a permanent vertical chemical and thermal stratification. In contrast to Barombi Mbo, Averno lake is rolling over occasionally in winter, so releasing low amounts of CO_2 and CH_4 into the atmosphere without causing risk for the surrounding population. Continuous profiling can contribute an improved geochemical characterization of the lake, and can allow detecting areas with higher pCO_2 that relate to local geotectonic-volcanologic structures.

As for goal (ii), a main objective of this work is to evaluate and compare the behaviour of gaseous CO_2, H_2S, SO_2 and H_2 in volcanic plumes issuing from lakes of different pH (acidic), chemistry and temperature conditions (Chapter 6). To this aim, a lake gas plume compilation is assembled by compiling data available from literature (Boiling Lake, Dominica; Copahue, Argentina; Kawah Ijen and Sirung, Indonesia; Poás, Costa Rica; Ruapehu, New Zealand; Vasca degli Ippopotami, Vulcano, Italy; Yudamari, Japan), unpublished data (Kaba and Kawah Ijen, Indonesia; Rincón de la Vieja, Costa Rica) and novel data acquired during this PhD (El Chichón, Mexico; Ruapehu, New Zealand; Vasca degli Ippopotami, Vulcano, Italy; Frying Pan Lake and Inferno Lake, Waimangu, New Zealand; Champagne Pool and Oyster Pool, Waiotapu, New Zealand; Yugama, Japan; Víti, Iceland; Taal,

Philippines; East Lake, Newberry, USA; Santa Ana, El Salvador). Gas scrubbing by lake water is an important process affecting both water chemistry and lake plume composition, and an attempt is made to identify systematic patterns in composition. In addition, we aim at establishing new insights on sulfur (H_2S and SO_2) degassing and aqueous speciation in relation with the physical and chemical characteristics of acidic lakes (pH 2 to 6). In particular, at El Chichón (Mexico) and Víti (Iceland), two lakes of pH~2.7, we determine for the first time with a Multi-GAS the lake gas composition and the effects of the lake water on the degassing by comparing gas ratios between fumaroles, hot pools and lake gases (Chapter 4). Finally, the composition of Santa Ana hyperacidic crater lake (El Salvador) is determined for the first time (Chapter 5). After the phreatic eruption in 2007, the lake activity decreased until 2010, but then increased by the time of writing. The gas composition, representative of a high level activity state, will serve as baseline for the future monitoring of the volcano.

CHAPTER 1

INTRODUCTION

1.1. VOLCANIC LAKES: GENERAL ASPECTS

The limnic eruption of Lake Nyos (Cameroon), that killed 1700 inhabitants in 1986 (Sigvaldason, 1989; Kusakabe et al., 2000b), has evidenced that volcanic lakes could be potentially dangerous by themselves and boosted their study. With more than 500 volcanic lakes identified worldwide (VOLADA database, Rouwet et al., 2014b), hazards evaluation became an important focus of investigation in volcanology (Kling et al., 1987; Sigurdsson et al., 1987; Kusakabe et al., 1989; Costa and Chiodini, 2015). In addition, crater lakes can provide useful information for volcano monitoring (e.g. Giggenbach 1974, Giggenbach and Glover, 1975; Takano, 1987; Brown et al., 1991; Rowe et al., 1992b; Armienta et al. 2000; Tassi et al. 2005; Zlotnicki et al. 2009; Martini et al. 2010). Actually, crater lakes represent the superficial "blue windows" (Christenson et al., 2015) of processes occurring deep in a volcanic system (Varekamp et al., 2000). By being located in the crater, where the main volcano-related heat and fluid fluxes are dissipated, volcanic lakes trap and integrate changes occurring in the underlying hydrothermal-magmatic systems (e.g. Pasternack and Varekamp, 1997; Barbier, 2010). Depending on their residence time (Varekamp, 2003; Taran and Rouwet 2008; Taran et al. 2013; Rouwet et al. 2014b), they can be highly or more weakly dynamic systems.

Specific conditions are required for volcanic lakes to persist (Pasternack and Varekamp, 1997; Rouwet and Tassi, 2011; Terada and Hashimoto, 2017). First, the lake bottom needs to be (partially) sealed. However, Terada and Hashimoto (2017) recently suggested that this condition is not always necessary for the persistence of hot crater lakes. Secondly, a transient equilibrium between mass and energy inputs and outputs must exist, such that the amount of fluid inputs (meteoric or volcanic) is sufficient to compensate the mass lost by evaporation, outflow and/or seepage. Also, the energy inputs (enthalpy of the deep fluids, heat from a shallow magma transferred by conduction and radiation

coming from the solar flux) do not have to exceed the heat outputs dissipated by evaporation, conduction and radiation or transfer to meteoric input.

Wet volcanoes are more dangerous than *dry volcanoes* (Torres et al., 1995; Mastin and Witter, 2000; Delmelle et al., 2015; Manville, 2015; Kusakabe, 2015; Rouwet and Morrissey, 2015). Actually, only 8% of the eruptions are subaquatic (Siebert et al., 2010) but they are responsible of 20% of the death toll due to volcanic eruptions (Mastin and Witter, 2000). Volcanic lakes present their own types of volcanic hazards (Mastin and Witter, 2000; Rouwet et al., 2014a; Delmelle et al., 2015; Kusakabe, 2015; Manville, 2015; Rouwet and Morrissey, 2015), such as phreatic (Rouwet et al., 2016) or phreatomagmatic eruptions (Christenson, 2000; Agusto et al., 2013), limnic gas bursts (e.g., Lakes Monoun and Nyos in 1984 and 1986, respectively; Kling et al., 1989; Zhang and Kling, 2006; Tassi and Rouwet, 2014), lahars (Cronin et al., 1997; Schaefer et al., 2008; Carrivick et al., 2009; Kilgour et al., 2010; Manville, 2015), tsunamis, seiches, flooding, base surges, acid rain, water contaminations (Sriwana et al., 1998; Delmelle and Bernard, 2000; van Rotterdam-Los et al., 2008; van Hinsberg et al., 2010), or flank failure (Kempter and Rowe, 2000; Wagner et al., 2003; Rouwet et al., 2014b; Delmelle et al., 2015). These events can be difficult, or even impossible, to predict (de Moor et al., 2016b; de Moor and Stix, 2018; Manville, 2015; Rouwet et al., 2014b).

In particular, phreatic eruptions can be highly destructive and violent. They can be triggered by the rapid input of heat and/or fluids from the underlying deep magmatic system into a shallower aquifer (Rouwet and Morrissey, 2015), or by the accumulation of gas under a mineral seal (e.g. Barberi et al., 1992; Browne and Lawless, 2001; Christenson et al., 2007, 2010, 2017; Agusto et al., 2017; Caudron et al., 2018). These events are almost impossible to forecast (Christenson et al., 2007, 2010; Jolly et al., 2010; Kilgour et al., 2010), although some prospect have recently been offered by real-time gas observations (de Moor et al., 2016b). To breach the crater lake surface, the hydrostatic pressure of the water column needs to be lower than the fluid pressure beneath the lake. If the pressure on the underlying magmatic-hydrothermal system drops (e.g., decrease of the lake level, or due to phreatic eruption), magma can start rising, eventually leading to phreatomagmatic eruptions (Rouwet et al., 2014b; Stix and de Moor, 2018).

1.2.   STATE OF THE ART

1.2.1. Chemical composition

The chemical composition of volcanic lakes ranges from dilute (meteoric) waters to hyper-acidic fluids and is related to (Varekamp et al., 2000):

(i)   The *magmatic/hydrothermal fluid discharge* (i.e. their composition and flux rate) at the lake bottom. Volcanic gases consist mainly of H_2O, CO_2, SO_2, H_2S, HCl, HF, HBr, N_2, H_2, CO, NH_3 and metal halides (e.g., Giggenbach, 1996). In hydrothermal systems and/or lakes, gases can be partially or totally scrubbed (Christenson and Wood, 1993; Symonds et al., 2001), enriching the water in dissolved components such as anions (Cl^-, SO_4^{2-}, etc) principally derived from the volcanic gases (Gemmell, 1987; Symonds et al., 1987).

(ii)   *Dilution/evaporation processes* (e.g. variations of the heat flux, intense rain). For example, if a shallow magma directly discharges high temperature magmatic gases, it can lead to intense evaporation or disappearance of the lake if the water input (e.g. rainfall) cannot balance water loss (e.g. Rowe et al., 1992a; Pasternack and Varekamp, 1997)

(iii)   The extent of the *water-rock interactions* into the lake and in the underlying hydrothermal system. Rock dissolution by hydrolysis reactions consumes acidity by (Christenson and Wood, 1993):

$$M_{2/z}O + zH^+ = M^{z+} + H_2O \qquad (1.1)$$

where M is the oxidic rock component, and liberates the RFE (Rock Forming Elements)-cations in the water (mainly Na, K, Ca, Mg, Fe and Al; Christenson and Wood, 1993; Rouwet et al., 2014b)

(iv)   The *dissolution and/or precipitation of secondary minerals*. Na, K, Ca, Al, Fe, SiO_2 and S are involved in precipitation of minerals (Giggenbach, 1974; Christenson and Wood, 1993). F can precipitate as fluorite or fluoroapatite (Christenson and Wood, 1993), while Cl, Mg, Mn, Zn, Li, Rb and possibly B are considered conservatives; they do not

participate into reactions between fluids and minerals (Giggenbach, 1974; Hurst et al., 1991). However, HCl evaporates in hyperacidic waters (Truesdell et al., 1989; Rouwet and Ohba, 2015; Capaccioni et al., 2017).

Hydrothermal fluids are classified in function of their main anions (Cl^-, SO_4^{2-} and HCO_3^-) (Figure 1.1; e.g. White, 1957; Ellis and Mahon, 1977; Giggenbach et al., 1990; Christenson et al., 2015; Varekamp, 2015) as:

(i)   *Acid sulfate-chloride waters* are highly acidic (pH = 0-4) and contain large amounts of SO_4 (up to 100,000ppm) due to the direct absorption of acidic magmatic gas. Examples of this type of lakes are Sorik Marapi (Indonesia; Barbier, 2004), Kawah Ijen (Indonesia; Delmelle and Bernard, 1994; van Hinsberg, 2017), Taal (Philippines; Maussen et al., 2018), Yudamari (Japan; Ohsawa et al., 2003, 2010; Shinohara et al., 2015), Yugama (Kusatsu-Shirane volcano, Japan; Ohba et al., 1994, 2000, 2008), Santa Ana (El Salvador; Bernard et al., 2004; this study), Poás (Costa Rica; Rouwet et al., 2017), Rincón de la Vieja (Tassi et al., 2005), El Chichón (Mexico; Taran et al., 1998; Rouwet et al., 2008; Casas et al., 2016), and Ruapehu (New Zealand; Christenson et al., 2010).

(ii)   *Neutral chloride waters* are fed by mature fluids, from which the initial acidity has been neutralised by extensive water-rock hydrolysis. They are rich in Cl (up to 100,000 ppm). Examples are Soufrière (Saint Vincent; Sigurdsson, 1977), Quilotoa (Ecuador ; Aguilera et al., 2000) and Segara Anak (Indonesia ; Barbier, 2010).

(iii)   *Neutral bicarbonate waters* contain huge amounts of dissolved CO_2 (mostly as HCO_3^-, up to 100,000 ppm) having magmatic, mantel, metamorphic or organic origins (Marini et al., 2003). These waters are slightly acidic (pH 4-7). They do not contain SO_4 and Cl. Examples are the Cameroonian lakes Nyos and Monou (Kusakabe, 2017 and references therin).
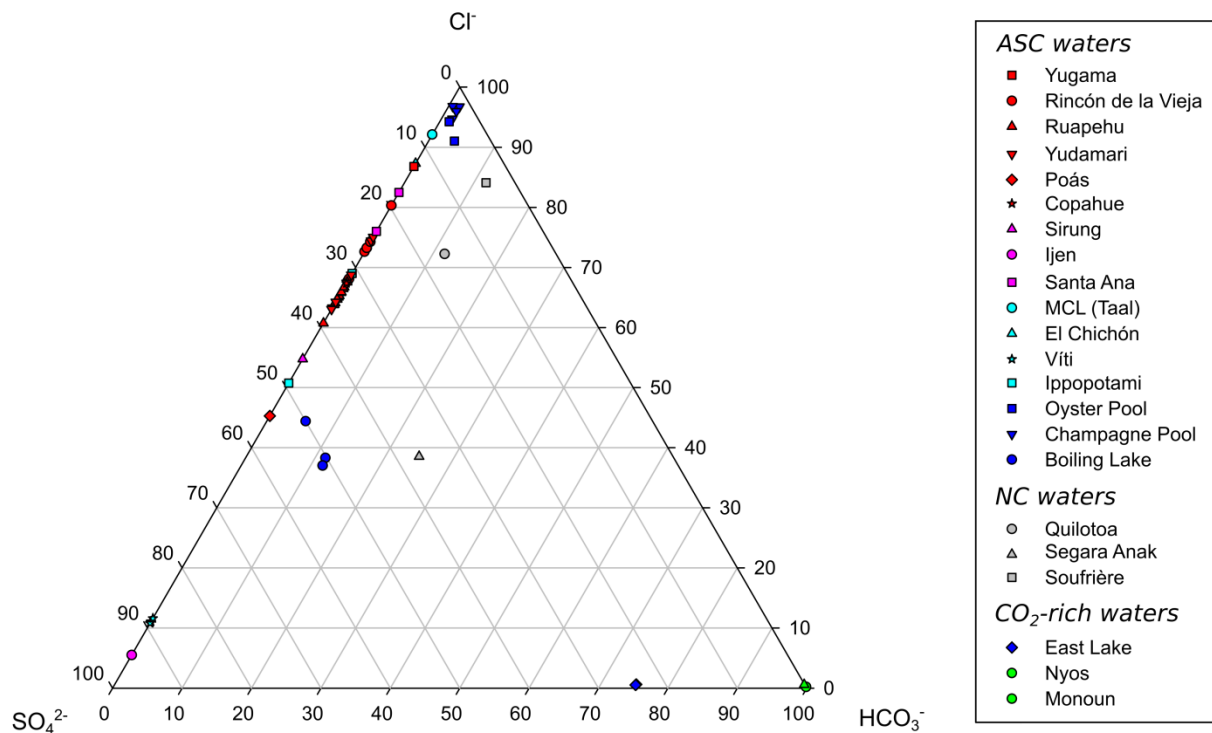
Figure 1.1 - Triangular diagram illustrating the composition of volcanic lakes in function of the main anions concentrations (Cl-SO₄-HCO₃). Most of the volcanic lakes discussed in this work are included. The water chemistry comes from: Yugama (Terada et al., 2018), Rincón de la Vieja (Tassi et al., 2005), Ruapehu (Christenson et al., 2010), Yudamri (Ohsawa et al., 2003, 2010; Miyabuchi and Terada, 2009; Shinohara et al., 2015), Poás (Rouwet et al., 2017), Copahue (Tamburello et al., 2015), Sirung (Bani et al., 2017), Ijen (van Hinsberg et al., 2017), Santa Ana (this study), MCL (Maussen et al., 2018), El Chichón and Víti (this study), Vasca degli Ippopotami (Mazor et al., 1988), Oyster Pool and Champagne Pool (Pope and Brown, 2014), Boiling Lake (Jospeh et al., 2011), Quilotoa and Segara Anak (Aguilera et al., 2000), Soufrière (Sigurdsson, 1977), East Lake (Lefkowitz et al., 2017), Nyos (Giggenbach, 1990) and Monoun (Sigurdsson et al., 1987). ASC is Acid Sulfate-Chloride and NC is Neutral Chloride.

1.2.2. Volcanic lakes classifications

Several physico-chemical classifications of volcanic lakes exist (Giggenbach, 1974; Pasternack and Varekamp, 1997; Varekamp et al., 2000; Varekamp, 2015), but none of them is of universal use because of the non-volcanic inputs such as seawater, evaporate-connate waters, or spring waters at some lakes (e.g. El Chichón, Mexico; Taal and Pinatubo, Philippines; Kelut (before 2007), Indonesia; Delmelle et al., 1998; Bernard and Mazot, 2004; Stimac et al., 2004; Peiffer et al., 2011, 2015). Recently, a genetic classification was introduced that permits to classify all the lakes independently of their fluid inputs, based on the origin of the lake basin (Christenson et al., 2015).

Here we detail some of the classification schemes for lakes that will be covered in this thesis.

1.2.2.1. Physicochemical classification

Pasternack and Varekamp (1997) proposed a physico-chemical classification of volcanic lakes (Figure 1.2) based on their volcanic activity, i.e. the intensity of the heat input, the capacity of the lake to dissipate this heat, the hydrodynamic mixing regimes transporting heat to the surface, and the composition of the lake/gas input. They divided volcanic lakes into 6 classes: (1) *erupting lakes*, (2) *peak activity lakes*, (3) *high activity lakes*, (4) *medium activity lakes*, (5) *low activity lakes*, and (6) *no activity lakes*. *Erupting lakes* and *peak activity lakes* deviate from steady-state equilibrium (where mass/energy inputs balance mass/energy outputs), contrary to the other volcanic lake classes. Both are hyperacid and hot. *Peak activity lakes* are highly saline (TDS > 300g/L). *Erupting lakes* are localized in erupting craters and are characterized by variable volumes. They typically do not often survive to high volcanic activity, with the exception of Voui (Vanuatu) in 2005 (Bani et al., 2009), Poás (Costa Rica; Brantley et al., 1987; Rouwet et al., 2016), Santa Ana (El Salvador; Bernard et al., 2004; Scolamacchia et al., 2010), Gorely (Kamchatka; Melnikov and Ushakov, 2011). If the fluids input from below is not sufficient (Terada and Hashimoto, 2017), a local rainfall of > 5000mm/y is needed to avoid a > 45°C-lake to shrink and dry out. This high water temperature is reached when the
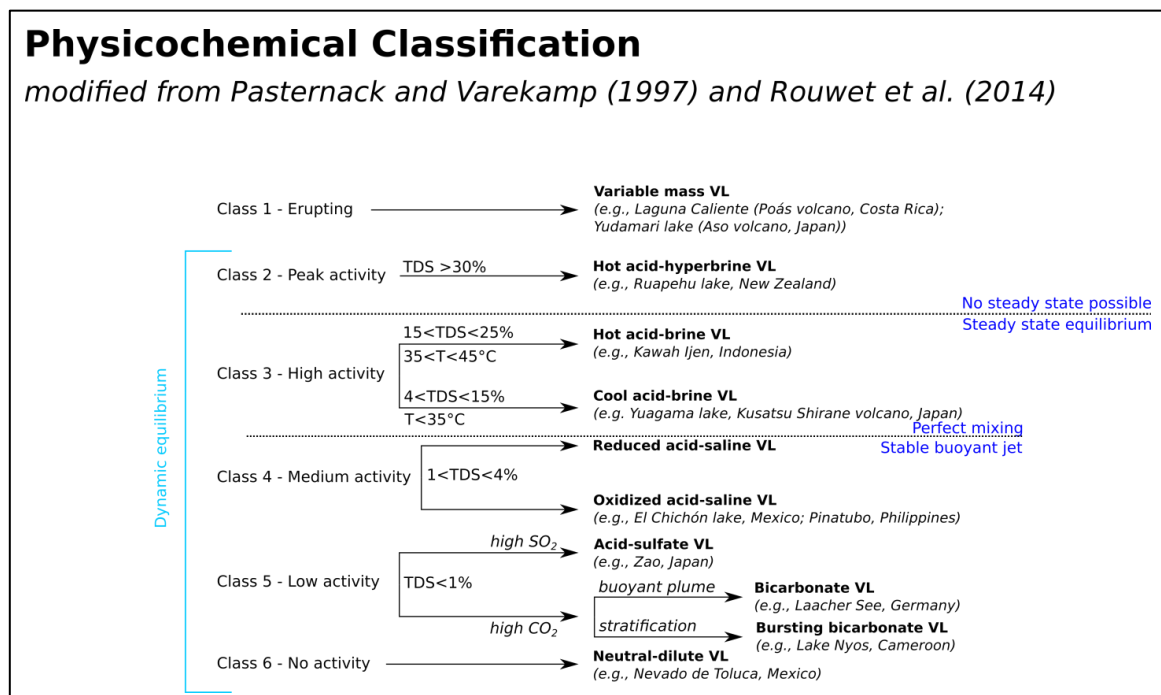
Figure 1.2 - Physico-chemical classification of volcanic lakes modified from Pasternack and Varekamp (1997). VL refers to Volcanic Lake.

volcanic activity increases, and only lakes located in tropical climatic conditions might be able to persist (e.g., Laguna Caliente, Poás, Costa Rica from 2006 to 2018; Rouwet et al., 2016). *High activity lakes* are mostly characterized by the presence of a powerful and permanent jet inlet at their bottom that mixes the lake water. They are acidic (pH<1.5), highly saline, and fed by magmatic/hydrothermal fluids rich in SO_2, HCl and HF. They are subdivided into hot (T = 35-45°C and TDS = 150-250 g/L) or cool (T = 20-35°C and TDS = 40-150 g/L) acidic lakes. *Medium activity lakes* present a stable buoyant jet at the bottom. Fluid inputs are mainly of hydrothermal origin (rich in $CO_{2(g)}$ and $H_2S_{(g)}$). The pH (2-2.5) and TDS (10-40 g/L) of those lakes are lower than high activity lake. They are subdivided in oxidized and reduced acid-saline lakes with variable water temperature, often higher than ambient temperature. *Low activity lakes* are characterized by low TDS (<10 g/L) and low or absent jet inlet. They are further divided into SO_4-dominated and CO_2-dominated lakes. Acid sulfate lakes are steam-heated pools fed by H_2S. Bicarbonate lakes have a relatively high pH and contain high concentrations of dissolved CO_2, without SO_2 or H_2S (hence SO_4). The CO_2 generally originates from a regional scale CO_2-degassing feeding ground waters recharging the lake. In rare cases, CO_2 originates from a magmatic or hydrothermal system. Bicarbonates lakes, depending on their depth and thermal stratification, may accumulate CO_2 in their deepest layers (Nyos-type lakes; Tassi and Rouwet, 2014), or allow CO_2 to escape into the atmosphere at the surface by diffusion or bubbling degassing (Mazot et al., 2011; Pérez et al., 2011). *No activity lakes* have a meteoric origin. They are neutral and diluted.

1.2.2.2. Chemical classifications

1.2.2.2.1. Cl + SO$_4$ concentrations vs. pH

This classification was introduced by Varekamp et al. (2000) and is based on the pH and the sum of Cl + SO_4 concentrations (Figure 1.3). Three classes are distinguished: (i) CO_2-dominated lakes (5 < pH < 9, SO_4+Cl < 10mg/L), (ii) quiescent lakes (1.5 < pH < 9, 10 mg/L < SO_4+Cl < 3000mg/L), and (iii) "active" crater lakes (-1 < pH < 3, SO_4+Cl > 3000mg/L).
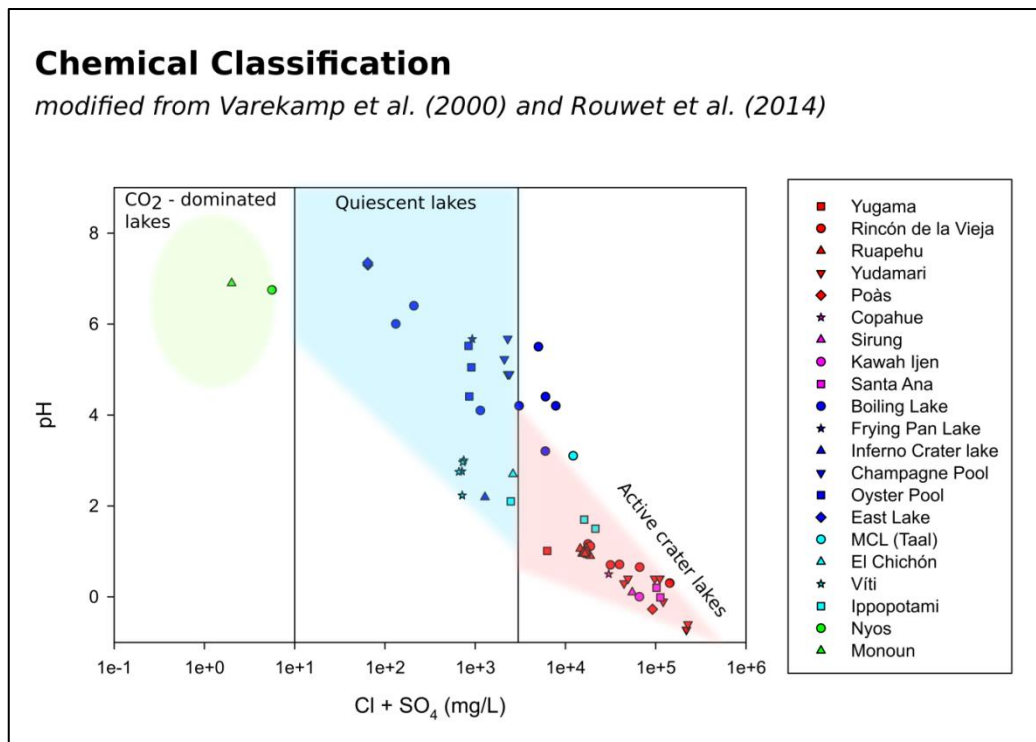
Figure 1.3 - Chemical classification modified from Varekamp et al. (2000) and Rouwet et al. (2014b). The green, blue and red areas represent the CO_2-dominated, quiescent and active crater lakes, respectively. It also illustrates that some lakes, such as Boiling Lake (Domenica) or Main Crater Lake (MCL; Taal volcano, Philippines), do not fit in this classification. The examples cited covered most of the volcanic lakes presented in this thesis.

1.2.2.2.2. Percentage of residual acidity

The percentage of residual acidity (PRA) represents the amount of original protons remaining into the lake water after neutralization by water-rock interaction (WRI) of the magmatic fluids discharging into the lake. Two classes are distinguished: (i) Rock-dominated lakes with low PRA and (ii) Gas-dominated lakes with high PRA (Varekamp et al., 2000; Figure 1.4).
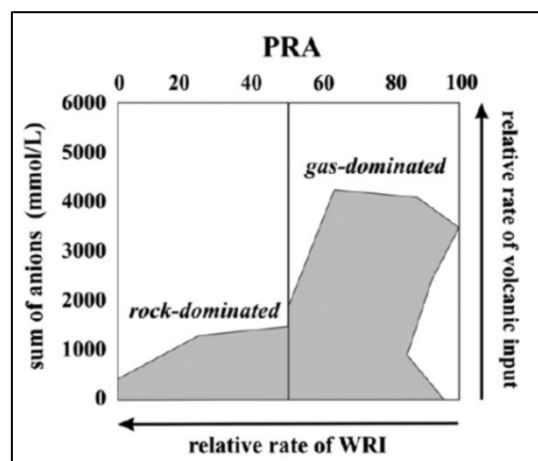
Figure 1.4 - Classification of volcanic lakes based on the pourcentage of residual acidity (Rouwet et al., 2014b).

1.2.2.3. Genetic classification

Christenson et al. (2015) proposed a genetic classification of volcanic lakes taking into account the processes (tectonic, geomorphic and volcanologic) contributing to the formation of these lakes (Figure 1.5). This coding classification depends on four parameters (i) the geo-tectonic context (G) of the volcanic systems, monogenetic (0) or polygenetic (1), where the lake is located; (ii) the relationship (R), weak (0) or strong (1), between volcanic activity and lake formation; (iii) the timing (T), long (0) or short (1), of lake formation after a volcanic eruption; (iv) the position of the lake relative to the vent (L), off (0) or over (1) the vent. In this study, we will focus on lake type classified as crater lakes (G1, R1, T1, L1), maar lakes (G0, R1, T1, L1) and geothermal lakes (G0-1, R1, T1, L0-1).
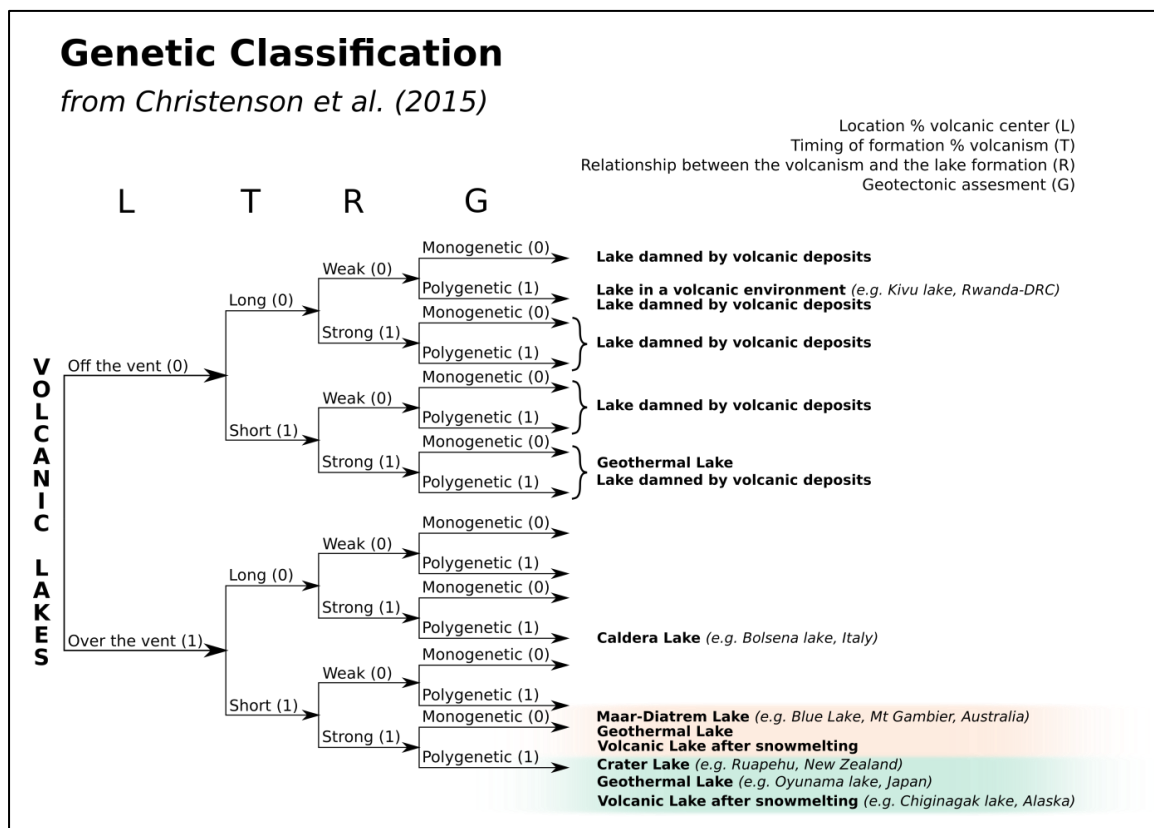
Figure 1.5 - Genetic classification of volcanic lakes (Christenson et al., 2015).

1.3.   GASES IN VOLCANIC LAKE ENVIRONMENTS

In this study, we will mostly focus on studying gases dissolved in, and emitted by, volcanic lakes. Indeed, lake waters can dissolve large amounts of gas but they also contribute to global volcanic gas emissions (Sriwana et al., 2000; Pérez et al., 2011; Tamburello et al., 2015). Gases in volcanic lakes are composed of a mixture of magmatic (e.g. CO_2, SO_2, H_2S, HCl, HF), hydrothermal (e.g. CH_4, NH_2, H_2S), meteoric (e.g. N_2, O_2, Ar, CO_2) and/or biogenic (e.g. CO_2, CH_4, N_2, O_2, H_2, H_2S) gases (Christenson and Tassi, 2015 and references therein).

The original magmatic gases entering a lake are mainly composed (>93%) of H_2O, CO_2 and SO_2 (listed in order of abundance), while the remaining 7% is made of H_2S, H_2, HCl, HF and CO (Carroll and Webster, 1994; Symonds et al., 1994; Giggenbach, 1996; Webster and Mandeville, 2007; Aiuppa et al., 2009a; Oppenheimer et al., 2011). Gas species have different solubilities in magma (Giggenbach, 1996). The less soluble gases are CO_2 and noble gases that can exsolve as deep as 40 km depth (e.g. Sigvaldason, 1989; Bourdier, 1994; Lowenstern, 2001; Schmincke, 2004). The following gases to outgas from a rising magma are H_2O and sulfur gases (Giggenbach, 1996). Halogens are the last gas species to exsolve, typically at depths of <1 km (Carrol and Webster, 1994; Giggenbach, 1996). Therefore, when the magma is deep, such as under Nyos-type lakes, the main gas detected at the surface is CO_2. This separate depths of magma degassing make gas monitoring an efficient parameter to forecast volcanic eruptions at "dry" volcanoes, when magma rises towards the surface (Aiuppa et al., 2002, 2004, 2007, 2009a) but also potentially at hyperacidic lakes which behave as "open-air" fumaroles (Rouwet et al., 2016; de Moor et al., 2016b). However, many volcanoes have an extensive hydrothermal system, which can manifest at the surface as a volcanic lake, which can strongly absorb magmatic gases depending on the physico-chemical properties (e.g., Eh, pH, water temperature; Symonds et al., 2001). Hydrothermal gases are composed of more than 99% of H_2O and CO_2, H_2S is lower than 1%, H_2 lower than 0.1%, and HCl and HF are typically absent (Symonds et al., 2001).

Depending on their solubilities in water (Figure 1.6), dissolved gases can ultimately diffuse to the atmosphere according to Henry's Law (Capasso and Inguaggiato, 1998; Sander, 1999, 2015):

$$[X] = pX \times K_H(X) \tag{1.2}$$

where [X] is the concentration of the dissolved gas (in mol/L), pX is the partial pressure of the gas X in the vapor phase (in atm) and $K_H(X)$ is the Henry constant which depends on temperature and salinity (in mol/L.atm).
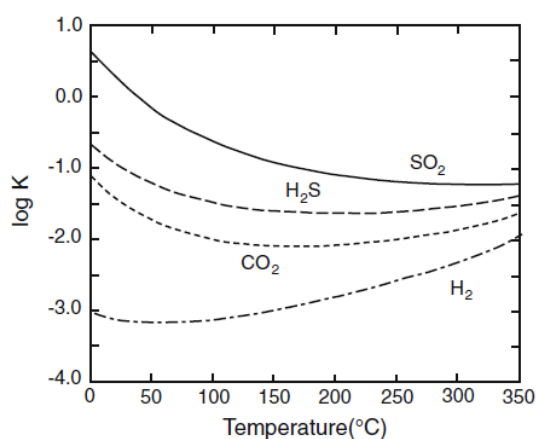
Figure 1.6 - Log of the Henry's solubility constant in function of the temperature for volcanic gas species studied in this thesis (Schulte et al., 2001 in Shinohara et al., 2015). It showed the gas solubility as $SO_2 > H_2S > CO_2 > H_2$.

The speciation of CO_2 in water is strongly dependent on pH. In water, $CO_{2(g)}$ can dissolve as $CO_{2(aq)}$, $H_2CO_{3(aq)}$, $HCO_3^-{}_{(aq)}$ and $CO_3^{2-}{}_{(aq)}$. The sum of these carbon species is called Total Dissolved Inorganic Carbon (TDIC, expressed in mol/L; Stumm and Morgan, 1981). Below a pH value of 3.8, the following reaction dominates (Stumm and Morgan, 1981):

$$CO_{2(aq)} + H_2O_{(l)} = H_2CO_{3(aq)} \tag{1.3}$$

When the pH is between 3.8 and 8.3, bicarbonate is produced by:

$$H_2CO_{3(aq)} = H^+{}_{(aq)} + HCO_3^-{}_{(aq)} \tag{1.4}$$

At pH above 8.3, bicarbonate dissociates to produce CO_3^{2-} as:

$$HCO_3^-{}_{(aq)} = H^+{}_{(aq)} + CO_3^{2-}{}_{(aq)} \tag{1.5}$$

At pH <3.8, CO_2 can flush through the lake as it was not there. Therefore, the study of CO_2 degassing at volcanic lakes has proved useful to volcano monitoring (Mazot and Taran, 2009; Hernández et al., 2011; Pérez et al., 2011; Caudron et al., 2012; Bernard et al., 2013).

The composition of sulfur species discharged at the Earth surface by open-vent degassing volcanoes, high or low temperature fumaroles or hyperacidic volcanic lakes, is primarily dependent on the magmatic H_2S/SO_2 fluid ratios. It is also a function of magma temperature, pressure and oxidation state (e.g., Symonds et al. 1994; Rye 2005; Gaillard et al., 2011). The following equilibria buffer the redox potential at high temperature (>300°C) fumarole discharges (Giggenbach, 1987):

$$H_2S + 2\ H_2O = SO_2 + 3H_2 \qquad\qquad (1.6)$$

At high temperature and low pressure, SO_2 is the dominant sulfur species in the gas phases. At low temperature, the fluid-rock buffer is the main process controlling the redox potential as (Giggenbach, 1987):

$$SO_2 + 6\ (FeO) + H_2O => H_2S + 6\ (FeO_{1.5}) \qquad\qquad (1.7)$$

This reaction is efficient to remove all the SO_2 after long and intense rock and fluid interactions. However, in most fluids, this reaction does not reach equilibrium as inferred by the presence of SO_2 emissions in fumaroles (Giggenbach, 1987).

Many secondary processes can affect sulfur speciation in fluids discharged at the surface (e.g. Symonds et al., 2001). Sulfur speciation produced by gas-water interaction is highly complex (e.g., Takano, 1987; Xu et al., 1998, 2000; Kusakabe et al., 2000a; Delmelle and Bernard, 2015 and references therein). S-gases can be affected by gas dissolution into water, and by chemical reactions in the water and gas phases producing, among others, native sulfur, aqueous sulfur species (mainly sulfates), polythionate and sulfide (Casadevall et al., 1984; Takano and Watanuki, 1990; Rowe et al., 1992b; Pasternack and Varekamp, 1994; Rowe, 1994; Takano et al., 1994; Symonds et al., 2001; Shinohara et al., 2015; Delmelle and Bernard, 2015 and references therein).

Except in hyperacidic lakes (Shinohara et al., 2015; Tamburello et al., 2015; de Moor et al., 2016b; Gunawan et al., 2016), SO_2 is believed to be totally scrubbed in water (Symonds et al., 2001).

At hyperacidic lakes, lake gases have lower H_2S/SO_2 ratios than fumarolic gases (e.g. during high lake volume at Yudamari Lake, Shinohara et al., 2015). Generally, the H_2S/SO_2 ratios at high temperature fumarolic gases are lower than in low-temperature fumarolic gases (Mizutani and Sugiura, 1966; Giggenbach, 1987). But, low-temperature fumaroles and lake gases can also exhibit very low H_2S/SO_2 ratios due to elemental sulfur (S°) precipitation (Mizutani and Sugiura, 1966; Giggenbach, 1987; Shinohara et al., 2015):

$$SO_2 + 2H_2S = 2H_2O + 3S° \qquad (1.8)$$

The amount of S° formed will depend on the original H_2S/SO_2 ratios (Shinohara et al., 2015). If the initial H_2S/SO_2 ratios is high (>2), the amount of S° that can be formed by reaction (1.8) will be large, and the resulting gas measured will have low H_2S/SO_2 ratios. On the contrary, with low original H_2S/SO_2 ratios, precipitation of S° by reaction (1.8) will be limited (Shinohara et al., 2015). The presence of liquid sulfur pools are common in the bottom of hyperacidic lakes and indicated at the surface by floating native sulfur. These pools indicate a bottom temperature ~116°C (Hurst et al., 1991) which is relatively low with respect to high temperature fumarolic gases.

At hyperacidic crater lakes, sulfur isotopic composition of dissolved bisulfate and elemental sulfur (i.e. molten sulfur or sulfur spherules) can give insights into their formation pathways and can be used to monitor volcanic activity (Kusakabe et al., 2000a; Delmelle and Bernard, 2015 and references therein):

(i)   *Insights on the magmatic SO_2 supply (hyper-acidic crater lakes).* Dissolved bisulfate and elemental sulfur can be produced by the following reactions of SO_2 disproportionation (Iwasaki and Ozawa, 1960; Ellis and Mahon, 1977; Symonds et al., 2001):

$$3SO_2 + 2H_2O = S° + 2H_2SO_4 \qquad (1.9)$$

or

$$4SO_2 + 4H_2O = H_2S + 3H_2SO_4 \qquad (1.10)$$

These reactions will produce heavy sulfur isotope ratios of HSO_4^- (high $\delta^{34}S_{HSO4}$) and low $\delta^{34}S_S$ values (Rye et al., 1992; Kusakabe et al., 2000a), resulting in large Δ_{HSO4-S} values

(typically ranging between 21 and 28‰ in active lakes such as Yugama, Maly Semiachik, Poás, Ruapehu, Kawah Ijen and Keli Mutu; Kusakabe et al., 2000a). These are the main processes generating HSO_4^- in hyper-acidic lakes (Kusakabe et al., 2000a; Delmelle and Bernard, 2015). A decrease of the $\delta^{34}S_{HSO4}$ values (e.g. from 21 (1955-1985) to 13‰ (1985-1990) at Yugama; Kusakabe et al., 2000a) can indicate a decrease of the magmatic SO_2 supply (Ohsawa et al., 1993; Kusakabe et al., 2000a).

(ii)   *H_2S origin*. At high oxygen concentrations, H_2S is oxidized by (Chen and Morris, 1972):

$$H_2S + 2O_2 = SO_4^{2-} + 2H^+ \tag{1.11}$$

When the oxygen concentration is low, H_2S is oxidized abiotically by (Delmelle and Bernard, 2015):

$$2H_2S + 2O_2 = S_2O_3^{2-} + H_2O + 2H^+ \tag{1.12}$$

At low pH, thiosulfate is unstable and forms S° and sulfite by (e.g. Davis, 1958):

$$S_2O_3^{2-} = S° + SO_3^{2-} \tag{1.13}$$

Then, a rapid oxidation of sulfite will produce SO_4^{2-} (Delmelle and Bernard, 2015):

$$SO_3^{2-} + 0.5\ O_2 = SO_4^{2-} \tag{1.14}$$

Sulfur isotope fractionation of H_2S-SO_4 (reaction 1.11) and H_2S-S (reactions 1.12 and 1.13) is limited at hydrothermal temperature (Sakai, 1968; Grinenko and Thode, 1970; Ohmoto and Rye, 1979; Kusakabe et al., 2000a) and will produce low $\delta^{34}S_{SO4}$ and $\delta^{34}S_S$ values.

(iii)   *Contribution of the bacterial oxidation (volcanic lakes with pH >1)*. $\delta^{34}S_{HSO4}$ originating from bacterial oxidation of sulfides, elemental sulfur or H_2S, such as (e.g. Kelly, 1982):

$$S° + 1.5O_2 + H_2O => SO_4^{2-} + 2H^+ \tag{1.15,}$$

is characterized by a low value (e.g. 1±1‰ in the surface water incoming into Yugama lake; Nakai and Jensen, 1964; Kusakabe et al., 2000a). At Yugama lake, the type of sulfur-oxidizing bacteria present (*Thiobacillus thiooxidans*) can only grow and survive in acidic (pH 1 to 3) and warm (T 10-60°C) waters but not at pH <1 (Kusakabe et al., 2000a).

(iv)   *Insights into the H_2S/SO_2 ratios of the gas feeding the magmatic-hydrothermal systems and its redox conditions*. The following relation was established assuming isotopic equilibration

between HSO_4^-, H_2S and S resulting from SO_2 disproportionation (Taran et al., 1996; Kusakabe et al., 2000a):

$$\delta^{34}S_{HSO_4} = \delta^{34}S_{\Sigma S} + \Delta_{H_2S}\frac{r}{1+r} + \Delta_S \frac{1}{3}\frac{1}{1+r} \tag{1.16}$$

where, $\delta^{34}S_{HSO_4}$ and $\delta^{34}S_{\Sigma S}$ are the sulfur isotopic ratio of HSO_4 and total sulfur, respectively, Δ_{H_2S} and Δ_S are the equilibrium fractionation factor for HSO_4^--H_2S and HSO_4^--S systems respectively and r is the H_2S/SO_2 ratio of magmatic gases.

When $\delta^{34}S_{HSO4}$ is plotted versus temperature (the equilibrium sulfur isotope fractionation between $S°$ and HSO_4^- is temperature dependent, Kusakabe et al., 2000a) at fixed $\delta^{34}S_{\Sigma S}$, high $\delta^{34}S_{HSO4}$ (e.g. 22‰, Kawah Ijen and 20‰, Yugama; Demelle et al., 2000; Kusakabe et al., 2000a) indicate a reduced volcanic gas (r between 1 and 10). While lower $\delta^{34}S_{HSO4}$ values (e.g. 20‰ for Keli Mutu, and 18‰ for Ruapehu; Kusakabe et al., 2000a; Varekamp and Kreulen, 2000;) suggest a slightly oxidizing gas (r between 0.1 and 1) (Kusakabe et al., 2000a).

Lake degassing is influenced by internal features such as the rate of gas discharges at the bottom, water temperature, lake water convection and bubbling degassing and by atmospheric factors (wind intensity; Rouwet and Ohba, 2015).

1.4. NYOS-TYPE LAKES AND ACID CRATER LAKES: DISTINCT PERSPECTIVES OF MONITORING

Nyos-type lakes and medium to erupting active crater lakes are monitored for distinct reasons. The former are mostly investigated to assess gas accumulation in their hypolimnion favoured by their specific limnological features (i.e. meromictic lakes have a stable and permanent thermal stratification; Schmid et al, 2005; Tassi et al., 2009; Cabassi et al., 2013) and to evaluate of hazards related to the potential gas release into the atmosphere, caused by either lake overturning driven by seasonality under temperate climate (e.g. Albano, Monticchio and Averno lakes, Italy; Caliro et al., 2008; Carapezza et al., 2008; Chiodini et al., 2012; Cabassi et al., 2013; Caracausi et al., 2013), or by gas overpressure and/or external unpredictable factors (e.g. Lakes Nyos and Monoun, Cameroon) (Tassi and Rouwet, 2014). Acidic lakes are firstly studied to detect changes in the underlying magmatic-

hydrothermal system, to monitor volcanic activity, and to evaluate global volcanic gas emissions (e.g. Pérez et al, 2011). Actually, physico-chemical changes such as water temperature (Giggenbach and Glover, 1975; Giggenbach, 1983; Christenson, 2000), lake volume, colour (Oppenheimer, 1997; Murphy et al., 2018), and water chemistry (Giggenbach, 1974, 1983; Giggenbach and Glover, 1975; Takano, 1987; Takano and Watanuki, 1990; Hurst et al., 1991; Rowe et al., 1992a; Christenson, 2000; Martínez et al., 2000; Taran et al., 2000; Mazot et al. 2008; Ohba et al., 2008; Christenson et al., 2010, 2017; Agusto and Varekamp, 2016; Rouwet et al., 2016) can indicate an increase of volcanic activity that need to be distinguished from seasonal variations.

The frequency of lake monitoring can be determined by the *residence time* (Rouwet et al., 2014b) which permits to estimate the sensitivity of a lake to potential external changes (e.g. rising magma). The residence time (RT) is defined by the following relation:

RT = V/Q (1.9)

where V is the lake volume (in m³) and Q (in m³/s) is the input or output flux of water entering or leaving the lake. Residence times of months to years are achieved for large lakes and/or low input fluxes, whereas small lakes and/or high input fluxes will lead to residence times of weeks to months. For example, bicarbonate lakes have longer residence times (decade to years); the monitoring frequency (to estimate the recharge rate of CO_2-enriched ground waters with time) of these lakes can be every 1-2 years (Rouwet al., 2014b).

Up to now, volcanic lake monitoring has principally been achieved by fluid geochemistry (Giggenbach, 1974; Ohba et al., 2008), geophysical investigations (Rymer et al., 2000, 2009; Vandemeulebrouck et al., 2005; Fournier et al., 2009; Caudron et al., 2012) and hydrogeology (Mazza et al., 2015) but currently new methods are emerging for – continuous – monitoring:

(i) Distance thermal imagery (e.g., Oppenheimer et al., 1993; Calvari et al., 2005; Harris et al., 2005, 2012; Spampinato et al., 2012 ; Witter et al., 2012) such as space-borne infrared imagery (e.g., Laguna Caliente, Poás volcano, Costa Rica, Oppenheimer et al., 1993;

Trunk and Bernard, 2008; Murphy et al., 2018) and ground-based thermal images (FLIR) (e.g., Ramírez et al., 2013)

(ii)   Gas flux measurements such as CO_2-flux station near an active crater lake, underwater hydroacoustic monitoring (Vandemeulebrouck et al., 1994, 2000) and echosounding surveys at the lake surface (Caudron et al., 2012)

(iii)   Multi-GAS measurements (e.g., Di Napoli et al., 2013 ; Shinohara et al., 2015; Tamburello et al., 2015 ; de Moor et al., 2016b; Gunawan et al., 2016)

(iv)   Numerical modeling (Christenson et al., 2010; Christenson and Tassi, 2015 ; Todesco et al., 2015)

(v)   Monitoring indirect hazards, such as lahars and volcano flank instabilities (Rowe et al., 1995; Taran and Peiffer, 2009; Delmelle et al., 2015)

(vi)   Statistical approaches such as pattern recognition and event trees (Sandri et al., 2004, 2005; Mendoza-Rosas and De la Cruz-Reyna, 2008; Tonini et al., 2016; Strehlow et al., 2017)

In this study, we use the Multi-GAS instrument to assess the relationship between the lake gas composition and acidic lake water physico-chemical features and the influence of lake scrubbing on the subaquatic fumarolic feeding gases.

CHAPTER 2

METHODS

2.1. INTRODUCTION

Here, we present the two main instruments used in this study to determine volcanic gas concentrations in water and air, (i) the CONTROS HydroC® CO_2 sensor (CONTROS System and Solutions GmbH, Kiel, Germany) to measure dissolved CO_2 partial pressure at meromictic lakes and (ii) the Multi-GAS instrument (Aiuppa et al., 2005a, Shinohara et al., 2005) to determine the gas composition (CO_2, SO_2, H_2S, H_2 and H_2O) of diverse volcanic emissions (acid lakes, hot pools and fumarolic gases). Finally, we will give details on the water sampling and analysis.

2.2. HYDROC® CO_2 SENSOR

2.2.1. Introduction

Current climate and environmental issues claimed for efficient instrumentation able to measure dissolved carbon dioxide in the ocean. The sensors have to be polyvalent and to work efficiently both installed on fixed platforms or during surveys (e.g. Fietzek et al., 2011a; Fietzek et al., 2011b; Fietzek et al., 2013; Fietzek et al., 2014; Frank et al., 2014). Sensors requirements are small size, reliability, efficiency for long period of measurements, low power consumption, high power autonomy, fast response time for profiling, high frequency of acquisition (1 Hz) and real-time measurements (Fietzek et al., 2011a; Fietzek et al., 2011b).

The CONTROS HydroC® CO_2 sensor (Figure 2.1) was initially developed for those purposes (Fietzek et al., 2014). It is equipped with a Seabird SBE 5T pump (flow rate 100 mL/s) and is powered by an external battery (CONTROS HydroB® battery pack). The sensor is robust, versatile and portable (90×376 mm and weight 4.7 kg). The pCO_2 measurement range is from 100 to 6000 µatm (resolution < 1 µatm); it has high accuracy ($\pm$ 1 % of reading) and fast response time ($t_{63} = 60$ s ($\pm$10s) at 25°C).

It can therefore be deployed in non-turbid, poorly CO_2-concentrated volcanic lakes for vertical and spatial profiling.
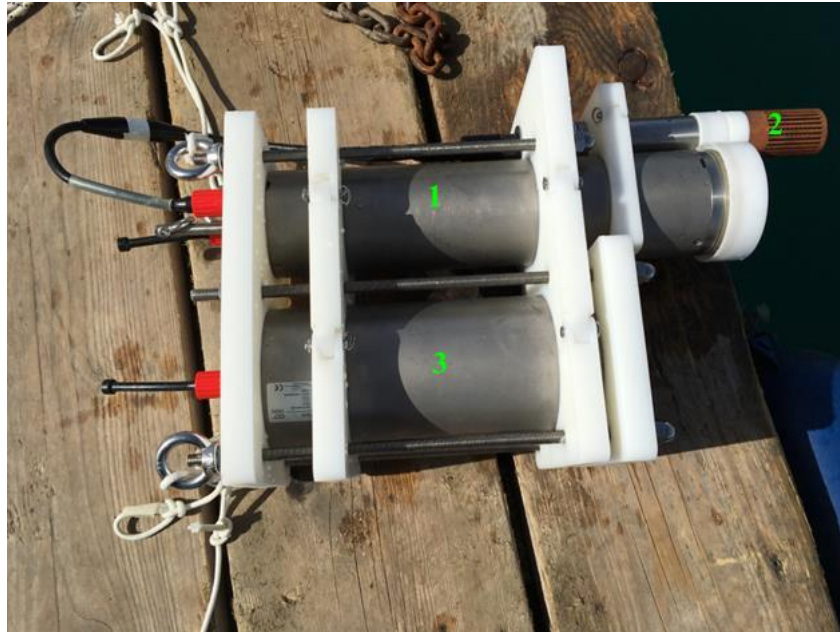
Figure 2.1 – Configuration of our sensor for lake measurements: (1) HydroC® CO_2 sensor (CONTROS System and Solutions GmbH, Kiel, Germany), (2) Seabird SBE 5T pump and (3) CONTROS HydroB® battery pack (Picture: R. Di Napoli).

2.2.2. Measurement principle

The HydroC® CO_2 sensor measures optically the partial pressure of dissolved CO_2 by the headspace method (CONTROS System and Solutions GmbH, 2011). The dissolved gas equilibrates into the sensor headspace by diffusing from the water through a hydrophobic silicone composite membrane (Figure 2.2). The concentration of CO_2 in the gas stream is then measured by a dual-beam non-dispersive inferred spectrometer (NDIR), together with internal gas temperature, pressure and relative humidity (Figure 2.2).
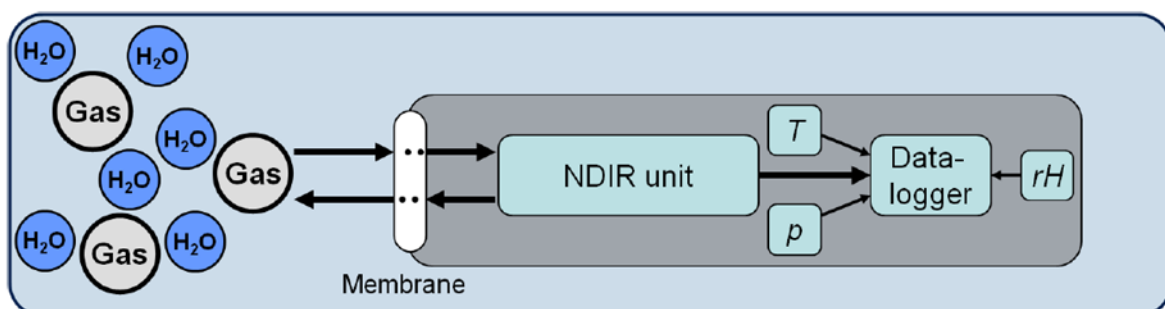
Figure 2.2 - CONTROS HydroC® CO_2 sensor principle (CONTROS Systems & Solutions GmbH; 2011)

2.2.3. Data Acquisition

Before use of the sensor in the field, the measuring cycle times (warm-up, zeroing, flush and measure; Figure 2.3) are configured with the CONTROS[TM] Detect 2.0 software (CONTROS System and Solutions GmbH). This requires the sensor head (pump + membrane) to be flooded into water and powered by electricity, which is binding during field work. The warm-up time depends on water temperature (e.g. ~10 min at 25°C and ~25 min at 17°C). The zeroing phase removes CO_2 that could have remained in the gas stream and gives a zero signal. A zeroing measurement is required at the end of the survey for potential drift-correction. The flushing phase permits to easily filter the data during the equilibrium phase. Actually, the response time of the sensor with the pump (t_{63}) is 60 s (± 10s) at 25°C, and decreases with a water temperature increase. All the campaigns were made in collaboration with researchers from the University of Florence, who provided a CTD (Hydrolab multiparameter probe, Idroprobe) that was attached to the HydroC® CO_2 sensor. It was necessary when profiling vertically because our HydroC® CO_2 sensor is not equipped with a pressure sensor. The CTD measured water depth (precision ± 0.05 m), temperature (± 0.03 °C), pH (± 0.1), electrical conductivity (± 0.01 mS/cm) and dissolved oxygen concentration ($\pm$ 1.56 µmol/L).
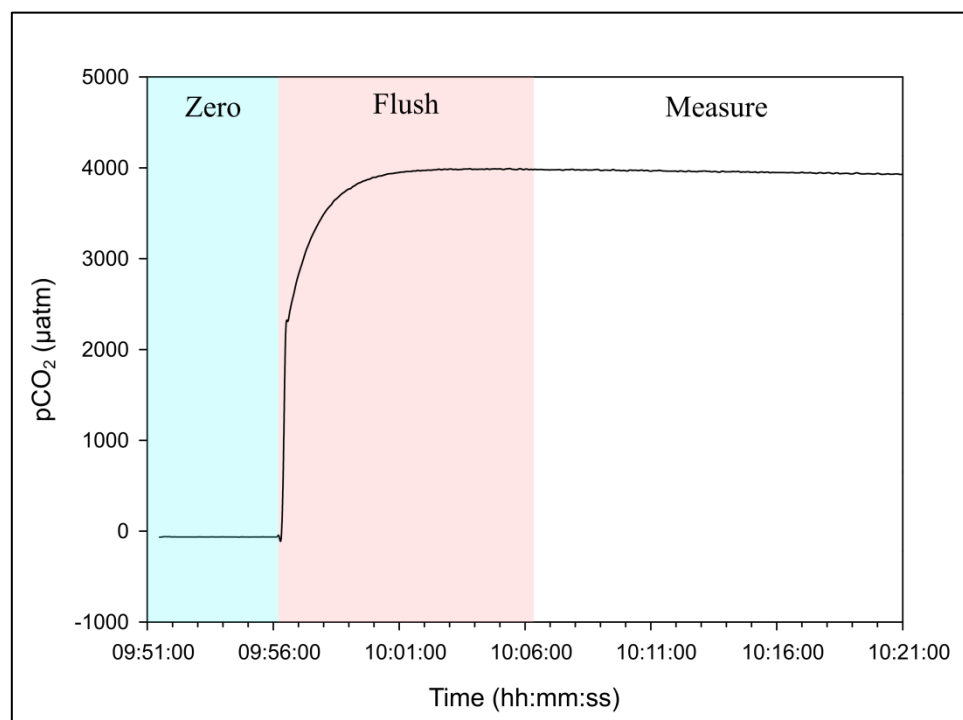
Figure 2.3 - Example of a measuring cycle including the variations of CO_2 partial pressure during zeroing, flush and measuring phases.

Some measurement requirements are necessary not to damage the membrane and the pump; the sensor cannot be run in turbid water or too close to the lake bottom. In addition, for profiling, a maximum profiling speed of 0.3 m/s is required.

2.2.4. Data Post-Processing

2.2.4.1. Zero Drift Correction

The two-beam signal (S_{2beam}) provided by the NDIR detector is calculated by (Fietzek et al., 2014):

$$S_{2beam} = \frac{S_{raw}}{S_{ref}}$$
(2.1)

where S_{raw} and S_{ref} are the sensor raw and reference signals, respectively.

The two-beam signal is also obtained for zero signals ($S_{2beam,Z}$) during the zeroing phases. The zero two-beam signal at the time t ($S_{2beam,Z}(t)$) is calculated from linear interpolation in time of the pre- and post-zero measurements.

The drift-corrected signal ($S_{DC}(t)$) is given by (Fietzek et al.,2014):

$$S_{DC}(t) = \frac{S_{2beam}(t)}{S_{2beam,Z}(t)}$$
(2.2)

where $S_{2beam}(t)$ is the two-beam signal at the time t.

2.2.4.2. Time-Lag Correction

The measured pCO_2 values were corrected to take into account the variation in the sensor response time with water temperature as follow (time-lag correction; Fiedler et al., 2013; Miloshevich et al., 2004):

$$pCO_{2,TLC}(t_i) = \frac{pCO_{2,NDIR}(t_i) - \left[pCO_{2,NDIR}(t_{i-\Delta t}).e^{-\Delta t/\tau}\right]}{1 - e^{-\Delta t/\tau}}$$
(2.3)

where $pCO_{2,NDIR}(t_i)$ is the pCO_2 measured by the sensor at the step i (in atm), $pCO_{2,NDIR}(t_{i-\Delta t})$ is the pCO_2 measured by the sensor at the step before i (in atm), Δt is time difference between the two following steps (in s), and τ is the reciprocal e-folding time (in s). The reciprocal e-folding time (τ)

was calculated empirically from the response-time evaluated during the zero-flush cycle before and after measurements on the field, assuming its linear variation with temperature.

2.2.5. Calibration

The sensor has to be calibrated annually, depending on the number of measurements done, by the manufacturer (Kongsberg, Germany). The calibration is made with three gas standards (100.74, 3001.0 and 6199.9 ppm of CO_2 in air) and 8 calibration steps are about 100, 200, 400, 900, 1800, 3000, 4500 and 6000 µatm at 21.5°C.

The mole fraction of CO_2 in wet air ($x_{CO2,wet}$) in the headspace, corrected for pressure and temperature, is calculated as followed (Data Processing Sheet for CONTROS HydroC® CO_2; Kongsberg Maritime Contros GmbH):

$$x_{CO_2,wet} = \left(k_3 . S_{proc}^3 + k_2 . S_{proc}^2 + k_1 S_{proc}^1 \right) \cdot \frac{p_0 \cdot T_{gas}}{T_0 \cdot p_{NDIR}} \tag{2.4}$$

where k_1, k_2 and k_3 are the calibration coefficients, S_{proc} is the processed NDIR signal (in digits), p_0 is the normal pressure (1013.25 bar), T_0 is the normal temperature (273.15 K), T_{gas} is the gas temperature (in K) and p_{NDIR} is the cell pressure (in bar).

Then the CO_2 partial pressure (p_{CO2}, in µatm) behind the membrane is calculated as (Data Processing Sheet for CONTROS HydroC® CO_2; Kongsberg Maritime Contros GmbH):

$$p_{CO_2} = x_{CO_2,wet} \cdot \frac{p_{in}}{1013.25} \tag{2.5}$$

where p_{in} is the total pressure in the gas behind the membrane (in atm).

2.3. MULTI-GAS

2.3.1. Introduction

The Multi-sensor Gas Analyzer System (Multi-GAS; Shinohara 2005; Aiuppa et al., 2005a) is a fully-automated compact instrument designed to measure simultaneously the in-plume concentrations of volcanic gases (CO_2, SO_2, H_2S, H_2 and H_2O) at high frequency (1 Hz). The gas ratios obtained from the concentration measurements are thought to be independent on source-instrument distance when the gas transport duration is not higher than tens of seconds (Aiuppa et al., 2005a). It is a main advantage for evaluating gas composition when the access to the source is difficult or impossible.
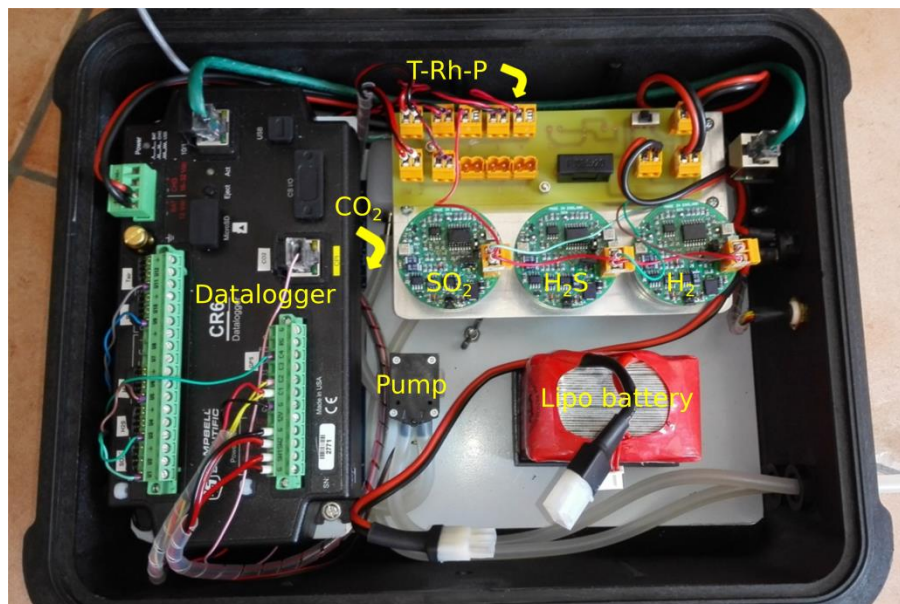
Figure 2.4 - Internal view of the Multi-GAS box (Pelicase 1400; 30.1 × 22.8 × 13.1 cm). The hand-made instrument is composed of a CR6 datalogger, sensors for CO_2, SO_2, H_2S and H_2 concentration measurements, sensors for temperature (T), pressure (P) and relative humidity (Rh) measurements, a 12V Lipo battery and a pump.

The instrument can be used for daily surveys but also installed as a (semi-)permanent station for monitoring purpose. During punctual surveys, the acquisition is done by walking into the dilute-to-concentrated gas plume. The installation of a (semi-)permanent station requests locating a strategic site, depending on the degassing characteristics (e.g. gas concentration, degassing intensity) and atmospheric conditions (e.g. down-wind), but also on accessibility and instrumental safety.

At Santa Ana volcano (El Salvador), a semi-permanent station was installed for a few days in 2017 and 2018 (see Chapter 5), whereas the gas concentration at El Chichón (Mexico), Víti (Iceland), Taal (Philippines), Yugama (Japan), Waimangu and Waiotapu geothermal systems (New Zealand), Newberry (USA), Vasca degli Ippopotami (Italy), Vulcano crater (Italy), Ruapehu (New Zealand), Kaba and Kawah Ijen (Indonesia), Rincon de la Vieja (Costa Rica) were measured on daily surveys.

2.3.2. Characteristics

Two instruments have been used for this study, one designed at the Istituto Nazionale du Geofisica e Vulcanologia (INGV), Sezione di Palermo and the other at the University of Palermo. Both instruments are equipped with a Non-Dispersive InfraRed (NDIR) spectrometer for measurement of CO_2 (Gascard II, measurement range 0-3000 ppmv, calibration range 293.7 and 2920 ppmv, accuracy $\pm$ 2%, resolution 0.8 ppmv) and three electrochemical sensors for measurement of SO_2 (CityTechnology, sensor type 3ST/F, measurement range 0-200 ppmv, calibration range 0 and 100.7 ppmv, accuracy $\pm$ 1%, resolution 0.5 ppmv, equipped with a H_2S filter) , H_2S (CityTechnology, sensor type EZ3H, measurement range 0-100 ppmv, calibration range 0-38 ppmv, accuracy $\pm$ 1%, resolution 0.25 ppmv, ~15% of interference with SO_2) and H_2 (CityTechnology, sensor type EZT3HYT "Easy Cal", measurement range 0-200 ppmv, calibration range 0-10, accuracy $\pm$ 2%, resolution 2 ppmv, equipped with a CO filter). H_2O concentrations are calculated from temperature, pressure and relative humidity (Galltex+Mela, sensor type KVM3/x, measurement range 0-100 % rh, accuracy $\pm$ 2% rh) measurements. The station is powered by a 12 V Lipo battery and the gas is pumped at a rate of 1.2 $L.min^{-1}$.

2.3.3. Data Processing

The gas concentrations of CO_2, SO_2, H_2S, H_2 and H_2O data are processed with Ratiocalc software (Tamburello, 2015). The gas plume is identified by peaks in a time-series plot (e.g. Figure 2.5) after removing the background in H_2O and CO_2 dataset and the eventual trends (e.g. instrumental drift). The molar gas ratios of the correlated gas peaks are calculated from linear regression in a scatter plot (Figure 2.6).
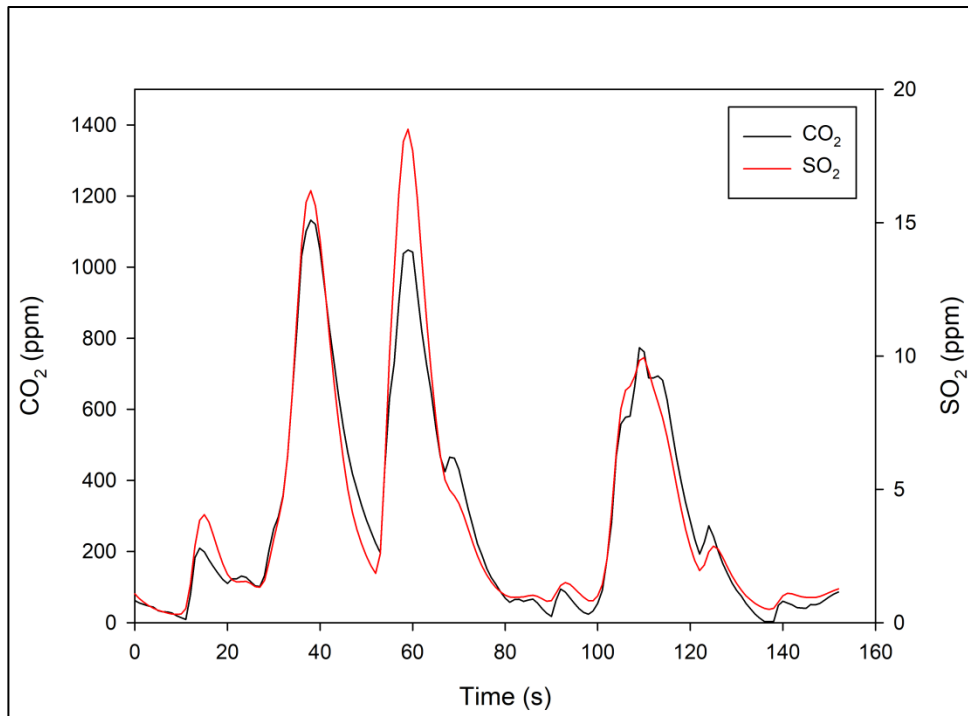
Figure 2.5 - Example of a CO_2 and SO_2 time-series plot showing the plume detection by gas concentrations increasing and decreasing at the same time.
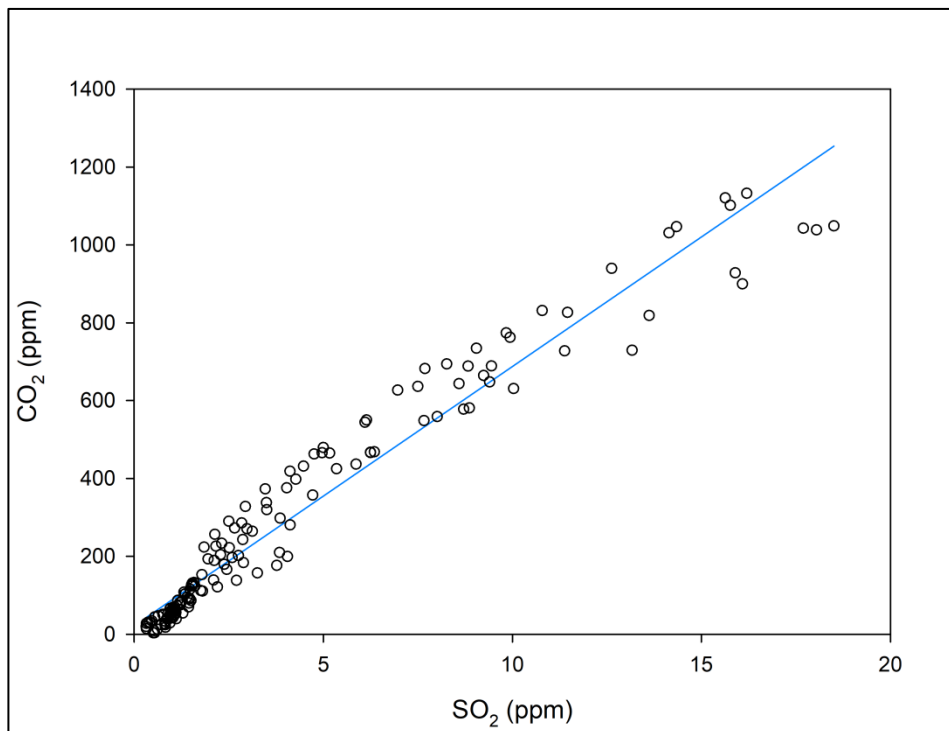
Figure 2.6 - Example of a SO_2-CO_2 scatter plot with the dataset from Figure 2.5. The correlation coefficient of the linear regression (in blue) is 0.95.

2.3.4. Application for low concentration measurements

The Multi-GAS is commonly used to measure concentrated gas plumes (SO_2 and/or H_2S >>1 ppmv) emitted by open-conduits volcanoes and fumarolic vents (e.g., Aiuppa et al., 2009b, 2011a,b, 2012) or highly-degassing volcanic lakes (e.g., Yudamari, Shinohara et al., 2015; Copahue, Tamburello et al., 2015; Poás, de Moor et al., 2016b; Kawah Ijen, Gunawan et al., 2016; Boiling Lake, Di Napoli et al., 2013).

In this study, we used the instrument at weakly sulfur-concentrated (<<1ppmv) lake plumes. Firstly, at El Chichón (Mexico), we sampled the lake gases from a slowly moving boat on March 03, 2016. To measure continuously the gas concentration, we used a tube rolled around a stick with the gas inlet (~0.5 cm diameter) at about 30-40 cm from the lake surface (Figure 2.7). It was difficult to extract SO_2 from the gas plume in the dataset during the data post-processing. The gases were probably already too mixed into the atmosphere to show good peaks above the background. At Víti lake (Iceland), we improved the method by adding an overturn funnel (~20 cm diameter) at the gas inlet. Here, the lake plume composition was measured at 10 cm from the surface. The data quality was better but the detection of SO_2 remained difficult. The same technique was used to measure the gas composition emitted by Vasca degli Ippopotami pond (Italy).

Figure 2.7 – Measurement method with the Multi-GAS at El Chichón (Mexico)

In order to assess the presence of SO_2 in the lake gas and the reliability of its detection as trace amounts, we did tests by keeping floating the overturn funnel directly on the lake surface at Víti lake (Iceland) and Vasca degli Ippopotami pond (Italy) (e.g. Figure 2.8a). The results showed strong

correlations between SO_2 peaks and other gases at concentrations as low as 0.03 – 0.1 ppmv indicating a higher sensitivity of the sensor than expected and the reliability of this low amount of gas in the dataset when it peaks slightly higher than the noise values (Figures 2.8b and c).
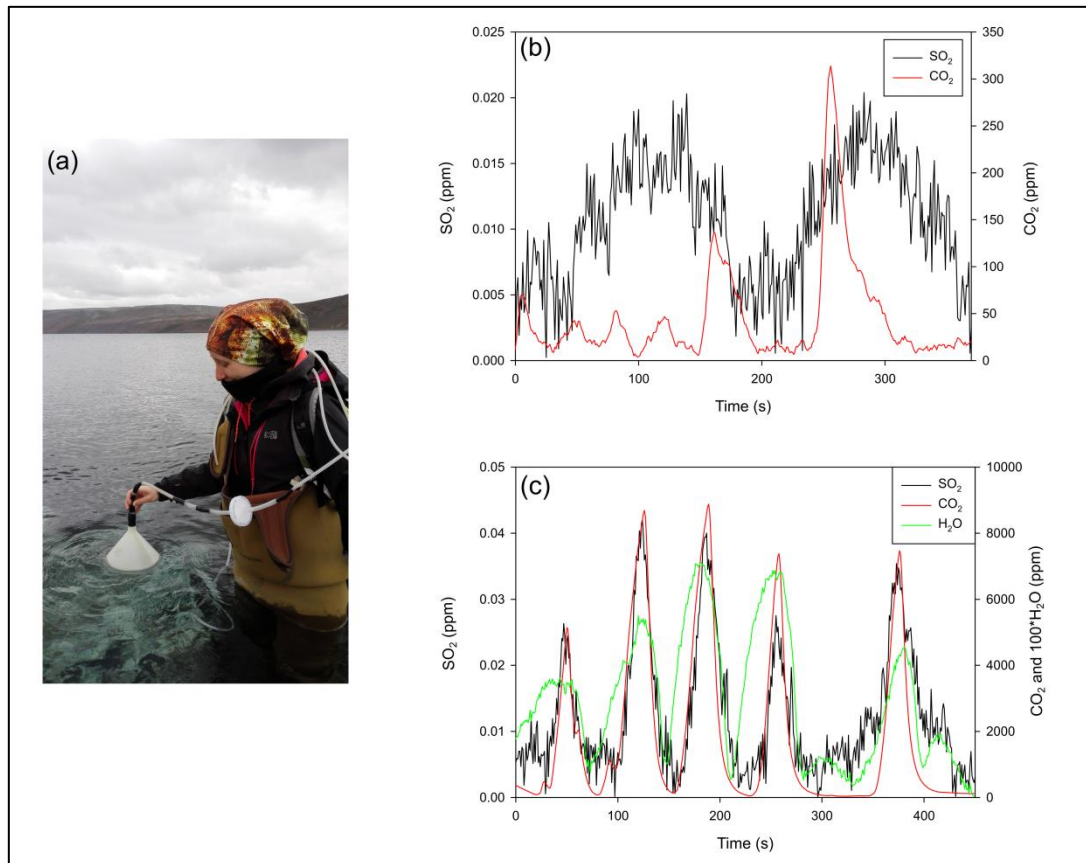
Figure 2.8 – (a) Multi-GAS measurements with the funnel kept floating on the lake surface. (b) and (c) show examples of the results of gas time-series experiments at Víti lake with the overturn funnel at 0.5 m above bubbling gases (b) and kept floating on the surface (c). In the first case, the Multi-GAS detects the bubbling gas (CO_2 peaks, up to 300 ppmv) but do not measure SO_2 concentrations above the instrumental noise. In the second experiment, SO_2 is detected (up to 0.04 ppmv) and correlated with CO_2 and H_2O when the funnel is kept on the surface (gas peaks). When the funnel is removed, gas concentrations return to noise and background values (in-between gas peaks). These experiments were also done in another lake in Iceland (Kleifarvatn lake (a), located in the Reykjanes Peninsula (SW of Iceland (Clifton et al., 2003)) above bubbles coming from subaquatic solfataras (Friðriksson, thesis 2014) and at Vasca degli Ippopotami pond (Italy) and the same kind results were obtained (not shown). These experiments aim to demonstrate the reliability of low SO_2 concentration measurements above the sensor noise.

2.4. WATER SAMPLING AND ANALYSIS

Temperature and pH were measured in situ by an ORION STAR A121 meter and the electrical conductivity by ORION STAR A122 meter. At Santa Ana crater lake, the pH was also measured by alkaline titration with NaOH 0.1M in laboratory (Capaccioni et al., 2017) and the main anions and

cations compositions were determined since 2007 at MARN (Ministerio de Medio Ambiente y Recursos Naturales, El Salvador) with Standard Methods for Examination of Water and Wastewater .

Main cations and anions from water samples were analysed by Dionex ICS 1100 chromatograph. Samples for cations analysis were filtered (0.45 μm) and acidified (ultrapure HNO_3), where those for anions analysis were only filtered.

CHAPTER 3

CONTINUOUS pCO₂ MEASUREMENTS ALONG VERTICAL AND HORIZONTAL PROFILES AT TWO MEROMICTIC LAKES

3.1. INTRODUCTION

Some quiescent volcanoes host meromictic lakes in their crater. Although these lakes only received low input of volcanic-hydrothermal fluids (Pasternack and Varekamp, 1997), they can accumulate gas in their hypolimnion (Tassi and Rouwet, 2014) which can lead to a serious hazard of CO_2 gas burst, such as the Lake Nyos catastrophe that occurred in 1986 and killed about 1700 people (Freeth and Kay, 1987, 1991; Sigvaldason, 1989; Kusakabe et al., 2000b; Kling et al., 2005) or the event that took place in 1984 at Lake Monoun (Sigurdsson et al., 1987).

Meromictic lakes are characterized by relatively cold, slightly acidic to neutral waters with low salinity (Rouwet et al., 2014b). The water column is typically stratified chemically and thermally (Rouwet et al., 2014b). Those conditions favour the development of a potentially large gas reservoir at depth (Tassi and Rouwet, 2014), mainly composed of CO_2 (originated from the deep fluids, and in smaller extent from microbial activity; e.g. Cabassi et al., 2013) and CH_4 (produced by microbial activity; Tietze et al., 1980; Schoell et al., 1988; Caliro et al., 2008; Carapezza et al., 2008; Cabassi et al., 2013). But, unexpectedly, the stable and permanent stratification can be broken by roll-over events releasing the stored dissolved and poisonous gases (e.g. CO_2 or H_2S) into the atmosphere (e.g. Sabroux et al., 1987; Kusakabe, 1996; Halbwachs et al., 2004; Kusakabe et al., 2008) and into the shallower lake water leading to fish kill events (e.g. Caliro et al, 2008).

A huge diversity of bacterioplanktons, distributed vertically in function of the physico-chemical characteristics of the water column, has been recognized at meromictic lake waters (e.g. Paganin et al., 2013; Tassi et al., 2018). Microbial activity has not only a strong influence on gas concentrations but

also on the water chemistry along the water column (Tassi et al., 2018). For example, low CO_2 concentrations at lake surfaces result from photosynthesis and speciation at slightly acidic to neutral pH. Therefore, meromictic lakes can be sinks for the atmospheric CO_2.

Methods available to investigate in-situ the dissolved gas partial pressure at deep lakes are few (Evans et al., 1993; Yoshida et al., 2010; Ohba et al., 2013; Zimmer et al., 2017). Here, I present the first application of the HydroC® CO_2 sensor (CONTROS System and Solutions GmbH, Kiel, Germany) in volcanic lakes which measures in-situ and continuously the dissolved CO_2 partial pressure. In order to assess the physico-chemical characteristics of the water columns, I also present vertical profiles of temperature, conductivity, pH and dissolved oxygen concentrations measured by a multiparameter probe (Hydrolab IP188A multi-probe; J. Cabassi pers. comm.; Tassi et al., 2018) and dissolved gas concentrations measured in the headspace of the water samples (F. Tassi pers.comm.; see Tassi et al., 2018 for details on the sampling and analytical methods). All the data were collected contemporaneously during the field campaigns.

The two studied lakes are Barombi Mbo in Cameroon (West Africa) and Averno in Italy. The former has been poorly studied and investigations were done at first to evaluate the amount of CO_2 dissolved in the water to assess the hazard of gas accumulation at depth and to provide a limnological characterization of the water column. The latter is the subject of regular monitoring to detect changes in the vertical physico-chemical profile and possible gas accumulation at depth. Vertical profiles are often executed at the lake centre but sources of CO_2 in other areas in the lake have never been investigated. The final aim of this study was to assess the potential of the HydroC® CO_2 sensor as a new tool for in-situ investigation of the pCO_2 in large and deep volcanic lakes to characterize the vertical and horizontal CO_2 distribution but also to locate sources of CO_2 at lake bottoms.

3.2. GENERAL SETTINGS ON THE STUDY SITES

3.2.1. Barombi Mbo Lake

Barombi Mbo (4°39'N, 9°24'E; 314 m a.s.l.) is a 110-m deep tropical maar lake located in the South-West region of Cameroon at 250 km NW of Yaoundé, the capital city (Figure 3.1). Barombi

Mbo is situated in the southern part of the Cameroon Volcanic Line (CVL; Figure 3.2; Cornen et al., 1992), in the Kumba Volcanic Field (800 km²; extending from Rump Hills and Bakassi Mountains in the North to Mount Cameroon in the South; Tchamabé et al., 2015).

The Cameroon Volcanic Line (CVL) is a 1600-km-long active volcano-tectonic ridge oriented NE-SW (Sato et al., 1990; Cornen et al., 1992) which extends from Ngaoundéré plateau (northern Cameroon) to Pagalú Island (Guinea) (Sato et al., 1990; Figure 3.2). It is composed of many extinct Cenozoic (Tsafack et al., 2009) monogenetic and polygenetic volcanoes (Sato et al., 1990; Fitton and Dunlop, 1985; Asaah et al., 2015), of which more than 40 have their craters filled by lakes (Figure 3.2; Kling, 1987; Ngwa et al., 2010; Tongwa et al., 2014).

Barombi Mbo is the largest maar lake (2.4-km diameter with a surface area of ~4.1 km²) in the CVL (Kling, 1988; Cornen et al., 1992). The lake fills the youngest maar (the easternmost) of two nested coalescing maar craters aligned W-E (Dumort, 1968; Cornen et al., 1992; Tchamabé et al., 2013). Volcanic activity at Barombi Mbo started in the Eocene (Dumort, 1968) and is not younger than 1 Ma (Cornen et al., 1992). The formation of Barombi Mbo maar includes three eruptive episodes that occurred respectively 500 ka BP, ~200 ka BP and ~80 ka BP (Tchamabé et al., 2014).

This volcano and its lake have not been extensively studied; research mainly focused on lake biodiversity (e.g., Green et al., 1973; Dominey and Snyder, 1988; Lebamba et al., 2012), palynology (e.g., Maley et al., 1990), sedimentology (e.g., Giresse et al., 1991; Cornen et al., 1992), stratigraphy (Tchamabé et al. 2013, 2014, 2015), limnology (e.g. Kling, 1987, 1988; Tongwa et al., 2014) and CO_2 emissions (Ohba et al., 2014).
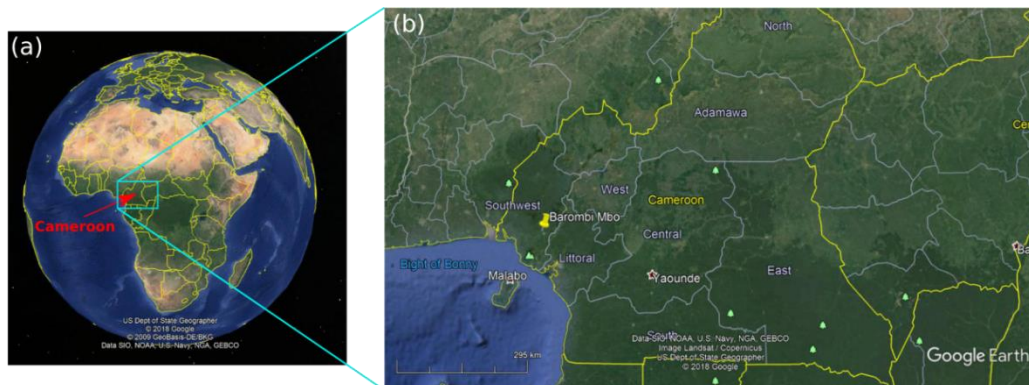
Figure 3.1 - Localisation of Barombi Mbo Lake (b) in Cameroon (a) (Google Earth 2018).

Barombi Mbo lake is a through-flow lake (Tongwa et al., 2014) with an outlet stream to the southeast (Cornen et al., 1992). Limnology studies have revealed the presence of a stable thermal stratification (Green et al., 1973; Kling, 1988) with a well-developed thermocline at above 35 m depth (end of the dry season; Kling, 1988) or shallower during the rainy season (Green et al., 1973). The surface water temperature is high (about 25-30°C) and varies seasonally (Green et al., 1973; Kling et al., 1987), as well as diurnally (Kling, 1988). The temperature in the hypolimnion was about 25.4 °C in 1985 (Kling, 1987). Occasionally, the lake turned over and the waters were mixed (e.g. in 1940s, Tongwa et al., 2014; in August 2012; Ohba et al., 2014). In 2013, after such an event, Tongwa et al. (2014b) investigated the isotopic composition (δD and $\delta^{18}O$) along the vertical profile and found a nearly homogeneous distribution (δD were of 3.4, 1.6 and 1.2 ‰ and $\delta^{18}O$ were of 4.1, 3.8 and 3.8 ‰ at depths of 0, 50 and 98 m, respectively) with values similar to that of the local rainfall. Dissolved oxygen concentration measurements revealed an anoxic hypolimnion (Green et al., 1973; Kling, 1988) and an oxic epilimnion which contained 8 mg/L of O_2 in February 1985 (Kling, 1988). The water was slightly saline in February 1985; the conductivity (at 25°C) was of 49.1 μS/cm at the surface and 80.2 μS/cm at the bottom (Kling 1988).

Figure 3.2 - Location of Barombi Mbo maar (red star) along the Cameroon Volcanic Line. The famous lake Nyos and Monoun emplacements are also shown (red star). Maar lakes of the CVL are represented by blue dots (Modified from Tchamabé et al., 2015).

Ohba et al. (2014) measured the CO$_2$ flux emitted by Barombi Mbo lake and found that it was not diffusing CO$_2$ into the atmosphere but that it rather was a sink for atmospheric CO$_2$ in April 2012 (-13 t/d; dry season, after lake overturn) and January 2014 (-0.87 t/d; end of the rainy season). Therefore the flux is not constant with time and may vary seasonally, daily or due the lake dynamic (Ohba et al., 2014). More surveys are required to clarify the influence of the above mentioned factors on the CO$_2$ emission process. Issa et al. (2014a) also determined the concentration of CO$_2$ in the bottom water (8.75 mmol/kg at 100 m depth) but could not infer on the origin.

3.2.2. Averno Lake

Lake Averno (40°50'N, 14°04'E, 2 m a.s.l.) is located in the northwestern part of the Phlegrean Fields caldera (Figure 3.3), an active volcano in the Naples area (Campania, Italy) which is constituted of a submerged and a continental part (Caliro et al., 2008). The two caldera collapses following the eruptions of the Neapolitan Yellow Tuff, 15 ky BP (Dellino et al., 2004 and references therein) and the Campanian Ignimbrite, 39 ky BP (Fedele et al., 2004 and reference therein) have formed the current caldera (Orsi et al., 1996). The last eruption in the area occurred in 1538 and formed Mt Nuovo, located 100 m SE of Averno lake (Di Vito et al., 1987). The remnant magma of the two main eruptions has been suggested to currently supply the fluid and heat emissions in the Phlegrean Fields caldera (De Vita et al., 1998, 1999; Chiodini et al., 2001; Dellino et al., 2001; Zimanowski et al., 2003; Caliro et al., 2008).
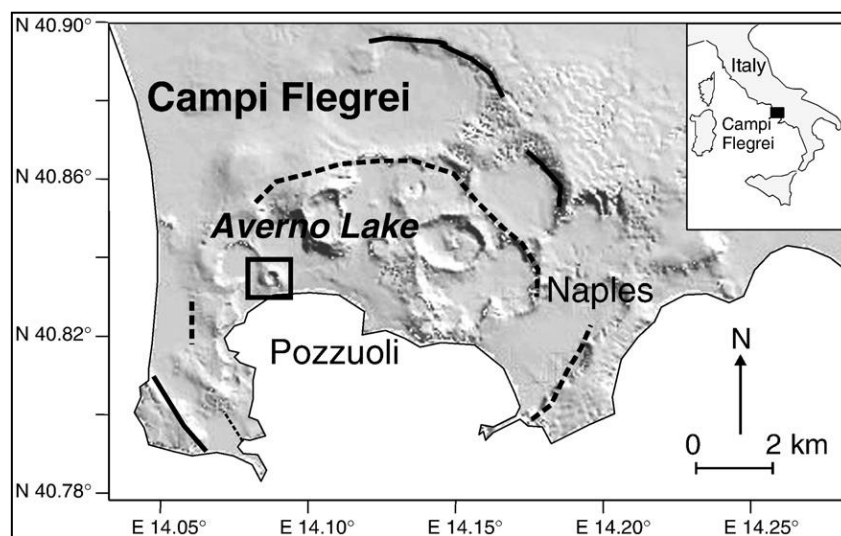
Figure 3.3 - Location and map of the Phlegrean Fields caldera with the situation of Averno Lake (Caliro et al., 2008).

The Averno crater (up to 110m high; Gruger and Thulin, 1998; Caliro et al., 2008) was built by two eruptions that occurred in 4500 yr BP and 3700 yr BP (Figure 3.4; Rosi and Sbrana, 1987; Orsi et al., 2004). The homonymous lake formed soon after the latter eruption (Rosi and Sbrana, 1987). The crater is located at the intersection of the dominant NW-SE, Pozzuoli bay, and NE-SW, San Vito-Averno, fault systems (Figure 3.4; Orsi et al., 1996, 2004).

The lake has a surface area of 0.55 km² and is 33 m deep (Grüger and Thulin, 1998; Caliro et al., 2008). It is fed by rainwater and submerged springs (originating from a Na-Cl hydrothermal fluid mixed with rich-HCO_3^- shallow water; Caliro et al., 2008) and has an outlet, a Roman canal, built in 37 BC, connecting it to the sea (Grüger and Thulin, 1998). In addition, sewages discharge into the lake and enrich the water and sediments in organic matter (Improta et al., 2004).
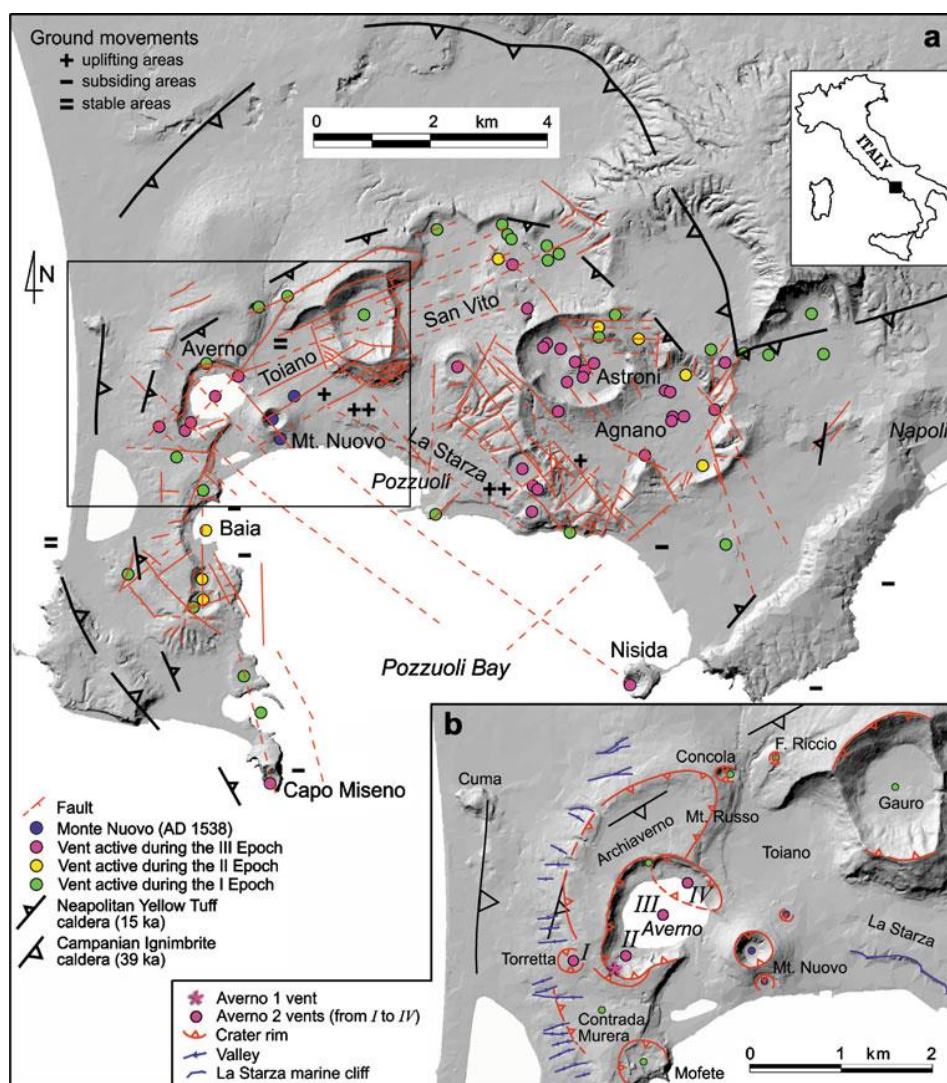
Figure 3.4 - (a) Structural map of the Phlegrean Fields caldera with the location of the faults and eruptive vents in history. (b) Location of the active vents at Averno and the respective crater rims (Di Vito et al., 2011).

Averno shows a permanent vertical chemical and thermal stratification (Caliro et al., 2008; Cabassi et al., 2013). Lake waters are neutral to slightly basic (Martini et al., 1991; Caliro et al., 2008; Cabassi et al., 2013; Tassi et al., 2018) and rich in bicarbonate (300-800 mg/L; Martini et al., 1991; Caliro et al., 2008; Cabassi et al., 2013; Tassi et al., 2018). The thermocline, situated between 5 and 15m depth (Caliro et al., 2008; Cabassi et al., 2013) separates the aerobic epilimnion, affected by seasonal temperature variations (surface temperatures varying from 9 to 27 °C; Caliro et al., 2008; Cabassi et al., 2013), from the cold and anoxic hypolimnion (stable temperature around 10°C; Caliro et al., 2008; Cabassi et al., 2013; Tassi et al., 2018). During the winter season, when the lake epilimnion temperature drops below 10°C (Caliro et al., 2008; Tassi et al., 2018), the lake can overturn (evidenced by fish kill events such as those reported in 2002, 2003, 2005 and 2017; Caliro et al., 2008; CVL reports). Even if the μmol concentration range of H$_2$S is toxic for fish (Bagarinao, 1992), the total amount of gas (mainly CO$_2$ and CH$_4$) released into the atmosphere during such rollover events is too low to be of risk for the local population.

Dissolved gases (O$_2$, CO$_2$, CH$_4$ and H$_2$S) concentrations display variations along the vertical profile (10^{-7}-10^{-4}; 10^{-5}-10^{-3}; 10^{-7}-10^{-3} and 10^{-6}-10^{-4} mol/L; respectively) while N$_2$ and Ar (3-7×10^{-4} and 1-2×10^{-5} mol/L, respectively; the main components of in the epilimnion) concentrations are nearly constant over the whole water column (Caliro et al., 2008). Below the epilimnion, a decrease in O$_2$ and an increase in CO$_2$, CH$_4$ and H$_2$S (the main gas below 30 m) concentrations are observed (Caliro et al., 2008). Dissolved gases at Averno have distinct origins. The main source of dissolved CO$_2$ is the hydrothermal fluid injected at the bottom (δ^{13}C-TDIC -5.4‰ at the lake bottom; Caliro et al., 2008), but CO$_2$ is also produced by bacterial processes (Cabassi et al., 2013; Tassi et al., 2018). Methane is produced by decomposition of the organic matter at the lake bottom by anaerobic bacteria (Caliro et al., 2008) while bacterial sulfate reduction is responsible for the production of H$_2$S. In the epilimnion, CO$_2$ is consumed by photosynthesis (Caliro et al., 2008).

3.3.   PHYSICOCHEMICAL PATTERNS AT BAROMBI MBO LAKE

On March 22, 2016, Barombi Mbo lake exhibited a sharp thermocline located between ~10 and 25m depth separating the hotter epilimion (30°C at the surface) from the ~26.5°C hypolimnion (Figure 3.5a). The lake water was nearly neutral (pH up to 7.57 at ~14m depth) to slightly acidic (pH down to 6.69 below 100 m) (Figure 3.5c) and contained low concentrations of dissolved solutes (the lowest values of electrical conductivity are found at 20 m depth (0.05 mS/cm) and the highest (0.12 mS/cm) at 100 m depth; Figure 3.5b). Dissolved oxygen showed a clinograde profile with a concentration of about 7.6 mg/L down to 7 m depth. Below 14 m depth, the water was anoxic (Figure 3.5d).

The composition of dissolved gases (Figure 3.6; Table 3.1) of the epilimnion is dominated by atmospheric gases, i.e. N_2 (~0.50 mmol/L), Ar (~0.012 mmol/L) and O_2 (~0.18 mmol/L), while the anoxic hypolimnion is mainly composed of CO_2 (up to 0.63 mmol/L) and CH_4 (up to 0.65 mmol/L), that derived from deep fluid inputs (only CO_2, supported by $\delta^{13}C$-CO_2 enrichment at depth; Boehrer et al., in prep.) or from biogeochemical processes (Boehrer et al., in prep.). Low amounts of H_2 (up to 0.00026 mmol/L), likely produced by bacterial processes (Tassi and Rouwet, 2014), were measured below 70 m depth.

The total gas pressure is mostly influenced by pN_2 (0.68-0.83 atm) over the whole water column (Figure 3.6, Table 3.1). The second most contributing gases to the total gas pressure are O_2 (pO_2 ~0.18 atm) in the epilimnion and CH_4 (pCH_4 up to 0.42 atm) below 20 m depth (Figure 3.6, Table 3.1). The pCO_2 only weakly contributed to the total gas pressure (1.4×10^{-3} and 0.016 atm at the lake surface and bottom, respectively) and is below the atmospheric pressure up to 7 m depth. In addition, the total gas pressure is below the hydrostatic pressure (~11.6 atm at 110 m depth; Figure 3.6).
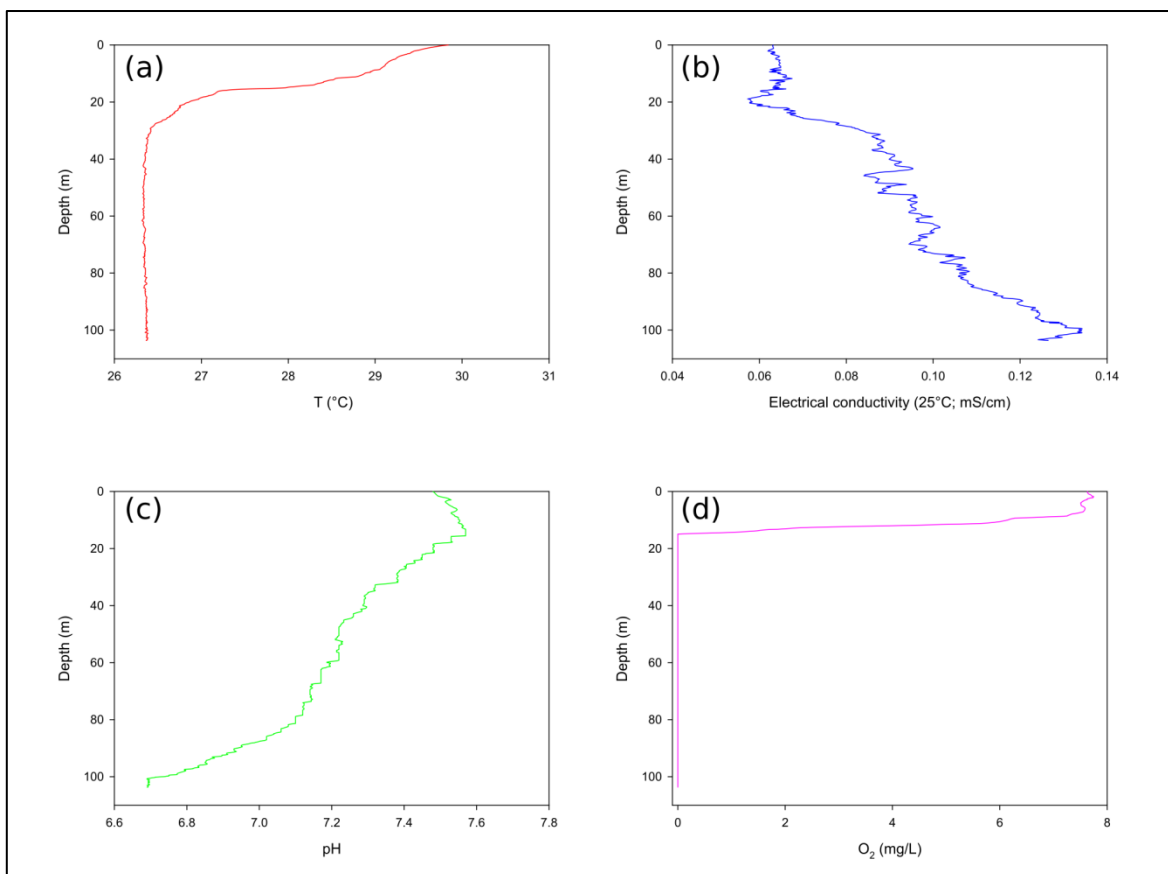
Figure 3.5 - Temperature (a), electrical conductivity (b), pH (c) and dissolved oxygen concentration (d) vertical profiles at Barombi Mbo.
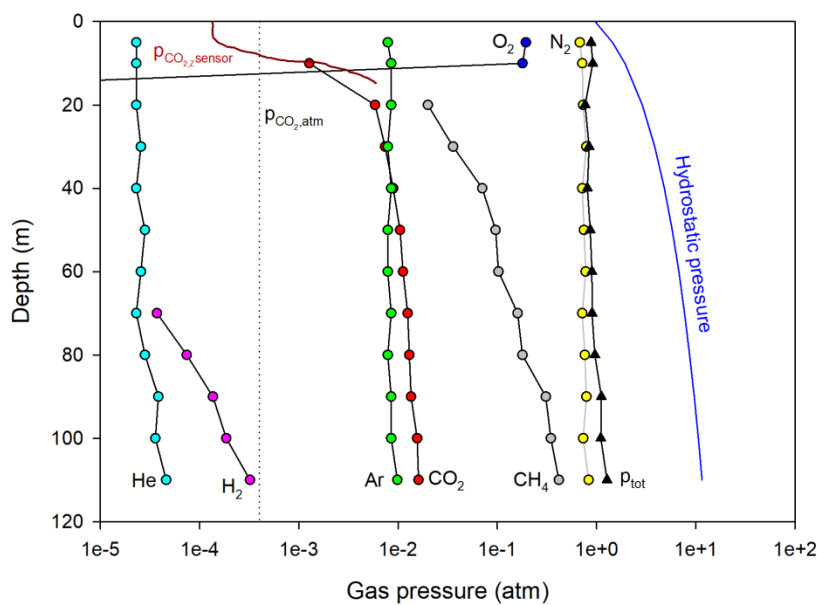
Figure 3.6 - Variations of the partial pressures of dissolved gas along the vertical profile at Barombi Mbo. The total dissolved gas pressure (p$_{tot}$), the hydrostatic pressure and the atmospheric pCO$_2$ (pCO$_{2,atm}$) are also shown. The pCO$_2$ measured by the HydroC® CO$_2$ sensor is represented by the continuous red line.

Table 3.1 - Dissolved gas concentrations and partial pressures in Barombi Mbo lake water along the vertical profile on March 22, 2016 (J.Cabassi and F.Tassi, pers.comm.). Temperature data come from the CTD. ptot is the total partial pressure.

Depth	T	CO_2	pCO_2	N2	pN_2	Ar	pAr	CH_4	pCH_4	O_2	pO_2	H_2	pH_2	He	pHe	ptot
m	°C	mmol/L	atm	mmol/L	atm	mmol/L	atm	mmol/L	atm	mmol/L	atm	mmol/L	atm	mmol/L	atm	atm
5	29.2	-	-	0.48	0.68	1.20×10^{-2}	7.86×10^{-3}	-	-	0.27	0.19	-	-	9.00×10^{-6}	2.30×10^{-5}	0.88
10	28.9	0.05	0.0013	0.51	0.72	1.30×10^{-2}	8.52×10^{-3}	-	-	0.25	0.18	-	-	9.00×10^{-6}	2.30×10^{-5}	0.92
20	26.9	0.23	0.0059	0.52	0.73	1.30×10^{-2}	8.52×10^{-3}	0.031	0.020	-	-	-	-	9.00×10^{-6}	2.30×10^{-5}	0.77
30	26.4	0.29	0.0074	0.56	0.79	1.20×10^{-2}	7.86×10^{-3}	0.056	0.036	-	-	-	-	1.00×10^{-5}	2.56×10^{-5}	0.84
40	26.4	0.35	0.0089	0.51	0.72	1.30×10^{-2}	8.52×10^{-3}	0.11	0.071	-	-	-	-	9.00×10^{-6}	2.30×10^{-5}	0.81
50	26.3	0.41	0.010	0.53	0.75	1.20×10^{-2}	7.86×10^{-3}	0.15	0.096	-	-	-	-	1.10×10^{-5}	2.81×10^{-5}	0.86
60	26.3	0.44	0.011	0.55	0.78	1.20×10^{-2}	7.86×10^{-3}	0.16	0.10	-	-	-	-	1.00×10^{-5}	2.56×10^{-5}	0.90
70	26.3	0.49	0.012	0.51	0.72	1.30×10^{-2}	8.52×10^{-3}	0.25	0.16	-	-	3.00×10^{-5}	3.71×10^{-5}	9.00×10^{-6}	2.30×10^{-5}	0.90
80	26.4	0.51	0.013	0.54	0.76	1.20×10^{-2}	7.86×10^{-3}	0.28	0.18	-	-	6.00×10^{-5}	7.42×10^{-5}	1.10×10^{-5}	2.81×10^{-5}	0.96
90	26.4	0.53	0.013	0.56	0.79	1.30×10^{-2}	8.52×10^{-3}	0.48	0.31	-	-	1.10×10^{-4}	1.36×10^{-4}	1.50×10^{-5}	3.83×10^{-5}	1.12
100	26.4	0.61	0.016	0.52	0.73	1.30×10^{-2}	8.52×10^{-3}	0.54	0.35	-	-	1.50×10^{-4}	1.86×10^{-4}	1.40×10^{-5}	3.58×10^{-5}	1.11
110	-	0.63	0.016	0.59	0.83	1.50×10^{-2}	9.83×10^{-3}	0.65	0.42	-	-	2.60×10^{-4}	3.22×10^{-4}	1.80×10^{-5}	4.60×10^{-5}	1.28

3.4.   PHYSICOCHEMICAL PATTERNS AT AVERNO LAKE

In September 2016, the Multi-parameter probe did not work and the temperature, electrical conductivity, pH and pO$_2$ came from water sampling measurements and analysis. The surface temperature was 24.5 °C (Figure 3.7a), the pH 9.5 (Figure 3.7c), the electrical conductivity 2.5 mS/cm (Figure 3.7b) and the pO$_2$ 160 mbar (Figure 3.7d).

In July 2017, measurements were executed down to 20 m depth. The surface temperature was higher (27.7 °C) and the vertical profile showed a well pronounced thermocline between 4 and 10 m depth (Figure 3.7a). The epilimnion reached between 132 and 182 mbar in pCO$_2$, peaking at 4.5 m depth (385 mbar). Below 5 m depth, the water was anoxic (Figure 3.7d). The pH was constant at about 8.1 in the epilmnion, decreased sharply from 4 m to 6m, below which it remained stable around 7.0 (Figure 3.7c). The electrical conductivity was nearly constant at 2.35 mS/cm (Figure 3.7b).

The dissolved gases displayed similar vertical profiles between 2016 and 2017, but with slightly different partial pressure (Figure 8; Table 3.2). The atmospheric gases (Ar, N$_2$ and O$_2$) exhibited higher partial pressures in 2016 (10^{-2}, 0.6-0.7 and 0.05-0.2 atm, respectively) compared to 2017 (7-8 $\times$ 10^{-3}, 0.64-0.67 and 5-6 $\times$ 10^{-3} atm, respectively) while the gases sourcing at the bottom (CO$_2$ and CH$_4$) showed the opposite trend. pCO$_2$ varied from 2×10^{-5} (surface) to 9×10^{-2} (bottom) atm in 2016 and from 3×10^{-5} (surface) to 0.1 (bottom) atm in 2017. pCH$_4$ ranged from 2×10^{-5} (10 m depth) to 0.53 atm (bottom) in 2016 and from 1×10^{-4} (8 m depth) to 1 atm (bottom) in 2017. The water was anoxic below 14 m in 2016 and below 6 m depth in 2017. Methane was present at shallower depth in 2017 (below 8 m depth) compared to 2016 (below 10 m depth).

In 2017 as well as in 2016, the total gas pressure remained far from the hydrostatic pressure (Figure 3.8). In 2016, the total gas pressure decreased from 0.90 atm at the surface to 0.64 atm at 16-18 m depth. Below it increased up to 1.2 atm. In 2017, the total gas pressure was constant (0.66-0.67 atm) down to 12 m depth and the increased up to 1.9 atm at the bottom.
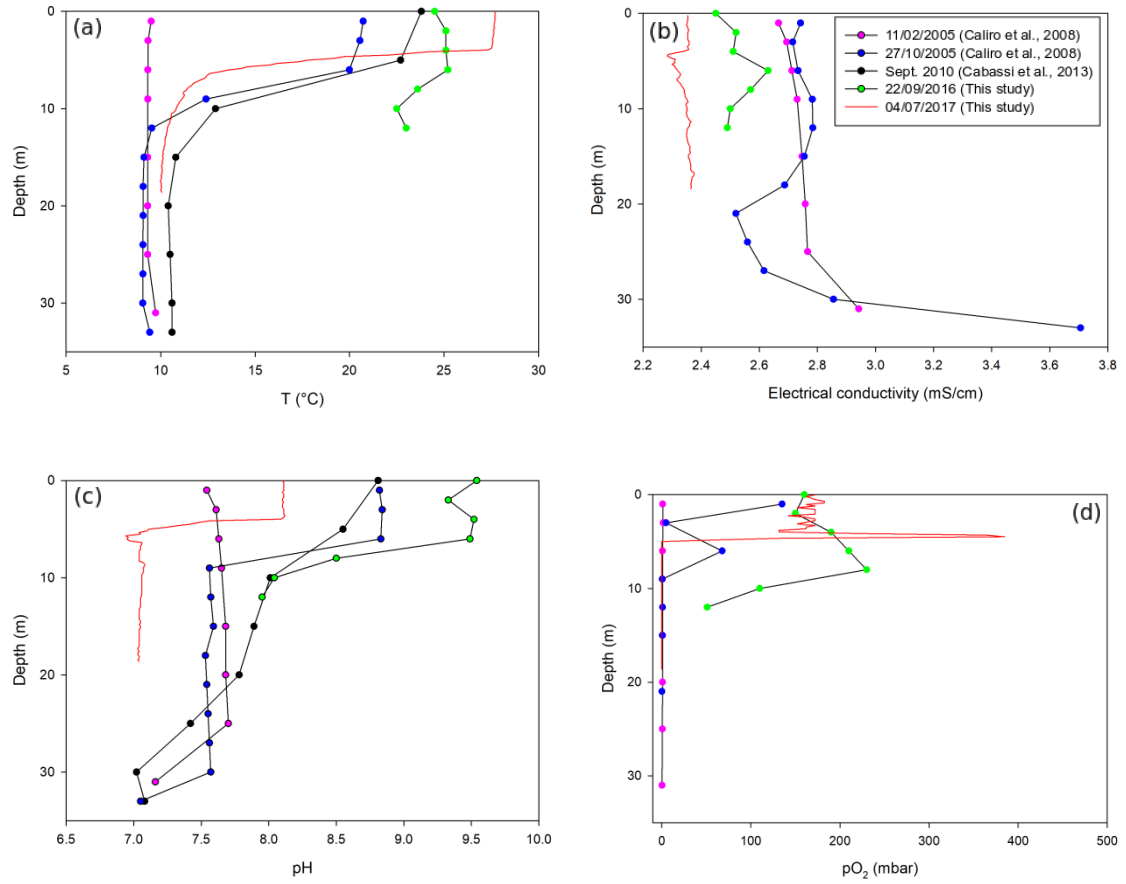
Figure 3.7 - Temperature (a), electrical conductivity (b), pH (c) and dissolved oxygen concentration (d) vertical profiles at Averno lake.
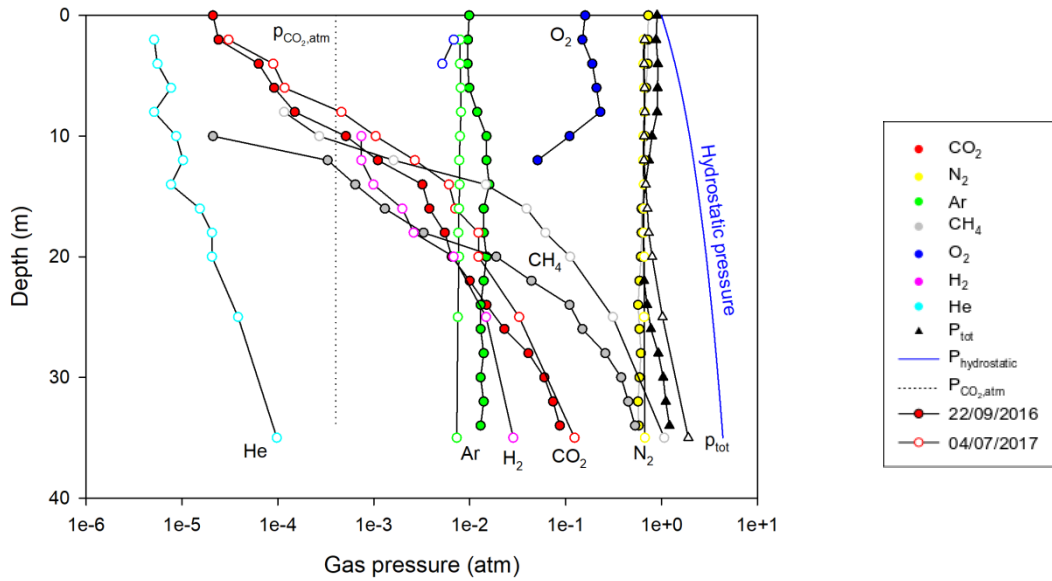
Figure 3.8 - Variations of dissolved gas partial pressures along the vertical profile at Averno lake in 2016 (full symbols) and 2017 (empty symbols) The total dissolved gas pressure (ptot), the hydrostatic pressure and the atmospheric pCO₂ (pCO₂,atm) are also shown.

Table 3.2 - Dissolved gas concentrations and partial pressures in Averno water along the vertical profile (J.Cabassi and F.Tassi, pers.comm.). Temperature data come from the CTD. ptot is the total partial pressure.

Date	Depth	T	CO_2	pCO_2	N_2	pN_2	Ar	pAr	CH_4	pCH_4	O_2	pO_2	pH_2	pH_2	pHe	pTot
	m	°C	mol/l	atm	mol/l	atm	mol/l	atm	mol/l	atm	mol/l	atm	mol/l	atm	atm	atm
22/09/16	0.00	24.5	7.24×10^{-7}	2.10×10^{-5}	4.49×10^{-4}	0.73	1.40×10^{-5}	9.90×10^{-3}	-	-	2.10×10^{-4}	0.16	-	-	-	0.90
22/09/16	2.00	25.1	8.14×10^{-7}	2.40×10^{-5}	4.39×10^{-4}	0.72	1.34×10^{-5}	9.60×10^{-3}	-	-	1.95×10^{-4}	0.15	-	-	-	0.88
22/09/16	4.00	25.1	2.14×10^{-6}	6.30×10^{-5}	4.37×10^{-4}	0.72	1.33×10^{-5}	9.50×10^{-3}	-	-	2.47×10^{-4}	0.19	-	-	-	0.92
22/09/16	6.00	25.2	3.08×10^{-6}	9.10×10^{-5}	4.20×10^{-4}	0.69	1.38×10^{-5}	9.90×10^{-3}	-	-	2.72×10^{-4}	0.21	-	-	-	0.91
22/09/16	8.00	23.6	5.30×10^{-6}	1.50×10^{-4}	4.11×10^{-4}	0.66	1.72×10^{-5}	1.20×10^{-2}	-	-	3.07×10^{-4}	0.23	-	-	-	0.90
22/09/16	10.00	22.5	1.86×10^{-5}	5.10×10^{-4}	4.24×10^{-4}	0.67	2.19×10^{-5}	1.50×10^{-2}	3.09×10^{-8}	2.10×10^{-5}	1.50×10^{-4}	0.11	-	-	-	0.80
22/09/16	12.00	23	3.95×10^{-5}	1.10×10^{-3}	4.21×10^{-4}	0.67	2.17×10^{-5}	1.50×10^{-2}	4.80×10^{-7}	3.30×10^{-4}	6.89×10^{-5}	0.05	-	-	-	0.74
22/09/16	14.00	-	-	3.20×10^{-3}	-	0.66	-	1.60×10^{-2}	-	6.40×10^{-4}	-	-	-	-	-	0.68
22/09/16	16.00	-	-	3.80×10^{-3}	-	0.62	-	1.40×10^{-2}	-	1.30×10^{-3}	-	-	-	-	-	0.64
22/09/16	18.00	-	-	5.50×10^{-3}	-	0.62	-	1.40×10^{-2}	-	3.30×10^{-3}	-	-	-	-	-	0.64
22/09/16	20.00	-	-	6.50×10^{-3}	-	0.61	-	1.50×10^{-2}	-	1.90×10^{-2}	-	-	-	-	-	0.65
22/09/16	22.00	-	-	1.00×10^{-2}	-	0.59	-	1.40×10^{-2}	-	4.40×10^{-2}	-	-	-	-	-	0.66
22/09/16	24.00	-	-	1.50×10^{-2}	-	0.57	-	1.30×10^{-2}	-	1.10×10^{-1}	-	-	-	-	-	0.71
22/09/16	26.00	-	-	2.30×10^{-2}	-	0.59	-	1.30×10^{-2}	-	1.50×10^{-1}	-	-	-	-	-	0.78
22/09/16	28.00	-	-	4.10×10^{-2}	-	0.61	-	1.40×10^{-2}	-	2.60×10^{-1}	-	-	-	-	-	0.93
22/09/16	30.00	-	-	6.00×10^{-2}	-	0.59	-	1.30×10^{-2}	-	3.80×10^{-1}	-	-	-	-	-	1.04
22/09/16	32.00	-	-	7.40×10^{-2}	-	0.57	-	1.40×10^{-2}	-	4.50×10^{-1}	-	-	-	-	-	1.11
22/09/16	34.00	-	-	8.70×10^{-2}	-	0.58	-	1.30×10^{-2}	-	5.30×10^{-1}	-	-	-	-	-	1.21

Table 3.2 - Continued

Date	Depth	T	CO_2	pCO_2	N_2	pN_2	Ar	pAr	CH_4	pCH_4	O_2	pO_2	pH_2	pH_2	pHe	pTot
	m	°C	mol/l	atm	mol/l	atm	mol/l	atm	mol/l	atm	mol/l	atm	mol/l	atm	atm	atm
04/07/17	2.00	27.6	9.69×10^{-7}	3.06×10^{-5}	3.83×10^{-4}	0.65	1.06×10^{-5}	7.93×10^{-3}	0	0	8.46×10^{-6}	6.84×10^{-3}	-	-	5.11×10^{-6}	0.67
04/07/17	4.00	27.3	2.85×10^{-6}	8.91×10^{-5}	3.83×10^{-4}	0.65	1.07×10^{-5}	7.93×10^{-3}	0	0	6.45×10^{-6}	5.18×10^{-3}	-	-	5.53×10^{-6}	0.66
04/07/17	6.00	13.54	5.49×10^{-6}	1.17×10^{-4}	4.78×10^{-4}	0.66	1.38×10^{-5}	8.06×10^{-3}	0	0	-	-	-	-	7.67×10^{-6}	0.67
04/07/17	8.00	11.4	2.29×10^{-5}	4.58×10^{-4}	4.98×10^{-4}	0.66	1.45×10^{-5}	8.12×10^{-3}	2.12×10^{-7}	1.16×10^{-4}	-	-	-	-	5.11×10^{-6}	0.67
04/07/17	10.00	10.8	5.31×10^{-5}	1.04×10^{-3}	4.92×10^{-4}	0.65	1.42×10^{-5}	7.93×10^{-3}	5.02×10^{-7}	2.70×10^{-4}	-	-	6.44×10^{-7}	7.42×10^{-4}	8.66×10^{-6}	0.66
04/07/17	12.00	10.3	1.38×10^{-4}	2.67×10^{-3}	4.92×10^{-4}	0.64	1.42×10^{-5}	7.80×10^{-3}	3.02×10^{-6}	1.60×10^{-3}	-	-	6.47×10^{-7}	7.42×10^{-4}	1.02×10^{-5}	0.66
04/07/17	14.00	10.2	3.15×10^{-4}	6.08×10^{-3}	5.01×10^{-4}	0.65	1.43×10^{-5}	7.86×10^{-3}	$2.78 10^{-5}$	1.48×10^{-2}	-	-	8.63×10^{-7}	9.89×10^{-4}	7.67×10^{-6}	0.68
04/07/17	16.00	10.1	3.68×10^{-4}	7.08×10^{-3}	5.04×10^{-4}	0.66	1.41×10^{-5}	7.73×10^{-3}	7.40×10^{-5}	3.92×10^{-2}	-	-	1.73×10^{-6}	1.98×10^{-3}	1.53×10^{-5}	0.71
04/07/17	18.00	10.1	6.41×10^{-4}	1.23×10^{-2}	5.00×10^{-4}	0.65	1.39×10^{-5}	7.60×10^{-3}	1.16×10^{-4}	6.16×10^{-2}	-	-	2.27×10^{-6}	2.60×10^{-3}	2.04×10^{-5}	0.74
04/07/17	20.00	-	-	1.23×10^{-2}	-	0.66	-	7.73×10^{-3}	-	1.12×10^{-1}	-	-	-	6.80×10^{-3}	2.04×10^{-5}	0.80
04/07/17	25.00	-	-	3.28×10^{-2}	-	0.66	-	7.53×10^{-3}	-	3.11×10^{-1}	-	-	-	1.48×10^{-2}	3.83×10^{-5}	1.02
04/07/17	35.00	-	-	1.24×10^{-1}	-	0.67	-	7.34×10^{-3}	-	1.07	-	-	-	2.84×10^{-2}	9.71×10^{-5}	1.90

3.5.   IN-SITU AND CONTINUOUS PCO$_2$ MEASUREMENTS

3.5.1. Data post-processing parameters

At both lakes, we attempted to measure a continuous pCO$_2$ vertical profile with the HydroC CO$_2$ sensor. Unfortunately, we could not measure the pCO$_2$ over the whole water columns because it exceeded 6000 µatm at the beginning of the thermocline at both lakes. Hereafter, we presented the parameters used for data post-processing (zero-drift and time-lag corrections) at both lakes (see Chapter 2, sections 2.2.4.1 and 2.2.4.2 for more details). The zero drift correction requires obtaining the zero signals before and after the measurements. If the two values are different, a linear correction will be applied to the entire dataset, and pCO$_2$ for each measurement will be modified consequently. The time-lag correction requires knowing the response time of the sensor (t_{63}) which can be estimated from the flush signals.

At Barombi Mbo lake, we used only the zero signal (11133.66) at the surface to correct the raw dataset along the vertical profile because it was not recorded at the lake bottom. At the surface the sensor response time (t_{63}) was ~45 s and was used for time-lag correction (Miloshevich et al., 2014).

At Averno, only a small part of the lake (centre and east) was surveyed in 2016 at a depth of 15m. The zero signal variation was of about 0.4% between the beginning and the end of the survey and the response time (t_{63}) of the sensor was 35 s. Because the CTD did not work during the vertical profiling in 2016, I could not locate the data at depth (the HydroC$^\circledR$ CO$_2$ sensor is not equipped with a depth sensor) and I was only able to obtain measurements at around 12.5 m depth thanks to the graduated rope when I stopped the profiling for a zero and flush phase. In 2017, the measurements done along the vertical profile showed a low zero signal variation between the surface and 6 m depth (lower than 0.05%). The sensor response time (t_{63}) was 50 s at the surface. In 2017, almost the entire Averno lake was investigated for the pCO$_2$ at 5 m depth. The maximum zero signal variation during our measurement was of 0.02% and the sensor response time of 35s. Unfortunately, the pump stopped working for a while and I attempted to correct the data by doing laboratory measurements (presented in the next section).

3.5.2. Pump off : Laboratory tests

Laboratory experiments were executed in July, September and October 2017 in order to correct field measurements data during which the pump was not switched on. Experiments were done at ambient temperature with the following pre-measurement configurations: warm up = 30 min, zero = 5 min, flush = 10 min. This configuration is the same than the one used at Averno lake in July 2017 when the probe's pump stopped working. Due to the sensor size and the facilities available in the laboratory, we were not able to use calibration solutions permitting to obtain a known pCO$_2$ in the water. Therefore, the alternative I found to obtain various pCO$_2$ was to use tap water (pCO$_2$ about 4000 µatm) and let it freely equilibrate with the laboratory air (pCO$_2$ about 600 µatm). The sensor was immersed in the tank filled with tap water the first day and remained inside during each experiment cycle (5 to 8 days). I alternated measurements with the probe pump on (30 minutes) and then off (30 minutes to 4 hours, depending on the pCO$_2$), with one "pump-off" measurement per day. I used the "pump-on" measurements to establish the relation between the equilibrated pCO$_2$ and the elapsed time since the beginning of the experiment in order to obtain an equation giving the "true" pCO$_2$ in the water at the time t. Thus, when the sensor was running with the pump turned off, I could know what was the "true" pCO$_2$ at the time t. The aim was to compare the pCO$_2$ values of the first "pump-off" data (not at equilibrium with the dissolved pCO$_2$) measured after the flushing phase (as I supposed it to be the closest with measurement in Averno lake while moving around the lake) with the true dissolved pCO$_2$ at that time t represented by the "pump-on" measurement and to understand how they are related (Figure 3.9).

From the laboratory measurements, I found that the water pCO$_2$ follows an exponential decay with time as y=y$_0$ + a.exp(-b.x) where x is the time elapsed since the beginning of each experiment both when the pump is on and off, y$_0$, a and b are constants depending of the exponential characteristics (Figure 3.9a-c). Then, I needed to establish the relation between the pCO$_2$ measured when the pump is off (Y$_{NP}$) and the true pCO$_2$ in the water (Y$_P$) at that time x=t. The water pCO$_2$ at x=t is given by the resolution of the pCO$_2$ equation found at x=t for "pump on". In the following equations, the subscripts NP and P refer to "pump-off" and "pump-on" respectively.
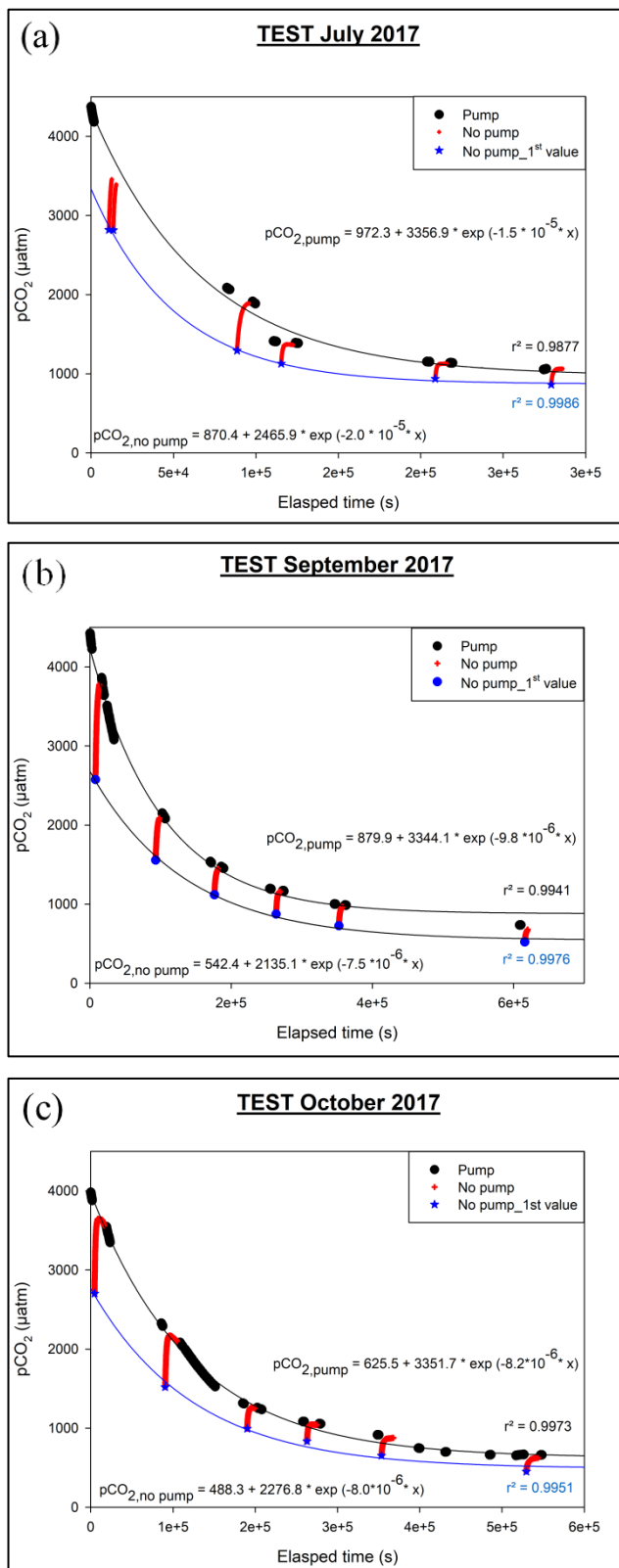
Figure 3.9 - Laboratory tests done with the pump switch on (black dots and lines) and off (blue and red symbols and lines) during which the CO₂ from the tap water freely equilibrated with the atmosphere over up to a week. The measurements were done in July (a) and repeated in September (b) and October (c) 2017.

In order to estimate Y_P, the concentration the probe should measure at time x=t, we rearrange the empirical equation to isolated x_{NP} and x_P:

<table>
<tr><td align="center">PUMP - OFF</td><td align="center">PUMP - ON</td></tr>
</table>

$$Y_{NP} = Y_{0,NP} + a_{NP} \cdot \exp(-b_{NP}*x_{NP}) \qquad\qquad Y_P = Y_{0,P} + a_P \cdot \exp(-b_P*x_P)$$

$$\exp(-b_{NP}*x_{NP}) = \frac{Y_{NP} - Y_{0,NP}}{a_{NP}} \qquad\qquad \exp(-b_P*x_P) = \frac{Y_P - Y_{0,P}}{a_P}$$

by taking the logarithm, we obtain: by taking the logarithm, we obtain:

$$-b_{NP}*x_{NP} = \ln\left[\frac{Y_{NP} - Y_{0,NP}}{a_{NP}}\right] \qquad\qquad -b_P*x_P = \ln\left[\frac{Y_P - Y_{0,P}}{a_P}\right]$$

$$x_{NP} = \frac{\ln\left[\frac{Y_{NP} - Y_{0,NP}}{a_{NP}}\right]}{-b_{NP}} \qquad\qquad x_P = \frac{\ln\left[\frac{Y_P - Y_{0,P}}{a_P}\right]}{-b_P}$$

The real pCO_2 at the time $x=x_{NP}$ is $Y_P(x=x_P)$. We have therefore to isolated Y_P for $x_{NP} = x_P$:

$$\frac{\ln\left[\frac{Y_{NP} - Y_{0,NP}}{a_{NP}}\right]}{-b_{NP}} = \frac{\ln\left[\frac{Y_P - Y_{0,P}}{a_P}\right]}{-b_P}$$

$$-b_P \cdot \ln\left[\frac{Y_{NP} - Y_{0,NP}}{a_{NP}}\right] = -b_{NP} \cdot \ln\left[\frac{Y_P - Y_{0,P}}{a_P}\right]$$

$$b_P \cdot \ln\left[\frac{Y_{NP} - Y_{0,NP}}{a_{NP}}\right] = b_{NP} \cdot \ln\left[\frac{Y_P - Y_{0,P}}{a_P}\right]$$

$$\frac{b_P}{b_{NP}} \cdot \ln\left[\frac{Y_{NP} - Y_{0,NP}}{a_{NP}}\right] = \ln\left[\frac{Y_P - Y_{0,P}}{a_P}\right]$$

By taking the exponential, we obtain:

$$e^{\frac{b_P}{b_{NP}} \cdot \ln\left[\frac{Y_{NP} - Y_{0,NP}}{a_{NP}}\right]} = \left[\frac{Y_P - Y_{0,P}}{a_P}\right]$$

$$a_P \cdot e^{\frac{b_P}{b_{NP}} \cdot \ln\left[\frac{Y_{NP} - Y_{0,NP}}{a_{NP}}\right]} = Y_P - Y_{0,P}$$

$$Y_P = Y_{0,P} + \left[a_P \cdot e^{\frac{b_P}{b_{NP}} \cdot \ln\left[\frac{Y_{NP} - Y_{0,NP}}{a_{NP}}\right]}\right]$$

$$\boldsymbol{Y_P = Y_{0,P} + \left[a_P \cdot \left(\frac{Y_{NP} - Y_{0,NP}}{a_{NP}}\right)^{\frac{b_P}{b_{NP}}}\right]}$$

To correct Averno pCO_2 data, I used a mean of the parameters found during our tests (Figure 3.9) as the best estimated of the real pCO_2 values. The data are therefore to be taken qualitatively instead of quantitatively.

3.5.3. pCO$_2$ vertical profiles

Few data are available to establish a clear comparison between the pCO$_2$ measured from water sampling and by the HydroC CO$_2$ probe. A general and logical trend shows higher pCO$_2$ values with the probe (Table 3.3). At Barombi Mbo, I measured pCO$_2$ values about 33% (uncorrected and zero-drift corrected data) up to 173 % (time-lag corrected data) higher with the probe compared to water samples analysis at 10 m depth. At Averno, in 2016, because of the problem exposed before, I could only compare pCO$_2$ at 12.5 m. The pCO$_2$ measured with the probe are 24% higher (with zero-drift correction) than the pCO$_2$ of the water sampling (Table 3.3). Fortunately, the measurements were done just after a cycle of zero and flush and the data did not require a time-lag correction. In 2017, pCO$_2$ of the shallow water (down to 4 m depth) were below the HydroC® CO$_2$ detection limit (100 µatm) whereas measurements done at 6 m depth with the probe were up to 5000 times higher than water analysis data.
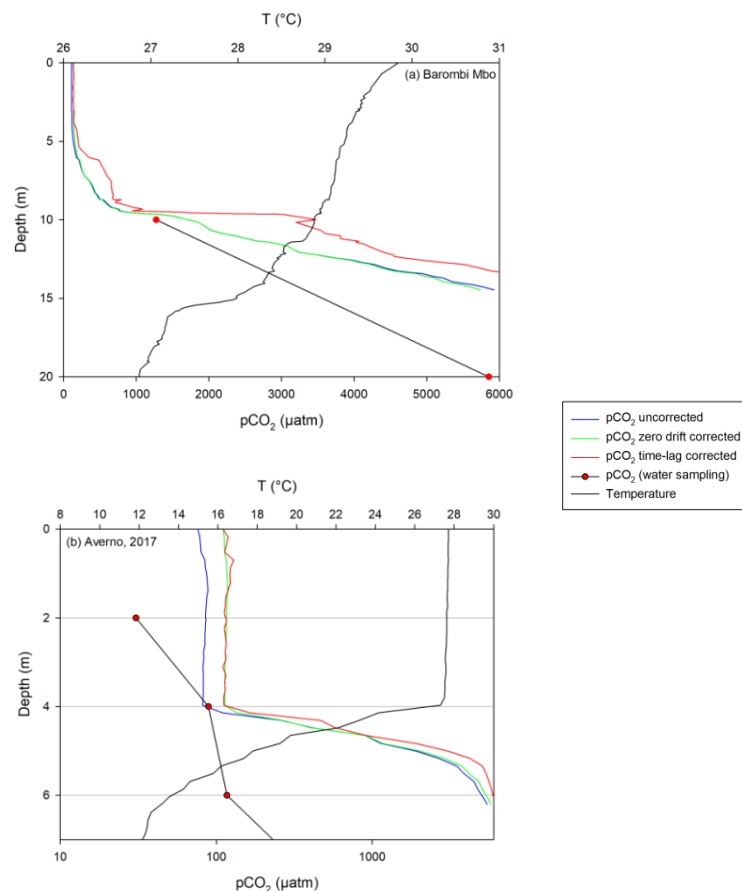
Figure 3.10 - pCO$_2$ vertical profiles up to 6000 µatm at Barombi Mbo (a) and Averno in 2017 (b). The data come from water sampling analysis (red dot-black line), HydroC® CO$_2$ sensor pCO$_2$ raw data (blue lines), zero-drift corrected (green lines) and time lag corrected (red line). Temperature profiles from the Multi-parameters probe are also displayed as black lines.

At Barombi Mbo, the HydroC CO$_2$ sensor was able to measure the pCO$_2$ in the epilimnion (down to 10 m depth) and to complete the shallower profile (Figures 3.6 and 3.10). It was constant from the surface to 4 m depth (~137 µatm, time-lag corrected) and then increase up 1085 µatm at 9.3 m depth.

Table 3.3 - pCO$_2$ measured from water sampling (pCO$_2$ sampling) and with the sensor and their differences at Barombi Mbo and Averno. pCO$_2$ uncorrected are the raw data; pCO$_2$ zero-drift are the data corrected for the zero-drift only and pCO$_2$ time-lag are the data corrected for the zero-drift and time-lag. The deviation (in %) from the pCO$_2$ measured with the probe and the water sampling are also listed.

Lake	Depth	pCO$_2$ sampling	pCO$_2$ uncorrected	pCO$_2$ zero-drift	pCO$_2$ time-lag	Difference (uncorrected)	Difference (zero-drift)	Difference (time-lag)
	m	µatm	µatm	µatm	µatm	%	%	%
Barombi Mbo	10	1273	1702	1700	3475	34	34	173
Averno 2016	12.5	1625	2230	2012	-	37	24	-
Averno 2016	15	3500	2880	2575	-	-18	-26	
Averno 2017	2	31	86	116	116	180	281	281
Averno 2017	4	89	82	113	112	-8	27	26
Averno 2017	6	117	5103	5430	5982	4258	4536	5008

3.5.4. pCO$_2$ Horizontal Patterns at Averno lake

In 2016, the data showed a pCO$_2$ (corrected for zero drift and time-lag) varying from 2492 µatm to 2913 µatm, with a mean value of 2701 µatm which was lower the one obtained by the water sampling analysis at ~15 m depth (~3500 µatm at the lake center). I observed an increase in pCO$_2$ from the centre towards the east part of the lake (Figure 3.11).

In 2017, a larger area was investigated (Figure 3.12). The horizontal profile was made at 5 m depth and pCO$_2$ varied from 1742 to 5929 µatm (mean pCO$_2$ of 4165 µatm), without considering the measurements done when the pump was off. These values are 10 times higher those that measured by the water analysis (~100 µatm) (Table 3.3).

The map of this horizontal survey (Figure 3.12) shows areas of higher pCO$_2$ (>5000µatm) (i) at the lake center, (ii) on the SW, along the lake shore, (ii) east and NNE from the lake center. The data have to been considered cautiously as they could represent false increase in area where the pump did not work. However the trend appears to be confirmed by data taken with the pump working.
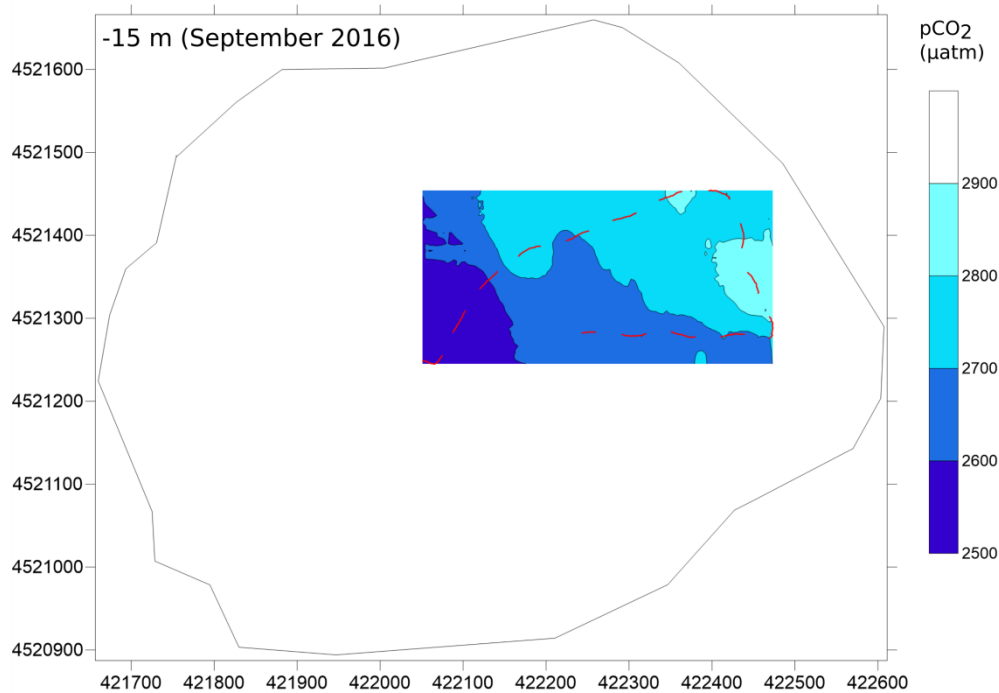
Figure 3.11 - Horizontal pCO₂ patterns at 15 m depth on September 22, 2016. The red dashed line is the GPS track.
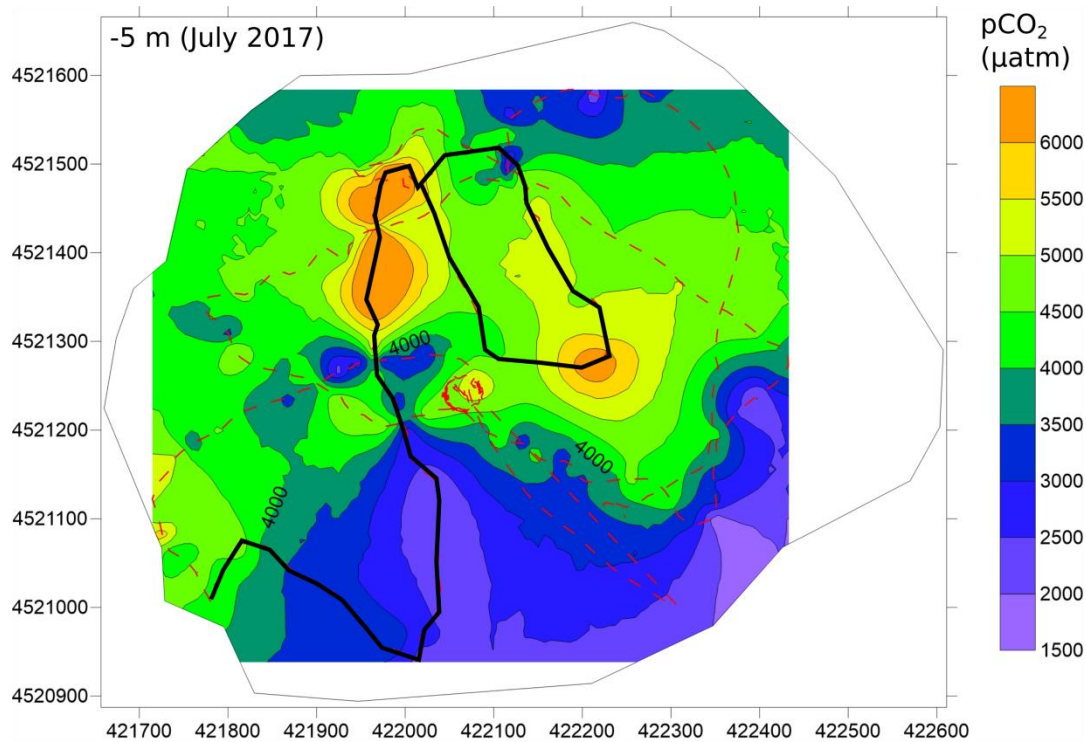
Figure 3.12 - Distribution of pCO₂ along horizontal patterns at 5 m depth on July 4, 2017. The red dashed line represents the track of the instrument when the pump was working, while the bold dark line corresponds to the track when the pump was not working.

3.6. DISCUSSION

3.6.1. Barombi Mbo: another potentially killer lake?

Barombi Mbo lake appears to exhibit a permanent and stable thermal stratification through time as suggested by similar temperature profile between March 2016 and February 1985 (Kling, 1988). Therefore it fills the conditions to potentially accumulate gases in the hypolimnion continuously. However, in March 2016, the maximum CO$_2$ concentrations, measured in the hypolimnion, were 10 times lower than those measured by Tongwa et al. (2014), suggesting a decrease of the bottom CO$_2$ concentrations likely due to lake overturn which would have released the deep CO$_2$ into shallower lake water or into the atmosphere. Moreover, the measured CO$_2$ concentrations at depth (up to 0.63 mmol/L) are about 600 times lower than at Lake Nyos (372.1 mmol/L at 210.0 m depth in January 2011; Ohba et al., 2017). In addition, the total gas pressure at depth is about 10 times lower than the hydrostatic pressure and a sudden limnic eruption by overpressuration at depth is quite unlikely.

The pCO$_2$ measured with the HydroC® CO$_2$ showed that Barombi Mbo was a sink for CO$_2$ in March 2016 (Figure 3.10a) as already suggested by Ohba et al. (2014). Thus this lake is pratically not contributing to the global volcanic lake CO$_2$ emissions (Pérez et al., 2011).

3.6.2. Temporal and spatial distribution of pCO$_2$ at Averno lake

The slightly distinct vertical profiles of dissolved gases partial pressure between 2016 and 2017 (in particular the higher partial pressure of dissolved CO$_2$ and CH$_4$ along the vertical profile in 2017) are consistent with the overturn event that happened during the winter of 2016-2017 and mixed the bottom CO$_2$- and CH$_4$ -rich and Ar-, N$_2$- and O$_2$ poor layer with the shallower layers. High CO$_2$ and CH$_4$ gas pressure distributions along the vertical profiles were also observed in February 2005 after a turnover event (Caliro et al., 2008). In addition, the lower pH along the entire water column compared to 2016 (>8 above 12 m depth) slightly favor a higher percentage of CO$_2$ over HCO$_3^-$ as dissolved carbon species (see Introduction). It is also consistent with the conductivity profiles. In fact, the conductivity can be indicative of the HCO$_3^-$ concentration; they exhibit a positive correlation (e.g.

Ohba et al., 2017). At Averno, a higher electrical conductivity was measured in 2016 compared to 2017.

Horizontal patterns in 2016 revealed a relatively homogeneous water layer at 15 m depth (deviating of maximum 8% from the mean, 2701 µatm). The CO$_2$ partial pressure increased from the middle of the lake towards the east. The 2017 surveys evidenced a more heterogeneous water layer at 5 m depth (pCO$_2$ ranging from 1742 to 5929 µatm). As already highlighted by vertical profiles at the lake center, the water layer at the respective depths show higher pCO$_2$ in shallower water in 2017 compared to 2016 (Figure 3.13). Although the density of pCO$_2$ measurements over the lake is quite low, I suggest that the heterogeneities at fixed depths are relatively consistent. High pCO$_2$ is measured at the lake center. From the center to the NE-E, I first observed a decrease in pCO$_2$ followed by an increase in pCO$_2$ with a maximum pCO$_2$ higher than 6000 µatm detected in 2017 (Figure 3.13).
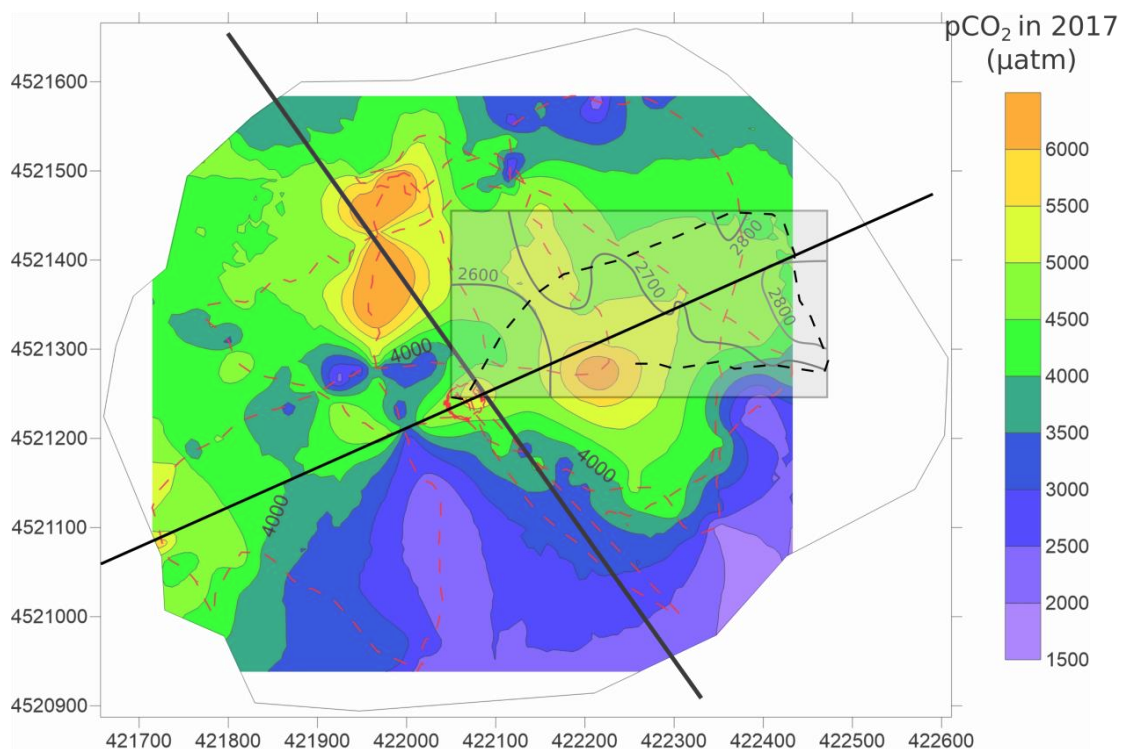
Figure 3.13 - Superposition of the pCO$_2$ spatial distribution map of 2016 (in grey) and 2017 (in color). The alignment of the area of higher pCO$_2$ along the local fault direction is highly by the SW-NE and NW-SE black lines.

In 2016, measurements revealed that the east part of the lake displayed the highest pCO_2 of the survey. When superposing both maps (Figure 3.13), I observed that the areas of higher pCO_2 may be aligned along the SW-NE and NW-SE directions which correspond (i) to the local direction of the fault system (Figure 3.4; Di Vito et al., 2011) and (ii) the SW-NE alignment of the vents that formed the Averno crater (Figure 3.4; Di Vito et al., 2011). Therefore, I suggest that areas of higher pCO_2 can be related to the volcano-tectonic local system and the location of subaquatic fluids injections. Degassing patterns related to local and regional tectonics has been observed at other volcanoes and volcanic lakes (e.g. Mazot et al., 2011; Melián et al., 2017). Other factors to potentially cause heterogeneity of water layers could be: due to (i) the local bathymetry and the depth of CO_2 injection, (ii) the CO_2 input rate at the lake bottom, (iii) the heterogeneity of bacterial distribution (Kling, 1988), (iv) internal waves or (v) wind action. To the best of my knowledge these horizontal surveys are the first in its kind executed on any volcanic lake. The observed heterogeneities in pCO_2, within the high detection precision of the HydroC® CO_2 sensor, could hence indicate that lake stratification in volcanic lakes affected by fluid input is less stable than previously postulated.

Bacterial activity is suggested to partially explain the significantly higher pCO_2 in the shallower depths of the lake in 2017 compared to 2016 in addition to the rollover event. In 2017, measurement have been done in early summer while in 2016, they have been done at the end of the summer. I hypothesize that the lake did not recover yet in July 2017 to the 2016 pCO_2 due to the lower CO_2 consumption by photosynthesis in early summer.

3.6.3. Evaluation of the HydroC® CO_2 sensor use at volcanic lake and insight for future applications

The HydroC® CO_2 sensor was able to consistently (i) reveal the shallower pCO_2 vertical distribution at Barombi Mbo lake and (ii) highlight heterogeneous water layers at Averno lake. Nevertheless, the results showed strong differences between the pCO_2 measured with the probe and those obtained from water analyses (Table 3.3). I hypothesize that the strong difference between pCO_2 measured with the HydroC® CO_2 sensor and the one obtained from water analyses can be caused by

(i) CO$_2$ exsolution during water sampling, and/or (ii) the impossibility to correct the HydroC$^®$ CO$_2$ data with decreasing temperatures along the vertical profiles. In fact, at both lakes a strong pCO$_2$ difference is observed between the water sampling and the HydroC$^®$ CO$_2$ data when profiles reach and cross the thermoclines (Figure 3.10a-b). It suggests that a zero-flush cycle would be required when the temperature changes by one degree Celsius in order to apply the right correction to the raw dataset. Therefore I recommend having a specific knowledge of the thermal profile before the acquisition of pCO$_2$ data with the HydroC$^®$ CO$_2$ probe in order to configure the sensor starting one new cycle for every 1°C change.

The HydroC$^®$ CO$_2$ sensor could therefore be used for applications at other low CO$_2$-concentrated volcanic lakes to investigate its vertical and spatial distributions at different depths. This will shed light on small-scale internal heterogeneities, undetectable by other methods that can be related to the hydrology and physical limnology of such lakes. It is a fast method to highlight the homogeneity of a water layer and to locate CO$_2$ sources at depth. In addition, due to the high measurement frequency and velocity of profiling it can be very useful to survey deep and/or large lakes.

CHAPTER 4

SULFUR DEGASSING FROM STEAM-HEATED CRATER LAKES: EL CHICHÓN (CHIAPAS, MEXICO) AND VÍTI (ICELAND)

4.1.   ABSTRACT

The composition of the gases released by El Chichón (Chiapas, Mexico) and Víti (Askja volcano, Iceland) volcanic lakes is examined by Multi-GAS for the first time. Our results demonstrate that H_2S and SO_2 are degassed by these pH 2-3 lakes. We find higher CO_2/H_2S and H_2/H_2S ratios in the lakes' emissions (31-5685 and 0.6-35, respectively) than in the fumarolic gases feeding the lakes (13-33 and 0.08-0.5, respectively), evidencing that only a fraction (0.2-5.4 % at El Chichón) of the $H_2S_{(g)}$ contributed by the subaquatic fumaroles ultimately reaches the atmosphere. At El Chichón, we estimate a H_2S output from the crater lake of 0.02-0.06 t·d^{-1}. Curiously, SO_2 is also detected at trace levels in the gases released from both lakes (0.003-0.3 ppmv). We propose that H_2S supplied into the lakes initiates a series of complex oxidation reactions, having sulfite as an intermediate product, and ultimately leading to SO_2 production and degassing.

4.2.   PLAIN LANGUAGE SUMMARY

Volcanic lakes are the site of some of the most unpredictable, and therefore dangerous, volcanic eruptions in nature. Their activity is driven by a feeding volcanic gas phase supplied by the underlying hydrothermal/magmatic system. These volatile species, entering the lake bottom, are absorbed into lake water at different rates/degrees depending on their water solubilities and the lake physical and chemical characteristics. Hyper-acidic crater lakes (pH <1) are degassing SO_2, a gas that was earlier believed to be totally dissolved into the water. In this study, we investigate for the first time the

presence of reactive S gases (SO_2 and H_2S) in the plumes of less acidic (pH 2-3) lakes El Chichón (Mexico) and Víti (Iceland). Our results demonstrate that H_2S, coming from the sub-limnic hydrothermal systems is only partially dissolved and oxidized by the lake water. In addition, we discover trace amount of SO_2 coming off both lakes. We propose that SO_2 is produced into the lake by H_2S oxidation, with dissolved sulfite as an intermediate product. Our results thus open new piece of knowledge to our understanding and monitoring the activity of restless volcanic lakes.

4.3.   INTRODUCTION

The volcanic lakes filling the craters of several dormant and active volcanoes worldwide (Rouwet et al., 2015) are known to act as traps of water-soluble volcanic volatiles escaping from the volcano's edifice (Rouwet et al., 2014b). Due to their high reactivity to aqueous solutions, sulphur species originating from deeper hydrothermal/magmatic sources are traditionally thought to be efficiently scrubbed by water bodies, including groundwaters, hydrothermal aquifers and volcanic lakes (Symonds et al., 2001; Varekamp, 2015; Varekamp et al., 2000). Recent Multi-GAS compositional measurements in the plumes of hyper-acidic crater lakes (Shinohara et al., 2015; Tamburello et al., 2015; Gunawan et al., 2016; de Moor et al., 2016b) have shown that SO_2 escapes through lake-water surfaces during pH<1 gas-water interactions. HCl, another acidic gas species generally considered reactive in aqueous solutions, was detected in emissions from hyper acid springs (e.g. Kalacheva et al., 2016). Recently, Capaccioni et al. (2017) and Rodríguez et al. (2017) experimentally demonstrated that HCl is increasingly released from a "lab-lake" when pH drops below -0.2.

In this study, we test the hypothesis of whether or not sulfur species are also actively degassed from two less acidic (pH~ 2-3) crater lakes. Our test sites are the volcanic lakes hosted in the volcanic craters of El Chichón, Chiapas, Mexico (Mazot et al. 2011; Rouwet et al. 2008; Taran & Rouwet 2008) and Askja (Víti lake, Iceland) (see Chapter 4 Appendix, Figure S4.1). El Chichón (17°22′N, 93°14′W) is a trachy-andesitic dome complex located in the northwest of Chiapas, Mexico, and was poorly known until its Plinian eruption in March-April 1982 which formed a 1.1-km-wide circular crater (Sigurdsson et al., 1984; Varekamp et al., 1984). Soon after the eruption, a hot (T=52-58°C) and

highly acidic (pH=0.56) lake appeared on the crater floor (Casadevall et al., 1984) that has changed (in 2016, T~30°C and pH~2.75) but persisted since. The lake and hydrothermal manifestations in the crater have been extensively studied (Armienta et al., 2000; Jácome Paz et al., 2016; Mazot & Taran, 2009; Mazot et al., 2011; Peiffer et al., 2015; Rouwet et al., 2004, 2008, 2009; Taran & Peiffer, 2009; Taran & Rouwet, 2008; Taran et al., 1998). Víti crater lake (65°02'N, 16°43'W), situated in east-central Iceland, was formed by a phreatic explosion inside the Askja volcano caldera, following its 1875 plinian eruption (Carey et al., 2009; Sigvaldason, 1979). Few low temperature fumaroles are located along the eastern and southern shores of the lake. Both lakes are large (in 2016, ~1.54×10^5 m² for El Chichón and ~7.8×10^3 m² for Víti) steam-heated pools where dissolved oxidized sulfur compounds originate mainly from oxidation of H_2S sourced at the lake bottom (maximum depth ~4.5 m at El Chichón and ~60 m at Víti) by the underlying hydrothermal systems.

Here, we report on Multi-GAS measurements made at the air-lake interface at both sites. We show that H_2S and trace SO_2 are effectively escaping these pH~2-3 lakes. By comparing the emissions from the lakes with the composition of emissions from subaerial fumaroles (treated as a proxy for the gas feeding to the lakes), we attempt at characterizing the chemical modifications driven by gas-lake water interactions, and the processes responsible for gas leakage through the lakes.

4.4.   METHODOLOGY

We investigate the composition of gases emitted by: (i) subaerial fumaroles around the lakes (*fumarole gas*), (ii) hot pools on the lake shore (only at El Chichón; *pool gas*), and (iii) gas at the air-lake interface (*lake gas*), sourced by surface degassing by either diffusion (no bubbling) or advection (bubbling lake degassing). Gas compositions were measured in-situ by Multi-GAS (Multicomponent Gas Analyser System) (Aiuppa et al., 2005a; Shinohara, 2005). We used a compact sensor unit containing a Non Dispersive InfraRed (NDIR) spectrometer (for CO_2; range = 0-3000 ppm), three electrochemical gas sensors for H_2S (range = 0-100 ppm), SO_2 (range = 0-200 ppm) and H_2 (range = 0-200 ppm) and a relative humidity sensor (range = 0-100%) for indirectly measuring H_2O. This instrument has been used previously to measure composition of gas released by fumarolic vents and

open-conduit volcanoes (e.g. Aiuppa et al., 2009b, 2011b, 2012, 2014), by hyper-acidic crater lakes (e.g. Yudamari, Shinohara et al., 2015; Copahue, Tamburello et al., 2015; Poás, de Moor et al. 2016b; Kawah Ijen, Gunawan et al., 2016) and at the less acidic Boiling Lake, Dominica (pH 4-6; Di Napoli et al., 2014). This is the first reported use of the Multi-GAS to measure weakly sulfur-degassing crater lakes without vigorous emissions.

Continuous measurements were made of lake gases, close to the lake surface, from a slowly moving boat. An anticipated challenge when measuring gases coming weakly from lakes are low concentrations, close to the sensor detection limits. Three sampling configurations were tested in order to measure the highest lake gases concentrations and minimize their atmospheric dilution: (i) measurements about 30-40 cm above the lake surface at the more vigorously degassing El Chichón lake, (ii) measurements about 10 cm above the surface, with a 20-cm-diameter overturned funnel attached to the inlet, and (iii) with the attached funnel kept floating on the surface of the lake at the more weakly degassing Víti lake. This latter configuration allows for the detection of very low SO_2 concentrations (<< 1 ppmv; see see Chapter 4 Appendix, Figure S4.2), but is complicated by the rapid saturation of the CO_2, H_2S and H_2 sensors. Moreover, as the relative humidity increases inside the funnel with time, functioning of electrochemical sensors (SO_2, H_2S, H_2) will be affected.

At El Chichón, gas measurements were made on 3 March 2016, with good meteorological conditions (no rain and low wind). Fumarole gas measurements were completed on 4 March 2016, after 3 hours of rain. At Víti, measurements were made on 16-17 August 2016. Due to wind, it was impossible to visually distinguish areas with bubbles on the lake, except close to the lake shore. Surface temperature and pH were measured at both lakes, and lake water samples were collected for later analysis for major cations and anions using standard ion chromatography methods (at IGF-UNAM and INGV-Palermo) (see Chapter 4 Appendix, Table S4.1).

4.5. RESULTS

4.5.1. Gas composition and SO_2 detection

The pH (2.76±0.37), temperature (21.8±1.1 °C) and chemical composition of Víti lake were homogenous (see Chapter 4 Appendix, Table S4.1). El Chichón lake was more heterogeneous with a mean pH of 2.75±0.02 and temperature of 30.1±1 °C (chemical composition at the lake center is detailed in Chapter 4 Appendix, Table S4.1).

Fumarole gases, pool gases and lake gases at both volcanoes were dominated by H_2O and CO_2 (10-1000s of ppmv). H_2S (up to ~7 ppmv at El Chichón and at ~100 ppmv at Víti) and H_2 (up to 50 and 70 ppmv at El Chichón and Víti, respectively) were unambiguously measured in the lake gases at both lakes (Figure 4.1a-c). Small amounts of SO_2 in the lake gases of both volcanoes (<0.3 ppmv and <0.003 ppmv for El Chichón and Víti, respectively; see Figure 4.1d) were also measured.

We caution that, given the low concentrations measured, well below the typical calibration range of SO_2 sensor (1-100 ppmv), our SO_2 ratios should not be viewed as truly quantitative for this gas. However, our SO_2 concentrations exhibit a positive correlation ($R^2>0.6$) with H_2S (Figure 4.1d), CO_2 and H_2O (Chapter 4 Appendix, Figure S4.2b), strongly suggesting that the SO_2 peaks are real, and not artefacts due to the sensor's noise. In addition, based on laboratory tests using 50-100 ppmv H_2S standard gases, we did not stimulate false SO_2 signals with H_2S gas (cross-sensitivity to H_2S of the SO_2 sensor is 0 according to our laboratory tests). As such, our El Chichón and Víti results should be intended as reflecting that SO_2 is actually present in the lake gases at sub ppmv levels.

At El Chichón, Taran et al. (1998) and Mazot et al. (2011) measured low amounts of SO_2, and interpreted its presence as not being magmatic, but rather due to secondary processes (i.e. saline water droplets in the collecting bottles). At Víti, very low SO_2 amounts were measured in fumarole gases (93°C) around the lake perimeter and in advected lake gases above very shallow sub-aquatic fumaroles (96°C) (Figure 4.1d). The detection of SO_2 in lake and pool gases is unusual. No SO_2 has previously been measured in gases emitted by pH 2-3 lakes as it has been believed to be completely dissolved at
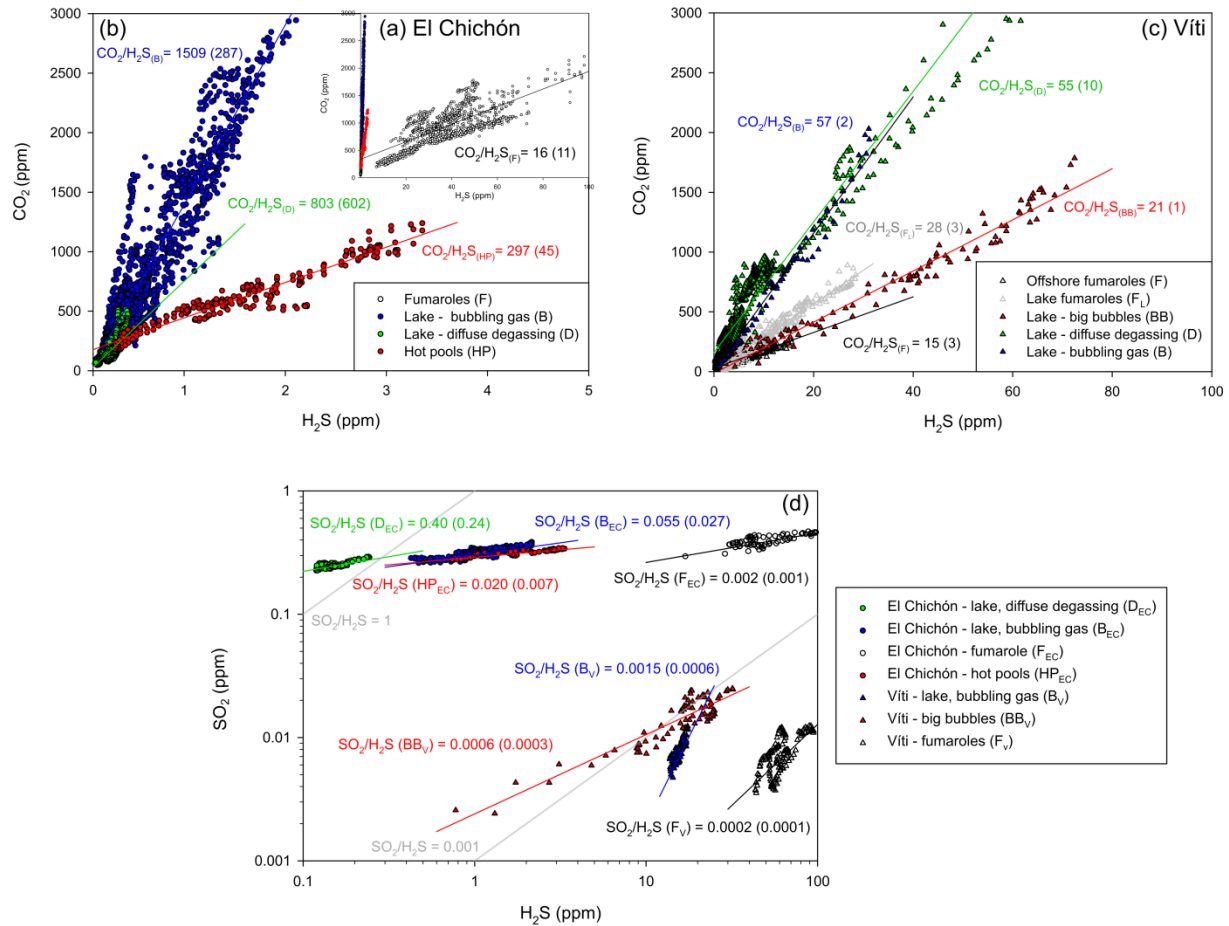
Figure 4.1 - Examples of CO_2 versus H_2S scatterplots at (a and b) El Chichón and (c) Víti and of SO_2 versus H_2S scatterplots at (d) both volcanoes. Ratios values corresponding to the regression lines are written in the plots with their errors in parenthesis. Plot (c) shows the fumarolic composition (CO_2/H_2S ratios between these of offshore fumaroles, located several meters from the lake shore, and lake fumaroles, situated at 30 cm from the shore) of gases coming off strong bubbling in shallow water (20–30 cm) at Víti (called lake-big bubbles). In the paper, those ratios are therefore assimilated to fumaroles. Plot (d) illustrates the lower SO_2 concentrations measured at Víti compared to El Chichón but also the increase of the SO_2/H_2S ratio as followed: Fumaroles < hot pools < bubbling lake gas < diffuse degassing.

such pH (Symonds et al., 2001). Hence, we suggest that it may be produced in the lake by a secondary oxidative process.

4.5.2. Gas ratios

Figure 4.2 shows scatter plots comparing fumarole gases and lake gases in terms of volatile ratios SO_2/H_2S vs. CO_2/H_2S and H_2/H_2S vs. CO_2/H_2S. El Chichón and Víti gas manifestations exhibit similar trends: the lowest values for all ratios are measured in fumarole gases, and the highest in the lake gases. Pool gases exhibit intermediate values (Figures 4.2a and 4.2b).
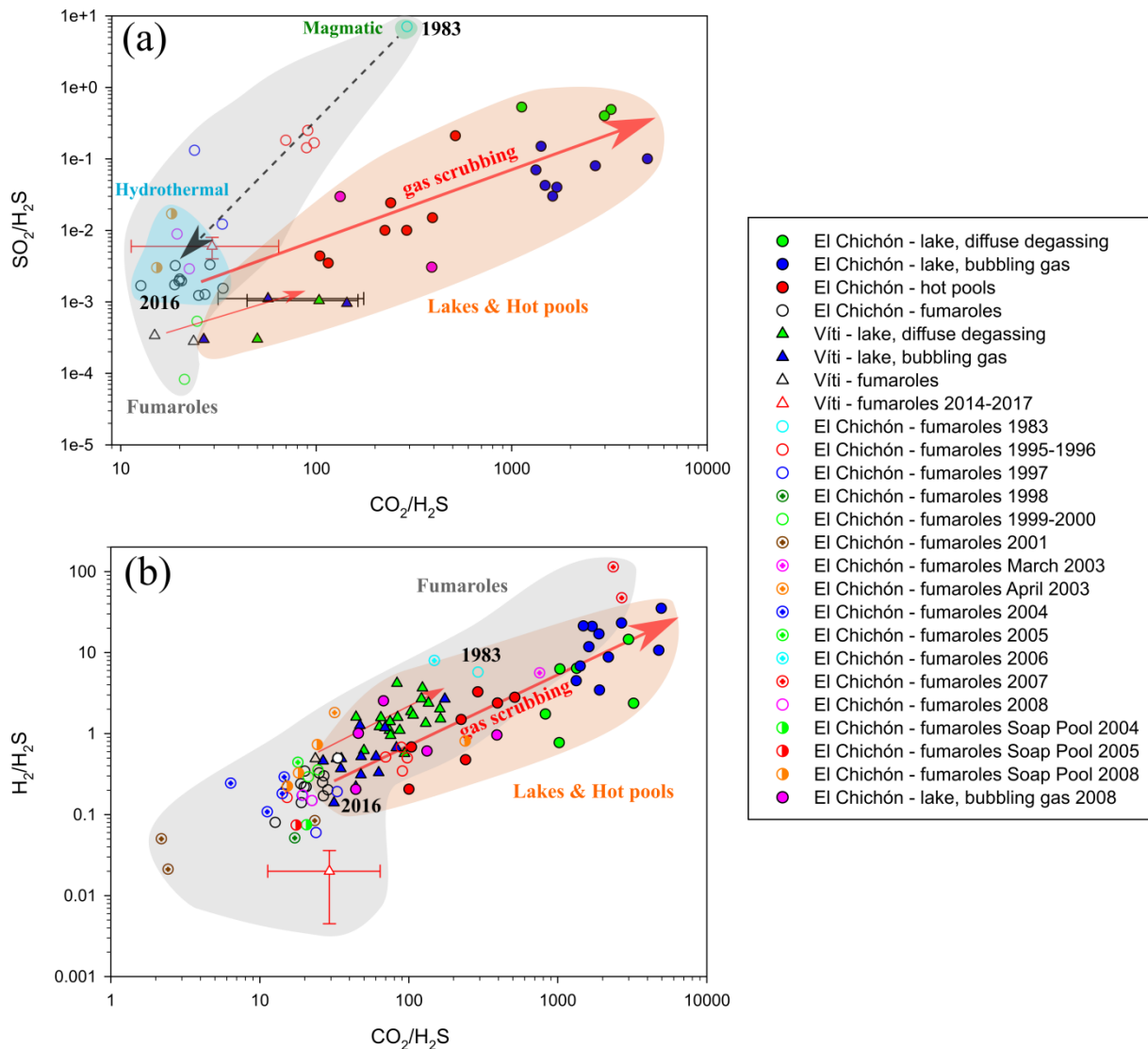
Figure 4.2 - (a) SO₂/H₂S versus CO₂/H₂S ratios and (b) H₂/H₂S versus CO₂/H₂S ratios measured in El Chichón and Víti plumes. Data references are listed in Table 4.1. The ratios symbolized by empty circles with a cross inside correspond to H₂ or CO₂ versus total sulfur instead of H₂S. At both volcanoes, red arrows show the scrubbing effect of lake waters on gas ratios. In addition, in plot (a), the transition from more magmatic (in 1983) to hydrothermal (since at least 2008) fumarolic gas composition is shown with decreasing SO₂/H₂S and CO₂/H₂S ratios through time at El Chichón (black arrow). Since 2008, the fumarolic SO₂/H₂S (10^{-2} to 10^{-3}), CO₂/H₂S (13–33), and H₂/H₂S (0.08–0.7) ratios are stable.

At El Chichón, the time-series for SO_2/H_2S and CO_2/H_2S ratios from fumarole gases (Figure 4.2a) are available dating back to the 1982 eruption (Casadevall et al., 1984; Mazot et al., 2011; Taran et al., 1998; Tassi et al., 2003; CCVG Newsletter, 2010). These clearly show a trend from more magmatic compositions in 1983 ($SO_2/H_2S = 7$, $CO_2/H_2S = 291$) to more hydrothermal compositions soon after (Taran et al., 1998; Tassi et al., 2003). Since 2008, fumarolic CO_2/H_2S ratios have clustered at values (13-33) representative of hydrothermal conditions, whereas SO_2/H_2S ratios have shown larger spread (10^{-2} to 10^{-3}) (Figure 4.2a). This H_2S-rich hydrothermal gas is assumed to be a proxy for the

composition of the sub-aquatic fumaroles feeding the lake today. El Chichón lake gases (bubbling and diffuse) plot at higher CO_2/H_2S and SO_2/H_2S ratios than this hydrothermal end-member (Figure 4.2a). The lake gases CO_2/H_2S ratios (615-5685) are 30 to 400 times higher than in fumaroles. Similarly, bubbling and diffuse lake gases have distinct SO_2/H_2S ratios (of respectively 0.03-0.15 and 0.4-0.53), but consistently above the fumarolic range (Figure 4.2a) (Table 4.1). H_2/H_2S ratios are also higher in the El Chichón lake gas (0.8 to 35) than in the fumaroles (0.08 to 0.5) (Figure 4.2b).

For Víti, a similar trend as for El Chichón is observed, with lake gases plotting at higher SO_2/H_2S, CO_2/H_2S and H_2/H_2S compositions than fumaroles (Figures 4.2a, b).

4.6. DISCUSSION

4.6.1. Inefficient gas dissolution and oxidation in steam-heated lakes

At both El Chichón and Víti, we find higher CO_2/H_2S and H_2/H_2S ratios in lake gases than in lake-shore fumaroles (Figure 4.2b). Higher CO_2/H_2S and H_2/H_2S ratios may be justified by either (i) CO_2 and H_2 addition in the lake, or (ii) preferential H_2S removal to the lake water aqueous phase. CO_2/H_2 ratios from fumarole and lake gases (bubbling and diffuse) vary within the same range (59-1429 for El Chichón, and 20-250 for Víti), suggesting that dissolution in acidic lakes poorly affects these gases (Badrudin, 1994; Shinohara et al., 2010). At the shallow El Chichón lake, Mazot et al. (2011) argued that the CO_2 flux emitted at the lake surface is very similar to the flux entering at the bottom. From our results, we can therefore estimate the fraction of H_2S and H_2 (x[%]) feeding lake that are ultimately degassed at El Chichón lake surface, using the relation:

$$x[\%] = [(CO_2/x)_{in} / (CO_2/x)_{out}] * 100 \qquad\qquad (4.1),$$

where x is either H_2S or H_2, and $(CO_2/x)_{in}$ and $(CO_2/x)_{out}$ are the gas ratios measured in fumaroles and lake gases, respectively. We evaluate that, on average, 1.1 % (range, 0.2 - 5.4 %) of the H_2S entering the lake bottom is ultimately flushing through the lake and discharged

Table 4.1 - Range of gas ratios and R_H (Giggenbach, 1987) measured with the MultiGAS (this study) or by direct gas sampling (literature data) in gas plumes at El Chichón and Víti volcanoes. The values in parenthesis are the means.

Volcano	Plume type	SO_2/H_2S	CO_2/H_2S	H_2/H_2S	H_2O/CO_2	CO_2/H_2	R_H	Reference
El Chichón	Lake – Diffuse degassing	$4.0-5.3\times10^{-1}$ (4.7×10^{-1})	615-5685 (2042)	0.8-14.5 (5.3)	0.6-32 (12)	167-1429 (333)	-3.2 to -2.7	This study
	Lake – bubbling gas	$3-15\times10^{-2}$ (7×10^{-2})	1330-5090 (2637)	3.4-35 (14.8)	0.5-4.4 (2.2)	71-556 (147)	-3.2 to -1.6	This study
	Hot pools	$10-24\times10^{-3}$ (16×10^{-3})	100-393 (256)	0.2-3.3 (1.6)	0.02-3.55 (0.97)	91-500 (200)	-3.2 to -0.7	This study
	Fumaroles	$1-7\times10^{-3}$ (3×10^{-3})	13-33 (23)	0.08-0.5 (0.25)	0.03-1.8 (0.51)	59-167 (100)	-2.4 to -0.4	This study
	Fumaroles (1983-2008)	$1-70000\times10^{-4}$	15-291	0.1-5.7	0.2-142 ; 2.5-84.3[b] (between 1996 and 2005)	17-333	-4.2 to -1.1	Casadevall et al., 1984 ; Taran et al., 1998 ; Tassi et al., 2003 ; Mazot et al., 2011 ; CCVG Newsletter, 2010
	Strongly bubbling gas (2008)	3×10^{-2}	44-390	0.2-2.5	0.08-0.9	25-333	-2.3 to -1.31	CCVG Newsletter, 2010
Víti	Lake – Diffuse degassing	$3-10\times10^{-4}$	44-163 (101)	0.6-4.2 (1.7)	n/a	20-167 (50)	n/a	This study
	Lake – Bubbling gas	$10-16\times10^{-4}$	31-175 (61)	0.14-2.7 (0.7)	0.05 – 0.3 (0.17)	33-250 (100)	-1.8 to -0.6	This study
	Fumaroles[a]	$28-34\times10^{-5}$ (31×10^{-5})	15-27 (22)	0.23-0.49 (0.39)	5 ($\pm$ 1.3[c])	48-67 (56)	-2.5	This study
	Fumaroles (2014-2017)	$4-8\times10^{-3}$ (6×10^{-3})	11.3-64.2 (29.3)	0.0045-0.036 (0.02)	1-23 (7)	1149-2632 (1471)	-4.1 to -3.3	This study

Note. [a]It includes the offshore fumaroles but also the shallow subaquatic fumaroles close to the shore (see Figures 1c and 1d for explanation). [b]The fumaroles before 1996 have higher temperature than 98°C and in 2008 the water vapor was mostly condensed in the sampling fumarolic gas. Therefore they cannot be used to compare to the present H_2O/CO_2 ratios. [c]Error

in the atmospheric plume. For H_2, the surface degassed fractions range 68% (range, 30 -100%) in bubbling areas and 30% (4 – 100%) in non-bubbling areas.

While thus H_2S dissolution in, and oxidation by, the lake (Symonds et al., 2001) is clearly supported by the higher (than fumaroles) lake gas CO_2/H_2S and H_2/H_2S ratios, the systematic H_2S in-plume detection at both volcanoes implies H_2S oxidative dissolution is not complete. The rate of H_2S dissolution into lake-water depends on initial bubble size, lake water depth and composition. We argue that transit of the feeding gas through both lakes is rapid enough to cause incomplete $H_2S_{(g)}$ removal, while more efficient dissolution and oxidation would only occur for longer gas residence times in the lake. Considering the similar fumarolic CO_2/H_2S ratios observed at both volcanoes, our results suggest more efficient H_2S escape in the deeper Víti lake than in the shallower El Chichón lake. We argue that El Chichón lake is probably better mixed and oxygenized than Víti lake, leading to higher rates of H_2S oxidation in the former.

4.6.2. Gas fluxes

In 2016, the surface area of El Chichón crater lake was estimated at 1.54×10^5 m², and the bubbling degassing area was estimated visually to be maximum 20% of the lake surface. In order to roughly estimate the CO_2, H_2S and H_2 fluxes for the lake, we used the last available CO_2 flux data for April 2015 (Jácome Paz et al., 2016) assuming that the specific (per unit surface area) CO_2 flux has not changed significantly since 2015 for each degassing population (bubbling vs. diffuse degassing). The mean CO_2 flux for the lake in 2016 was estimated at 223 t·d^{-1} (90% confidence interval of the mean 203-253 t.d^{-1}), based on a CO_2 flux of 3594 g·m^{-2}·d^{-1} for bubbling gas and 913 g·m^{-2}·d^{-1} for diffuse degassing in 2015 (Jácome Paz et al., 2016). By scaling to the CO_2/H_2S and CO_2/H_2 ratios, and using the mean CO_2 flux for each degassing population (i.e., 111 and 112 t·d^{-1} for bubbling and diffuse degassing, respectively), we calculated a maximum H_2S fluxes from El Chichón crater lake between 0.02 and 0.21 t·d^{-1}. Considering that H_2S is preferentially emitted in bubbling areas and not detected by the MutliGAS at the entire diffusive lake area, a more realistic flux would be 0.02-0.06 t.d^{-1}. For comparison, recent surveys conducted by one of us (M. P. Jácome-Paz) in 2014 and 2015, using a

floating accumulation chamber (West System, 2012) equipped with an electrochemical cell (WS-TOX-H2S, underestimation of 5% of H_2S fluxes; West system, 2012), yielded a H_2S lake flux of ~0.007 t.d^{-1} with mean values of 0.03 g.m^{-2}.d^{-1}. We also estimate the H_2 flux (in 2016) in the 0.01 to 0.1 t·d^{-1} range.

Our H_2S fluxes are in the same order of magnitude as those estimated for the similarly large, but more active, Ruapehu Crater Lake (New Zealand, Werner et al., 2006). Kawah Ijen released 75 t·d^{-1} of H_2S in September 2014 (Gunawan et al., 2016), but this flux includes the H_2S originating from the 400°C fumarolic field, in addition to the crater lake. Compared to open-conduit and high-T fumarolic degassing volcanoes (Etna, Stromboli, Vulcano), H_2S fluxes at El Chichón are, unsurprisingly, at least an order of magnitude lower (Aiuppa et al., 2005b). Tamburello et al. (2015) reports a H_2 flux of 3.3 t·d^{-1} for the peak-activity (post-eruptive) crater lake of Copahue (Argentina). Etna emits 1.8 t·d^{-1} of H_2 (Aiuppa et al., 2011b), one to two orders of magnitude higher than El Chichón. Both Etna and Copahue are actively degassing volcanoes, whereas El Chichón passes a stage of quiescent degassing.

In summary, the H_2S (and H_2) fluxes sustained by acidic (pH~ 2-3) crater lakes are relatively minor compared to more active volcanic systems, with or without crater lake, but their cumulative contribution may not be trivial globally, and requires full consideration in future assessments of the global volcanic H_2S budget.

4.6.3. Physical-chemical model of SO_2 degassing

The detection of SO_2 in lake gases (Figure 4.1d), and the SO_2/H_2S increase from fumaroles to lake gases (Figure 4.2a), are more puzzling. Previous studies demonstrated that SO_2 is released by hyper-acidic crater lakes (pH near 0, or below) (de Moor et al., 2016b; Gunawan et al., 2016; Shinohara et al., 2015; Tamburello et al., 2015). El Chichón and Víti crater lakes are not hyper-acidic (pH 2-3), however, SO_2 is released from their surfaces. Compositions of fumaroles reported in literature (Mazot et al., 2011; Taran et al., 1998; Tassi et al., 2003) and H_2/H_2O ratios measured in this study (reported as R_H in Table 4.1) strongly suggest the presence of a reduced hydrothermal system, hence, with H_2S

as the dominant S-gas species (Giggenbach, 1987). As magmatic SO_2 is virtually absent in the parental feeding gas, these observations imply that SO_2 is produced in the shallow, oxidizing lake-fumarole environment.

Casas et al. (2016) recently published the first detailed study of S-speciation in El Chichón lake surface waters. In order of abundance, they identified S^{2-} (< 0.77%), SO_3^{2-} (< 3.61%), $S_4O_6^{2-}$ (< 33.2%), and SO_4^{2-} (< 85.2%). No $S_2O_3^{2-}$ was detected. As we measured $H_2S_{(g)}$ with the MultiGAS, we should also add $H_2S_{(aq)}$ to the dissolved species, since its oxidation reaction:

$$H_2S + 2O_2 \rightarrow SO_4^{2-} + 2H^+ \tag{4.2}$$

although being the dominant mechanism generating sulfate in "steam heated" pools (Rouwet et al., 2008), appears not go to completion in our case.

In analogy with results demonstrating SO_2 production in acid sulfate-rich soils (pH near 4) (Macdonald et al., 2004), we propose sulfites as the potential SO_2 source in steam-heated lakes. Notably, our highest SO_2 gas concentrations are detected right above vigorously bubbling degassing areas at El Chichón crater-lake, where higher sulfite concentrations have consistently been observed by Casas et al. (2016).

Macdonald et al. (2004) identified a positive correlation between soil evaporation rate (and moisture) and SO_2 emission rates. They concluded that evaporation is the process that liberates gas from soil solutions. This process can be extended to evaporative degassing from acidic lakes, where SO_2 peaks in lake measurements correlate with H_2O peaks (Chapter 4 Appendix, Figure S4.2b). By analogy, in pH 2-3 crater lakes, SO_2 can be produced from sulfites following the equilibria (Barnett, 1985; Barnett & Davis, 1983; Macdonald et al., 2004):

$$H^+_{(aq)} + SO_3^{2-}_{(aq)} = HSO_3^-_{(aq)} \tag{4.3}$$

$$H^+_{(aq)} + HSO_3^-_{(aq)} = SO_2 \cdot H_2O_{(l)} \tag{4.4}$$

$$SO_2 \cdot H_2O_{(l)} = SO_{2(g)} + H_2O_{(g)} \tag{4.5}$$

Sulfite (SO_3^{2-}) in acid aqueous solutions is generated by H_2S oxidation, following the reactions (Morse et al., 1987):

$$H_2S_{(aq)} = H^+_{(aq)} + HS^-_{(aq)} \qquad (4.6)$$

$$HS^-_{(aq)} + 1.5O_{2(aq)} = SO_3^{2-}_{(aq)} + H^+_{(aq)} \qquad (4.7)$$

or via (Delmelle & Bernard, 2015, and references herein):

$$2H_2S_{(aq)} + 2O_{2(aq)} = S_2O_3^{2-}_{(aq)} + H_2O_{(l)} + 2H^+_{(aq)} \qquad (4.8)$$

followed by the rapid breakdown of thiosulfate ($S_2O_3^{2-}$) into sulfite (Delmelle & Bernard, 2015):

$$S_2O_3^{2-}_{(aq)} = S° + SO_3^{2-}_{(aq)} \qquad (4.9),$$

which is not thermodynamically favored at 29°C (Chapter 4 Appendix, Table S4.2).

Under high temperature and acidic conditions, an alternative reaction pathway is rapid thiosulfate oxidation to tetrathionate ($S_4O_6^{2-}$) (Delmelle & Bernard, 2015):

$$2S_2O_3^{2-}_{(aq)} + 0.5O_{2(aq)} + 2H^+_{(aq)} = S_4O_6^{2-}_{(aq)} + H_2O_{(l)} \qquad (4.10)$$
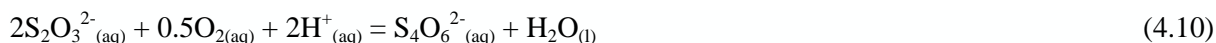
Despite the fact that sulfite is considered highly unstable through reactions (4.3) and:

$$SO_3^{2-}_{(aq)} + 0.5O_{2(aq)} = SO_4^{2-}_{(aq)} \qquad (4.11)$$

its presence in El Chichón lake water (Casas et al., 2016) suggests its continuous re-supply via H_2S oxidation (reactions (4.6)-(4.7) and (4.8)-(4.9)).

We use simple thermodynamic calculations to test if sulfite dissolved in the lake is a plausible source for lake gas SO_2. Equilibrium constants of reactions (4.2)-(4.11) at 29°C are listed in Table S4.2 (Chapter 4 Appendix), and are taken from the EQ3NR code database (Wolery, 1992). Using equilibrium constants for reactions (4.3) to (4.5), we calculate the SO_2 partial pressure (pSO_2) at equilibrium with a dissolved sulfite concentrations of 3.46×10^{-5} mol/l (the lowest measured by Casas et al., 2016). At 29°C and pH=2.7, the equilibrium pSO_2 is 0.14 atm, more than 5 orders of magnitude higher than the maximal pSO_2 measured with the MultiGAS (0.28 µatm) above the El Chichón lake.

From these calculations, we conclude that the measured in plume SO_2 can be easily accounted for by dissolved sulfite. In view of the modeled pSO_2 largely exceeding the measured pSO_2, we additionally argue that (i) only a small fraction of the "measured" dissolved SO_3^{2-} is ultimately available (perhaps for kinetic reasons) for participating into reactions (4.3)-(4.4) and/or (ii) that large part of the produced $SO_{2(aq)}$ is rapidly oxidized to sulfate before being outgassed as $SO_{2(g)}$. Similar calculations show that dissolved pH_2S at equilibrium with the sulfate content of the lake water is significantly lower (4.16×10^{-33} µatm) than the pH_2S measured with the MultiGAS (0.3-6.48 µatm), reinforcing the hypothesis that sulfur speciation is not at equilibrium with the pH-redox conditions of the lake. Kaasalainen and Stefánsson (2011) argue that sulfur speciation is controlled by kinetics and not by redox equilibrium.

In view of the above, we propose that, in a dynamic lake-water environment, the continuous supply of H_2S from the underlying hydrothermal system initiates a kinetically driven, oxidative mechanism with sulfite as a transient species, and SO_2-gas and dissolved sulfate as the final products. During this process, H_2S is only partially sequestered by the lake, and is in small part degassed via the lake gas.

Despite the fact that SO_2 concentrations are higher above bubbling areas than in diffuse degassing areas, the opposite is observed for SO_2/H_2S ratios (diffusive > bubbling). This can be explained by (i) lower $H_2S_{(g)}$ dissolution or (ii) reaction (4.10) dominating thiosulfate breakdown in bubbling areas. In areas of active gas transport through bubbles, gas dissolution into shallow lakes is physically delayed and limited (e.g. Caudron et al., 2012). Consequently, H_2S dissolution is less efficient for bubbling areas of lakes and pools, leading to lower SO_2/H_2S ratios in their degassing plumes. Moreover, if we assume ubiquitous presence of sulfites, SO_2 production occurs in the entire lake through reactions (4.7) and (4.9). Considering the absence of $S_2O_3^{2-}$ and magmatic SO_2, and the abundance of $S_4O_6^{2-}$ in the lake (Casas et al., 2016), it can be argued that, in hot bubbling areas, thiosulfate is preferentially decomposed into tetrathionate (reaction (4.10)), relative to non-bubbling and colder areas.

As SO_2 is also measured at Víti, arguably the same chemical processes occur to form SO_2 from this originally H_2S-dominated lake system. Unfortunately, S-speciation has so far not been reported for Víti to confirm our hypothesis.

4.7. CONCLUSIONS AND IMPLICATIONS FOR MONITORING

We have found clear evidence of H_2S release from steam-heated lakes. Our results thus point to incomplete H_2S dissolution and oxidation by lake water in acidic (pH 2-3) shallow crater lake conditions. Trace amounts of SO_2 in degassing plumes coming off non-hyperacid crater lakes was also measured for the first time. Both steam-heated lakes are fed by reduced H_2S-rich fluids entering from the underlying hydrothermal system, without the direct input of magmatic SO_2. Therefore, physical-chemical processes inside the lake's water body cause SO_2 formation, although in small amounts. Combining S-speciation results for El Chichón lake water with our in-plume gas measurements, we proposed SO_2 is formed by H_2S oxidation via sulfite as the transient S-species. Our observations highlight that sulfur degassing through pH 2-3 lakes is a highly kinetic, non-equilibrium process. The original H_2S is partially oxidized in the lake water (mainly as SO_4^{2-}), and partially released as a gas phase, as H_2S or SO_2, together with the abundant CO_2 and poorly reactive H_2.

More work is required to better constrain kinetics of this degassing process, arguably very fast. It appears that the various S-species are transient solutes strongly affected by S-rich (SO_2 and H_2S) gas flushing through lakes. This kinetics seems to be independent of the "residence time dependent monitoring time window" (Rouwet et al., 2014b), defined for "slower" solutes, such as Mg^{2+}, Cl^-, and SO_4^{2-}. As the definition of a time window is crucial in volcano monitoring, ideally fitting the time frame of the volcanic feature we aim to forecast, we strongly suggest combining the total S-speciation with gas chemistry (reactive and non-reactive gas species) at the interface between lake and atmosphere. Controlling parameters in experimental setups (e.g. lake water T, pH, bubbling vs non-bubbling, lake depth, f_{O2}) can also help to quantify and time-frame the degassing process.

CHAPTER 4 - APPENDIX
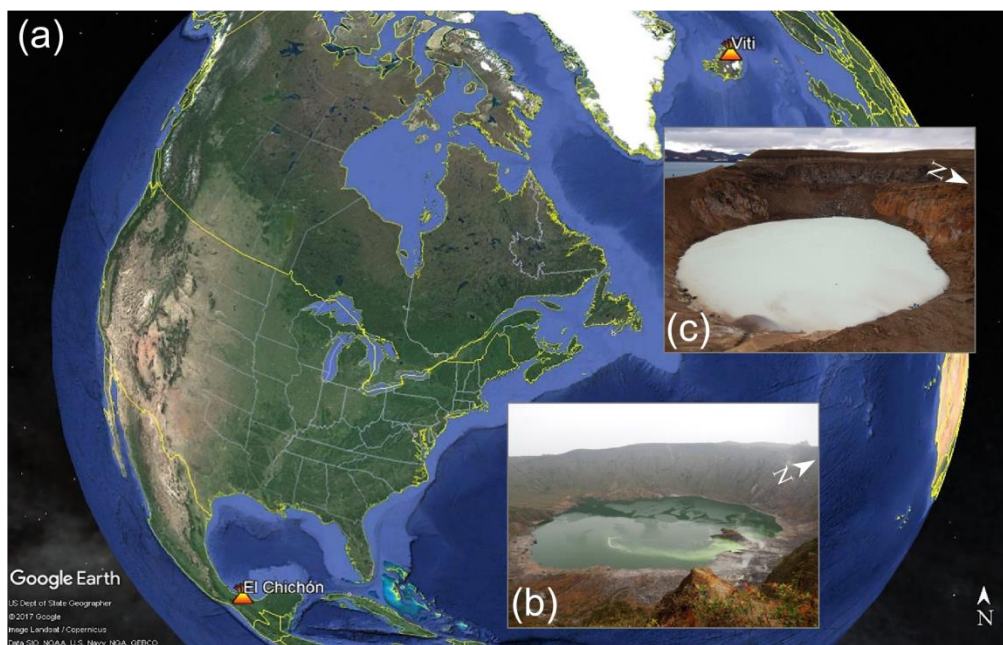
Figure S 4.1 - (a) Google Earth ProTM image showing the location of El Chichón (Mexico) and Víti (Island) volcanoes. The pictures (b) and (c) show the absence of vigorous degassing lake plume at El Chichón (b) and Víti (c) on 3 March and 16 August 2016, respectively
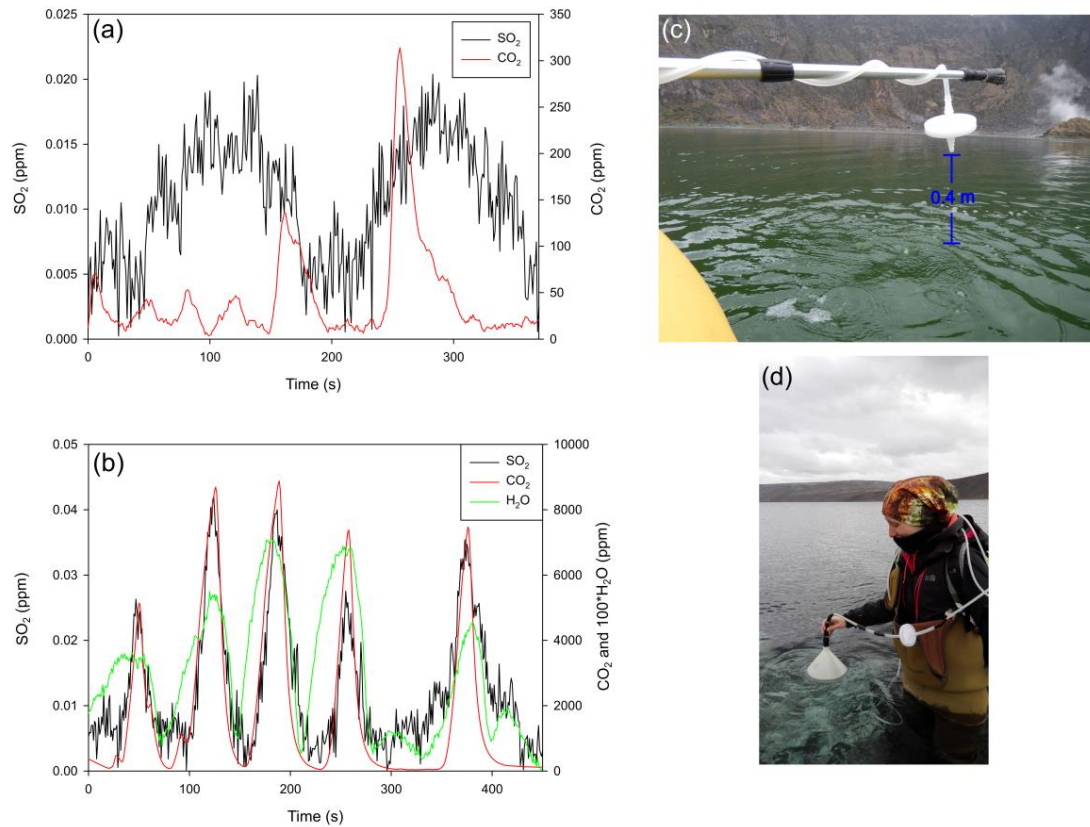
Figure S 4.2 ‐ Examples of CO_2, SO_2 and H_2O (only in (b)) time-series obtained during Multi-GAS configuration experiments at Víti lake with an overturned funnel at 0.5 m above bubbling gases (a) and kept floating on the surface (b). These experiments have for aim to demonstrate the reliability of low SO_2 concentrations measurement above the sensor noise. Here, CO_2 is used as a reference gas to detect the presence of the bubbling gas because it is able to flush through the lake as it was not there in pH 2-3 lakes. (a) Bubbling gases are detected (CO_2 peaks) but no SO_2 was measured. The variations are due to the sensor noise. (b) The funnel is kept on the surface (shown by the increase in gas concentrations) and then removed (gas concentrations decrease) several times. In absence of fast air dilution, we detected very low SO_2 concentrations as shown by the correlation between SO_2 and CO_2 peaks but also with H_2O. This experience was also done in another lake in Iceland (Kleifarvatn lake (d), located in the Reykjanes Peninsula (SW of Iceland (Clifton et al., 2003)) above bubbles coming from subaquatic solfataras (Friðriksson, thesis 2014) and the same kind results were obtained (not shown). Pictures (c) and (d) show the the Multi-GAS configurations used at El Chichón (c) (without funnel) and in Iceland (d) with the funnel kept on the water surface.

Table S 4.1 - Chemical composition of El Chichón and Víti lake waters at the surface. [a]Sampling at the lake center.

Samples	Date	Latitude	Longitude	T	pH	Conductivity	SO_4^{2+}	Cl^-	Mg^{2+}	Ca^{2+}	Na^+	K^+
				°C		mS/cm	mg/l	mg/l	mg/l	mg/l	mg/l	mg/l
El Chichón[a]	16-03-16	-	-	29	2.7	-	741.6	1880.6	7.6	188.8	776.4	142.6
Viti 1	17-08-16	N65.04744°	W16.72542°	22.5	3	2.15	715.7	32.5	31	79.4	35.6	3.9
Viti 2	17-08-16	N65.04672°	W16.72716°	20.7	2.76	2.22	682	31.1	29.8	76.5	33.1	3.6
Viti 3	17-08-16	N65.04650°	W16.72613°	21.3	2.23	2.21	688.8	31.7	29.8	76.3	33.3	3.7
Viti 4	17-08-16	N65.04707°	W16.72562°	21.4	2.96	2.2	697.9	31.2	30.1	77.4	33.3	3.6
Viti 5	17-08-16	N65.04655°	W16.72502°	21.2	2.75	2.18	629.2	30.5	29.8	75.9	32.6	3.5

Table S 4.2 - Equilibrium constants (K) for the forward reactions at the temperature of El Chichón lake (29°C) calculated with EQ3NR code (Wolery, 1992). K of the gas dissolution equilibriums correspond to the Henry's law constants.

	logK (29°C)	K
$H_{2(g)}$ dissolution : $H_{2(g)} = H_{2(aq)}$	-3.1141	7.69E-04
$CO_{2(g)}$ dissolution : $CO_{2(g)} = CO_{2(aq)}$	-1.5157	3.05E-02
$H_2S_{(g)}$ dissolution : $H_2S_{(g)} = H_2S_{(aq)}$	-1.0304	9.32E-02
$SO_{2(g)}$ dissolution : $SO_{2(g)} = SO_{2(aq)}$	0.1082	1.28E+00
$H_2S_{(aq)}$ oxidation:		
a) $\quad H_2S + 2O_2 = SO_4^{2-} + 2H^+$	123.5088	3.23E+123
b) $\quad H_2S = H^+ + HS^-$	-6.9351	1.16E-07
$\quad HS^- + 1.5O_2 = H^+ + SO_3^{2-}$	85.9055	8.04E+85
c) $\quad 2H_2S + 2O_2 = S_2O_3^{2-} + H_2O + 2H^+$	121.3226	2.10E+121
$SO_3^{2-}{}_{(aq)}$ production:		
a) $\quad$ Reaction (7)	85.9055	8.04E+85
b) $\quad S_2O_3^{2-} = S° + SO_3^{2-}$	-6.2647	5.44E-07
$SO_3^{2-}{}_{(aq)}$ oxidation: $SO_3^{2-} + 0.5O_2 = SO_4^{2-}$	44.5384	3.45E+44
$S_2O_3^{2-}{}_{(aq)}$ oxidation:		
$\quad 2S_2O_3^{2-} + 0.5O_2 + 2H^+ = S_4O_6^{2-} + H_2O$	30.2691	1.86E+30
$SO_{2(aq)}$ production :		
$\quad H^+ + SO_3^{2-} = HSO_3^-$	7.2273	1.69E+07
$\quad H^+ + HSO_3^- = SO_{2(aq)} + H_2O$	1.8999	7.94E+01

CHAPTER 5

THE CRATER LAKE OF ILAMATEPEC (SANTA ANA) VOLCANO, EL SALVADOR: FIRST INSIGHTS INTO LAKE GAS COMPOSITION AND IMPLICATIONS FOR FUTURE MONITORING.

5.1. ABSTRACT

We here present the first chemical composition of plume gas degassing from the Santa Ana crater lake, a hyper-acidic crater lake (pH -0.2 to 2.5) in NW El Salvador, by means of the Multi-GAS instrument. After a prospective survey of Multi-GAS measurements at various distances from the crater lake (lake shore, plateau and rim, in increasing distance from the lake) in March and June 2017, a semi-continuous instrument was installed at the most adequate site (i.e. plateau), acquiring additional in-plume gas composition data for the period April-June 2018.

After a re-evaluation of temporal variations in lake water chemistry for the 25-year long period 1992-2017 a conceptual model is presented on the degassing dynamics prior, during and after the October 2005 magmatic eruption and March-April 2007 phreatic eruptions. The 2017-2018 lake plume gas compositions are contextualized within this long-term degassing dynamics. The CO_2/SO_2 decreased by one order of magnitude between 2017 (37.2 ± 9.7) and 2018 (2.4 ± 0.5). This implies that gas feeding the Santa Ana crater lake had become more SO_2-rich, and in general more S-rich (as H_2S/SO_2 ratios increased) between 2017 and 2018. Nevertheless, the SO_2 flux did not increase during this period, whereas the volume of the crater lake decreased significantly due to higher evaporation rates and/or less meteoric recharge of the lake. The apparent more "magmatic" recent period, also manifested by peak SO_4 and Cl concentrations in crater lake water, could hence be highly overprinted by the small lake volume, hence reducing its S-scrubbing capacity.

Despite the lower level of study of the Santa Ana crater lake with respect to e.g. Poás (Costa Rica), Yugama (Japan), Ruapehu (New Zealand) and Kawah Ijen (Indonesia), the lower volume of Santa Ana makes it arguably more sensitive to variations in the underlying magmatic-hydrothermal system, as demonstrated by the fast reaction to the eruption 2005-2007 dynamics. The installation of the semi-continuous Multi-GAS, a major accomplishment of the present study, will enable to monitor changes in lake plume chemistry and hence volcanic activity form a safe distance of the phreatic eruption prone Santa Ana crater lake.

5.2. INTRODUCTION

At active volcanoes, physical-chemical properties of crater lakes have often been used to monitor volcanic activity (e.g. at Ruapehu, New Zealand; Poás, Costa Rica, Yugama, Japan; Copahue, Argentina; Kawah Ijen, Indonesia; Rowe et al., 1992b; Takano et al., 1994; Christenson, 2000; Martínez et al., 2000; Ohba et al., 2008; Christenson et al., 2010; Agusto and Varekamp, 2016; Caudron et al., 2017; Rouwet et al., 2016). Temporal variations in the lake's physical-chemical state are thought to result from various extents of interaction of heat and fluid fluxes, coming from the underlying magmatic-hydrothermal system. However, Rouwet et al. (2017) recently postulated that the chemistry of hyper-acidic crater lakes (Laguna Caliente, Poás in their case) is often just reflecting a transient situation of gas flushing through the lake, far from chemical equilibrium. They concluded that punctual water chemistry monitoring is not efficient as sampling frequency is too low, for logistical or safety matters.

The magmatic gas species usually monitored in fumaroles and plumes of open-vent volcanoes can also be detected in the gas plumes released by hyper-acidic lakes. At hyper-acidic lake conditions, CO_2 is not absorbed into lake water, SO_2 is scrubbed to a minor extent (e.g. Tamburello et al., 2015; de Moor et al., 2016b; Gunawan et al., 2016) and HCl release accelerates if pH<0 conditions are met (Cappaccioni et al., 2016). The Multi-GAS instrument (Aiuppa et al., 2005a; Shinohara et al., 2005), while traditionally used to monitor volcanic gas composition at "dry volcanoes" (e.g. Aiuppa et al., 2009a,b, 2011a,b, 2012, 2014; de Moor et al., 2016a; Moussalam et al., 2017), has recently proven

useful in measuring lake gas composition (Tamburello et al., 2015; de Moor et al., 2016b; Gunawan et al., 2016; Hasselle et al., 2018). Gunawan et al. (2016) demonstrated that lake gas measurements with a Multi-GAS can be efficient to monitor the activity of Kawah Ijen volcano. In addition, de Moor et al. (2016b) have suggested the potential of studying the lake plume CO_2/SO_2 ratios to predict phreatic eruptions at Laguna Caliente (Poás). Phreatic eruptions, which are quite common at active crater lakes (e.g., Laguna Caliente, Poás, and Rincón de la Vieja, Costa Rica), are almost impossible to forecast by geophysical methods and precursors, if presents, are only detectable at best few days before eruption (Maeda et al., 2015; de Moor et al., 2016b; Stix and de Moor, 2018). High frequency, or continuous analysis, of lake gas composition (e.g., de Moor et al., 2016b) can therefore be of paramount importance to monitor volcanic activity, and to forecast phreatic eruptions (Stix and de Moor, 2018).

In this chapter, we examined the temporal evolution of water and gas composition, and temperature of the Santa Ana hyper-acidic crater lake (El Salvador), since 1992 (based on data available in literature), and with a special focus on the period after the March-April 2007 phreatic eruptions (based on unpublished data and data from this study). Eventually, we also tracked these changes with variations in lake level, SO_2 fluxes and seismicity. In addition, we characterized for the first time the composition of the lake gas plume for the period March 2017-June 2018. Due to the difficult access to the lake-shore, a suitable, more distal location to monitor the gas plume composition was identified. Finally, we related the gas composition to the activity of the volcano, and speculated on possible changes for different hazardous scenarios in the future.

5.3. GEOLOGICAL AND VOLCANOLOGICAL SETTINGS

Ilametepec or Santa Ana volcano (13°51'N, 89°37.5'W; 2381 m asl; Scolamacchia et al., 2010) is located in western El Salvador (Figure 5.1) and is surrounded by two highly populated cities, Santa Ana (pop. 522 000) and Sonsonate (pop. 420 000) within a radius of 25 km (Pullinger, 1998; Colvin, 2008). It is one of the most active volcanoes in El Salvador, with 13 eruptions since AD 1500 (Mooser et al., 1958; GVP, 2018), mostly phreatic or phreatomagmatic (Simkin and Siebert, 1994; Pullinger, 1998). The last main eruption occurred on October 1, 2005 (Scolamacchia et al., 2010) and was

followed by small phreatic eruptions on March 15 and April 27, 2007. The youngest of the current four summit craters (0.5-km diameter; Hernández et al., 2007) hosts a small hyper-acidic crater lake (Bernard et al., 2004; Colvin, 2008) since its formation in 1904 (Carr and Pointer, 1981).

The Santa Ana-Izalco-Coatepeque volcanic complex (<200 ka; Pullinger, 1998) includes two stratovolcanoes (Santa Ana and Izalco), the Coatepeque caldera that is filled with a lake, many parasitic cones, cinder cones and explosion craters (Figure 5.2; Pullinger et al., 1998). The complex is part of the Central American Volcanic Arc, which results from subduction of the Cocos plate below the Caribbean plate (Figure 5.1; Molnar and Sykes, 1969; Carr, 1984; DeMets et al., 1990).

Two fault systems intersect the volcanic complex: (i) a E-W-trending fault system, corresponding to the southern boundary of the Median Trough or *Central American Graben* (a structural Plio-Pleistocene depression; Carr and Stoiber, 1977), and (ii) a NW-SE regional fault system (20 km long), active since Late Pleistocene (Williams and Meyer-Abich, 1955; Wiesemann, 1975; Pullinger, 1998). A common deep-seated parental magma body is thought to feed three independent, shallower magma plumbing systems underneath Santa Ana, Izalco and Coatepeque (Carr and Pontier, 1981; Halsor and Rose, 1988; Pullinger, 1998). Erupted magmas include LILE-enriched basaltic-andesites and andesite, and LILE-poor basaltic-andesites and rhyolites.
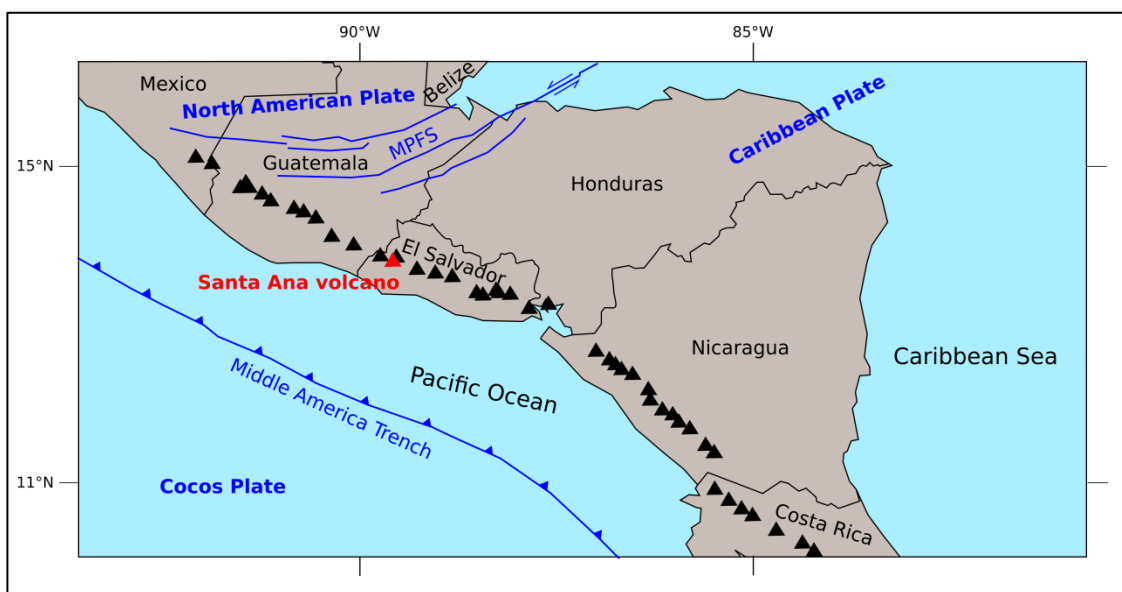
Figure 5.1 - Location of Santa Ana Volcano along the Central American Volcanic Arc (CAVA). The tectonic framework of the area is also shown. MPFS is Motagua-Polochic Fault System (modified from Carr et al., 2003).
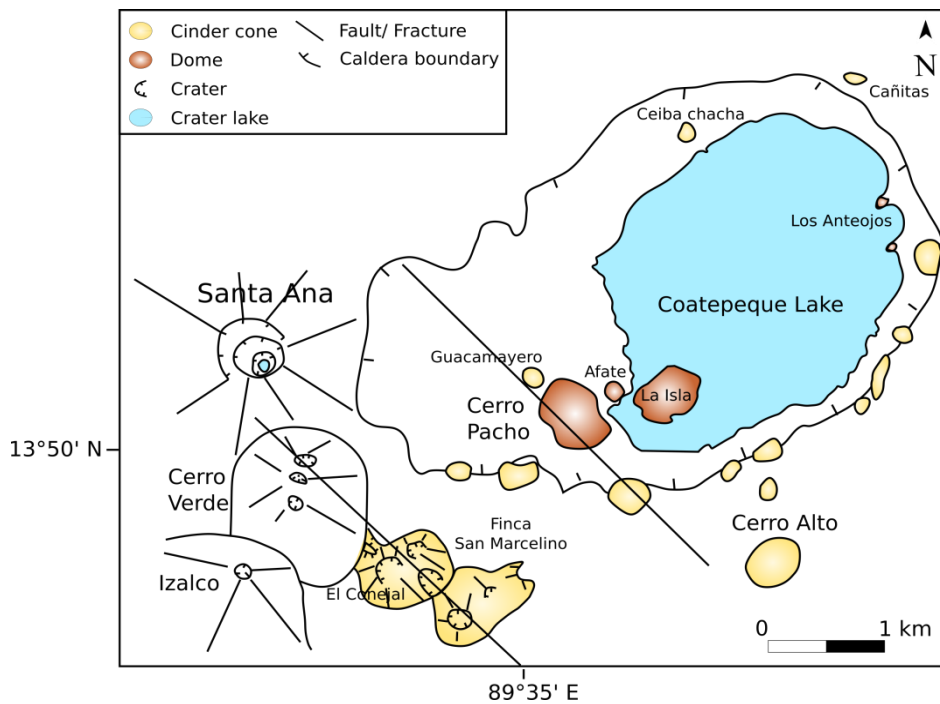
Figure 5.2 - Structural and morphological map of Santa Ana-Izalco-Coatepeque volcanic complex (modified from Carr and Pontier, 1981; Hernández et al., 2007)

5.4. THE SANTA ANA HYDROTHERMAL SYSTEM AND EVOLUTION OF THE CRATER LAKE

A large and permanent hydrothermal system beneath the volcano is implicated by Santa Ana eruptions that were mostly phreatic to phreatomagmatic in the last thousand years (Pullinger, 1998; Bernard et al., 2004). The hydrothermal system, topped by the hyper-acidic crater lake, manifests as hot springs along the lake shore, lake gas bubbling, and fumarolic emissions west of the lake. In 2000-2002, the lake was bowl-shaped, with a diameter of 200 m and a maximum depth of 27 m (Bernard et al., 2004). Along the shoreline, bubbling hot springs were observed (T~80°C; Bernard et al., 2004). Prior to the October 2005-eruption, high-temperature fumaroles discharged vigorously (532°C in January 2000, 875°C in June 2002, 264°C in December 2003, 360°C in January 2004; Bernard et al., 2004; Scolamacchia et al., 2010; SNET, Monthly Report). The October 2005 magmatic and March-April 2007 phreatic eruptions might have increased permeability under the lake (Colvin, 2008; Laiolo et al., 2017) and have drastically modified the lake geometry, temperature and water chemistry due to changes of rate and composition of the volcanic gas input (Colvin, 2008). Actually, the 2005-2007 period was characterized by drastic changes in water temperatures (Colvin et al., 2013), chemical

variations (Table 5.1; Colvin et al., 2013) and evaporation cycles (e.g. on April 10, 2006, the lake volume was 30% lower than prior to the October 2005 eruption; Laiolo et al., 2017). After the 2005-2007 eruptive period, the discharge rate and temperature of the fumaroles decreased (<100°C). The period 2010-2014 is poorly documented; few data are available, inhibiting detailed evaluation of the activity of Santa Ana crater lake.

During the period of observation of this study, in March 2017, only one low temperature fumarole was visible on the SW side of the lake, and no hot spring was identified (perhaps covered by the lake). In June 2017, we observed some hot springs along the lake shore and the presence of a few new subaerial fumaroles in addition to the SW fumaroles.

Colvin (2008) proposed a physical model of the Santa Ana magmatic-hydrothermal system. According to the author, a shallow degassing magma body (3-7 km depth, Carr and Pontier, 1981; Halsor and Rose, 1988) is overlain by a single-phase vapor zone, as supported by the high temperature fumarolic field on the west side of the lake (up to 875°C in 2002), and acid-sulfate hot springs before the 2005 eruption (Bernard et al., 2004). This vapor zone would be separated from a two-phase (liquid + gas) region, prevailing in the shallow hydrothermal system, by a low-permeability mineral seal (Pullinger, 1998; Bernard et al., 2004). The fumarolic field, present since at least 1950 (Meyer-Abich, 1956; Bernard et al., 2004), was ruptured during the 2005 eruption (Hernández et al., 2007). After the eruption, this part of the crater was flooded but the presence of sub-lacustrine fumaroles is highlighted by strong bubbling at the lake surface, still visible in 2018.

Periodical changes in activity are common in the recent history of Santa Ana crater lake. High activity levels were reported in 1920 and July 1992 (Gutiérrez and Escobar, 1994; Bernard et al., 2004). More recently, low-level activity periods (January-May 2000 and February 2002-June 2004) alternated with high activity periods (May 2000-February 2002 and June 2004-August 2005) and finally culminated into eruption on October 1, 2005 (Colvin, 2008). Before (October 2005-March 2007) and after (May 2007-December 2007) the March-April 2007 phreatic eruptions, Colvin (2008)

reported a high level of activity. Lake activity decreased slowly until 2010-2011, but then started to increase again to the high level of activity observed today.

5.5. METHODS

We investigated the composition of gases emitted by the Santa Ana crater lake. Gas compositions were measured in-situ by Multi-GAS (Multicomponent Gas Analyser System) (Aiuppa et al., 2005a; Shinohara, 2005). We used a compact sensor unit containing a Non Dispersive InfraRed (NDIR) spectrometer (for CO_2; range = 0-3000 ppm), three electrochemical gas sensors for H_2S (range = 0-100 ppm), SO_2 (range = 0-200 ppm) and H_2 (range = 0-200 ppm) and a relative humidity sensor (range = 0-100%) for indirectly measuring H_2O. This instrument has been used previously to measure composition of gases released by fumarolic vents and open-conduit volcanoes (e.g. Aiuppa et al., 2009b, 2011b, 2012, 2014), by hyper-acidic crater lakes (e.g. Yudamari, Shinohara et al., 2015; Copahue, Tamburello et al., 2015; Poás, de Moor et al. 2016b; Kawah Ijen, Gunawan et al., 2016) and at the less acidic Boiling Lake, Dominica (pH 4-6; Di Napoli et al., 2014) and El Chichón and Viti steam heated pools (Hasselle et al., 2018).

An explorative Multi-GAS survey was conducted at Santa Ana in March 2017 to investigate the composition of the lake gas plume for the first time. Measurements were obtained using a mobile Multi-GAS from three distinct sites in the crater area, located at different distances from the lake (Figure 5.3a): (i) on the S and SW outer crater rims, >400m from the lake; (ii) on the plateau, ~200m NNE from the lake and (iii) on the northern-eastern lake shore. The same operations, from the same measurement sites, were repeated in June 2017 and a semi-permanent station was installed on the plateau site between June 5 and 13 (Figure 5.3a). Based on the results of these initial surveys, the plateau site (Figure 5.3a, b) was selected as the best spot for deployment of a semi-permanent station, owing to relatively safe access (relative to the shore) and denser plume conditions (relative to the outer rim). This semi-permanent station operated between in April 2018 for 3 days while daily measurements were done on May 3 and June 28, 2018.
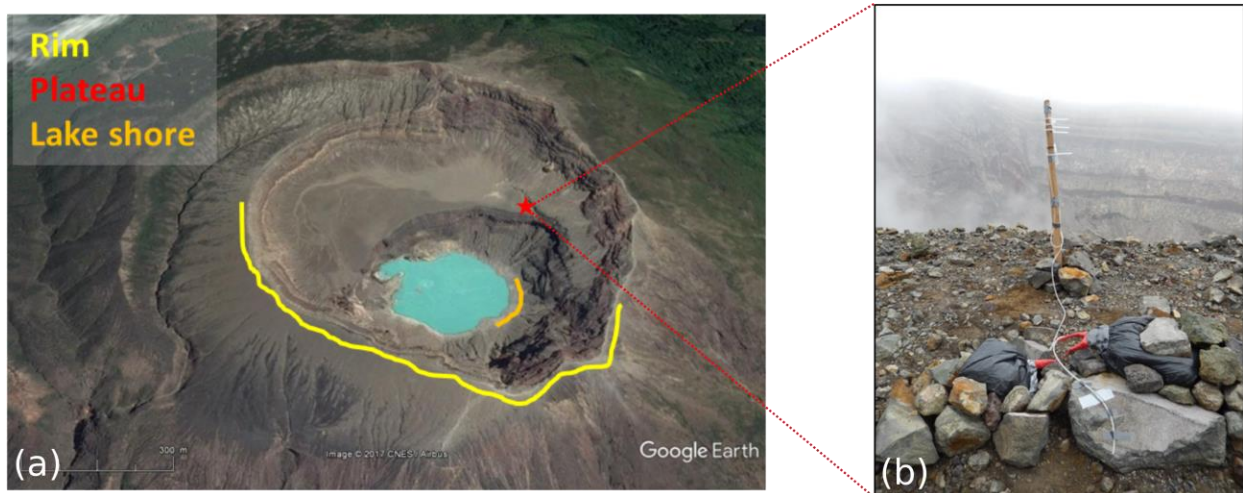
Figure 5.3 - (a) Satellite view of Santa Ana volcano (Google Earth, 2017) with the location and tracks of Multi-GAS measurements in March 2017. The yellow and orange tracks correspond to measurements done by walking on the rim and the lake shore, respectively. The red star is the site where we did measurements at the plateau. It is also the location where the station was installed in June 2017 and in 2018 (b).

SO_2 fluxes were measured with the permanent DOAS instrument installed at San Blas, 1 km SE from the crater by the MARN.

Surface temperature and pH (by alkaline titration with NaOH 0.1M (Cappacioni et al., 2017) at INGV-Palermo for June 2017 samples) were measured and lake water samples were collected for later analysis for major cations and anions using Standard Methods for Examination of Water and Wastewater (at MARN) and standard ion chromatography methods (at INGV-Palermo).

5.6. RESULTS

5.6.1. Long-term physical and chemical changes in the lake (1992-2017)

Temporal variations in temperature, pH, concentrations of main anionic species (SO_4 and Cl) and significant ratios (SO_4/Cl, Mg/Cl) of Santa Ana crater lake water for the period January 1992-June 2017 are presented in Figure 5.4. Prior to the October 2005 magmatic eruption, the lake water temperature did not show significant variations, suggesting a sealed lake system. These observations coincide with the fact that heat of the magmatic intrusion was transferred through the high-T dome/fumarole W of the crater lake since the summer of 2005 (Scolamacchia et al., 2010). After the lake was reformed after the October 2005 eruption, a slightly higher temperature (28-32°C) with

respect to the pre-2005 eruptive period was reported (Figure 5.4; Table 5.1). In March 2007 a sudden temperature rise of 10°C occurred, at that time the highest temperature measured since 2000 (Bernard et al., 2004; Figure 5.4; Table 5.1). This temperature increase preceded the March-April 2007 phreatic eruptive period, during which lake water temperature further increased to 65.6°C after the phreatic eruptions, suggesting that the phreatic eruptions breached the hydrothermal plumbing system beneath the lake, permitting an efficient heat dissipation. By Mid-2010 lake water temperature returned to pre-phreatic lake temperatures of 28-32°C (Figure 5.4). Since February 2011, the lake water temperature steadily increased with a peak temperature registered in June 2017 (Figure 5.4). Since 2015, the thermal regime of the lake was less stable, demonstrated by sudden temperature variations in the order of 10°C. The pre-phreatic eruptive temperature of 65.6°C was never reached again, so far (Figure 5.4).

The pH of the lake water since approximately four years prior to the October 2005 magmatic eruption showed strong fluctuations, between 2 and 0.5 (Figure 5.4 and Table 5.1). The pre-2007 phreatic stage was characterized by a lake water pH near 1; after the March-April 2007 phreatic eruptions the lake water pH dropped to -0.2, the lowest pH measured so far (Figure 5.4). This negative pH peak coincides with the highest lake water temperature measured right after the phreatic eruptions (Figure 5.4), suggesting that the lake heating was probably caused by the input of acidic fluids after vent opening, arguably of magmatic origin. During the following three years, the pH ranged from 0 to 1.5, reflecting a lake system in search of a new equilibrium after the phreatic eruptions. Most recent pH values are near zero (Figure 5.4; Table 5.1).

Temporal trends for SO_4 and Cl concentrations in Santa Ana crater lake water are similar (Figure 5.4; Table 5.1), suggesting a common source mechanism for both anionic species: probably magmatic degassing. In the early 1990s, Cl peaked up to >75000 mg/L (Figure 5.4). This peak did not coincide with any eruptive activity (Figure 5.4). For the 5-year period prior to the October 2005 magmatic eruption, SO_4 varied from 4500 to 15000 mg/L while Cl varied from approx. 1000 to <10000 mg/L (Figure 5.4). Peculiarly, the September 2005 (i.e. less than two weeks before the October 1 eruption) SO_4 and Cl concentrations were extremely low (80 and 150 mg/L, respectively; Figure 5.4; Table 5.1). Ruling out analytical uncertainties, this observation is clearly in favor of a sealed plumbing system

below the lake, and does not contradict the absence of any thermal anomaly prior to the 2005 eruption. After the lake reformed, "classical" pre-eruptive SO_4 and Cl concentrations were detected (<10000 mg/L; Figure 5.4), hence not providing any precursory sign to the March-April 2007 phreatic eruptions. After the 2007 phreatic eruptions, Cl concentration peaked up to >30000 mg/L while SO_4 concentrations remained stable (near 10000 mg/L; Figure 5.4). The SO_4 and Cl concentrations measured during this study (March-June 2017) were the highest ever measured (41000-47000 mg/L for SO_4, and 54000-71000 mg/L for Cl; Figure 5.4; Table 5.1). These clearly above background values require an explanation (see next sections).

Indicative ratios between species (SO_4/Cl and Mg/Cl), often effective tools in geochemical monitoring of active crater lakes for not being influenced by the dilution effect of the lake water volume, were useful to detail the degassing mechanism for the 2005-2007 eruptive period at Santa Ana volcano. Although SO_4 and Cl concentrations did not reveal significant variations for the pre-2005 magmatic eruption period, a clear SO_4/Cl ratio peak occurred in December 2002 (6.6) trending afterwards to lower values, and was followed by a second peak in August 2003 (3.5) (Figure 5.4; Table 5.1). Moreover, the Mg/Cl ratio peaked even a month earlier (November 2002) followed by a period of unstable Mg/Cl trends, with at least four other high Mg/Cl ratios prior to the October 2005 magmatic eruption (Figure 5.4). Such trends were not observed during any other moment of our 25-year long period of observation (1992-2017).

We here hypothesize that the October 2005 eruption was preceded, logically, by the intrusion of a fresh magma body prior to late-2002, reflected in the high Mg/Cl ratios (Giggenbach, 1975; Ohba et al., 2008; i.e. enhanced leaching of the highly mobile element Mg from a fresh magma batch, with respect to the more conservative Cl) and increased SO_2 degassing, resulting in high SO_4/Cl ratios (i.e. the less soluble SO_2 is released from the magma, while the more soluble HCl remains in the magma). This observation follows the yet classical hypothesis of Mg/Cl and SO_4/Cl peaks in many crater lake waters prior to magmatic eruptions (Giggenbach, 1975; Christenson, 2000; Ohba et al., 2008).
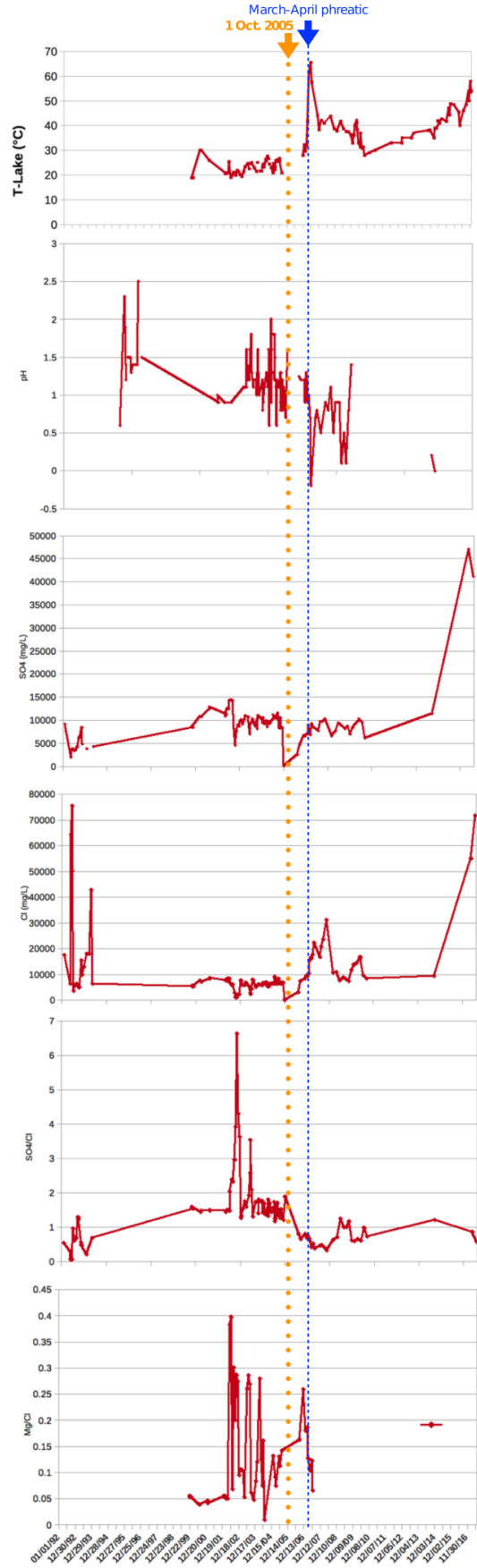
Figure 5.4 - Evolution of the water temperature, pH, SO₄ and Cl content, SO₄/Cl and Mg/Cl ratios of Santa Ane lake from 1992 to 2017

On the other hand, after the 2005 eruption, the SO_4/Cl ratio dropped despite the recovery to background concentrations of both SO_4 and Cl (Figure 5.4). The SO_4/Cl drop prior to the March-April 2007 phreatic eruptions arguably reflects that the 2002-2005 magma batch was exhausted of the less soluble SO_2. This SO_4/Cl decrease coincided with a clear Mg/Cl relative peak in December 2006 that occurred three months before the March 15, 2007 phreatic eruption (Figure 5.4). Phreatic eruptions can be instigated by migration of small magma batches of previously available magma in the plumbing system (e.g. Poás, Rouwet et al., 2017), shown by relative Mg/Cl peaks prior to phreatic eruptions. The post-2007 phreatic eruption period was characterized by a SO_4/Cl ratio below background (i.e. pre-2005 values; Figure 5.4). This observation, together with the Cl increase after the 2007 phreatic eruptions might indicate the exhaustion of SO_2 in the 2002-2005 magma and hence the release of the less soluble HCl at the end of the 2005-2007 eruptive cycle.

No data are available on the lake water chemistry for the period 2010-2014; the 2017 Cl and SO_4 peaks are yet puzzling and challenging. The approach of this study by reporting plume gas chemistry aims to shed light on this apparently "worrying" situation (see sections below).

5.6.2. Short-term Physical and chemical changes in the lake since the March-April 2007 phreatic eruptions

Since the 2007 phreatic eruptions, significant variations of the lake level (and hence volume; Figure 5.5) and surface temperature have been observed (Figures 5.4 and 5.6). The lake reappeared and its level increased from April 2007 until 2010-2011, when it stabilized (see SNET monthly reports on http://www.snet.gob.sv/ver/vulcanologia/monitoreo/informe+mensual/?id_volcan=6). Subsequently, it decreased until reaching a minimum in April 2018 (Figure 5.5). After the 2007 phreatic eruptions, when the lake level was not at maximum, sulfur spherules floating on the lake surface were common (Figure 5.5), indicating the presence of high temperature at the lake bottom (i.e. presence of a molten sulfur pool with T >116°C; Hurst et al., 1991; Takano et al., 1994).

Due to the difficult access to the lake shore, lake water was sampled discontinuously after the 2007 eruptions (Table 5.1). Since October 2010, the lake water was only sampled once in 2014 and

during our campaigns, on March 7 and 8 and June 13, 2017 (Table 5.1). Water was sampled on the NE

shore of the lake. We assumed the lake to be well mixed and not stratified (as it was the case in 2000;

Bernard et al., 2004) and the water samples hence to be representative of whole lake chemical

variations.

As observed in Figure 5.5, the volume of Santa Ana's crater lake has varied enormously during

the post-phreatic eruption period May 2007-June 2017. Due to difficult access to the crater lake, it was

impossible to measure distances and elevations in the field that would ideally permit us to estimate the

lake volume and hence volume changes through time. Needless to say that the lake volume can

strongly affect the concentrations of solute species: the smaller the lake, the higher the solute

concentrations will be for a stable fluid input, with respect to a larger lake. In the following

paragraphs, small variations in the detected absolute concentrations should hence be interpreted
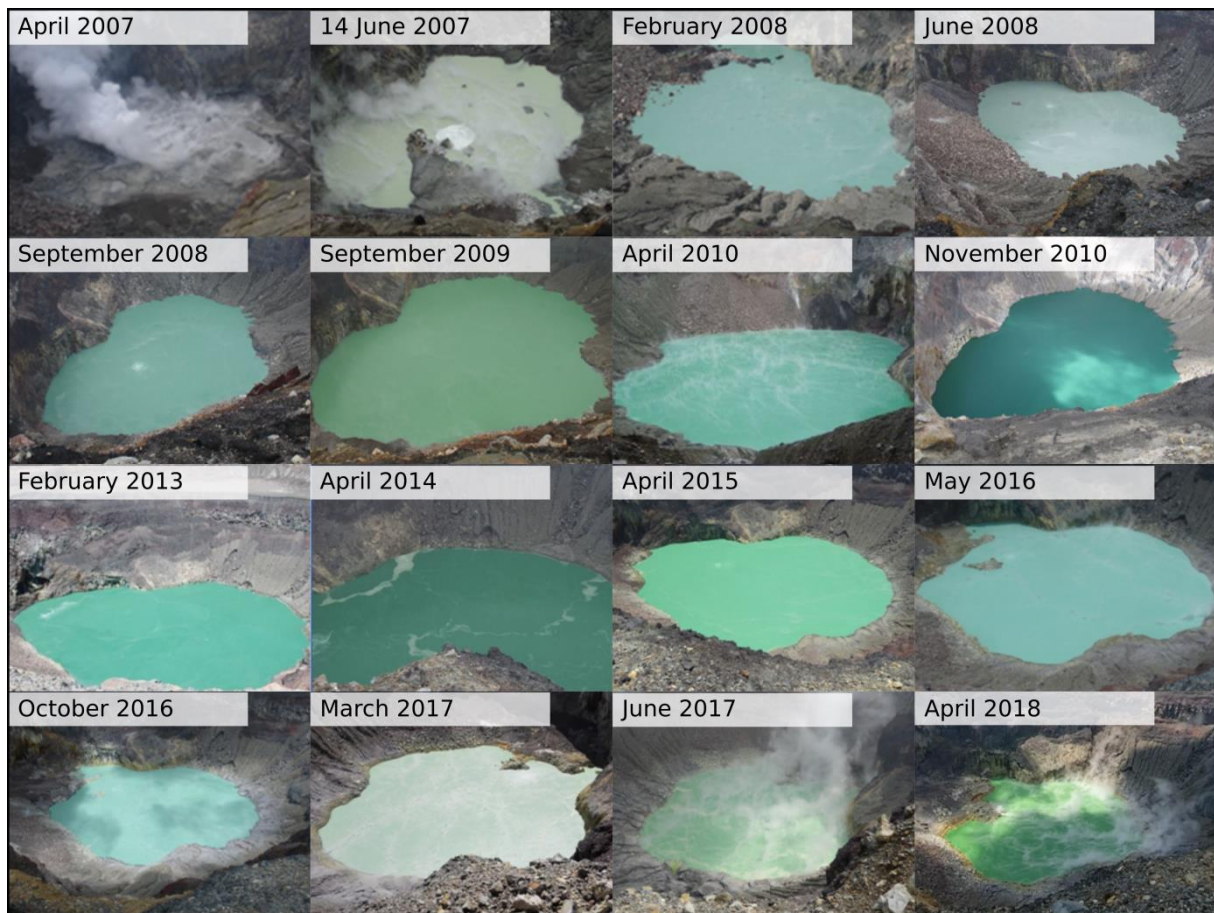
Figure 5.5 - Evolution of Santa Ana crater lake since 2007 (pictures from April 2007 to October 2016 are taken from http://www.snet.gob.sv/ver/vulcanologia/monitoreo/informe+mensual/?id_volcan=6). We observe the subaquatic fumaroles manifested as bubbling degassing at the lake surface.

cautiously. For instance, the maximum temperature and minimum pH (-0.2) measured in the recently reformed lake after the March-April 2007 phreatic eruptions are hence strongly overprinted by the small size of the lake, that is efficiently heated, strongly evaporating and thus highly acidic. Lakes with a pH <0 are often a sign of hyperconcentration upon evaporation (e.g. Poás, Varekamp et al., 2000; Rouwet et al., 2017).

We divided the observed post-2007 phreatic eruptive period into three sub-intervals, based on the observed changes in lake volume (Figure 5.5) and temperature (Figure 5.6) and, and also considering the data gaps in lake water sampling (i.e. November 2010-October 2014, marked by "no data" in Figure 5.5): (i) Phase 1: *post-eruptive period*, from May 2007 to February 2008, (ii) Phase 2: *period of decreasing activity*, from March 2008 to October 2010, and (iii) Phase 3: *recent period*, after November 2014.

Phase 1 (post-eruption period, May 2007-February 2008) in Figure 5.6 indicates the restoring of pre-eruption lake stability and chemistry. Active crater lakes topping voluminous magmatic-hydrothermal systems in tropical areas breached by an eruption often restore their pre-eruptive hydrothermal conditions soon after (e.g. El Chichón (Mexico), Pinatubo (Philippines) who were even disrupted by VEI 4-5 Plinian eruptions in 1982 and 1991, respectively). Phase 2 (period of decreasing activity, March 2008-October 2010) is manifested as a large volume and hence less sensitive lake (T 30-43°C, pH 0.1-1.4, stable SO_4 concentrations < 10000 mg/L; Figure 5.6). The initial Cl peak, explained through Figure 5.4 as the final release of HCl of the highly degassed 2002-2005 magma batch, is followed by a Cl drop and hence a SO_4/Cl increase. We propose a working hypothesis that this observation results from steady HCl degassing from a large volume lake due to preferential release of HCl with respect to SO_2 or H_2S in hyper-acidic environments (Capaccioni et al., 2017). Nevertheless, the small-scale trends and their relationship with pH and temperature are more complex and in the "high pH" end, not favoring HCl degassing.
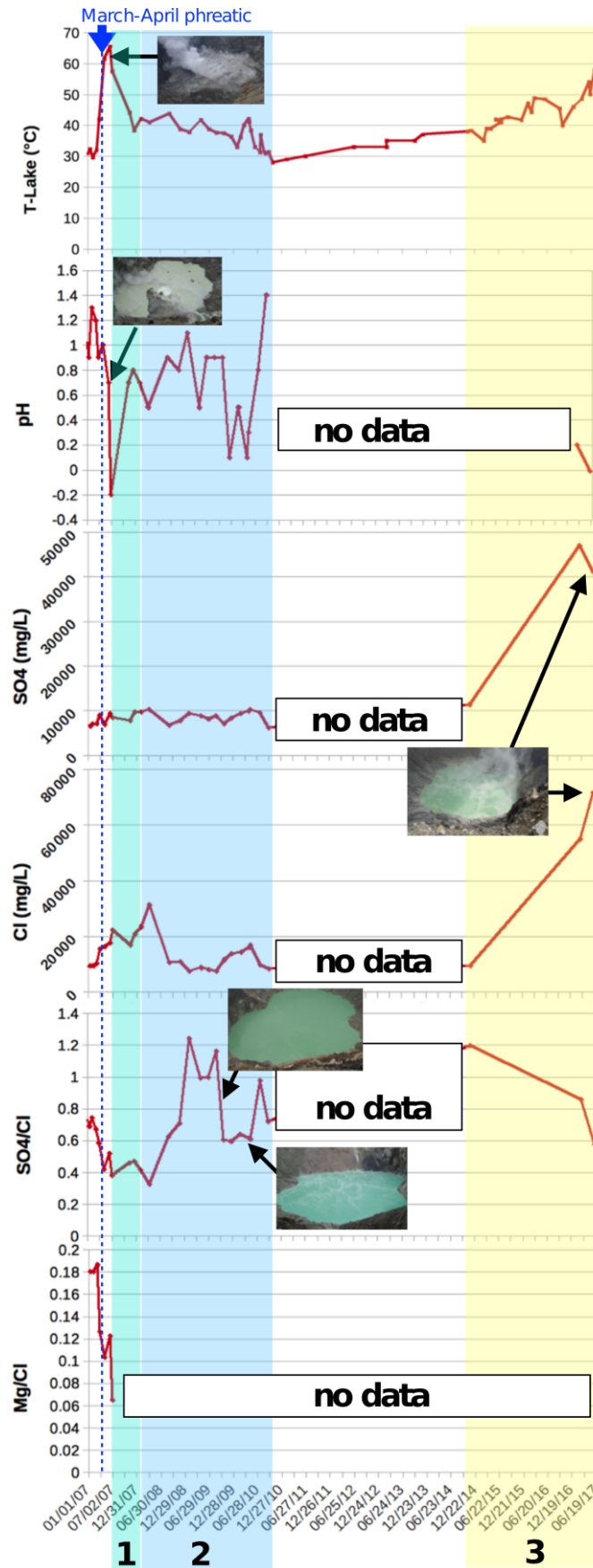
Figure 5.6 - Evolution of the water temperature, pH, SO₄ and Cl content, SO₄/Cl and Mg/Cl ratios of Santa Ane lake from 2007 to 2017. The green, blue and yellow areas correspond respectively to phase 1, 2 and 3.

A long-term SO_4/Cl ratio increase occurs during steady lake heating and evaporation (e.g. at Poás, Rouwet et al., 2017). Despite the absence of data on lake water chemistry for the period November 2010-October 2014, the lake water heating (i.e. high evaporation) and clear volume decrease of the crater lake towards Phase 3 (November 2014-June 2017, Figure 5.6) can explain the high SO_4/Cl ratio in late 2014. A small lake is observed since April 2015 (Figure 5.5) and decreases with time. In June 2017 the highest SO_4 and Cl concentrations ever were measured and coincided with a low lake volume (Figures 5.5 and 5.6). The lake in the pictures for June 2017 and April 2018 (no water chemistry data available) in Figure 5.5 manifest vigorous degassing and evaporation. Another hypothesis on the variations in SO_4/Cl ratios in lake water is provided in the "Gas section" below.

We conclude that (1) long-term tracking of T, pH, SO_4, Cl, SO_4/Cl and Mg/Cl can reveal detailed insights into magma migration and magmatic degassing, in relation to magmatic and phreatic eruptive activity, (2) short-term variations can indicate the instability of a system, often observed prior to or after eruptions; these observations would need a higher detail of data gathering in order to be more insightful, (3) temperature, pH and solute concentrations are intimately related to lake volume; higher solute concentrations do not necessarily reflect a higher fluid input from the underlying magmatic-hydrothermal system, and (4) the solute chemistry of a hyper-acidic and hot crater lakes (e.g. Santa Ana crater lake during our period of observation of this study, 2017-2018) merely reflects a transient phase of magmatic gases flushing through the lake water column, and scrubbed by various degrees depending on delicate pH-T-concentration conditions.

In the next section, coupling solute chemistry of crater lake water with the chemistry of the gas plume coming off the lake aims to increase our insights into the degassing dynamics of acid crater lakes.

5.6.3. Lake plume gas composition

Examples of Multi-GAS acquisitions at the three sites (rim, plateau and lake shore) are illustrated in Figure 5.7. At the crater rim, both in March and June 2017, we detected low amounts of SO_2 (~1 ppm) and H_2O (~1000s ppm above atmospheric background) (Figure 5.7a). H_2S concentrations were

very low (~0.1-0.4 ppm) and poorly correlated with SO_2 peaks, and the volcanic plume was typically too diluted for a volcanic CO_2 signal to be resolved over the atmospheric background (Figure 5.7a). At the plateau and the lake shore, all the target volcanic gases (CO_2, SO_2, H_2 and H_2O) were detectable in the plume at concentrations higher than 1 ppm (Figures 5.7b, c). At the plateau, peak concentrations were ~30 ppm for SO_2, ~150 ppm for CO_2 (above background), ~20 ppm for H_2, ~3000 ppm for H_2O (above background), and ~1.3 ppm for H_2S. Measurements at the lake shore were complicated by erratic, mostly unfavorable wind directions dispersing the plume in unreachable parts of the lake shore.

The acquired concentration time-series were processed using the techniques described elsewhere (this Thesis, Chapter 2). In brief, starting from the raw concentration data, plume gas ratios were calculated by building sequences of gas vs. gas scatter plots (e.g. Figure 5.8) in all sub-intervals where well correlated concentration peaks were observed. The procedure was run iteratively using the Ratiocalc software (Tamburello, 2015), which allowed to sequentially scan the dataset, select the appropriate temporal windows, and calculate the ratios from the gradients of the best-fit regression lines in each scatter plot (e.g. Figure 5.8). The obtained ratios are listed in the Appendix (Table S1).

We find that, even at the plateau site (where the most dense gas plume was detected), the obtained gas/SO_2 ratios were typically anti-correlated to SO_2 concentrations (Figure 5.9). The high ratios at the
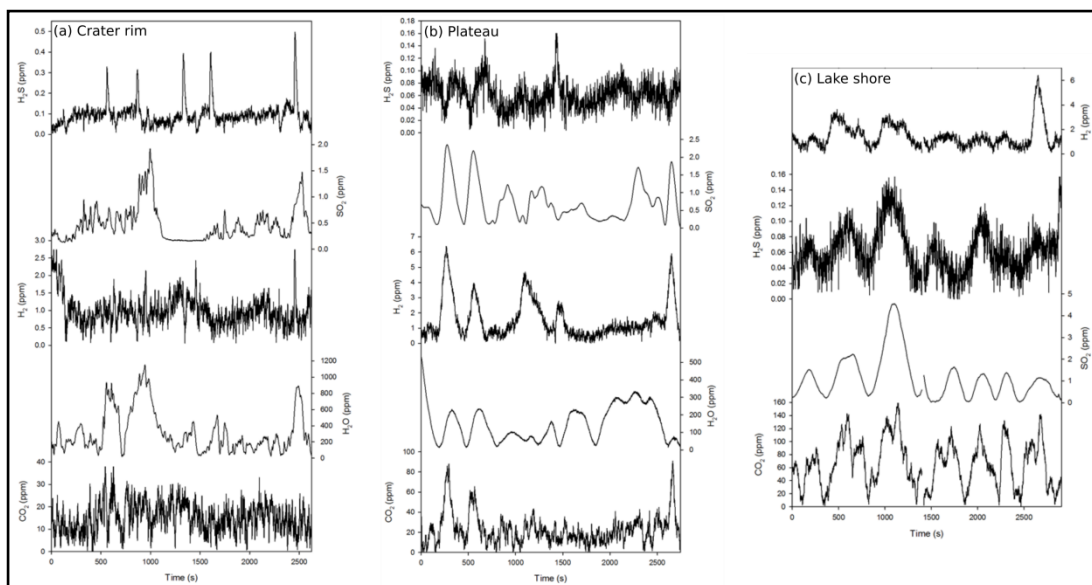
Figure 5.7 - Examples of Multi-GAS measurements at the crater rim (a), plateau (b) and lake shore (c) in March 2017.
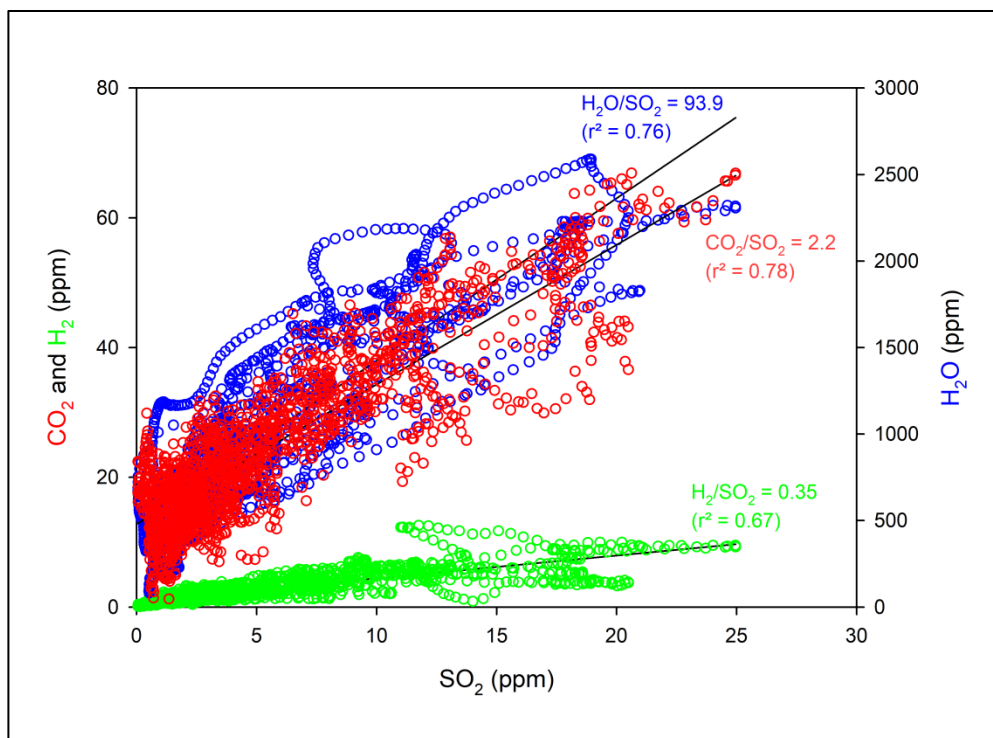
Figure 5.8 - Example of a CO_2, H_2, H_2O vs. SO_2 scatter plot of June 28, 2018.

low SO_2 concentrations may imply either (i) the presence of an SO_2-poor, reduced (high in H_2) gas source of hydrothermal (CO_2-rich) nature, or (ii) that volcanic H_2 and CO_2 signals are more difficult to resolve from their atmospheric backgrounds in dilute plume conditions (low SO_2 concentrations, eventually implying that H_2/SO_2 and CO_2/SO_2 ratios are over-estimated). Because of this possible concern, we find it therefore more prudent to filter the dataset by accepting only those ratios obtained for sub-intervals having SO_2 above the 7 ppm concentration threshold (above which the ratios become independent of SO_2 concentrations) (Figure 5.9). This filtered ratio dataset is listed in Table 2.

The filtered dataset (Table 5.2) highlights sizeable changes in gas composition during the investigated period (Figures 5.10 and 5.11). In March 2017, we were only able to obtain CO_2/SO_2 and H_2/SO_2 ratios at both the plateau and lake shore (Figure 5.10). The measured CO_2/SO_2 ratios were similarly high at both lake shore (31.0 ± 13.7) and plateau (37.2 ± 9.7). The H_2/SO_2 ratios were 0.42 ± 0.11 at the lake shore and higher (2.39 ± 0.27) at the plateau. In June 2017, the CO_2/SO_2 ratios were drastically lower than in March (see Table 5.2), and again similar at both measurement sites (5.4 ± 0.1 at the lake shore and 4.2 ± 1.4 at the plateau; Figure 5.10). The same contrast in H_2/SO_2 ratios (already seen in March) between lake shore (0.06 ± 0.02) and plateau (0.46 to 0.84 ± 0.75) was observed, but at
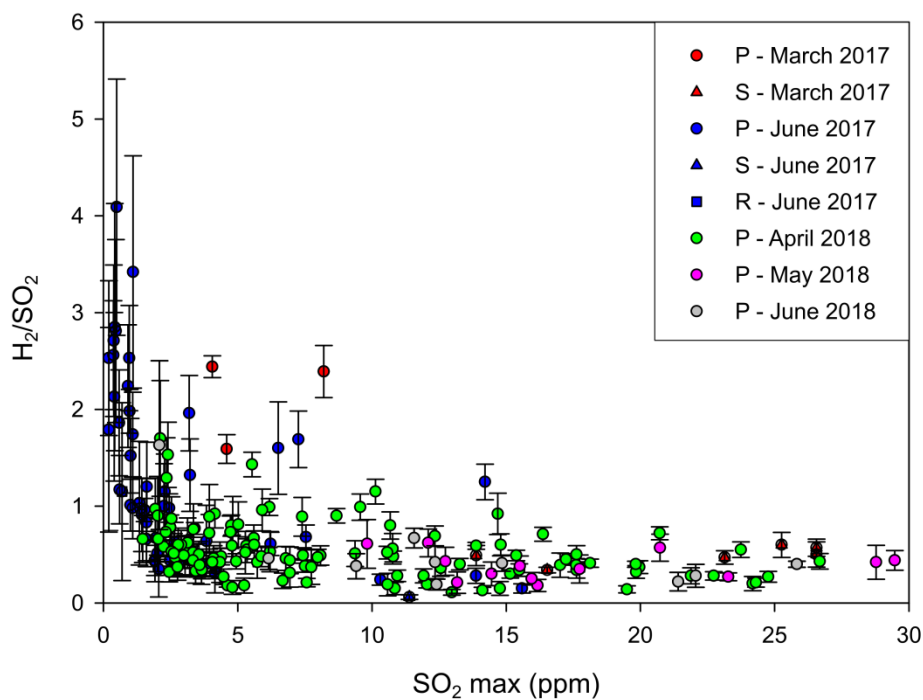
Figure 5.9 - Variations of the H_2/SO_2 ratios with the maximum SO_2 concentration for each single gas peak. It shows that lake gases are clearly detected above 7 ppm of SO_2 when measured at the plateau in 2017 and above 10 ppm in 2018.

both sites an H_2-poorer (SO_2-richer) gas than in March was detected. The H_2S/SO_2 ratios were similar in March and June 2017 (0.03 to 0.06). In March 2017, we were not able to resolve any volcanic H_2O from the background, but in June we derived H_2O/SO_2 ratios of 75.8 to 77.4 (Table 5.2).

A further decrease in CO_2/SO_2 ratios was observed at the plateau in April, May and June 2018, when the ratio ranged between 4.1 ± 1.6 (April) and 2.4 ± 0.5 (June) (Figures 5.10 and 5.11). The H_2/SO_2 ratios in June 2018 were also the lowest (from 0.37 ± 0.14 to 0.39 ± 0.15) observed at the plateau since observations started at Santa Ana (Figure 5.11). In 2018, the gas composition remained H_2O-rich (H_2O/SO_2 between 32.0 ± 18.5 and 177.2 ± 10.8), and the H_2S/SO_2 ratio varied between 0.08 ± 0.07 and 0.11 ± 0.07 (Table 5.2).

Table 5.2 - Daily mean of lake gas ratios measured at the plateau and lake shore and the respective gas fluxes.

Date	Location	SO_2 max (ppm)	CO_2/SO_2 (1σ)	H_2/SO_2 (1σ)	H_2O/SO_2 (1σ)	H_2S/SO_2 (1σ)	SO_2 (t/day)	CO_2 (1σ) (t/day)	H_2 (1σ) (t/day)	H_2O (1σ) (t/day)	H_2S (1σ) (t/day)
07-03-17	Lake shore	14-16.5	31.0 (13.7)	0.42 (0.11)	-	-	240	5117 (2260)	3.1 (0.8)	-	-
07-03-17	Plateau	8.2	37.2 (9.7*)	2.39 (0.27*)	-	-	240	6128 (1594)	18.0 (2.0)	-	-
08-03-17	Lake shore	18.7-26.6	54.5 (24.9)	0.54 (0.06)	-	0.03 (0.01*)	329	12317 (5628)	5.6 (0.6)	-	5.3 (1.8)
05-06-17	Plateau	7.5-10.3	4.7 (1.9)	0.46 (0.31)	-	0.03 (0.02*)	51	165 (66)	0.7 (0.5)	-	0.8 (0.4)
13-06-17	Lake shore	11.3-20	5.4 (0.1)	0.06 (0.02*)	77.4 (3.9)	-	41	151 (3)	0.1 (0.03)	893 (45)	-
13-06-17	Plateau	7.3-15.6	4.2 (1.4)	0.84 (0.75)	75.8 (48.2)	0.06 (0.03)	41	117 (41)	1.1 (1.0)	874 (556)	1.3 (0.6)
06-04-18	Plateau	13.0-14.7	4.1 (1.6)	0.52 (0.57)	177.2 (10.8)	0.08 (0.02)	87	245 (96)	1.4 (1.6)	4335 (264)	3.7 (0.9)
12-04-18	Plateau	10.1-26.7	3.3 (1.1)	0.44 (0.27)	82.4 (34.3)	0.11 (0.07)	214	479 (167)	3.0 (1.8)	4959 (2066)	12.0 (7.7)
13-04-18	Plateau	10.6-24.8	3.2 (0.7)	0.39 (0.17)	62.2 (37.2)	0.08 (0.07)	61	135 (30)	0.7 (0.3)	1167 (638)	2.6 (2.3)
14-04-18	Plateau	10.6-17.6	3.3 (0.5)	0.44 (0.21)	32.0 (18.5)	-	81	184 (28)	1.1 (0.5)	729 (421)	-
03-05-18	Plateau	12.9-29.5	2.9 (0.8)	0.39 (0.15)	74.6 (26.5)	-	117	233 (64)	1.4 (0.6)	2454 (872)	-
28-06-18	Plateau	11.6-25.8	2.4 (0.5)	0.37 (0.14)	107 (18.9)	-	231	381 (79)	2.7 (1.0)	6950 (1228)	-

Note. The gas fluxes were calculated by scaling the SO_2 fluxes from the DOAS station and scale to the daily mean gas ratios. 1σ is the standard deviation. At the plateau, the lake plume was detected by a maximum SO_2 concentration higher than 7 ppm in 2017 and 10 ppm in 2018. The plume measured at the lake shore had a maximum SO_2 concentration higher than 10ppm.

*Correspond to one single data and the value in parenthesis is the error coming from Ratiocalc.
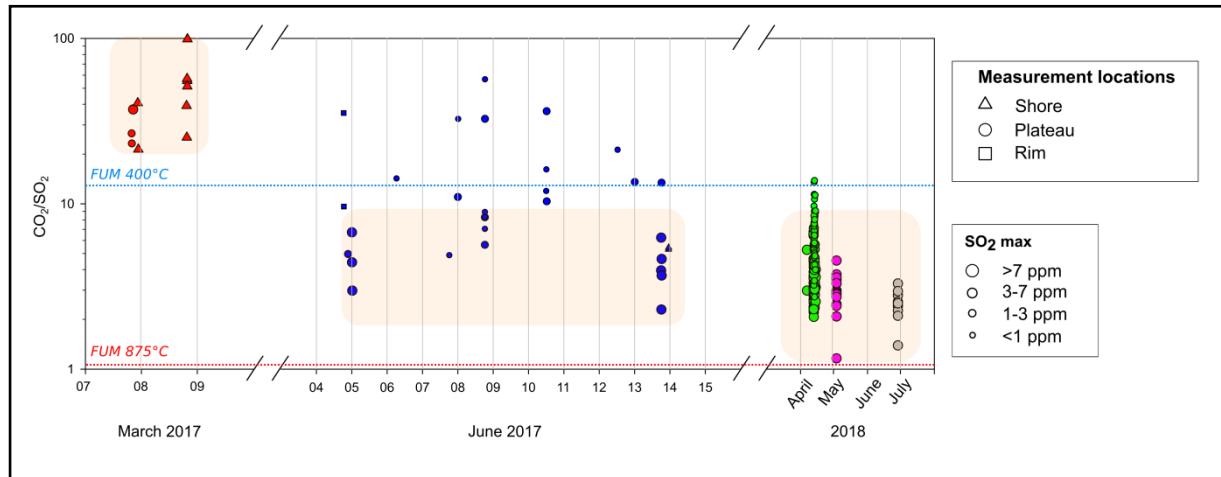
Figure 5.10 - Variations of the CO_2/SO_2 ratios between March 2017 and June 2018. Dashed lines are the CO_2/SO_2 gas ratios of high temperature fumaroles in 2005 (data courtesy of Tobias Fischer). The light orange areas show the pure lake gas composition.
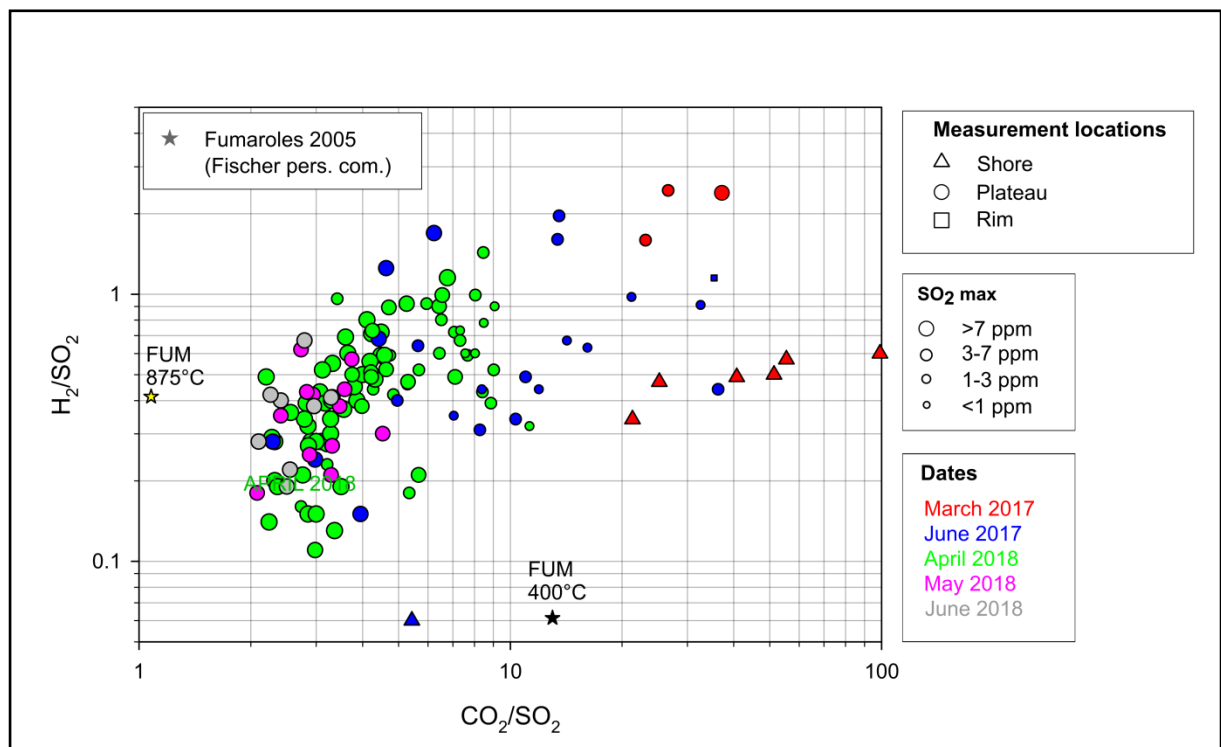
Figure 5.11 - H_2/SO_2 vs CO_2/SO_2 ratios of Santa Ana lake emissions in 2017 and 2018. The composition of high temperature fumaroles measured in 2005 are added (Fischer, pers. comm.). This plot also illustrates that below 7 ppm of SO_2, the gas measured have higher CO_2/SO_2 ratios compared to pure lake gases.

5.7.   DISCUSSION

5.7.1. State of activity of the crater lake

Colvin et al. (2013) postulated that in early 2008, Santa Ana crater lake was reaching a new state of quiescence, but at higher energy input. In the absence of anomalous seismicity (Figure 5.12a-c), background SO_2 fluxes (Figure 5.12d) and the relative stability of the lake temperature and chemistry until early 2010, we confirm this trend towards quiescence. The low fluctuations of lake chemistry and surface temperature are likely mostly due to seasonal changes (e.g., rain vs. dry season).

At the end of October 2010, a new unrest started, as suggested by inversion of trends in lake surface temperature and lake volume (Figures 5.4 and 5.5). Trends in chemistry cannot be inferred due to an interrupted dataset, but anion species concentrations in 2014 were higher than at the end of 2010 (Table 5.1). The highest anion concentrations since 2000 were measured in 2017 (Figure 5.4). Heating and evaporation of the lake can reflect changes in input rate and/or enthalpy of hot fluids entering the lake from below (Bernard et al., 2004). Seismicity data do not indicate clear fluid or magma movements. On July 27, 2011 and September 26, 2012, the number of daily volcano-tectonic earthquakes peaked at 19 and 11, respectively. RSAM remained at background levels (below 20 units; Olmos et al., 2004). Since May 2016, the RSAM exceeded 20 units (up to 86 units on March 19, 2017), and it remains at high level by the time of writing, suggesting a new background level of circa 40 units has been reached (Figure 5.12c). The increase in RSAM unit is not correlated with an obvious change in SO_2 flux. The higher surface lake temperature in 2017 coincided with increasing RSAM.

Changes in SO_4/Cl ratios can be indicative of changes in the fluids input composition, but also of the degree of evaporative degassing from the lake surface (see Introduction and Figures 5.4 and 5.6). Decreasing SO_4/Cl ratios below 1 since the 2005 phreatomagmatic eruption may reflect increasing HCl input into the lake as suggested by the Cl peak concentration after the March-April 2007 phreatic eruptions (SO_4/Cl ratio until 0.33 on April 9, 2008; Figure 5.4 and 5.6). This phenomenon was also described at Ruapehu Crater Lake (Christenson and Wood, 1993). Additionally, this decrease in SO_4/Cl ratio can also be explained by the precipitation of native S and S-bearing minerals (e.g.

Christenson et al., 2010; Rouwet et al., 2014b, 2016; Scolamacchia and Cronin, 2016; Takano et al., 1994), which have been reported at saturation at Santa Ana earlier (Bernard et al., 2004; Colvin et al., 2013).

Unfortunately, due to incomplete data chemistry, we are not able to model the mineral phases in saturation in the lake water after 2008. Common minerals in saturation in the Santa Ana water were
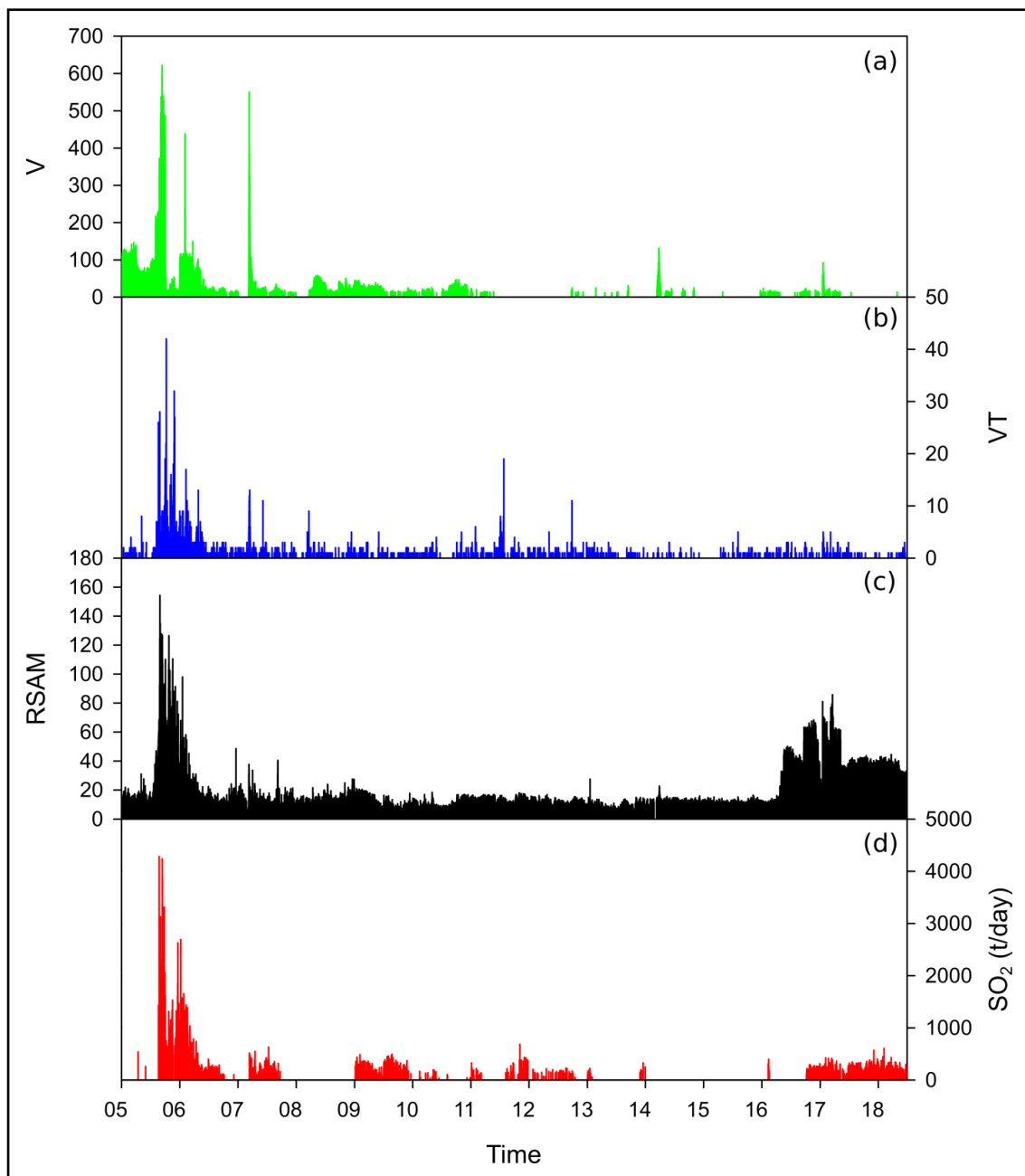
Figure 5.12 - 2005-2018 time-series of the seismic activity (number of volcanic (a) and volcano-tectonic (b) earthquakes and RSAM (c)) and SO₂ flux (d) at Santa Ana. Data are personal communication from MARN.

alunite, gypsum, iron sulfide and anhydrite (Colvin et al., 2013). Total concentrations of SO_4, Ca, Na and Fe varied simultaneously over the period 2008-2010 (Table 5.1). After the Cl peak, and consequent low SO_4/Cl ratios, following the 2007 phreatic eruptions the SO_4/Cl ratio remained lower than background values prior to the 2005 eruption. During this period the low SO_4/Cl ratio are more likely due to precipitation/dissolution of S-bearing minerals, instead of a change in the gas composition or HCl evaporative degassing (as shown by the decrease of SO_4/Cl ratios with surface lake water temperature; Figure 5.13). Indeed, no significant increase in SO_2 flux was measured over the 2007-2018 period (Figure 5.12d). Within the pH range of Santa Ana crater lake, less extreme than at e.g. Poás, but at higher temperatures, loss of SO_4 from solution due to the S-sealing capacity of the underlying hydrothermal system is the dominant process with respect to HCl degassing from the lake, which would instead lead to a SO_4/Cl increase. Only for the most recent, and smallest lakes observed in 2017-2018 (Figure 5.5) evaporative degassing of HCl can come into play, explaining the slightly higher SO_4/Cl ratios (note the temporal succession in Figure 5.13).

It is difficult to infer the origin of changes of lake physico-chemical patterns since 2010. Still, these changes require further scrutiny with additional observations. Actually, before volcanic eruptions, changes in lake temperature, volume and chemistry have been often reported (e.g.
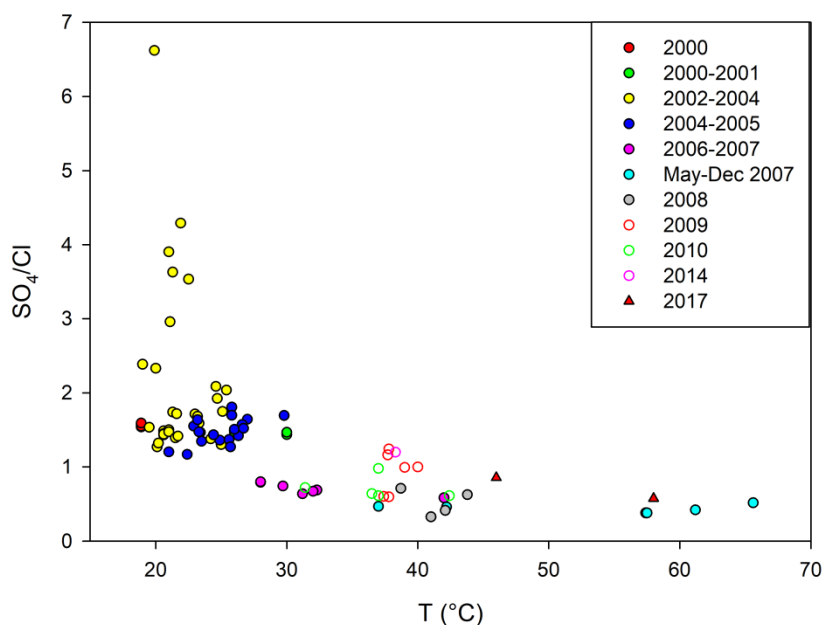
Figure 5.13 - SO₄/Cl ratios vs temperature of Santa Ana crater lake waters for the period 2000-2017.

Giggenbach, 1974, 1983; Hurst and Dibble, 1981; Takano, 1987; Brown et al., 1989; Pardyanto, 1990; Rowe et al., 1992b; Badrudin, 1994; Pasternack and Varekamp, 1997; Vandermeulebrouck et al., 2000; Hernández et al., 2001; Varekamp et al., 2001; Dehn et al., 2002). Despite the general lower level of study of the Santa Ana crater lake, compared to the four most monitored crater lakes of Ruapehu, Poás, Kusatsu-Shirane (Yugama) and Kawah Ijen, long- and short-term trends in chemical composition, temperature and recent additional plume gas data have led to sound hypotheses on how magma migrated and degassed below the crater lake during the >25-year long period 1992-2018. In terms of eruptive activity, Santa Ana is certainly not less active and dynamic with the mentioned four crater lakes.

5.7.2. Clues from lake gas composition and flux

Interpreting the implications of the compositional signature of the lake gas plume for assessing the current Santa Ana volcanic activity state is hampered by the lack of previous data. Notwithstanding, our 2017-2018 data offer novel and interesting insights.

One first important observation is that the compositional features of the Santa Ana plume are widely heterogeneous, in both space and time. Measurements taken in 2017 from three distinct locations (rim, plateau, shore), at different distances from the gas emission source, imply some spatial heterogeneity in plume composition. Sulfur gases and hydrogen in young plumes are thought to behave relatively conservative (i.e. poorly reactive) over timescales of seconds to a few minutes, implicated by the short plume traveling distances between the lake and the Multi-GAS, also the case at Santa Ana (Aiuppa et al., 2005b, 2011b; Ehhalt and Rohrer, 2009). As such, gas plume composition should only be affected by atmospheric dilution, and hence gas ratios should be invariant independently on distance from the source. However, our complete dataset (see Appendix Table S1) identifies systematic differences in gas ratio between the three manifestations (rim, plateau, shore). At the rim, gas observations are complicated by the very dilute plume detected; we consider the derived ratios strongly affected by analytical uncertainty, e.g., by the difficulty in resolving volcanic gases over background, especially for H_2O, CO_2 and H_2. Our filtered dataset, in which measurements taken at higher plume density ($SO_2 > 8$ ppm) were considered, confirms a more restricted compositional

range between plateau and shore (Table 5.2). Even there, however, while CO_2/SO_2 ratios exhibit overlapping ranges at plateau and shore at each given time (March and June 2017), H_2/SO_2 ratios do not, and are systematically higher at the plateau than at the shore. We are confident that these spatial compositional changes (at one single time) cannot reflect variable extents of plume atmospheric dilution, at least in the filtered dataset. We find it instead more likely that the compositional change between shore and plateau reflect some additional H_2 contributions from other sources, perhaps weakly degassing hydrothermal fumaroles and steaming grounds in the inner crater slope. We suggest that these additional, diffuse gas contributions get mixed with the lake plume upon plume transport between emission at the lake surface and measurement at the plateau, thus justifying part of the compositional variability observed (Figure 5.11).

In addition to spatial heterogeneity, our measurements also highlight important temporal changes in gas composition (Figures 5.10 and 5.11). It is observed that the CO_2/SO_2 ratio decreased by more than one order of magnitude in one year, from March 2017 (shore: 31.0 ± 13.7; plateau: 37.2 ± 9.7) to June 2018 (2.4 ± 0.5) (Figure 10). The H_2/SO_2 ratios at the plateau were also lower (and far less variable) in May-June 2018 than in March 2017. Overall, these observations imply a gas composition becoming more SO_2-rich over time, and more S-rich in general (in view of the H_2S/SO_2 ratios being the higher in April 2018 than in 2017; see Table 5.2).

The S composition of gas leaving the lake surface reflects a complex balance between the proportion of magmatic vs hydrothermal gas entering at the lake-bottom, and extents/mechanisms of S-dissolution and saturation relations in the lake water. These gas-water-rock reactions into the lake can remove S from the input gas via (Kusakabe et al., 2000a; Christenson and Tassi, 2015):

$$3SO_2 + 2H_2O \rightarrow 2HSO_4^- + S_{(e)} + 2H^+ \tag{5.1}$$

$$4SO_2 + 4H_2O \rightarrow 3HSO_4^- + H_2S + 3H^+ \tag{5.2}$$

$$2H_2S + SO_2 \rightarrow 3S_{(e)} + 2H_2O \tag{5.3}$$

The increasing S compositions of the Santa Ana lake plume gas in 2018 relative to 2017, imply a shift of the above reactions toward the left, i.e., a lower consumption of the reagents during gas-water-rock reactions into the lake. If this happens, then the gas leaving the lake (our lake plume gas) will become increasingly more magmatic in nature, i.e. more similar to the input gas at the lake bottom.

The composition of the Santa Ana input gas in 2017-2018 is unknown, in view of the lack of measurable fumaroles. However, two high-temperature (400 to 875 °C) gas samples were collected at Santa Ana by Tobias Fischer (Pers. Comm.) during increased activity in 2005. If these composition are taken as representative of the current (2017-2018) magmatic gas input into the lake, it becomes evident that the lake plume gas has become increasingly more magmatic in nature in 2018 relative to 2017 (Figures 5.10 and 5.11).

Less S scrubbing into the lake in 2018 imply faster magmatic gas transit through the lake. In turn, this can be explained by (i) higher magmatic gas input into the lake, and/or (ii) lower lake water volume. The two mechanisms are not mutually exclusive.

Gas flux measurements (and calculations) can help distinguishing which of the two factors are more significant in the Santa Ana case. During the study period, the SO_2 flux was systematically measured by a DOAS fixed station operated by MARN (Figure 5.12d). These results imply similar SO_2 degassing rates in 2017 and 2018, and point in general to much lower SO_2 emissions in 2017-2018 than during the 2005 eruptive unrest (Olmos et al., 2007). During our specific Multi-GAS measurement intervals, the SO_2 flux varied from 41 and 329 t/day, and was somewhat higher in 2017 than in 2018 (Table 5.2). By scaling the SO_2 fluxes to our mean lake gas ratios, we calculate the fluxes of CO_2, H_2, H_2S and H_2O released by the lake into the atmosphere (Table 5.2). The highest CO_2 (5117 to 12317 t/day) and H_2 (3.1 to 18 t/day) fluxes were observed in March 2017, relative to June 2017-June 2018 when the CO_2 (117 to 479 t/day) and H_2 (0.7 to 3.0 t/day) fluxes remained at lower levels. These results thus demonstrate that the more magmatic gas compositions in 2018 cannot be explained by a higher magmatic gas input from the sub-limnic magmatic-hydrothermal system. Rather, we propose that the decreasing lake volumes in 2018 caused an overall reduction in gas-water-rock

interactions. This interpretation is consistent with our measured H_2O fluxes, which seem to have varied in response to increasing evaporation rates of the lake, consistent with the higher lake water temperatures (874-893 t/day in June 2017; 729-4959 t/day in April 2018; 2454 t/day on May 3, 2018 and 6950 t/day on June 28, 2008). The decrease in lake volume is probably also caused by the lower contribution of rainwater, as El Salvador is passing anomalously dry seasons recently. During 2017-2018, the small volume Santa Ana crater lake is thus more sensitive to variations in temperature and chemistry, and has become a less efficient gas scrubber as such. This fact might lead to an apparent, and probably wrong, over interpretation of the "more magmatic" state of degassing at Santa Ana.

5.8. IMPLICATION FOR FUTURE ERUPTION FORECASTING

Our results highlight a dynamic evolution of the Santa Ana crater lake for the period 1992-2018, and deal with the most recent extreme changes (2017-2018). The lake is heating, reducing in volume, and becoming more acidic and rich in dissolved solutes. Available information on gas chemistry is too limited in number and temporal interval to allow firm conclusions to be made on the current state of the volcano. Nevertheless, our results show that from early-2017 to mid-2018, the lake plume gas has become increasingly rich in S, and therefore more magmatic in nature. The SO_2 flux, for which a long temporal record exists, argues against an increase in magmatic gas input into the lake, which suggests that the observed changes may more likely result from reduced S deposition into the lake due to a lower lake volume, and thus, a more rapid transit of magmatic gases through the lake. The dynamic evolution of Santa Ana volcano (Figures 5.4, 5.5, 5.6, 5.10), highlighted in the present study, clearly raises the need of further observations and careful scrutiny of water/gas compositional features in the near future.

The triangular plots of Figure 5.14 compare the Santa Ana Lake gas composition (this study) with (i) available magmatic gas compositional data for the volcano (Fischer, pers. comm., and Aiuppa et al., 2017), and (ii) lake gas plume compositions recently obtained at other quiescent and recently erupting lakes worldwide (this Thesis and references listed in the Figure 5.14 caption). The plots

confirm the temporal evolution of the Santa Ana lake gas composition. In only one year of observations, the gas has evolved from CO_2-H_2-rich and S-poor, to more S-rich compositions. As such, the Santa Ana lake gas in 2018 sits in an intermediate position between the CO_2-H_2-H_2S-rich lake plumes seen at "quiescent" lakes (El Chichón and Viti; see Chapter 4 and Hasselle et al., 2018), and the far more SO_2-rich plumes issuing from recently erupting lakes (Poás, Copahue and Yudamari) (Fig. 5.14). The 2018 lake plume is also approaching the "magmatic" composition of the high-T (875 °C) fumarole courageously sampled by T. Fischer in a restless Santa Ana crater in 2005. As such, a further migration of the Santa Ana lake plume gas toward the SO_2-rich magmatic gas pole should seriously be taken as evidence of further activity escalation. At Laguna Caliente (Poás, Costa Rica), a decrease in CO_2/SO_2 ratios, and increasing SO_2 fluxes, are generally observed prior to phreatic eruption (de Moor et al., 2016b; Stix and de Moor, 2018), and are explained by increasing magmatic gas influx entering the lake. Although this critical situation has not yet been reached at Santa Ana, our results reinforce the need of reinforcing volcano monitoring at this potentially hazardous volcano.
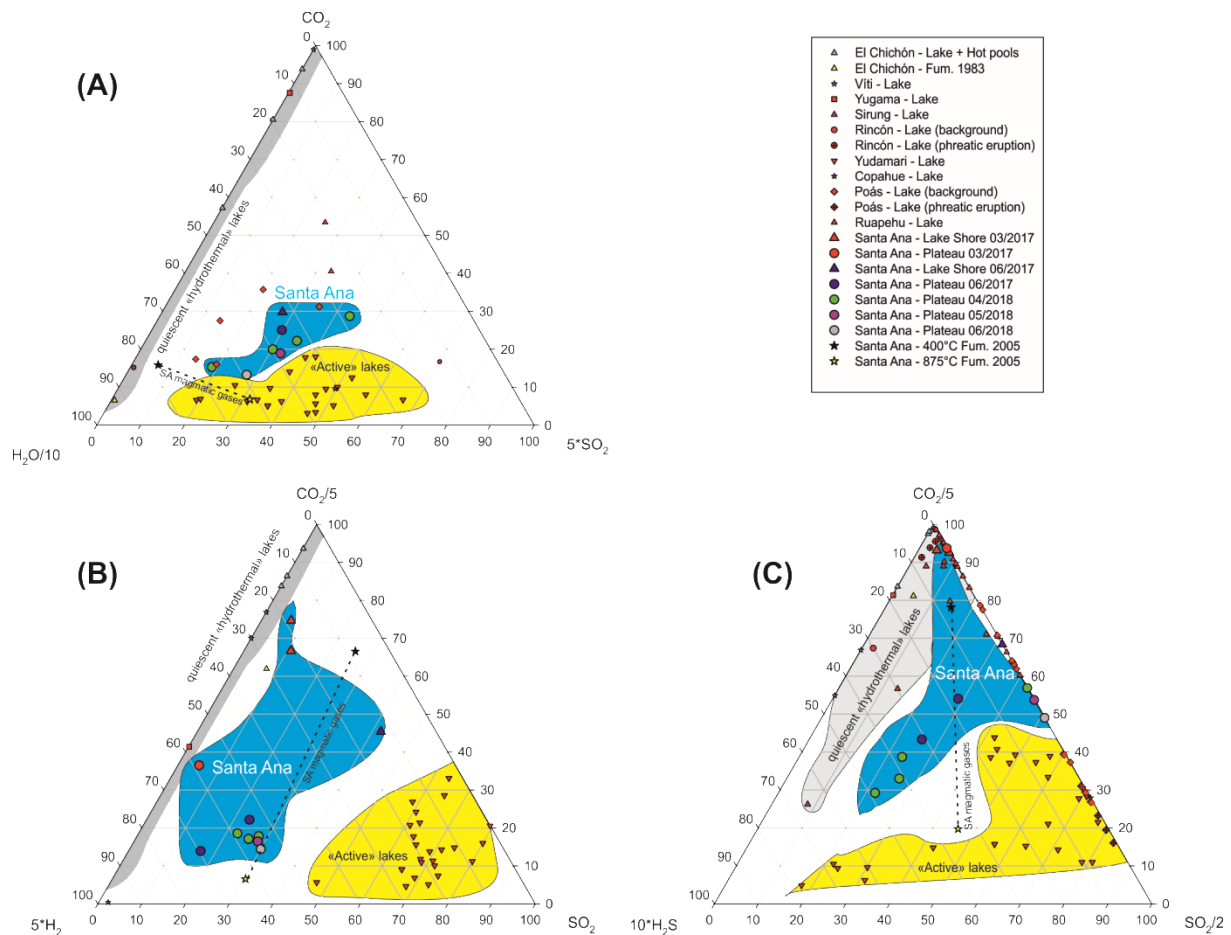
Figure 5.14- Triangular plots (H_2O-CO_2-SO_2 (a), CO_2-H_2-SO_2 (b) and CO_2-H_2S-SO_2(c)) showing the chemical composition and its temporal and spatial evolution of the gas plume coming off Santa Ana crater lake, compared to those of degassing lakes of El Chichón (Mexico; Hasselle et al., 2018; this thesis), Viti (Iceland; Hasselle et al., 2018; this Thesis), Yugama (Kusatsu-Shirane volcano, Japan; this Thesis), Yudamari (Aso volcano, Japan; Shinohara et al., 2015), Copahue (Argentina-Chile; Tamburello et al., 2015) and Ruapehu (New Zealand; this Thesis), and Kawah Ijen (Indonesia; Gunawan et al., 2016). The 2018 Santa Ana plume gases have increasingly become more magmatic (high-T fumaroles courtesy of T. Fischer) with respect to the 2017 plume gases. Santa Ana crater lake gas occupies an intermediate position between "quiescent hydrothermal lakes" (El Chichón, Viti and Yugama) and "active lakes" (Copahue, Yudamari, Kawah Ijen).

Table 5.1 - Chemical composition of Santa Ana lake water since 1992. C, is for Center and N, for Northern shore.

Date	Location	Depth	T	pH	Cl	SO₄	F	B	Mg	Ca	Na	K	Fe total	SiO₂	TDS	SO₄/Cl	Mg/Cl	References
		m	°C		mg/l	mg/l	mg/l	mg/l	mg/l	mg/l	mg/l	mg/l	mg/l	mg/l	mg/l			
22-02-92	-	-	-	0.6	17470	9130	-	-	-	-	-	-	-	114	-	0.52	-	Colvin et al., 2013
02-07-92	-	-	-	2.3	6350	1900	-	-	-	-	-	-	-	48	-	0.30	-	Colvin et al., 2013
22-07-92	-	-	-	1.9	64380	3700	-	-	-	-	-	-	-	107	-	0.06	-	Colvin et al., 2013
13-08-92	-	-	-	1.4	75480	3850	-	-	-	-	-	-	-	97	-	0.05	-	Colvin et al., 2013
21-08-92	-	-	-	1.2	50200	3500	-	-	-	-	-	-	-	-	-	0.07	-	Colvin et al., 2013
24-09-92	-	-	-	-	3500	3370	-	-	-	-	-	-	-	71	-	0.96	-	Colvin et al., 2013
23-10-92	-	-	-	1.5	5770	3500	-	-	-	-	-	-	-	72	-	0.61	-	Colvin et al., 2013
25-11-92	-	-	-	1.5	6290	4300	-	-	-	-	-	-	-	-	-	0.68	-	Colvin et al., 2013
08-01-93	-	-	-	1.5	4950	6300	-	-	-	-	-	-	-	-	-	1.27	-	Colvin et al., 2013
22-01-93	-	-	-	1.3	5180	6300	-	-	-	-	-	-	-	-	-	1.22	-	Colvin et al., 2013
10-03-93	-	-	-	1.4	15400	8400	-	-	-	-	-	-	-	118	-	0.55	-	Colvin et al., 2013
23-03-93	-	-	-	-	10060	4800	-	-	-	-	-	-	-	106	-	0.48	-	Colvin et al., 2013
18-05-93	-	-	-	1.4	12900	-	-	-	-	-	-	-	-	126	-	-	-	Colvin et al., 2013
07-07-93	-	-	-	1.4	17940	3800	-	-	-	-	-	-	-	-	-	0.21	-	Colvin et al., 2013
30-08-93	-	-	-	2.5	17940	-	-	-	-	-	-	-	-	138	-	-	-	Colvin et al., 2013
22-10-93	-	-	-	-	42760	-	-	-	-	-	-	-	-	142	-	-	-	Colvin et al., 2013
25-11-93	-	-	-	1.5	6290	4300	-	-	-	-	-	-	-	-	-	0.68	-	Colvin et al., 2013
28-01-00	SAL1	0	18.9	0.9	5470	8420	215	6.6	294	799	378	136	738	235	17600	1.54	0.05	Bernard et al., 2004
01-01-00	SAL2	0	18.9	0.9	5650	8750	211	6.7	296	812	378	137	756	240	18100	1.55	0.05	Bernard et al., 2004
01-01-00	SAL3	0	18.9	0.9	5660	8740	235	6.9	296	802	374	134	750	237	-	1.54	0.05	Bernard et al., 2004
01-01-00	SAL4	0	18.9	0.9	5520	8630	209	7.1	308	840	376	138	779	250	18000	1.56	0.06	Bernard et al., 2004
01-01-00	SAL5	20	18.9	0.9	5610	8700	223	7	300	831	377	137	771	252	18100	1.55	0.05	Bernard et al., 2004
01-01-00	SAL6	25	18.9	1	5430	8630	212	7.1	302	832	377	137	773	255	17800	1.59	0.06	Bernard et al., 2004

Table 5.1 - Continued

Date	Location	Depth	T	pH	Cl	SO$_4$	F	B	Mg	Ca	Na	K	Fe total	SiO$_2$	TDS	SO$_4$/Cl	Mg/Cl	References
		m	°C		mg/l	mg/l	mg/l	mg/l	mg/l	mg/l	mg/l	mg/l	mg/l	mg/l	mg/l			
05-07-00	SAN1	0	30	0.9	7600	10910	194	6	307	862	395	145	832	282	22500	1.44	0.04	Bernard et al., 2004
01-08-00	SAN2	0	30	0.9	7270	10660	194	5.7	283	805	367	139	720	276	21600	1.47	0.04	Bernard et al., 2004
01-02-01	SAP1	0	26	0.9	8370	12460	379	12.8	392	1140	506	209	1070	359	26200	1.49	0.05	Bernard et al., 2004
01-02-01	SAP2	0	26	0.9	8760	12900	386	11.4	366	1110	485	196	974	357	26800	1.47	0.04	Bernard et al., 2004
20-02-02	ANA21	0	20.6	1.1	7620	11320	341	10.2	417	1010	487	174	1310	303	24300	1.49	0.05	Bernard et al., 2004
01-02-02	ANA22	0	20.6	1.1	7630	10920	333	10.2	424	1030	481	173	1310	301	23900	1.43	0.06	Bernard et al., 2004
01-02-02	ANA23	0	20.6	1.1	7700	11160	314	-	428	1030	481	171	1320	305	24200	1.45	0.06	Bernard et al., 2004
01-02-02	ANA24	0	20.6	1.1	7940	11450	337	-	434	1050	491	181	1330	309	24800	1.44	0.05	Bernard et al., 2004
20-03-02	MARC02	0	21	1.1	8400	12600	372	10.2	423	1010	463	177	1310	302	26400	1.50	0.05	Bernard et al., 2004
20-04-02	APR02	0	21	1.1	8400	12380	357	9.1	422	1010	457	178	1330	295	26200	1.47	0.05	Bernard et al., 2004
02-05-02	-	0	25.4	1.6	7000	14250	-	-	-	3240	-	-	-	-	-	2.04	-	SNET
06-06-02	-	0	19	1.2	6030	14380	-	-	2310	2610	-	-	-	-	-	2.38	0.38	SNET
10-07-02	-	0	20	1.2	6120	14250	-	-	2432	2210	-	-	-	-	-	2.33	0.40	SNET
15-08-02	-	0	21.1	1.6	2750	8130	-	-	188	1210	-	-	-	-	-	2.96	0.07	SNET
11-09-02	-	0	21	1.8	1150	4500	-	-	347	762	-	-	-	-	-	3.91	0.30	SNET
07-10-02	-	0	19.9	1.3	1150	7630	-	-	231	762	-	-	-	-	-	6.63	0.20	SNET
06-11-02	-	0	21.9	1.1	2080	8940	-	-	596	2060	-	-	-	-	-	4.30	0.29	SNET
05-12-02	-	0	21.3	1.2	2390	8690	-	-	656	179	-	-	-	-	-	3.64	0.27	SNET
01-01-03	-	0	20.1	1.2	7670	9750	-	-	726	1800	-	-	-	-	-	1.27	0.09	SNET
21-01-03	-	0	20.2	1.2	7670	10130	-	-	-	-	-	-	-	-	-	1.32	-	SNET
19-02-03	-	0	19.5	1	5950	9130	-	-	632	898	-	-	-	-	-	1.53	0.11	SNET
04-04-03	-	0	21.3	1.6	5890	10250	-	-	605	1300	-	-	-	-	-	1.74	0.10	SNET

Table 5.1 - Continued

Date	Location	Depth	T	pH	Cl	SO$_4$	F	B	Mg	Ca	Na	K	Fe total	SiO$_2$	TDS	SO$_4$/Cl	Mg/Cl	References
		m	°C		mg/l	mg/l	mg/l	mg/l	mg/l	mg/l	mg/l	mg/l	mg/l	mg/l	mg/l			
05-07-00	SAN1	0	30	0.9	7600	10910	194	6	307	862	395	145	832	282	22500	1.44	0.04	Bernard et al., 2004
01-07-03	C	0	24.7	1.1	5590	10750	-	-	1458	1200	-	-	-	-	-	1.92	0.26	SNET
04-08-03	-	0	22.5	1.2	2720	7000	-	-	777	961	-	-	-	-	-	2.57	0.29	SNET
04-08-03	C	0	-	0.8	2330	8250	-	-	-	1280	-	-	-	-	-	3.54	-	MARN
01-09-03	C	0	24.6	0.9	4500	9380	-	-	1214	801	-	-	-	-	-	2.08	0.27	SNET
01-10-03	C	0	25	1.1	7880	10250	-	-	486	801	-	-	-	-	-	1.30	0.06	SNET
01-12-03	C	0	23	1.3	5100	8750	-	-	243	1600	-	-	-	-	-	1.72	0.05	SNET
18-01-04	-	0	21.5	1.1	5830	10250	-	-	486	1200	-	-	-	-	-	1.76	0.08	SNET
18-01-04	C	0	-	-	5830	8130	-	-	-	801	-	-	-	-	-	1.39	-	MARN
10-02-04	-	0	25.1	1.6	6080	10630	-	-	729	-	-	-	-	-	-	1.75	0.12	SNET
12-02-04	C	0	-	0.6	6080	11000	-	-	-	8500	-	-	-	-	-	1.81	-	MARN
15-04-04	-	0	21.6	2	5970	10250	-	-	1672	2300	-	-	-	-	-	1.72	0.28	SNET
26-04-04	C	0	-	0.9	5960	10500	-	-	-	2260	-	-	-	-	-	1.76	-	MARN
13-05-04	-	0	21.7	1.6	6710	9500	-	-	836	1380	-	-	-	-	-	1.42	0.12	SNET
15-05-04	N	0	-	-	6710	9500	-	-	-	1380	-	-	-	-	-	1.42	-	MARN
08-06-04	-	0	23.2	1.3	6310	10630	-	-	468	1760	-	-	-	302	-	1.68	0.07	SNET
09-06-04	N	0	-	-	6310	10630	-	-	-	1760	-	-	-	302	-	1.68	-	MARN
19-06-04	-	0	24.2	1.8	6710	9250	-	-	1084	894	-	-	-	290	-	1.38	0.16	SNET
22-06-04	N	0	-	-	6710	9250	-	-	-	894	-	-	-	290	-	1.38	-	MARN
22-06-04	C	0	-	-	6710	9750	-	-	-	894	-	-	-	302	-	1.45	-	MARN
08-07-04	N	0	23.4	1.3	6310	9250	25	0.5	900	751	-	-	-	313	-	1.47	0.14	SNET
22-07-04	N	0	24.9	1.2	6800	9250	7.5	6.5	1897	1790	-	-	-	450	-	1.36	0.28	SNET
26-07-04	C	0	-	1.8	6310	9250	13	5.9	-	1790	-	-	-	434	-	1.47	-	MARN
11-08-04	N	0	26.3	1.5	6960	9880	29	7.4	542	1790	-	-	-	368	-	1.42	0.08	SNET
12-08-04	C	0	-	-	6960	9630	19	7.0	-	1340	-	-	-	347	-	1.38	-	MARN
31-08-04	N	0	25.8	1.1	5470	9880	90	2.6	2249	1390	-	-	-	278	-	1.81	0.41	SNET

Table 5.1 - Continued

Date	Location	Depth	T	pH	Cl	SO₄	F	B	Mg	Ca	Na	K	Fe total	SiO₂	TDS	SO₄/Cl	Mg/Cl	References
		m	°C		mg/l	mg/l	mg/l	mg/l	mg/l	mg/l	mg/l	mg/l	mg/l	mg/l	mg/l			
01-09-04	C	0	-	1.2	6460	8500	88	-	-	1390	-	-	-	258	-	1.32	-	MARN
16-09-04	N	0	27	0.6	5710	9380	66	1.8	559	1380	-	-	-	299	-	1.64	0.10	SNET
29-09-04	N	0	27.7	1	5460	9250	89	5.1	839	923	-	-	-	324	-	1.69	0.15	SNET
30-09-04	C	0	-	1	5460	-	96	5.1	-	963	-	-	-	324	-	-	-	MARN
19-10-04	N	0	26.6	1.2	6200	9750	80	6.3	1206	802	-	-	-	318	-	1.57	0.19	SNET
20-10-04	C	0	-	1.2	6450	-	75	6.3	-	802	-	-	-	324	-	-	-	MARN
09-11-04	N	0	24.4	1.1	6450	9250	69	5.9	1703	1200	-	-	-	357	-	1.43	0.26	SNET
11-11-04	C	0	-	-	6450	9630	64	6.7	-	1610	-	-	-	258	-	1.49	-	MARN
16-12-04	-	0	22.9	1.1	6450	10000	54	6.5	1700	1200	-	-	-	312	-	1.55	0.26	SNET
21-01-05	-	0	21.8	1.3	6960	10250	73	6.5	1457	1200	-	-	-	312	-	1.47	0.21	SNET
21-01-05	N	0	23.3	0.8	6960	10250	73	6.5	-	1200	-	-	-	312	-	1.47	-	MARN
21-01-05	C	0	23.3	0.9	6460	11130	83	6.3	-	801	-	-	-	293	-	1.72	-	MARN
05-02-05	-	0	20.9	1.3	9200	10750	-	-	1214	1200	-	-	-	276	-	1.17	0.13	SNET
07-02-05	N	0	24.7	-	9200	10750	150	-	-	1200	-	-	-	276	-	1.17	-	MARN
07-02-05	C	0	22.4	-	8700	10880	154	-	-	1200	-	-	-	279	-	1.25	-	MARN
04-03-05	N	0	23.2	0.87	6490	10630	10	-	-	1200	-	-	-	376	-	1.64	-	MARN
15-03-05	-	0	22.3	1.2	7990	10750	71	-	729	801	-	-	-	355	-	1.35	0.09	SNET
16-03-05	N	0	23.6	0.8	7980	10750	71	-	-	801	-	-	-	355	-	1.35	-	MARN
16-03-05	C	0	23.5	1.2	7490	10380	8.7	-	-	801	-	-	-	489	-	1.39	-	MARN
05-04-05	N	0	25.8	1.1	6490	11000	72	-	486	1600	-	-	-	383	-	1.69	0.07	MARN
03-05-05	N	0	26.1	0.9	8480	11630	76	-	-	1200	-	-	-	317	-	1.37	-	MARN
03-05-05	C	0	25.6	1.1	8480	11630	77	-	-	1200	-	-	-	340	-	1.37	-	MARN
02-06-05	N	0	-	0.8	6490	8250	50	3.1	-	801	-	-	-	209	-	1.27	-	MARN
17-06-05	-	0	-	0.7	6990	10530	55	6.5	913	897	-	-	-	410	-	1.51	0.13	SNET
28-06-05	N	0	26.7	0.7	6990	10630	55	6.5		897	-	-	-	410	-	1.52	0.00	MARN
30-06-05	-	0	25.7	0.8	6490	8250	50	3.1	729	801	-	-	-	209	-	1.27	0.11	SNET

Table 5.1 - Continued

Date	Location	Depth	T	pH	Cl	SO$_4$	F	B	Mg	Ca	Na	K	Fe total	SiO$_2$	TDS	SO$_4$/Cl	Mg/Cl	References
		m	°C		mg/l	mg/l	mg/l	mg/l	mg/l	mg/l	mg/l	mg/l	mg/l	mg/l	mg/l			
16-08-05	N	0	21	1.6	6970	8380	28	4.4	991	769	-	-	-	242	-	1.20	0.14	MARN
18-09-05	N	0	-	-	80	150	1.0	-	-	42	23	5.2	-	75	376	1.88	-	MARN
20-07-06	N	0	-	1.24	3160	2500	34	0.7	486	1200	2210	75	-	238	27500	0.79	0.15	MARN
05-09-06	N	0	-	1.2	7450	4750	27	1.1	1214	1600	627	57	-	78	41750	0.64	0.16	SNET
13-12-06	N	0	28	1.2	8450	6750	28	1.8	2186	1600	231	117	-	362	37600	0.80	0.26	SNET
15-01-07	N	0	32.3	0.9	9440	6500	-	6.3	1700	1600	7580	47	-	419	45500	0.69	0.18	SNET
07-02-07	N	0	29.7	1.3	9440	7000	-	3.1	1700	1600		109	-	386		0.74	0.18	SNET
08-03-07	N	0	32	1.2	10430	7000	-	6.3	1943	2410	3330	148	2190	344	102500	0.67	0.19	SNET
28-03-07	N	0	42	0.9	15400	9000	103	2.9	1943	2000	25500	160	2320	359	74250	0.58	0.13	SNET
04-05-07	N	0	61.6	1	16400	6880	42	6	1700	2400	6450	238	2460	519	68750	0.42	0.10	SNET
16-06-07	N	0	65.6	0.7	17870	9250	59	2.6	2186	1200	2190	85	1160	373	99250	0.52	0.12	SNET
05-07-07	N	0	57.5	-0.2	22340	8500	180	4.6	1457	2000	1180	76	1710	206	150250	0.38	0.07	SNET
13-11-07	N	0	44.1	0.7	16880	7750	23	5.7	-	2000	628	498	205	569	43250	0.46	-	SNET
18-12-07	N	0	38.3	0.8	20850	9750	24	6.0	-	4000	713	177	2740	470	85750	0.47	-	MARN
07-02-08	N	0	42.1	0.7	23580	9750	22	7.8	-	2400	663	254	2660	382	129000	0.41	-	MARN
09-04-08	N	0	41	0.5	31280	10250	21	4.7	-	2800	1540	2240	1530	369	94750	0.33	-	MARN
04-09-08	N	0	43.8	0.9	10600	6630	37	5.7	-	1040	722	603	1600	381	28070	0.63	-	MARN
27-11-08	N	0	38.7	0.8	10920	7750	49	6.4	-	1200	540	408	2030	423	35250	0.71	-	MARN
04-02-09	N	0	37.8	1.1	7550	9380	73	1.9	-	1280	558	1170	2750	375	31500	1.24	-	MARN
30-04-09	N	0	41.8	0.5	8810	8750	100	8.5	-	2680	408	1165	2840	584	39150	0.99	-	MARN
29-06-09	N	0	38.8	0.9	8140	8130	78	6.0	-	2040	2130	1680	2340	710	36250	1.00	-	MARN
27-08-09	N	0	37.7	0.9	7520	8750	79	5.9	-	1520	717	1160	2250	724	33000	1.16	-	MARN
22-10-09	N	0	37.4	0.9	11630	7000	73	5.7	-	1760	1010	406	2010	658	22820	0.60	-	MARN
17-12-09	N	0	36.4	0.1	13860	8250	70	5	-	2160	810	835	2340	741	33250	0.60	-	MARN
25-02-10	N	0	36.1	0.5	14470	9250	93	7.7	-	1600	1160	60	2480	737	36750	0.64	-	MARN
29-04-10	N	0	41.2	0.1	16140	9880	88	5.5	-	3720	1170	62	3300	1280	42000	0.61	-	MARN

Table 5.1 - Continued

Date	Location	Depth	T	pH	Cl	SO$_4$	F	B	Mg	Ca	Na	K	Fe total	SiO$_2$	TDS	SO$_4$/Cl	Mg/Cl	References
		m	°C		mg/l	mg/l	mg/l	mg/l	mg/l	mg/l	mg/l	mg/l	mg/l	mg/l	mg/l			
13-05-10	N	0	38.4	0.3	16770	10250	85	ND	-	3040	1140	48	2780	1260	37000	0.61	-	MARN
22-07-10	N	0	31.4	0.8	9700	9500	46	9.0	-	865	738	42	1690	621	16040	0.98	-	MARN
24-09-10	N	0	31.4	1.4	8500	6130	33	8.9	-	1200	676	80	1620	710	14360	0.72	-	MARN
25-11-14	N	0	-	-	9490	11370	388	20.0	-	859	623	164	3850	329	55600	1.20	-	MARN
07-03-17	N	0	50	0.2	54960	47050	1000	17.0	292	1240	2580	651	6000	213	264130	0.86	0.01	MARN
13-06-17	N	0	58	-0.01	71620	41210	1490	16.7	1531	3470	3320	766	8020	319	263500	0.58	0.02	MARN

CHAPTER 6

EXPLORING THE COMPOSITIONAL VARIABILITY OF VOLCANIC LAKE PLUMES

6.1. INTRODUCTION

In this chapter, we will investigate the compositional range (CO_2, SO_2, H_2S, H_2 and H_2O) of gas plumes emitted by different acidic volcanic lakes. We attempt at understanding the relationships between lake gas composition and lake water chemistry, especially pH and dissolved Cl and SO_4 contents (taken as proxies for volatile inputs originating from the deep system). We also analyse the influence of water temperature on lake gas composition. Finally, we infer the relation between the composition of the gas feeding the lakes at the bottom and the gas discharges at the lake surface.

In order to achieve these aims, we review an extensive lake gas dataset we assembled by combining together gas observations taken at El Chichón (Mexico; Chapter 4), Víti (Iceland; Chapter 4), Santa Ana (El Salvador, Chapter 5) and Vasca degli Ippopotami (Vulcano Island, Italy, this Chapter) with measurements made (from partner researchers travelling/working abroad) at Ruapehu (New Zealand, measured by B. Christenson), Frying Pan Lake and Inferno Lake, (Waimangu, New Zealand, measured by G. Giudice and M. Liuzzo), Champagne Pool and Oyster Pool (Waiotapu, New Zealand, measured by G. Giudice and M. Liuzzo), Yugama (Japan, measured by T. Ohba), Main Crater Lake (Taal volcano, Philippines, measured by K .Maussen and A. Bernard), East Lake (Newberry volcano, USA; measured by A. Aiuppa). We also complete the dataset with unpublished gas results from Kaba (Indonesia, P. Bani), Kawah Ijen (Indonesia; A. Aiuppa) and Rincón de la Vieja (Costa Rica; A. Battaglia, Phd Thesis), and published gas data from Boiling Lake (Dominica; Di Napoli et al., 2013), Copahue (Argentina; Tamburello et al., 2015), Kawah Ijen and Sirung (Indonesia; Bani et al., 2017; Gunawan et al., 2016), Poás (Costa Rica; de Moor et al., 2016b), Ruapehu (New
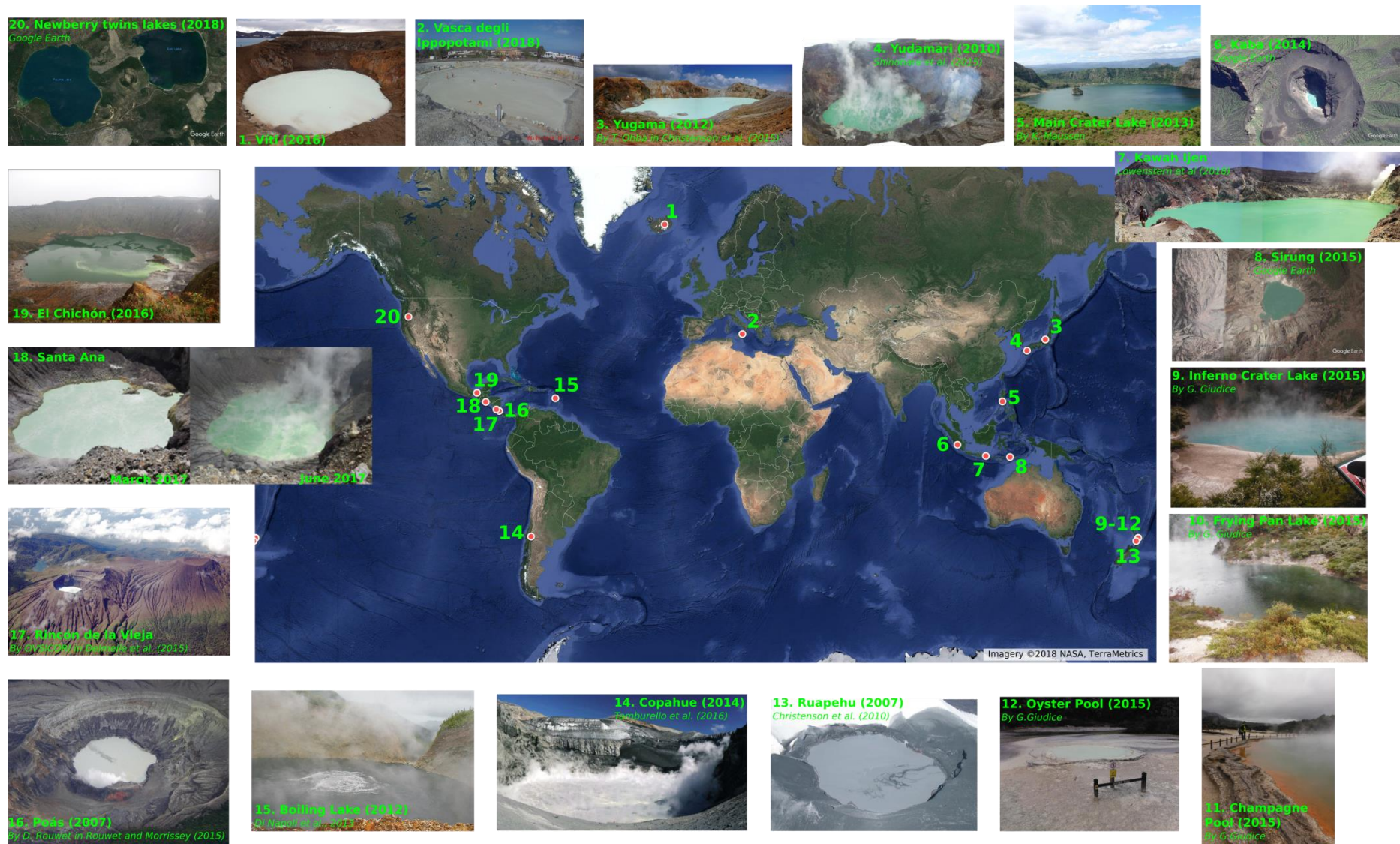
Figure 6.1 - Location of the volcanic lakes presented in this chapter. World Map from Google MyMAPS

Zealand, Christenson et al., 2010), Vasca degli Ippopotami (Vulcano, Italy; Mazor et al., 1988; Capaccioni et al., 2001) and Yudamari (Japan, Shinohara et al., 2015, 2018).

Water chemistry can change fast depending of the variation of fluids input/outputs (Chapter 1). Therefore, in order to establish the possible relationship between lake gas composition –arguably reacting even faster than water chemistry – and water chemistry, we attempt at using data sampled the most closely in time to gas measurements.

6.2. BRIEF OVERVIEW OF GEOLOGICAL, VOLCANOLOGICAL AND LIMNOLOGICAL SETTINGS

6.2.1. Asia

6.2.1.1. Main Crater Lake (Taal volcano, Philippines)

Taal volcano (14°00'N, 120°59'E, 311m a.s.l.) is located on the southwestern sector of Luzon Island (Philippines; Figure 6.1 and 6.2a). It is one of the most active (33 eruptions since 1572; Reyes et al., 2017) and dangerous (Torres et al., 1995; Zlotnicki et al., 2009) volcanoes in the country. The last eruptive cycle occurred from 1965 to 1977 (Zlotnicki et al., 2009). Since then, several unrests occurred (e.g. in 1994-1995; 1999-2000; 2010-2011) that did not lead to an eruption (Maussen et al., 2018).

Taal volcano is situated at the intersection of the Macolod corridor (a pull-apart basin oriented NE-SW; Defant et al., 1988; Förster et al., 1990) and the Bataan-Mindoro arc (Cardwell et al., 1980; Delmelle et al., 1998). Its volcanic activity is associated with the subduction, along the Manila Trench, of the South China Sea plate under the Philippine Archipelago (Hamburger et al., 1983; Figure 6.2a).

The active complex (Taal Volcano Island, TVI, 6 km diameter) is hosted in a large caldera (25 x 30 m) filled with freshwater (Lake Taal; Figure 6.2b). A large hydrothermal system manifests at the surface of TVI as hot springs, geysers and an acid crater lake (Main Crater Lake, MCL; Maussen et al., 2018). MCL is a hot (30-33°C) and acid (pH 2-3) crater lake rich in Na and Cl (Delmelle et al.,

1998; Maussen et al., 2018). The lake is about 75 m deep and is well mixed (inferred by constant conductivity and temperature along the vertical profile; Maussen et al., 2018). Maussen et al. (2018) identified two fluid components, a first sulfate-rich and acidic and a second Na-K-Cl-rich and neutral. These mix together to define the MCL composition. Maussen et al. (2018) also suggested the presence of H_2S in MCL waters, due to its requirement for the creation of acid sulfate waters (steam heated lake), pyrite formation in the sediments, and the smelling bubbles at the lake surface.
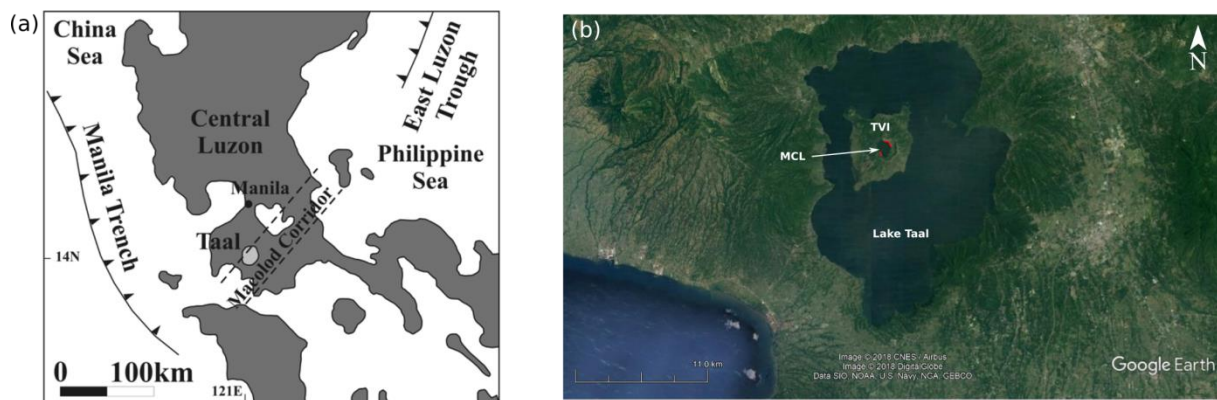
Figure 6.2 - (a) Location of Taal Volcano and tectonic settings of the region (Hernández et al., 2017). (b) Location of Taal active volcanic complex (TVI, Taal Volcanic Island) and crater lake (MCL, Main Crater Lake) inside the large caldera filled by Lake Taal (Google Earth, 2018)

6.2.1.2. Kawah Ijen (Indonesia)

Kawah Ijen volcano (8°03'S, 114°14'E, elevation 2769 m a.s.l.) is part of the Kawah Ijen volcanic complex, located in the eastern side of Java island (Indonesia; Figure 6.3). It is an active stratovolcano (11 eruptive periods since 600 BC; Caudron et al., 2015a,b; GPV, 2018) composed of basaltic to dacitic rocks (van Hinsberg et al., 2017). The last magmatic eruption occurred in 1817 whereas the last phreatic activity took place in 2010-2012 (Kemmerling 1921; Caudron et al., 2015a). Kawah Ijen is located along a structural margin of the 20 km-wide Kawah Ijen caldera (Handley et al., 2007; van Hinsberg et al., 2010). Volcanism is related to the Sunda volcanic arc (Hall et al., 2011; Figure 6.3).

A hyperacidic lake (1000×600 m, 30 Mm³, ~200 m deep; Takano et al., 2004; Caudron et al., 2015b; Gunawan et al., 2016) fills the volcano's summit crater (Figure 6.1) and is the largest natural reservoir of hyperacidic brine on Earth. The lake water has a pH~0, T~38°C and is highly concentrated (e.g. Delmelle and Bernard, 1994, 2000; Gunawan et al., 2016; van Hinsberg et al.,

2017). A high temperature (<450°C; Gunawan et al., 2016) fumarolic field is present on the silicic dome, east of the lake.
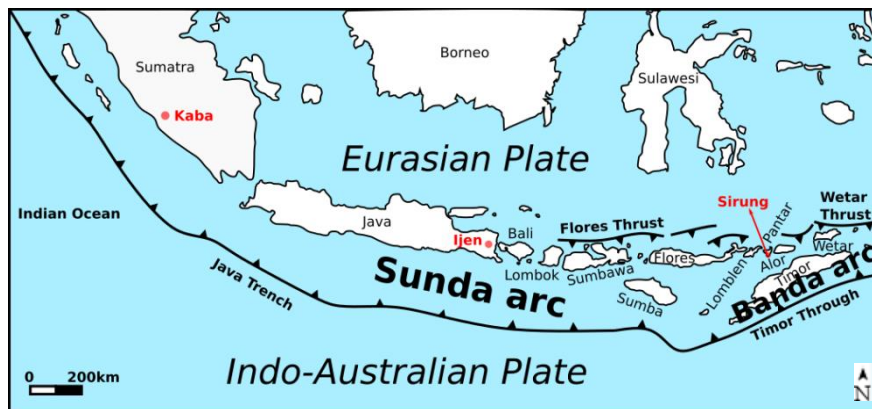
Figure 6.3 - Tectonic settings of Indonesia with location (red spots) of Kaba, Kawah Ijen and Sirung volcanoes (modified from Bani et al., 2017 and Vigouroux et al., 2012).

6.2.1.3. Kaba (Indonesia)

Kaba volcano (3°30'S, 102°37'E; elevation 1940 m a.s.l.) is located in the SW of Sumatra island (Indonesia; Figure 6.3). This stratovolcano last erupted in 2000 (33 eruptions have been reported since 1833; GPV, 2018). Rocks are andesitic to basaltic-andesite in composition (GVP, 2018).

The volcanic complex is composed of three craters aligned ENE-WSW (Figure 6.4). The central crater hosts a poorly studied acidic lake (Figure 6.4). The lake water is hot (45°C in 1971 and 34°C in 1978, 72°C on October 15, 2009). The pH was 3.24, last measured on October 15, 2009 (GVP, 2018).

Figure 6.4 – Satellite view of Kaba volcanic complex and its three main craters (Google Earth, 2018).

6.2.1.4. Sirung (Indonesia)

Sirung stratovolcano (8°29'S, 124°07'E, 862 m a.s.l.) is located on the southern part of Pantar Island (Western Timor, Indonesia; Figure 6.3). It is an andesitic volcanic complex poorly studied due to its remoteness. Since 1852, at least 12 eruptions (mostly phreatic) have been reported (Bani et al., 2017). It is part of the eastern Sunda-Banda arc (Figure 6.3) which is related to the subduction of the Australian plate underneath the Eurasian plate (Vroon et al., 1993).

The volcano summit consists of 2 km-wide caldera which hosted in 2015 a main crater lake (Figures 6.1 and 6.5), bubbling mud pools, more than 4 fumarolic fields on the SW part, a 100 m-wide gas vent (sub-crater B), SW of the main crater and thermal springs (Bani et al., 2017; Caudron et al., 2018; Figure 6.5). The craters are aligned NE-SW (Bani et al., 2017; Figure 6.5). The main crater lake (0.3 km² in 2015; Bani et al., 2017) is hot (35°C), hyperacidic (pH 0.1-0.2), concentrated, and contains acid sulfate chloride water (Bani et al., 2017; Caudron et al., 2018). Sulfur spherules are floating at the surface (Caudron et al., 2018).
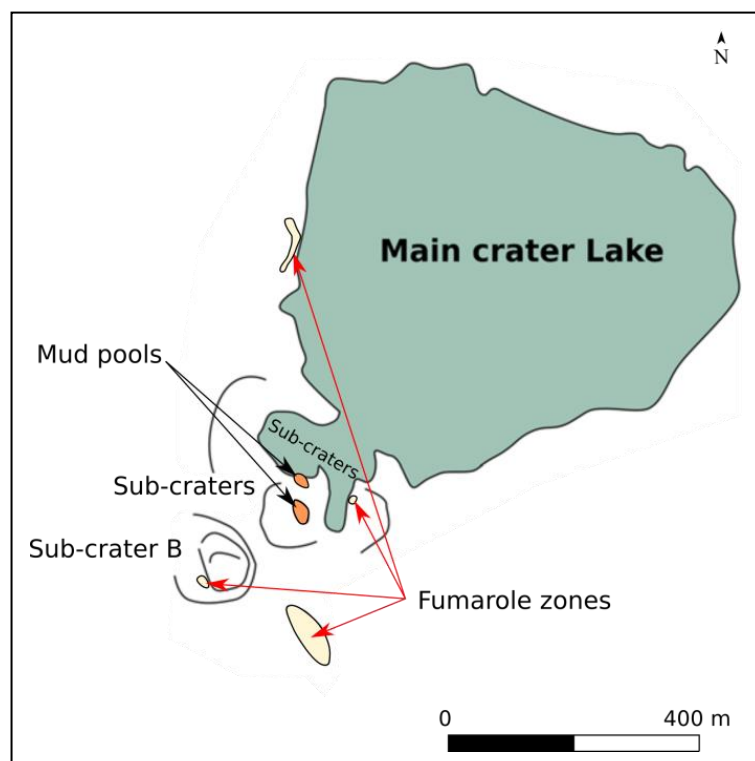
Figure 6.5 - Sirung volcanic complex in 2015 (modified from Bani et al., 2017)

6.2.1.5. Yudamari (Nakadake cone, Aso volcano, Japan)

Aso volcano (32°53'N, 131°05'E, 1592 m a.s.l.) is located in the center of Kyushu island (South Japan; Figure 6.6). It is an active arc volcano (Figure 6.6) with 185 eruptions reported in the Holocene (GVP, 2018), mostly taking place in the basalt to basaltic-andesitic Nakadake stratocone (Shinohara et al., 2015). The last eruptions occurred in 2014-2016 (GVP, 2018).

The Nakadake stratocone contains the Yudamari crater lake (Shinohara et al., 2015; Figure 6.1). This is a hot (40-80°C) and acidic (pH -1 to +1) lake (Ohsawa, 2003; Miyabuchi and Terada, 2009; Ohsawa et al., 2010) fed by a large volcanic gas input (Shinohara et al., 2015). Kanda et al. (2008) have suggested the presence of a hydrothermal fluid reservoir a few hundred meters below the crater lake. A close relation between eruptive activity and changes in Yudamari crater lake activity has been established (Ono et al., 1995; Sudo et al., 2006). The lake level varied dynamically through time; during high level, the lake water volume ranged from 2 to 8 x 10^5 m³ (Saito et al., 2008; Terada et al., 2008). A high temperature fumarolic field is located on the southern wall of the crater (Shinohara et al., 2015), degassing in a thermally isolated manner with respect to the lake (similar as happened prior to the October 2005 Santa Ana eruption, object of study of this thesis).
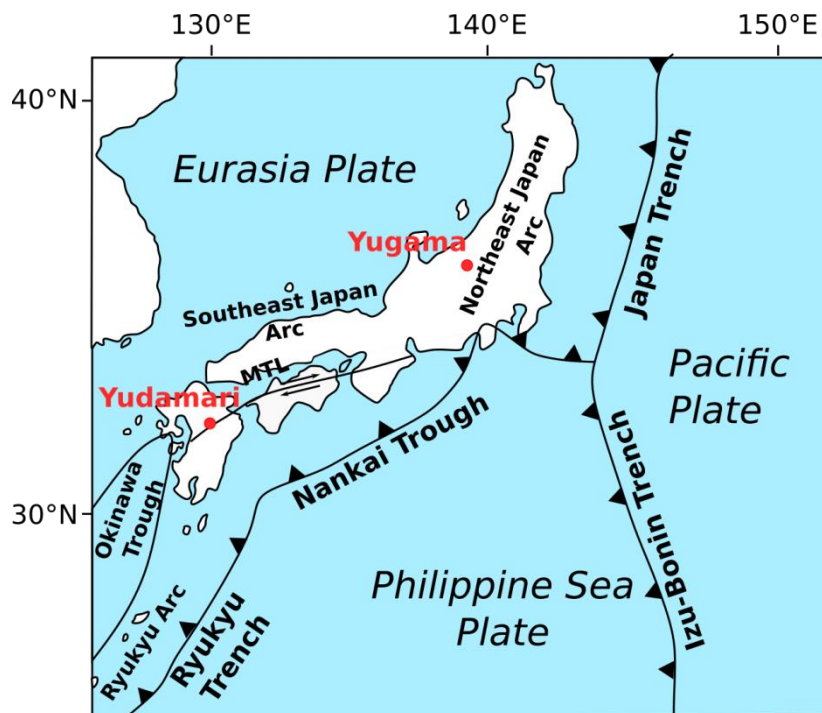
Figure 6.6 - General tectonic in Japan region and location of Yugama and Yudamari lakes. MTL is Median Tectonic Line (modfied from Kamata and Kodama, 1999)

6.2.1.6. Yugama (Yugama crater, Kusatsu-Shirane volcano, Japan)

Yugama crater (36°38'N, 138°32'E, 2165 m a.s.l.) is one of the craters of Mt. Kusatsu-Shirane volcano. It is located on Honshu Island (Japan) along the volcanic front (Sugimura, 1960; Figure 6.6). First historical activity was recorded in 1882 and was followed by frequent phreatic eruptions at Yugama crater lake (Minakami et al., 1943; Ossaka et al., 1980, 1997).

This crater hosts a hot and hyperacidic lake (pH ~1; Ohba et al., 2008; Terada et al., 2018; Figure 6.1), classified as high-activity crater lake. The average lake depth is 15 m and the diameter is 290m (Ohba et al., 1994). Hydrothermal circulation is well developed and characterized with a 200°C bi-phase reservoir (Ohba et al., 2000). An intense discharge of hot chloride-rich spring water occurs on the east flank of the volcano, 5 km from the summit (Ohba et al., 2000). A recent phreatic eruption occurred in January 2018, but not from the Yugama crater lake.

6.2.2. Europe

6.2.2.1. Víti (Askja volcano, Iceland)

See Chapter 4.

6.2.2.2. Vasca degli ippopotami (Vulcano Island, Italy)

Vasca degli Ippopotami (38°24'N, 14°57'E, 1 m a.s.l.) is located along the northern beach (Baia di Levante) of Vulcano Island (Aeolian Archipelago, Sicily, sourthern Italy), 2 km north of La Fossa Crater (391 m; Figure 6.7). Vulcano is an arc volcano (Barberi et al., 1974; Beccaluva et al., 1985) which last erupted from August 1888 to March 1890 (Mercalli and Silvestri, 1888; Silvestri and Mercalli, 1891).

Nowadays, fumarolic activity concentrates on the northern part of the La Fossa crater (rim and inner slopes, with temperatures up to 400°C; Aiuppa et al., 2005a), and along the Baia di Levante beach (T <100°C, Chiodini, 1991), the seashore near Vasca degli Ippopotami. Both are believed to be

fed by a common magmatic fluid source (Martini et al., 1980; Cioni and D'Amore, 1984; Mazor et al., 1988; Chiodini et al., 1991, 1995; Paonita et al., 2013).

Vasca degli Ippopotami is a small (15x25 m; Mazor et al., 1988) and shallow pond (<1 m). Many subaquatic fumaroles (T~90°C) are covered by the pond and visible at the surface as bubbling. The pond is used by tourists to take mud baths. Variations in water chemistry are partially due to occasional cleaning of the pond (Mazor et al., 1988) but the pond is always highly acidic (1.5-2.1, Mazor et al., 1988) and the water is of Na-SO$_4$-Cl composition (Mazor et al., 1988).

Figure 6.7 - Satellite view of Vulcano Island with the location of the active crater, La Fossa and Vasca degli Ippopotami Pond (Google Earth, 2018).

6.2.3. Central America

6.2.3.1. Santa Ana (El Salvador)

See Chapter 5.

6.2.3.2. Laguna Caliente (Poás Volcano, Costa Rica)

Poás volcano (10°12'N, 84°13'; 2708 m a.s.l.; Figure 6.1) is located in the centre of Costa Rica (Figure 6.8). It is part of the Central American Volcanic Arc (CAVA), formed by the subduction of the Cocos Plate underneath the Caribbean Plate (Carr et al., 2003; Husen et al., 2003; Johnston and

Thorkelston, 1997; Figure 6.8). Poás is part of the Quaternary Cordillera Central together with Turrialba, Irazú, Barva and Platanar-Porvenir (Rowe et al., 1992a). These stratovolcanoes exhibit compositions varying from basaltic to dacitic (Castillo, 1984). Poás is a frequently active volcano with 59 eruptions reported during the Holocene (Casertano et al., 1983; GVP, 2018). The last occurred in April 2017 and expelled the crater lake. Poás eruptive activity is mainly phreatic and rarely phreato-magmatic (Krushensky and Escalante, 1967; Casertano et al., 1983; de Moor et al., 2016b; GVP, 2018).

The summit of the volcano is composed of three cones oriented NS (Von Frantzius, Active Crater and Botos; Tassi et al., 2009). Poás Active Crater hosts a hot (~50°C; de Moor et al., 2016b) and hyperacidic (pH~0; de Moor et al., 2016b) lake, Laguna Caliente. The lake has a maximal depth of 55 m and diameter about 300 m (Rowe et al. 1992b). The physico-chemical characteristics of the lake have varied strongly in time depending on the seismic activity, thermal output and precipitation (Brown et al., 1989: Rowe et al., 1992a, b; Rouwet et al., 2017). A fumarolic field is located on the southern edge of the lake (Casertano et al., 1983, 1987; Rowe et al., 1992a b; Vaselli et al., 2003; Tassi et al., 2009; Fischer et al., 2015).
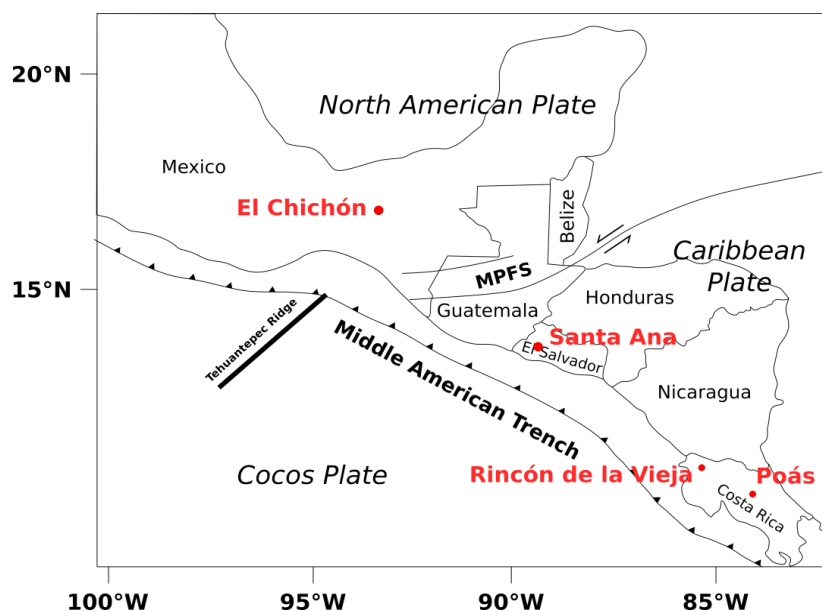
Figure 6.8 - Tectonic settings of North and Central America. MPFS is Motagua-Polochic Fault System (modified from Carr et al., 2003; Tassi et al., 2009 and Casas et al., 2016). The red dots indicated the emplacement of El Chichón, Santa Ana, Rincón de la Vieja and Poás volcanoes.

6.2.3.3. Rincón de la Vieja (Costa Rica)

The Rincón de la Vieja volcanic complex (10°49'N, 85°20'W, 1916 m a.s.l.) is an active basaltic-andesitic stratovolcano located in NW Costa Rica (Kempter et al., 1996; Figure 6.8). It is part of the Guanacaste Volcanic Range that is related to the subduction of the Cocos plate along the Middle American Trench (Carr, 1984; Johnstone and Thorkelson, 1997; DeMets et al., 2001; Figure 6.8). Since 1851, the frequent volcanic activity is mostly phreatic to phreatomagmatic (Boudon et al., 1996; Battaglia et al., submitted).

Seven nested craters, oriented NW-SE, compose the summit of the volcano (Boudon et al., 1996; Kempter et al., 1996; Tassi et al., 2009). Thermal fluid manifestations include a hyperacidic lake (in the Active Crater; Figure 6.1), numerous thermal springs, mud pools, boiling pools and gas discharges (Tassi et al., 2005). The hyperacidic lake is hot (31-47°C; Tassi et al., 2005) and has a high TDS (up to 154,216 mg/L). It is directly fed by magmatic, poorly processed, fluids (Tassi et al., 2005).

6.2.4. Southern America

6.2.4.1. Copahue (Argentina)

Copahue volcano (37.53°S, 71.10°W, 2997 m a.s.l.) is located at the border between Chile and Argentina (Figure 6.9). It is an active (17 eruptions, mostly phreatic, in recent history; GVP, 2018) strato-volcano of the Southern Volcanic Zone (Stern, 2004). It is situated on the SW margin of the Caviahue Caldera (formed 2 Ma years ago; Bermúdez and Delpino, 1995; Ramos and Folguera, 2000; Melnick et al., 2006; Varekamp et al., 2006; Vera et al., 2010; Sruoga and Consoli, 2011).

The volcano hosts a hot (63°C in 2014) and hyperacidic (pH< 0.5) crater lake (300 m diameter; Tamburello et al., 2015). Hydrothermal manifestations include hot springs, boiling pools, bubbling pools and mud pools (Mas et al., 1996, 2000; Agusto et al., 2013; Tamburello et al., 2015). The volcano erupted in 2012 and in March 2013, when the crater was emptied. In March 2014, the lake had reappeared but no bubbling activity was visible, instead, vigorous degassing was obvious (Tamburello et al., 2015). Eruptions have continued, though irregularly, by the time of writing.
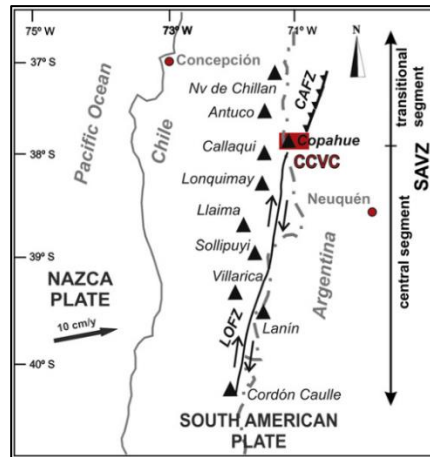
Figure 6.9 - Simplified map showing the main tectonic and active volcanoes of a part (central and transitional segment) of the Southern Andean Volcanic Zone (SAVZ) (Agusto et al., 2013). CCVC is Caviahue-Copahue Volcanic Complex; LOFZ is Liquiñe-Ofqui fault zone; CAFZ is Copahue-Antiñir fault zone.

6.2.5. North America

6.2.5.1. El Chichón (Mexico)

See Chapter 4

6.2.5.2. East Lake (Newberry Volcano, USA)

Newberry Volcano (43°43'N, 121°13'W, 2434 m a.s.l.) is located in Oregon, USA (Figure 6.1 and 6.10). It is situated on the east side of Cascade Range (MacLeod and Sherrod, 1988) and was active during the Holocene (25 eruptions; MacLeod and Sherrod, 1988). The last eruption occurred 1.3 ka ago (Sherrod et al., 1997). The 8-km summit caldera hosts two twins crater lakes, Paulina Lake on the west side and East Lake on the east side separated by a 2-km wide volcanic ridge (Figure 6.1 and 6.10).

An active hydrothermal system is present in the volcano, manifested at the surface as hot springs along lakes shores and fumaroles (Forcella, 1982; Lefkowitz, 2012) suggesting the existence of hot magma at depth (Forcella, 1982; Ingebritsen et al., 2014). East lake (1945m a.s.l.) has a surface area of 4.2 km², a maximum depth of 55 m (average 20m) and a volume of $86 \cdot 10^6$ m³ (Johnson, 1985). Lefkowitz et al. (2017) suggested that rain water is the main water recharge at East Lake. It is a dimictic lake that freezes in winter (Morgan et al., 1997). The pH is around 7.8 in winter and from 6.5 (bottom) to 8.3 (surface) in summer (Lefkowitz et al., 2017). The deep water has a temperature of 4-

5°C whereas the surface water can reach 20°C in summer (Lefkowitz et al., 2017). The lake turns over in spring and is thermally stratified (Lefkowitz et al., 2017). The lake is classified as carbonate-rich, and CO_2-rich bubbles are injected into the lake, probably carrying some H_2S as well (Lefkowitz et al., 2017).
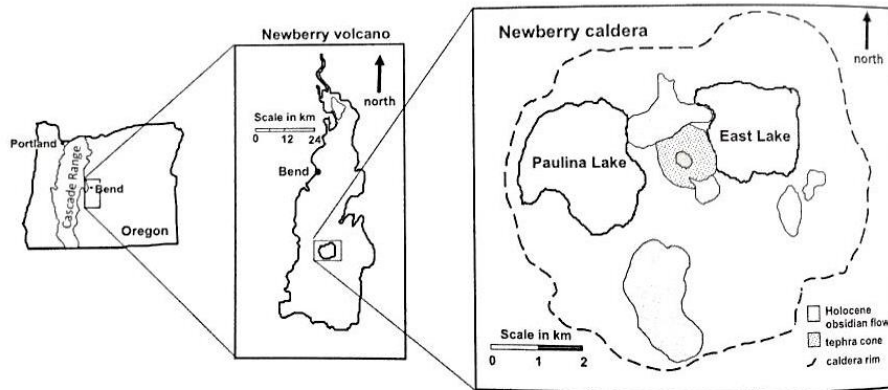
Figure 6.10 - Geographical location of Newberry Volcano and detailled view of the caldera composed of the twins lakes, Paulina Lake and East Lake (Lefkowitz et al., 2017)

6.2.5.3. Boiling Lake

Boiling Lake (15°19'N, 61°17'W, 800 m a.s.l.) is located in SE Dominica (West Indies), in the so-called Valley of Desolation (Di Napoli et al., 2013; Figure 6.1 and 6.11). Dominica is part of the Lesser Antilles volcanic arc (Wadge, 1984), resulting from the subduction of the American Plate underneath the Caribbean Plate (Maury et al., 1990; Dixon et al., 1998; DeMets et al., 2000; Figure 6.11). On the island, rock compositions range from basalts (Miocene to Pliocene) to andesites-dacites (Pleistocene to Recent; Roobol and Smith, 2005). No magmatic eruption has been reported in historical times on the island, but phreatic explosions occurred recently in the Boiling Lake/Valley of Desolation area in 1880 (Nicholls, 1880a, b) and in 1997 (Di Napoli et al., 2013). In addition, in 1901, the Boiling Lake was the theatre of a CO_2-gas burst event (Elliot, 1938; Bell, 1946).

Many hydrothermal manifestations are present all over the island, such as fumaroles, hot springs and bubbling pools (Joseph et al., 2011, and reference therein). The most impressive is the hot (80-90°C) and acidic (pH, 4-6) volcanic lake Boiling Lake, in the SE part of the island (Fournier et al.,

2009; Di Napoli et al., 2013; Rouwet and Morrissey, 2015). In that part of the island, ascent of CO_2-H_2S rich hydrothermal fluids gives rise to widespread steam-heated meteoric waters.

Boiling Lake is the second largest boiling lake in the world (~10^4 m³; Fournier et al., 2009) after Frying Pan Lake (New Zealand; Vandemeulebrouck et al., 2008). It has a diameter of 50 m and a depth of 15 m (Fournier et al., 2009). It is vigorously discharging gases and steam at its centre (Di Napoli et al., 2013). Water chemistry and isotopic composition have been reported by Pedroni et al. (1999) and Joseph et al. (2011). The lake alternates steady-state periods (T~80-90°C, pH 4-6, TDS up to 14000ppm, Na-Cl(SO$_4$) waters and vigorous gas upwelling at the centre; Joseph et al., 2011) with emptying events, associated with the cessation of the steam input, lower temperature (<20°C), and neutral low-Cl low-SO$_4$ waters (Fournier et al., 2009; Rouwet and Morrissey, 2015).

Figure 6.11 - Main tectonic settings of the Lesser Antilles arc region and location of Boiling Lake (red dot; modified from Di Napoli et al., 2013).

6.2.6. Oceania

6.2.6.1. Ruapehu, Waimangu and Wai-O-Tapu (New Zealand)

6.2.6.1.1.   Tectonic setting of New Zealand

Ruapehu volcano, Waimangu and Wai-O-Tapu geothermal systems are part of the Taupo Volcanic Zone (TVZ; Dibble, 1974) and are located in the North Island of New Zealand (Figure 6.12). The TVZ extends 300 km in a SW-NE direction, parallel to the Hikurangi Margin along which the Pacific plate subducts beneath the Australian Plate (Hurst et al., 1994) (Figure 6.12). Ruapehu (39°16'S, 175°33'E) is located at the south-western end of the zone (andesitic volcanism) whereas the Waimangu and Wai-O-tapu geothermal systems are located at the centre (rhyolitic volcanism; Figure 6.12).

6.2.6.1.2.   Ruapehu

Ruapehu (39°16'S, 175°33'E) is an andesitic volcano which erupted frequently during the last century, in 1945, 1969, 1972, 1976, 1978, 1982, 1988, 1995, 1996 (Christenson and Wood, 1993; Werner et al., 2006). Most of the eruptions were phreatic or phreatomagmatic (Werner et al., 2006). Ruapehu volcano and its Crater Lake have regularly been investigated since 1970 (Dibble, 1974; Giggenbach, 1974; Giggenbach and Glover, 1975; Hurst, 1986; Hurst et al., 1991; Christenson and Wood, 1993; Hurst and Sherburn, 1993; Takano et al., 1994; Hurst and Vandemeulebrouck, 1996;
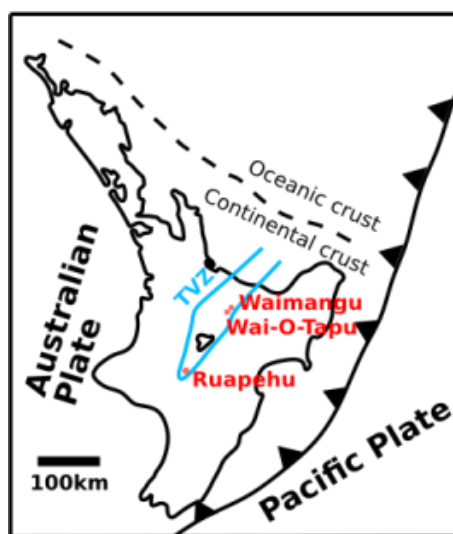
Figure 6.12 - North Island (New Zealand) simplified tectonic map (modified from Cole et al., 2014) with the location of Ruapehu volcano and the Waimangu and Wai-O-Tapu geothermal fields (red dots). TVZ is Taupo Volcanic Zone.

Christenson, 2000; Werner et al., 2006; Christenson et al., 2010). The lake is <50 m deep in its shallowest part, and deepens in correspondence of two sub-aquatic vents (up to 267 m in 1966; Dibble, 1974 and 80 m in 1970; Irwin, 1972; 180 m in 1982; Nairn et al., 1982). The lake surface temperature is spatially constant (±1°C) (Hurst et al., 1991). The quiescent activity state (after 1979) of the Crater Lake is characterized by fluctuations in lake temperature (Werner et al., 2006), with long periods of decreasing temperature followed by sudden temperature increases that never culminated into an eruption. Contrarily, phreatic eruptions at Ruapehu are often "blue sky events", occurring during apparent periods of quiescence (e.g. low lake water temperature and no medium-term chemical precursory signals, September 2007 eruption) (Christenson et al., 2010; Jolly et al., 2010). Lake chemistry (main ions and polythionates) at different depths and locations suggested that the lake water is well mixed (Takano et al., 1994; Giggenbach, 1974; Christenson et al., 1992; Hurst et al., 1991). Heat is transfered to the lake by a heat pipe (Hurst et al., 1991), a conceptual model that is revised by Christenson et al. (2010).

6.2.6.1.3. Inferno Crater Lake and Frying Pan Lake (Waimangu)

The Waimangu geothermal field was formed by the 1886 eruption of Mt Tarawera (Keam, 1988; Hunt et al., 1994) and is characterised by numerous hot acid-sulfate lakes, boiling springs, sinter terraces and crater lakes (Hunt et al., 1994). The Inferno Crater Lake is located in a crater formed by the eruption of Mount Tarawera in 1886 (Glover et al., 1994). Frying Pan Lake sits in the Echo Crater formed in 1917 (Glover et al., 1994).

The Inferno Crater Lake (38°16'S, 176°23'E; 28 m depth; 110×80 m; 7500 m² at maximum; Glover et al., 1994) is hot (37-84°C; Hunt et al., 1994) and contains acid chloride-sulfate water (Hunt et al., 1994). Its low pH (2-4) is due to H_2S oxidation (Mahon, 1965; Glover, 1968; Sheppard, 1986; Keywood and Nicholson, 1990; Balmes, 1991; Glover et al., 1994). The volume of Inferno varied from 45600 m³ to 65200 m³ (Glover et al., 1994). Many geochemical characterisations of Inferno Crater Lake have been done (Mahon, 1965; Sheppard, 1986; Balmes, 1991; Keywood, 1991).

Frying Pan Lake (38°17S, 176°23'E; 200 000 m³; Glover et al., 1994) is acidic (pH 2-4, same acidity origin as Inferno Crater lake) and hot (45-55°C; Hunt et al., 1994), and contains alkali-chloride waters (Hunt et al., 1994). It is the largest hot pool of the world (38000 m²; Glover et al., 1994; Vandemeulebrouck et al., 2008).

Both lakes exhibit cyclic flow behaviour (Lloyd, 1974; Glover et al., 1994). At both lakes, Cl concentrations do not fluctuate with time (over 1992-1993; Glover et al., 1994). SO_4 has remained constant at Frying Pan Lake, while it varied cyclically at Inferno Crater Lake (Glover et al., 1994).

6.2.6.1.4.   Champagne Pool and Oyster Pool (Wai-O-Tapu)

The Wai-O-Tapu geothermal system includes boiling springs, steaming grounds, geysers, mud volcanoes, fumaroles and sinter terraces (Hunt et al., 1994). The lakes we studied in this area are Champagne Pool and Oyster Pool.

Champagne Pool (38°21'S, 176°22'E) is hot (~75°C; Pope and Brown, 2014) and slightly acidic (pH ~5.5 due to CO_2 addition; Pope and Brown, 2014). The pool is large (2000 m²; Hunt et al., 1994) and contains sulfate-chloride waters. Sulfate originates from H_2S oxidation (Hunt et al; 1994). At Champagne Pool, water chemistry changes are linked to changes in the gas flow entering the lake (Hedenquist, 1983).

Less data are available for Oyster Pool (38°21'S, 176°22'E). This is a hot (60-70°C) and acidic (pH ~5; Pope and Brown, 2014) pool filled with sulfate-chloride waters (Pope and Brown, 2014). Cl concentrations at Champagne Pool and Oyster Pool (~2000 and 700-800 mg/L, respectively) have shown little variation over the last 20 to 80 years (Pope and Brown, 2014).

6.3.   OVERVIEW ON THE COMPOSITION OF LAKE GAS PLUMES

6.3.1. Plumes from hyper-acidic lakes

6.3.1.1. Kawah Ijen (data from Gunawan et al., 2016)

Lake and fumaroles gas composition at Kawah Ijen were determined with a Multi-GAS instrument during a period of quiescence (Caudron et al., 2015a; Gunawan et al., 2016) in September 2014 (Gunawan et al., 2016 and Aiuppa pers. comm.), i.e. two years after the 2011-2012 volcanic crisis (Caudron et al., 2015a, b), and a few months after an increase in activity on May, 6-7, 2014 (increase in tremor, lake bubbling and upwelling; Gunawan et al., 2016). During the investigations, the temperature of the fumarolic field was high (up to 450°C; Gunawan et al., 2016). The lake surface temperature varied between 21 and 28 °C (Caudron et al., 2017). Bubbling water was visible at the edge of the lake, which was strongly evaporating (Gunawan et al., 2016).

The fumarolic plume was characterized by low CO_2/S_{tot} ratios (2.27 ± 0.19), the dominant sulfur species being SO_2 (H_2S/SO_2=0.50 ± 0.05). H_2O/CO_2 ratios (16.5 ± 1.8) were poorly constrained because H_2O was detected at concentration slightly above the background. At Kawah Ijen, fumarolic H_2S/SO_2 ratios are thought to be more influenced by H_2S combustion at high temperature into the atmosphere (strongly temperature-dependent) than by injection of a new magma. In addition, fumarolic H_2S/SO_2 ratios are also affected by precipitation of native sulfur that, by primarily removing $H_2S_{(g)}$, can modify sulfur speciation and redox conditions of the gas phase (Christenson et al., 2010; Gunawan et al., 2016).

Lake gases were composed of H_2O, SO_2 and CO_2, while H_2S was absent. The H_2O/CO_2 and CO_2/SO_2 ratios were assessed at 55±5 and 90±10, respectively (Gunawan et al., 2016). The same authors also detected lower CO_2/SO_2 ratios (e.g. 38±3 on September 17 during 25 min, without detection of H_2S which could indicate a fumarolic contamination). They suggested that excess SO_2 could be periodically released from the lake.

6.3.1.2. Copahue (data from Tamburello et al., 2015)

Tamburello et al. (2015) measured gas composition in March 2013 (direct fumarolic gas sampling) and March 2014 (Multi-GAS measurements of lake gases). The volcano erupted in 2012 and no lake was present between December 2012 and April 2013. In March 2014, the lake had reappeared but no bubbling activity was visible (the lake appeared to release gas in diffuse form; Tamburello et al., 2015) while sulfur was floating at the lake surface. A shallow magma body (~5km below the summit craters; Vélez et al., 2011) is thought to supply fluids at the lake bottom (Varekamp, 2004).

Fumarolic gases (431 and 102°C) were composed of H_2O, CO_2, SO_2, HCl, H_2S, HF and H_2 (Tamburello et al., 2015). Fumarolic gas ratios in Table S2, S3 (Appendix) are calculated from the chemical composition of direct gas sampling analyses. The ranges in gas ratios were 13-19 (SO_2/H_2S), 4.5-7 (CO_2/SO_2), 57-125 (H_2O/SO_2) and 0.05-0.55 (H_2/SO_2).

The lake gas plume data composition was measured with a semi-permanent Multi-GAS installed at the crater rim (~100 m from the lake shore) for 5 days, and with a walking survey where gas was measured in air at 30 cm from the ground, starting at the lake shore and moving toward the crater rim (Tamburello et al., 2015). No significant variation in lake gas ratios was observed at the different measurement distances. The bulk lake plume composition was characterized by $CO_2/SO_2 = 0.97 \pm 0.3$, $H_2O/SO_2 = 340.87 \pm 14.7$ and $SO_2/H_2 = 0.11 \pm 0.05$. The lake plume had a H_2S/SO_2 ratio $< 10^{-3}$ (H_2S was below 0.1 ppm, the detection limit).

6.3.1.3. Poás (data from de Moor et al., 2016b, 2017)

de Moor et al. (2016b) used a fixed Multi-GAS installed at the east shore of the lake to determine lake gas composition. Measurements were taken between April and June 2014. This period was characterized by intense phreatic activity (14 eruptions were seismically registered during the time of the Multi-GAS measurements). Additional data were presented by de Moor et al. (2017). Surveys were also conducted to measure the dome fumarole (up to 800°C) gas composition.

During non-eruptive periods, the SO_2/CO_2 ratio was 0.88±0.12 and 2.28 in lake gas and fumaroles, respectively, whereas during eruptive phases the ratios were of 1.47±0.21 and 2.37, respectively. The H_2S/SO_2 ratio of fumaroles was on average 0.12. H_2S was not detected in the lake gas (<1ppm).

6.3.1.4. Sirung (data from Bani et al., 2017)

Gas was sampled in August 2015. Fumaroles (divided in four zones) were located on the south-western of the caldera, and degassing was also observed at the sub-crater B (which was not hosting a lake), and two mud-pools southwest of the main crater lake (Bani et al., 2017). Multi-GAS measurements were done by walking traverses through the main degassing areas.

The lake gas H_2S/SO_2 ratios were of 0.4 ± 0.1, similar to fumaroles (0.2-1.2). CO_2/SO_2 ratios of lake gas (8.0 ± 2.3) were higher than fumaroles (1.2-5.7). The low H_2S/SO_2 ratios (0.2-1.2) at Sirung point to a shallow magmatic gas source (Bani et al., 2017). Caudron et al. (2018) proposed a parent fluid with a SO_2/H_2S ratio around ~1 (as for Poás, Maly Semiachik, or Ruapehu; Marini et al., 2011)

6.3.1.5. Yudamari (data from Shinohara et al., 2015, 2018)

Gas composition was determined with a Multi-GAS from 2003 to 2014 (Shinohara et al., 2015, 2018). During this period, a magmatic eruption took place between November 27, 2014 and May 21, 2015 (Shinohara et al., 2018). The lake is permanently degassing (200 to 400 t/d of SO_2, Shinohara et al., 2015). The high-temperature fumaroles are located on the southern wall of the crater (Shinohara et al., 2015). Lake and fumaroles are suggested to be fed by a common magmatic source (Shinohara et al., 2015).

Between 2003 and 2009, the lake level was high (volume ranging from 2 to 8×10^5 m³; Saito et al., 2008; Terada et al., 2008). In 2004, 2005, 2010, 2011 and 2012, the lake level dropped a few times (Shinohara et al., 2015, 2018), and the lake nearly dried up at the end of 2013 (Shinohara et al., 2018). Fluids discharging into the lake originate from a shallow (few hundred meters below the crater) hydrothermal reservoir (Kanda et al., 2008).

High H_2 and SO_2 contents, typical for magmatic gas composition, were measured in fumarolic and lake gases (Shinohara et al., 2015). Between 2003 and 2014, the lake gas had CO_2/SO_2 ratios of 0.3-2.6, always lower than the contemporaneously measured fumarolic gas ratios (1.7-10) (Shinohara et al., 2015, 2018). Lake and fumarolic CO_2/SO_2 ratios varied inversely (with a mean values of 2). SO_2/H_2S ratios of lake gas (4.5-2000) were systematically larger (and more variable) than in fumarolic gas (5-30; common for high-temperature gas; Giggenbach, 1996), except during low lake volume periods, when lake and fumaroles exhibited similar ratios. When the lake volume was lower, SO_2/H_2S ratios of lake gas was low. Similar H_2/CO_2 ratios were measured in lake and fumarolic gases (Shinohara et al., 2015). H_2/SO_2 ratios varied from 0.01 to 0.34 in fumarolic gases and from 0.01 to 0.2 in lake gases.

6.3.1.6. Ruapehu (data from Christenson et al., 2010)

Gas ratios at Ruapehu were calculated from gas fluxes published in Christenson et al. (2010) as no direct Multi-GAS measurements exist. Ruapehu lake gases were SO_2-dominated (SO_2/H_2S 9.1-230 between 2004 and 2016). The CO_2/SO_2 ratios ranged between 2.9 and 179.

6.3.2. Plumes from H_2S-dominated lakes

6.3.2.1. Boiling Lake (data from Di Napoli et al., 2013)

Lake gas was characterized for the first time in late February 2012 (Di Napoli et al., 2013), and exhibited CO_2/H_2S ratios of 4.8-5.2 and H_2O/CO_2 ratios of 31 ± 6. Fumaroles in the nearby Valley of Desolation had average CO_2/H_2S and H_2O/CO_2 ratios of 5.7 of 20, respectively. No SO_2 was detected in lake gas, and fumaroles had a mean SO_2/H_2S ratio of 0.0002.

Di Napoli et al. (2013) modelled the gas composition obtained by evaporation/degassing at equilibrium from the dissolved gas in the lake water. The model results demonstrated a lake plume composition highly depleted in S, compared to the measured Multi-GAS compositions. The authors concluded that, at the Boiling Lake, the feeding gas bubbles rise so rapidly through the lake to undergo only minor scrubbing (by condensation or reaction). This hypothesis is also supported by the Boiling

Lake gas compositions being not too dissimilar from the magmatic gas signature of the Lesser Antilles arc (e.g. gas samples from Soufrière Hills in Montserrat).

6.3.2.2. Vasca Degli Ippopotami (data from this study)

Pond and shore fumarole gas composition was measured by Multi-GAS in April 2016 and June 2018. The main sulfur species in fumaroles was H_2S (SO_2/H_2S ratios of 0.008±0.005 and 0.009±0.001 in 2016 and 2018, respectively). In 2016, trace amounts of SO_2 were detected in the pond gas (H_2S/SO_2 ratios of 0.017 ± 0.008) and in bubbling gas, with the Multi-GAS kept floating above the water surface (H_2S/SO_2 ratios of 0.0006±0.0001).

Pond and fumarole CO_2/H_2S ratios remained relatively constant since 1982 (39.3-57.7 and 33.4-46.3, respectively; Mazor et al., 1998; Capaccioni et al., 2001; this study), while H_2/H_2S showed more variations (0.019-0.71 and 0.15-0.54, respectively; Mazor et al., 1998; Capaccioni et al., 2001; this study).

In 2018, we also performed a Multi-GAS survey in the La Fossa crater, and we measured SO_2/H_2S ratios of 4.8 ± 1.6, CO_2/H_2S ratios of 548 ±346 and H_2/H_2S ratios of 0.08 ± 0.02 (this being much higher than in the pond gases, 0.28 ± 0.06). We did not observe the H_2 enrichment in pond gases (relative to La Fossa fumaroles), as observed by Mazor et al. (1988).

6.3.2.3. Waimangu and Wai-O-Tapu (data from this study)

The atmospheric plumes of Wai-O-Tapu (Champagne Pool and Oyster Pool) and Waimangu (Frying Pan Lake and Inferno Crater Lake) were investigated in November and December 2015, respectively. Measurements were made with a Multi-GAS in the walking traverse mode (Aiuppa et al., 2005a).

Trace amounts of SO_2 were detected in emissions of Frying Pan Lake ($SO_2/H_2S = 0.03 ± 0.02$), Champagne Pool ($SO_2/H_2S = 0.01 ± 0.002$) and Oyster Pool (0.001 ± 0.0004). CO_2/H_2S ratios varied strongly between the lakes, Frying Pan Lake ($CO_2/H_2S = 161 ± 8$), Inferno Crater Lake ($CO_2/H_2S =$

1103 ± 289), Champagne Pool (CO_2/H_2S = 15.7 ± 0.8) and Oyster Pool (CO_2/H_2S = 14 ± 1). H_2/H_2S ratios varied from 0.04 ± 0.01 (Champagne Pool) to 0.1 ± 0.02 (Frying Pan Lake and Oyster Pool).

Since measurements were taken several meters downwind the lakes, it is problematic in this specific case if the tiny amounts of SO_2 detected in the lake plumes originated from either (i) reactions into the lakes (Hasselle et al., 2018) or (ii) from H_2S oxidation in air (Caponi et al., 2018).

6.3.2.4. Main Crater Lake (Taal volcano) (data from this study)

At the Main Crater Lake, lake gas plume composition was measured with the Multi-GAS (in July 2016) using a boat. In addition, the atmospheric plumes of mud pools, geyser and fumaroles were also investigated for their composition.

Lake plume gases had CO_2/H_2S (4792-9624) ratios higher than mud pools (155 ± 35), geysers (206 ± 53) and fumaroles (248 ± 113) gases. Lake plume H_2/H_2S (36.9-171) ratios were also higher than mud pool (0.27 ± 0.10), geyser (0.41 ± 0.15) and fumaroles (0.53 ± 0.23) gases.

Although the fumarole CO_2/H_2S ratios in 2016 were similar to those measured in 2009-2011 (310–478; Arpa et al., 2013), the SO_2/H_2S ratios were strongly different. The dominant sulfur species were H_2S in 2016 and 2019 (SO_2/H_2S of 0.0027 and 0.45, respectively) and SO_2 in 2010-2011 (SO_2/H_2S ratios 4.5 and 5.1, respectively; coinciding with a phase of unrest; Maussen et al., 2018). In 2016, SO_2 was also detected in trace amounts in mud pool gases, while it was below detection in the lake plume gas. Our detection of H_2S in the lake gas supported the earlier suggestions of Maussen et al. (2018).

6.3.2.5. East Lake (data from this study)

The bubbling southern shore of East Lake, and its adjacent fumaroles, were investigated for gas composition with the Multi-GAS in August 2017. Bubbling gases were only composed of CO_2 and H_2S. SO_2 and H_2 were not detected. Very tiny amounts of SO_2 were measured in fumarolic plumes (SO_2/H_2S of 0.007 ± 0.001). Both plumes (lake and fumarole) had similar CO_2/H_2S ratios (167 and 237, respectively).

6.3.2.6. **Yugama (data from this study)**

Lake plume and fumarole gas compositions were measured at Yugama in October 2016. Lake gas compositions were measured from the lake shore, and the fumaroles were measured in a geothermal area on the outer north flank of Yugama crater.

At both gas emissions, the dominant sulfur specie was H_2S. The SO_2/H_2S ratio was 0.15 ± 0.08 in lake gas, and 0.0015 ± 0.0004 in fumarolic gases. The CO_2/H_2S and H_2/H_2S ratios were higher in lake gas (220 ± 131 and 12.4 ± 4.3, respectively) than in fumaroles (6.1 ± 1.5 and 0.018 ± 0.006, respectively).

6.4. DISCUSSION

6.4.1. Synthesis of the observations

Active and quiescent lakes can be partially distinguished based on their SO_4+Cl contents (threshold of 3000mg/L; Varekamp et al., 2000). Broadly speaking, active lakes have a lower pH than quiescent lakes (Figure 1.3), and highly active ("peak lakes") are hyperacidic (pH<1).

Our dataset here (Table S2 and S3 in the Appendix), the first attempt to catalogue available gas information on the chemistry of plumes issuing from volcanic lakes, can now be explored to test if lake gas plume compositions can also be used to categorise volcanic lakes into active and quiescent. At this aim, we integrate the results described in section 3 in the scatter plots of Figures 6.13 to 6.16. These plots demonstrate that lake gas compositions define systematic compositional arrays, which in turn imply substantial communalities in the processes that drive/determine plumes issuing from degassing volcanic lakes on Earth.

In our dataset, the lake gas plumes are, logically, intrinsically and invariably H_2O-rich, but the steam/gas ratios (e.g., the gas plume H_2O/CO_2 ratios) systematically increase with lake water temperature (Figure 6.13). In low temperature lakes, water loss by diffusion/evaporation is limited. In high-temperature lakes, instead, increased lake evaporation, perhaps combined with less effective magmatic gas condensation (at least in case of vigorous gas jets rapidly transiting through the lakes),

lead to higher lake plume H_2O/CO_2 ratios, approaching the values measured in hydrothermal/magmatic fumaroles (Figure 6.13).
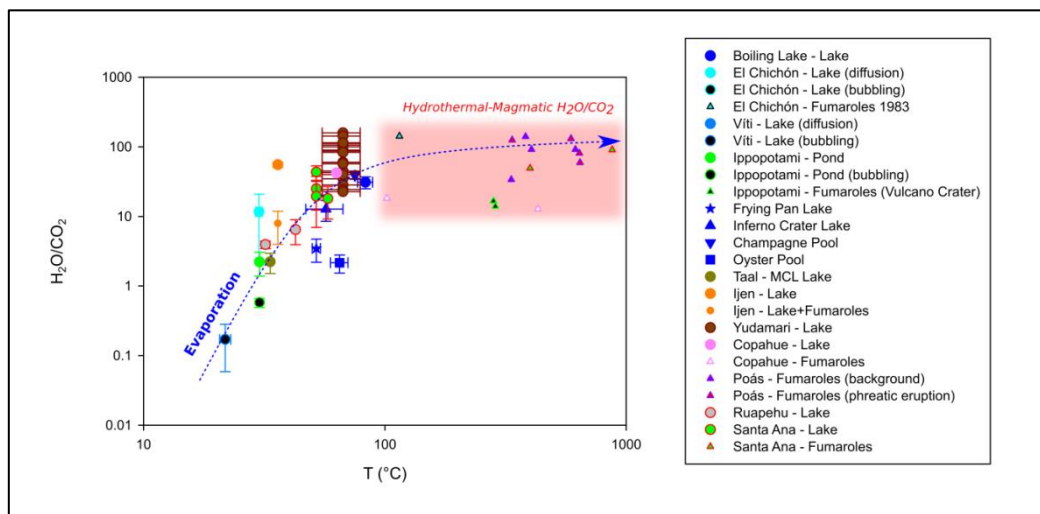
Figure 6.13 - Variations of the H_2O/CO_2 ratios in lake and fumarolic gases in function of temperature. Blue arrow shows the increasing evaporation; red area, the range of high-temperature H_2O/CO_2 ratios.

Secondly, we find that S speciation in volcanic lake gas plumes varies in systematic fashion (Figure 6.14). Our compilation shows that hyperacidic lakes, apart from being richer in SO_4+Cl (Figure 6.14a), are typically associated with plumes with SO_2/H_2S ratios > 1 (range, $1-10^5$), and are therefore SO_2 (magmatic)-dominated (Figure 6.14). In contrast, less acidic (pH 2-6) lakes emit plumes with SO_2/H_2S ratios < 1 (range, $10^{-4}-1$), i.e. they are H_2S (hydrothermal)-dominated (Figure 6.14). The plumes issuing from geothermal pools/lakes exhibit SO_2/H_2S ratios similar to medium-low activity lakes (e.g. El Chichón; Figures 14a, b). We conclude that lake gas plume SO_2/H_2S ratios allow gaining insights into the nature (magmatic vs. hydrothermal) of the sub-limnic feeding gas, and as such make a key proxy for identifying the state of activity of the volcanic lake system overall.

Thirdly, we also demonstrate that plumes from hyperacidic SO_2-dominated lakes systematically exhibit lower (more magmatic) CO_2/SO_2 ratios (range, 0.1s-100s) than H_2S-dominated lakes (range, 10^3-10^5) (Figures 6.14c and 6.15a-c). CO_2/SO_2 ratios in lake gas plumes are inversely correlated to H_2O/CO_2 ratios (Figure 6.15b) and positively correlated to H_2/SO_2 ratios (Figure 6.15c), implying that SO_2 release via lake surfaces can only happen in sizeable amounts at the condition that lakes are strongly heated by the feeding gas at the lake bottom, and that dissolution of otherwise reactive SO_2 is

132

hampered by fast gas transport and high gas flux (i.e. physical-kinetic, and non-chemical equilibrium process). In less active lakes, where gas dissolution (scrubbing) into lake water prevails, lake plumes are invariably SO_2-poor, and enriched in less water-soluble species (CO_2 and H_2). Copahue lake plume appears to be anomalously rich in H_2 (H_2/SO_2 of 9.1) compared to other SO_2-dominated lakes, characterized by a H_2/SO_2 gas ratios ranging from 0.01s to 2.3.

Similar "scrubbing" trends are obtained if total S (S_{tot}) (Figure 6.15d) or H_2S (Figure 6.15e) are used in place of SO_2. Hyperacidic lakes discharge plumes with the lowest CO_2/S_{tot} ratios (0.1s-100s), while the highest CO_2/S_{tot} ratios are observed in pH 2-3 lake gases (>1000). Geothermal lakes (pH 3.5-6) are associated to comparatively less CO_2-rich plumes, eventually due to increasing C dissolution (as dissolved CO_2 and HCO_3^-) into lake water. In terms of CO_2/H_2S vs. H_2/H_2S ratios (Figure 14e), lake plumes still vary as a function of the extent of S scrubbing into lake water, but the trends are more scattered. According to Shinohara et al. (2015, 2018), the negative trend between CO_2/H_2S and H_2/H_2S in Yudamari lake gases is related to the lake level, whereby low CO_2/H_2S and high H_2/H_2S are emitted when the lake level is low, while the opposite gas composition is emitted at high lake level.

6.4.2. Feeding gas vs. lake plume gas composition

One very convenient way to confirm that S dissolution into lake water is a primary mechanism driving the compositional variability of lake plumes is to compare, for those volcanoes where both are constrained, the surface gas output versus the feeding gas input. The latter is of course not amenable to measurement, but the composition of nearby crater fumaroles can, at least in principle, be taken as a convenient proxy. For example, the chemical compositions of fumaroles on the shores of H_2S-dominated lakes (Figure 6.16a, Tables S2 and S3 in the Appendix) are strongly suggestive for that that H_2S-rich gas (with no magmatic SO_2) is feeding the lake bottoms of El Chichón, Main Crater Lake, Víti, Vasca degli Ippopoatami and Yugama. At El Chichón, these hydrothermal fumaroles were used as a proxy for the composition of the subaquatic fumaroles (Chapter 4; Hasselle et al., 2018).

Our systematic comparison study here indicates higher CO_2/H_2S and H_2/H_2S ratios in gas fluxing through pH 1-3 lakes, compared to their corresponding fumarolic gases (Figure 6.16a). Diffuse and

bubbling lake gases are found to have relatively similar CO_2/H_2S and H_2/H_2S for each lake (Figure 6.16a). CO_2/H_2S ratios increase, from fumarolic to lake gas, from 23.0 to 2042-2637 at El Chichón, from 22 to 61-101 at Víti, from 33.4-33.6 to 45.3-57.7 at Vasca degli Ippopotami, from 248 to 4792-9624 at MCL (Taal) and from 6 to 220 at Yugama (Tables S2 and S3; Figure 6.16a). H_2/H_2S ratios also increase from fumarolic to lake gas, from 0.25 to 5.3-14.8 at El Chichón, from 0.39 to 0.74-1.7 at Víti, from 0.15-0.16 to 0.28-0.65 at Vasca degli Ippopotami, from 0.53 to 37 to 171 at MCL (Taal), and from 0.02 to 12.4 at Yugama. We also observe that, although Vasca degli Ippopotami and Vulcano crater are thought to be fed by the same deep magmatic gas source (Martini et al., 1980; Cioni and D'Amore, 1984; Mazor et al., 1988; Chiodini et al., 1991a, 1995), the Crater fumaroles cannot be taken as proxies for the feeding gas into the pond, owing to extensive chemical processing in the Vulcano Porto hydrothermal system that converts SO_2 into H_2S (Figure 6.16a, Tables S2 and S3).

Figure 6.16b contrasts the composition of fumaroles and lake gases (in terms of their CO_2/SO_2 and H_2/SO_2 ratios) at Santa Ana, Copahue and Yudamari. Even at these hyperacidic lakes, the lake gas compositions are strongly different from those in the nearby (shore) fumaroles. However, only the Santa Ana dataset, where fumaroles have lower CO_2/SO_2 and H_2/SO_2 ratios than the lake gases, is fully consistent with S scrubbing (note, however, that fumaroles and plumes were measured in 2005 and 2017-18, respectively, so that their comparison is not immediate). In contrast, lake vs. fumarole chemical trends are more complicated at the two other hyperacidic lakes. At Copahue, fumaroles have higher CO_2/SO_2 ratios (4.5-6.8) and lower H_2/SO_2 ratios (0.05-0.6) than lake gases (0.97 and 9.1, respectively), while at Yudamari fumaroles have higher CO_2/SO_2 ratios (1.7-10) than lake gases (0.3-2.6) but H_2/SO_2 ratios (range, 0.01-0.34) are overlapping at the two manifestations. These trends are not consistent with SO_2 scrubbing into the lake, and imply that the directly sampled fumaroles are themselves strongly modified by hydrothermal processing compared to the feeding (magmatic) gas phase supplying the lakes (Tamburello et al., 2015). Tamburello et al. (2015) and Shinohara et al. (2015) suggested that volcanic gases below Copahue and Yudamari crater lakes are hotter and more oxidized than shore fumaroles (rich in H_2S). Shinohara et al. (2015) proposed that Yudamari

fumaroles are mixtures of magmatic gases and CO_2-rich vapour separated (in various degree) from hydrothermal fluids (CO_2-poor liquid) feeding the lake.

6.4.3. Gas-lake water interactions in hyperacidic lakes

SO_2-dominated lake gas compositions, with their SO_2/H_2S ratios >1, CO_2/SO_2 ratios <10^3, and H_2/SO_2 ratios <10, approach the compositions of high-temperature arc volcanic gases (Aiuppa et al., 2017), and imply gas equilibrium temperatures far higher than lake water temperature (Tamburello et al., 2015; de Moor et al., 2016b). Hyperacidic lake degassing is thus a non-equilibrium process; rather, it is controlled by the (typically fast) rates and dynamics of magmatic gas transport into the lake, and in the underlying hydrothermal system (Tamburello et al., 2015; de Moor et al., 2016b). Gases are injected at the lake bottom at such high supply rate that can rapidly transit through (shallow) hyperacidic lakes without undergoing major S scrubbing/dissolution (Tamburello et al., 2015).

A number of potential dissolution mechanism for magmatic SO_2 in crater lakes have been proposed (Giggenbach et al., 2003; Delmelle et al., 2000; Kusakabe et al., 2000a; Werner et al., 2008; Shinohara et al., 2015). One often invoked mechanism is:

$$3SO_{2(g)} + 2H_2O_{(l)} = S^\circ_{(s,l)} + 2HSO_4^-{}_{(aq)} + 2H^+{}_{(aq)} \qquad (6.1)$$

This reaction mechanism, however, becomes less efficient with increasing temperature and decreasing pH (de Moor et al., 2016b), e.g. in hyperacidic lakes and in their "hot" feeding pipe systems.

SO_2 can also be disproportionated by the following reaction (Symonds et al., 2001; Giggenbach et al., 2003; Werner et al., 2008):

$$4\ SO_{2(g)} + 4\ H_2O_{(l)} = 3\ H_2SO_{4(aq)} + H_2S_{(aq)} \qquad (6.2)$$

Our lake gas plume results imply that reaction (6.2) is also likely to be minor in hyperacidic lakes (Shinohara et al., 2015; de Moor et al., 2016b)

The high SO_2/H_2S gas ratios of hyperacidic lake plume gases, apart from indicating feeding by magmatic (SO_2-rich) gases, are also likely to reflect elemental sulfur formation (sulfur deposition is observed at most hyperacidic lakes; Shinohara et al., 2015; this study) via (Mizutani and Sugiura, 1966; Giggenbach, 1987):

$$SO_{2(g)} + 2H_2S_{(g)} = 2H_2O + 3S° \tag{6.3}$$

This reaction can lead to either S oxidation or reduction in the (residual) post-scrubbing gas phase, depending on the initial SO_2/H_2S ratios in the feeding gas. de Moor et al. (2016b) proposed that H_2S injected in the Poás hydrothermal system is totally scrubbed before entering the lake. In contrast, low SO_2/H_2S ratios in the Yudamari lake gas (during low lake level phases) are explained by lower interactions between gas and water (less gas scrubbing; Shinohara et al., 2015). It is also suggested at Santa Ana lake (see Chapter 5) to explain the decrease of CO_2/SO_2 ratios when the lake level is lower.

By studying the correlation between eruptive activity (i.e. phreatic eruptions) and changes in lake gas composition (mostly SO_2/CO_2 ratios), de Moor et al. (2016b) proposed that increased magmatic gas influx at the lake bottom kinetically inhibits SO_2 hydrolysis into the lake (Symonds et al., 2001; Werner et al., 2008; Tamburello et al., 2015). In addition, increased magmatic acid gas inputs lead to decreasing pH and increasing temperature (Kusakabe et al., 2000a), which concur to shift reaction (6.1) to the left, ultimately leading to inefficient SO_2 removal from the gas (Tamburello et al., 2015). If such, our results (Figures 6.14-6.16) imply higher magmatic gas inputs into Copahue, Poás and Yudamari lakes, compared to Rincón de la Vieja, Sirung, Ruapehu, Kawah Ijen and Santa Ana (the latter exhibiting less SO_2-rich plumes).

It is also possible that changing degassing pressure can concur to determine (at least partly) the temporal/spatial variability in lake plume composition. Shinohara et al. (2018) argued that the CO_2/SO_2 ratio temporal variations observed in Yudamari lake gases and fumaroles might be due to variations in magma degassing pressures.

6.4.4. Gas-lake water interactions in H$_2$S-dominated lakes

Gas plumes issuing from H$_2$S-dominated lakes are inherently more S-poor (CO$_2$-H$_2$-rich) than SO$_2$-dominated lake plumes (Figures 6.15d-e). This reflects the concurrent action of more S-poor (hydrothermal) feeding gas, and the higher extents of S dissolution during lake-gas interactions. This notwithstanding, even in such less active lake systems, S (H$_2$S) dissolution into lake water is far from reaching completion. Similarly to what already noted for El Chichón and Víti lakes (Chapter 4; Hasselle et al., 2018), the plumes of Taal Main Crater Lake, Vasca degli Ippopotami and Yugama are active H$_2$S sources to the atmosphere, implying that only part of the feeding gas H$_2$S is ultimately trapped into lake water (Figure 6.16). At the low input gas fluxes that prevail in these systems, the lake water column depth probably plays a role. For example, feeding fumaroles at Vasca degli Ippopotami and El Chichón fumaroles have similar CO$_2$/H$_2$S (33.6 ± 9.9 vs. 23.0 ± 4.8) and H$_2$/H$_2$S (0.15 ± 0.04 vs. 0.25 ± 0.08) ratios. However, lake plume CO$_2$/H$_2$S (from 2042 ± 1513 to 2637 ± 1453) and H$_2$/H$_2$S (from 5.3 ± 5 to 14.8 ± 9.6) ratios in the ~4.5 m deep El Chichón lake are respectively ~100 and ~10 times higher than in the plume gas (CO$_2$/H$_2$S, 45.3 ± 7.5; H$_2$/H$_2$S, 0.28 ± 0.06) of the <1 m deep Vasca degli Ippopotami. A less thick water column at Vasca degli Ippopotami likely results into faster gas transit and minor S scrubbing, further highlighting the kinetic nature of the process (Kaasalainen and Stefánsson, 2011; Hasselle et al., 2018).

One additional key aspect of our study is the detection of tiny but persistent SO$_2$ amounts in plumes released by lake fed by otherwise SO$_2$-free (and H$_2$S-rich) input gas (Figures 6.14 and 6.15). SO$_2$ is a magmatic gas, and its discharge from hyperacidic lakes (cfr 6.4.3) claims for an active shallow magma source underneath these systems (e.g. Tamburello et al., 2015; de Moor et al., 2016b). In contrast, the fumaroles surrounding H$_2$S-dominated lakes are typically venting hydrothermal gas with no magmatic SO$_2$ (the low amounts of SO$_2$ measured in these fumaroles have been explained by H$_2$S oxidation by atmospheric oxygen; Kaasalainen and Stefánsson, 2011; Caponi et al., 2018). If the subaquatic fumaroles feeding pH>2 lakes are thus SO$_2$-free (Hasselle et al., 2018), then the trace amounts of SO$_2$ detected in the lake plumes require a formation mechanism in the lake water. We therefore argue that the mechanism discussed in Chapter 4 (and in Hasselle et al., 2018), in which SO$_2$

is produced into the lake by dissolved SO_3^{2-}, is more frequently happening than previously believed. SO_3^{2-} is a very reactive sulfur species, with very short lifetime in acidic lakes, but increased stability into less acidic lakes (e.g. Eldridge et al., 2016). The similar SO_2/H_2S lake gas ratios in pH 2-4 lakes and geothermal lakes (pH 4-6) (Figures 14a-c) might thus reflect higher SO_2 production in the latter systems, where sulfite contents are typically higher (Xu et al., 2000). We cannot rule out, however, that in some geothermal lakes (at least those measurements were taken meters downwind the lake surface(s)) the detected plume SO_2 is formed by H_2S oxidation during atmospheric transport and dispersion (e.g. Caponi et al., 2018). Similarly, the comparable CO_2/SO_2 lake plume ratios in pH 2-4 lakes and geothermal lakes (Figure 6.15a) can be explained by (i) higher CO_2 into lake water at higher pH, and/or (ii) higher SO_2 production in less acidic lakes due to the higher SO_3^{2-} contents. CO_2 is an ubiquitous volcanic species and it is known to feed both crater lakes and geothermal lakes (Mazot et al., 2011; Lowenstern et al., 2015; Paz et al., 2016). Its atmospheric release is dependent on the physico-chemical characteristics of the lakes, and at pH > 3.8 CO_2 conversion to dissolved bicarbonate becomes appreciable.
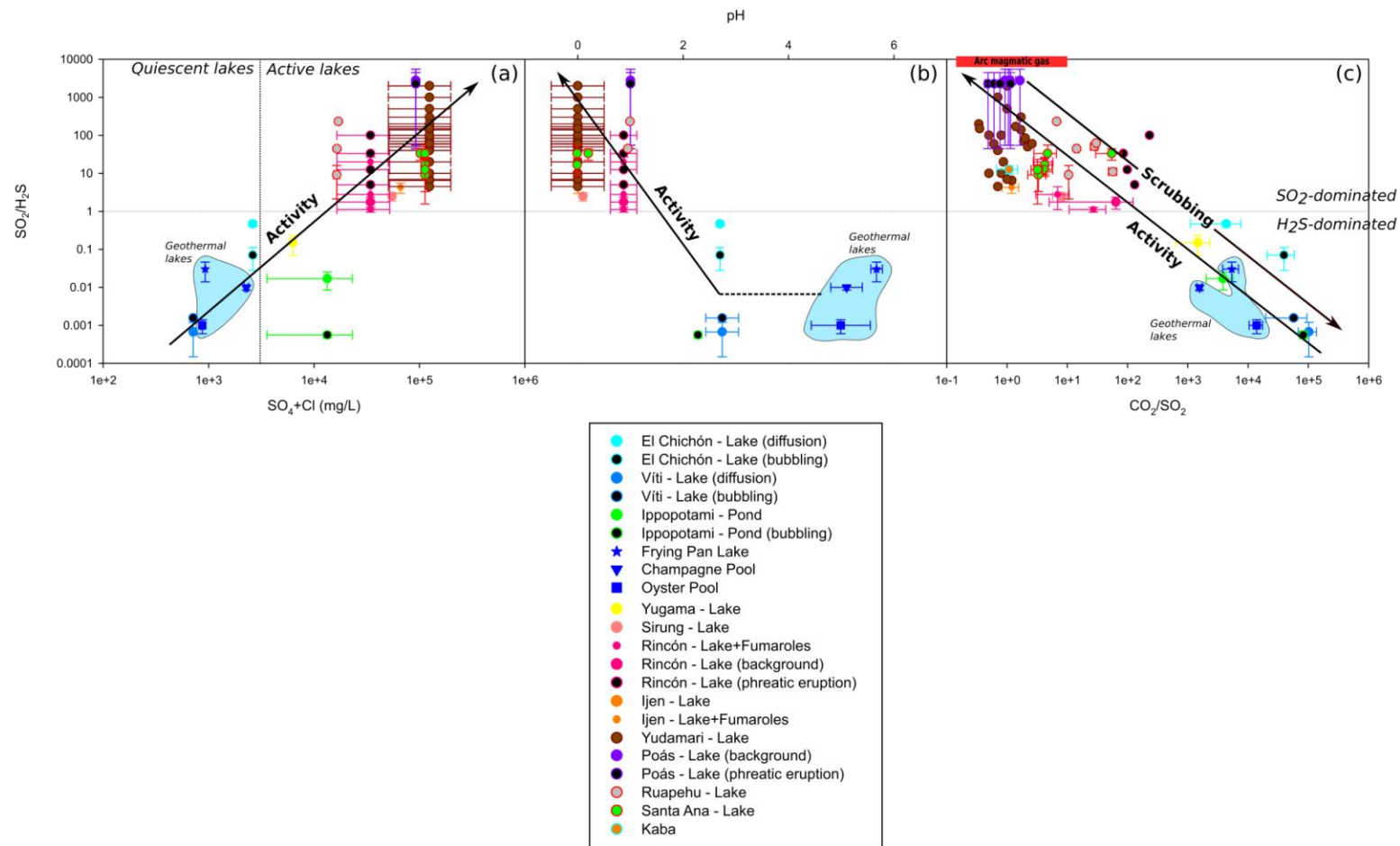
Figure 6.14 - Lake gas SO_2/H_2S ratios variations in function of the SO_4+Cl contents (a) and the pH (b) of the lake waters and the CO_2/SO_2 ratios of the lake plumes (c). The arrows show the direction of increase lake activity (a-c) and the effect of gas scrubbing (c) from the original magmatic gas composition towards the lake gas composition, highlighting that in H_2S-dominated lake emissions, the original gas has been more extensively scrubbed, while in SO_2-dominated lakes, i.e. highly more active lakes, gas emissions are less scrubbed and have a composition closer to the original magmatic gas (rich in SO_2 and H_2S-poor). Blue area highlights geothermal lakes.
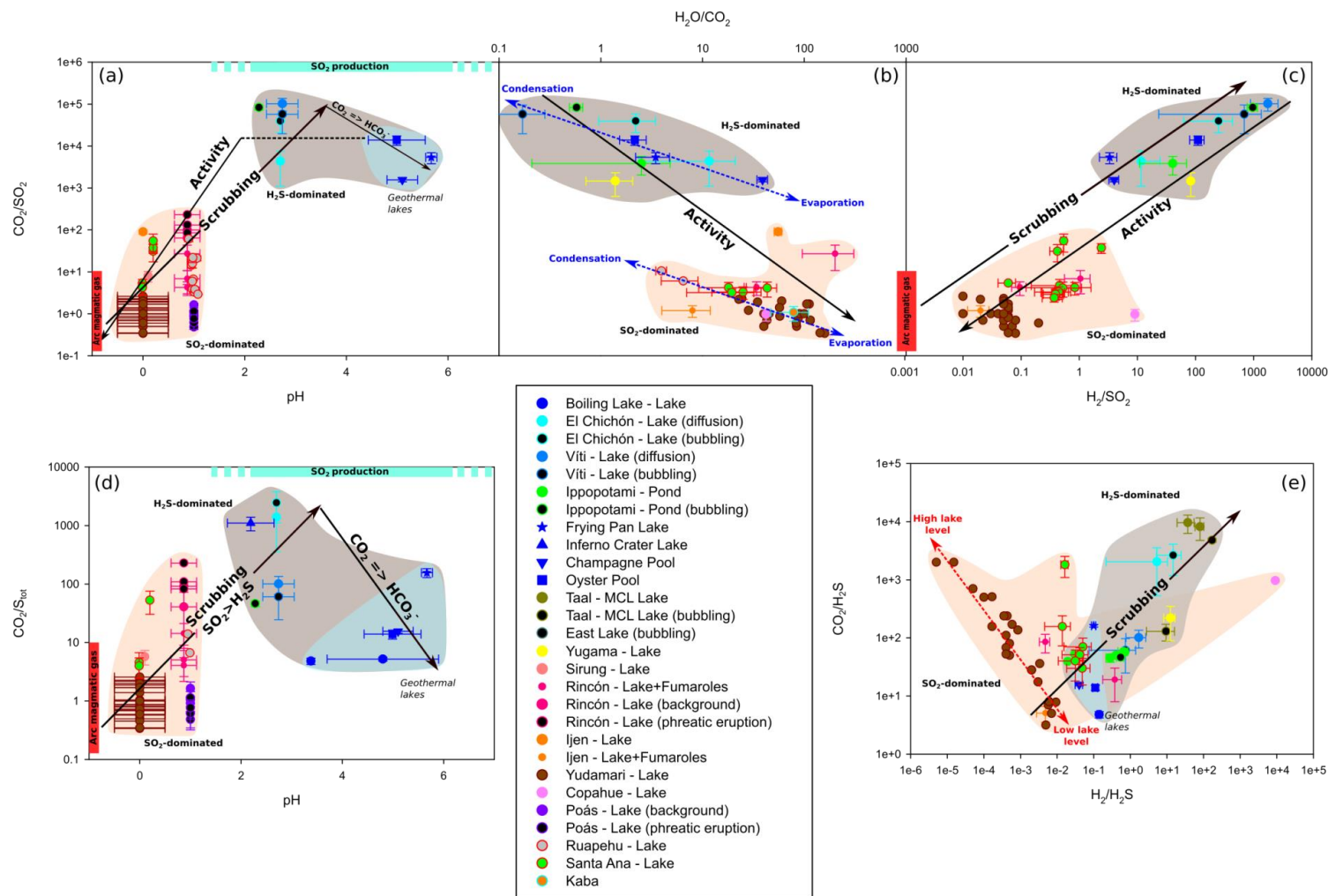
Figure 6.15 - Lake gas CO_2/SO_2 ratios variations in function of the pH (a) of the lake waters, the H_2O/CO_2 (b) and H_2/SO_2 (c) ratios of the lake plumes. The variations of $CO_2/Stot$ in function of the pH (d) and CO_2/H_2S in function of H_2/H_2S (e) are also shown. Orange, grey and blue areas highlight respectively, SO_2-dominated, H_2O-dominated and geothermal lakes. Black arrows show the direction of increasing activity and gas scrubbing. Blue dashed arrows (b) show the evaporation/condensation effect on lake gas composition. Red dashed arrow (e) shows the changes in lake level at Yudamari.
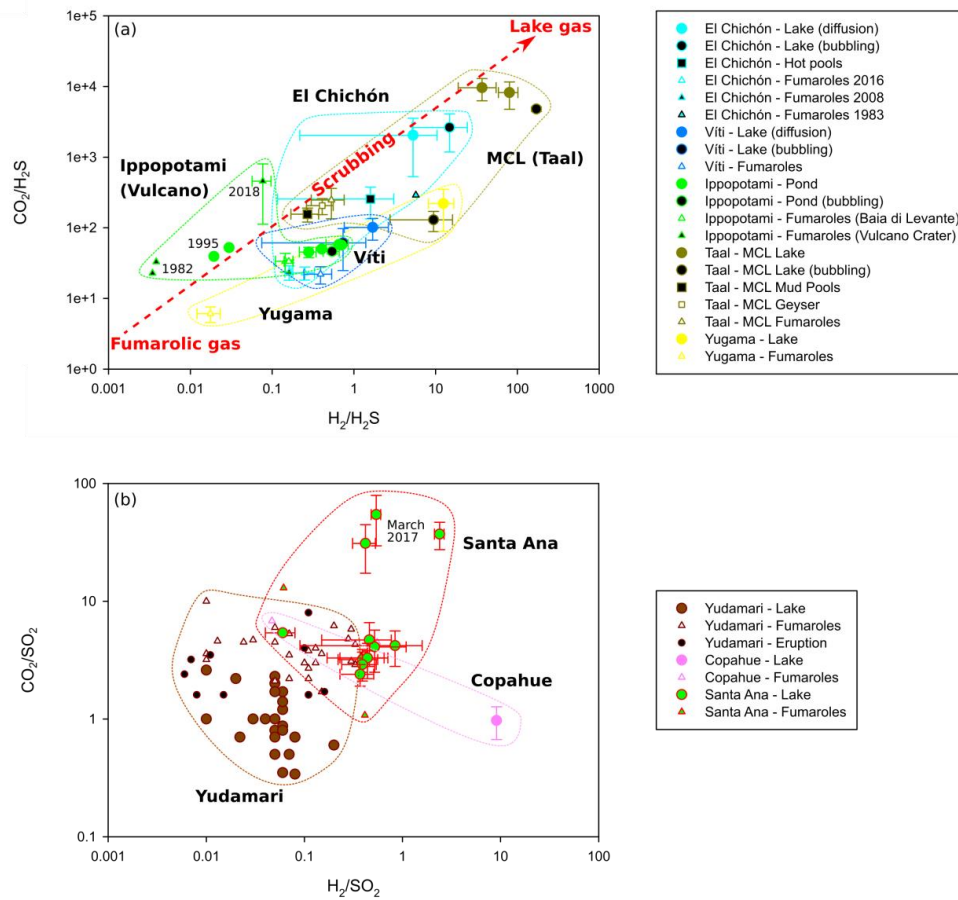
Figure 6.16 - Variations of the CO₂/S ratios vs. H₂/S ratios in H₂S-dominated lake (a; S=H₂S) and SO₂-dominated lake (b; S=SO₂) gases. The red dashed arrow in Figure (a) highlights the direction of increasing gas scrubbing from offshore fumarolic gas (proxy of the subaquatic fumaroles composition) to lake gases.

CHAPTER 7

GENERAL CONCLUSIONS

The findings of this study permitted (i) to highlight the physico-chemical characteristics of Barombi Mbo maar lake (Cameroon) and to define its weak killer-lake potential, (ii) to establish the spatial pCO_2 distribution at Averno lake (Campi Flegrei, Italy), (iii) to evaluate the potential application of the HydroC® CO_2 sensor to measure pCO_2 at volcanic lakes, (iv) to distinguish degassing patterns through acidic volcanic lakes, (v) to identify SO_2 emissions from pH 2-6 crater lakes, and (vi) to characterize Santa Ana lake plume gas composition for the first time.

Investigations executed at Barombi Mbo showed that this permanently stratified lake contains a large amount of dissolved gases (mostly atmospheric) of which CO_2 contributed only in a small fraction (pCO_2 1.4 x 10^{-3} atm at the surface increasing up to 0.016 atm at the lake bottom). Actually, the maximum total gas partial pressure was measured at the bottom (1.28 atm) and is far from the hydrostatic pressure (11.6 atm at 110 m depth), highlighting that the risk a sudden gas burst by overpressure is quite low.

In 2016 and 2017, Averno lake water did not encounter significant physico-chemical changes compared to data of the last decade. During the winter of 2017, the lake turned over and in July 2017, the shallow lake water contained a slightly higher dissolved pCO_2 compared to September 2016. In 2016, the incomplete horizontal profile revealed a relatively homogeneous water layer (at 15 m depth), with a mean of 2701 µatm (± 8%). The 5 m deep water layer investigated in 2017, was more heterogeneous (pCO_2 ranging from 1743 to 5929 µatm). I suggested that the spatial pCO_2 heterogeneities are likely due to fluid emissions at the lake bottom; higher pCO_2 could highlight the emplacement of a CO_2 source at the lake bottom. This hypothesis is reinforced by the alignment of the pCO_2 anomalies (trending SW-NE and NW-SE) coinciding with the main direction of the local fault

systems. However, other sources (changes in bathymetry, CO_2 input rate at the bottom or heterogeneity of bacterial distribution) could not be excluded.

The HydroC® CO_2 sensor was used for the first time to study pCO_2 in volcanic lakes and revealed its potential to investigate the pCO_2 distribution of CO_2-poor large and deep lakes. Actually, low surface pCO_2 (below the atmospheric pCO_2) at Averno and Barombi Mbo lakes were well detected with the sensor and allowed to complete and provide large detail of the shallow vertical pCO_2 profiles when water sampling data was failing. However, strong pCO_2 discrepancies were observed between data measured by the sensor (drastically higher pCO_2) and water sample analyses. A slightly higher pCO_2 was expected from the sensor data compared to water sample analyses but not as large as observed. We argue that the post-processing corrections may be the reason for such a discrepancy and stress for the need of numerous zero-flush cycles along the thermocline allowing to more accurately correct the raw data.

The study of acidic volcanic lake gas composition by Multi-GAS measurements permitted to distinguish two main degassing patterns of volcanic degassing through lakes: (i) hyper-acidic lakes poorly affect gas composition emitted at the crater (i.e. the lake bottom) and the lake gas signature remains more magmatic ($SO_2/H_2S > 1$; low CO_2/SO_2), and (ii) H_2S-dominated, steam-heated lakes strongly affect the original volcanic gas composition and emitted a sulfur-poor (and CO_2-poor at lake with pH 3.8-6) plume. In particular, pH 2-3 lake emissions have higher CO_2/H_2S and H_2/H_2S ratios compared to the offshore fumaroles (taken as a proxy of the subaquatic fumaroles composition). The systematic detection of H_2S in gas emissions from shallow pH 2-6 lakes, point to an incomplete dissolution and oxidation into the lake waters. This was investigated in detail at El Chichón (Mexico) and Víti (Iceland) lakes, but gas emissions at other H_2S-dominated lakes point to a more general pattern. The degree of H_2S gas scrubbing in a lake is not an equilibrium process, only depending on lake chemistry and temperature, but appears to be strongly influenced by kinetics. Actually, if fumarolic gases are well representative of subaquatic fumarole gas and with similar CO_2/H_2S and H_2/H_2S fumarolic gas ratios, the shallow Vasca degli Ippopotami (Vulcano, Italy) pond may scrub less

H$_2$S than the deeper El Chichón lake, pointing to an effect of the water column thickness (and thus the kinetics of the degassing) on H$_2$S transfer from the bottom to the surface.

An important discovery of this study was the emission of trace amounts of SO$_2$ in gas emissions from H$_2$S-dominated lakes. While hyperacidic lakes are degassing magmatic SO$_2$, which transit rapidly through the lake, the emission of trace amounts of SO$_2$ from pH 2-6 lakes was surprising. Indeed, reduced H$_2$S-rich fumaroles feeding those lakes are magmatic-SO$_2$-free. Therefore, SO$_2$ has to be produced inside the lake or in the atmosphere above the lake surface. We proposed that the formation of SO$_2$ is caused by physical-chemical processes inside the lakes. The S-speciation at El Chichón reported in literature helped to hypothesize that H$_2$S oxidation formed SO$_2$ via sulfite as a transient S-species. However, we cannot totally exclude the formation of SO$_2$ by oxidation of H$_2$S in the air, while in the absence of ubiquitous SO$_2$ emissions during our boats surveys at Víti and El Chichón lakes, we argue that trace amount of SO$_2$ measured close to the water surface where H$_2$S is emitted everywhere is likely not due to H$_2$S oxidation in air but rather due to the release by the lake itself.

Finally, the first Mulit-GAS investigation of the hyperacidic Santa Ana (El Salvador) lake plume gases revealed, unsurprisingly, a magmatic composition with H$_2$S/SO$_2$ ratios varying from 0.03 to 0.09, whereas the CO$_2$/SO$_2$ ratios decreased from 54.5 in March 2017 to 4.7 in June 2017, remaining similar until June 2018 (2.4). Rapid changes in water temperature, chemistry and CO$_2$/SO$_2$ ratios over time revealed a highly dynamic system, also disrupted by two eruptive phases, a magmatic eruption on October 1, 2005 and phreatic eruptions in March-April 2007. In such a system, the acquisition of safe and continuous gas monitoring is challenging in order to track short-term changes in the activity, as the traditional water chemistry monitoring is not efficient enough on the short-term due the lower sampling frequency. The determination of a site for semi-continuous Multi-GAS measurements for future monitoring was an ground-breaking endeavour of this study.

CHAPTER 8

REFERENCES

Aguilera, E., Chiodini, G., Cioni, R., Guidi, M., Marini, L., & Raco, B. (2000). Water chemistry of Lake Quilotoa (Ecuador) and assessment of natural hazards. Journal of volcanology and geothermal research, 97(1-4), 271-285.

Agusto, M., & Varekamp, J. (2016). The Copahue volcanic-hydrothermal system and applications for volcanic surveillance. In Copahue Volcano (pp. 199-238). Springer, Berlin, Heidelberg.

Agusto, M., Tassi, F., Caselli, A. T., Vaselli, O., Rouwet, D., Capaccioni, B., ... & Darrah, T. (2013). Gas geochemistry of the magmatic-hydrothermal fluid reservoir in the Copahue–Caviahue Volcanic Complex (Argentina). Journal of volcanology and geothermal research, 257, 44-56.

Agusto, M. R., Caselli, A., Daga, R., Varekamp, J., Trinelli, A., Afonso, M. D. S., ... & Guevara, S. R. (2017). The crater lake of Copahue volcano (Argentina): geochemical and thermal changes between 1995 and 2015. In: Ohba, T., Capaccioni, B. & Caudron, C. (eds) Geochemistry and geophysics of Active Volcanic Lakes. Geological Society, London, Special Publications, 437, 107-130. First published online December 23, 2016.

Aiuppa, A., Federico, C., Paonita, A., Pecoraino, G., & Valenza, M. (2002). S, Cl and F degassing as an indicator of volcanic dynamics: the 2001 eruption of Mount Etna. Geophysical Research Letters, 29(11).

Aiuppa, A., Federico, C., Giudice, G., Gurrieri, S., Paonita, A., & Valenza, M. (2004). Plume chemistry provides insights into mechanisms of sulfur and halogen degassing in basaltic volcanoes. Earth and Planetary Science Letters, 222(2), 469-483.

Aiuppa, A., Federico, C., Giudice, G., & Gurrieri, S. (2005a). Chemical mapping of a fumarolic field: la Fossa crater, Vulcano Island (Aeolian Islands, Italy). Geophysical Research Letters, 32(13).

Aiuppa, A., Inguaggiato, S., McGonigle, A. J., O'dwyer, M., Oppenheimer, C., Padgett, M. J., . . . Valenza, M. (2005b). H_2S fluxes from Mt. Etna, Stromboli, and Vulcano (Italy) and implications for the sulfur budget at volcanoes. Geochimica et Cosmochimica Acta, 69, 1861-1871. https://doi.org/10.1016/j.gca.2004.09.018

Aiuppa, A., Moretti, R., Federico, C., Giudice, G., Gurrieri, S., Liuzzo, M., ... & Valenza, M. (2007). Forecasting Etna eruptions by real-time observation of volcanic gas composition. Geology, 35(12), 1115-1118.

Aiuppa, A., Baker, D. R., & Webster, J. D. (2009a). Halogens in volcanic systems. Chemical Geology, 263(1-4), 1-18.

Aiuppa, A., Federico, C., Giudice, G., Giuffrida, G., Guida, R., Gurrieri, S., . . . Papale, P. (2009b). The 2007 eruption of Stromboli volcano: insights from real-time measurement of the volcanic gas plume CO_2/SO_2 ratio. Journal of Volcanology and Geothermal Research, 182, 221-230.

Aiuppa, A., Burton, M., Allard, P., Caltabiano, T., Giudice, G., Gurrieri, S., ... & Salerno, G. (2011a). First observational evidence for the CO_2-driven origin of Stromboli's major explosions. Solid Earth, 2(2), 135-142.

Aiuppa, A., Shinohara, H., Tamburello, G., Giudice, G., Liuzzo, M., & Moretti, R. (2011b). Hydrogen in the gas plume of an open-vent volcano, Mount Etna, Italy. Journal of Geophysical Research: Solid Earth, 116(B10).

Aiuppa, A., Giudice, G., Liuzzo, M., Tamburello, G., Allard, P., Calabrese, S., ... & Taran, Y. (2012). First volatile inventory for Gorely volcano, Kamchatka. Geophysical Research Letters, 39(6).

Aiuppa, A., Robidoux, P., Tamburello, G., Conde, V., Galle, B., Avard, G., . . . Muñoz, A. (2014). Gas measurements from the Costa Rica-Nicaragua volcanic segment suggest possible along-arc variations in volcanic gas chemistry. Earth and Planetary Science Letters, 407, 134-147. https://doi.org/10.1016/j.epsl.2014.09.041

Aiuppa, A., Fischer, T. P., Plank, T., Robidoux, P., & Di Napoli, R. (2017). Along-arc, inter-arc and arc-to-arc variations in volcanic gas CO_2/S_T ratios reveal dual source of carbon in arc volcanism. Earth-science reviews, 168, 24-47.

Armienta, M. A., De la Cruz-Reyna, S., & Macıas, J. L. (2000). Chemical characteristics of the crater lakes of Popocatetetl, El Chichon, and Nevado de Toluca volcanoes, Mexico. Journal of Volcanology and Geothermal Research, 97(1-4), 105-125.

Asaah, A. N., Yokoyama, T., Aka, F. T., Usui, T., Wirmvem, M. J., Tchamabe, B. C., ... & Hell, J. V. (2015). A comparative review of petrogenetic processes beneath the Cameroon Volcanic Line: Geochemical constraints. Geoscience Frontiers, 6(4), 557-570.

Badrudin, M. (1994). Kelut volcano monitoring: Hazards, mitigation and changes in water chemistry prior to the 1990 eruption. Geochemical Journal, 28, 233-241. https://doi.org/10.2343/geochemj.28.233

Bagarinao, T. (1992). Sulfide as an environmental factor and toxicant: tolerance and adaptations in aquatic organisms. Aquatic Toxicology, 24(1-2), 21-62.

Balmes, C. P. (1991). Geochemistry of Waimangu Geothermal System. Project Report.

Bani, P., Oppenheimer, C., Varekamp, J. C., Quinou, T., Lardy, M., & Carn, S. (2009). Remarkable geochemical changes and degassing at Voui crater lake, Ambae volcano, Vanuatu. Journal of Volcanology and Geothermal Research, 188(4), 347-357.

Bani, P., Alfianti, H., Aiuppa, A., Oppenheimer, C., Sitinjak, P., Tsanev, V., & Saing, U. B. (2017). First study of the heat and gas budget for Sirung volcano, Indonesia. Bulletin of Volcanology, 79(8), 60.

Barberi, F., Innocenti, F., Ferrara, G., Keller, J., & Villari, L. (1974). Evolution of Eolian arc volcanism (southern Tyrrhenian Sea). Earth and Planetary Science Letters, 21(3), 269-276.

Barberi, F., Bertagnini, A., Landi, P., & Principe, C. (1992). A review on phreatic eruptions and their precursors. Journal of volcanology and geothermal research, 52(4), 231-246.

Barbier, B. (2004). Etude minéralogique et géochimique du lac de cratère, des sources thermales et du système hydrothermal associé au volcan Sorik Marapi (Sumatra, Indonésie). Mémoire de licence, Université Libre de Bruxelles, Bruxelles.

Barbier, B., & Bernard, A. (2010). Bilan thermique et caractérisation géochimique de l'activité hydrothermale du volcan Rinjani, Lombok, Indonésie.

Barnett, D., & Davis, E. G. (1983). A GC method for the determination of sulphur dioxide in food headspaces. Journal of chromatographic science, 21, 205-208.

Barnett, D. (1985). Sulphites in foods: their chemistry and analysis. Food Technology in Australia, 37, 503-505.

Beccaluva, L., Gabbianelli, G., Lucchini, F., Rossi, P. L., & Savelli, C. (1985). Petrology and K/Ar ages of volcanics dredged from the Eolian seamounts: implications for geodynamic evolution of the southern Tyrrhenian basin. Earth and Planetary Science Letters, 74(2-3), 187-208.

Bell, H. (1946). Glimpses of a Governor's Life – Dominica, Samson Low, London.

Bermudez, A., & Delpino, D. (1995). Mapa de los peligros potenciales en el área del Volcán Copahue–sector Argentino. Volcanic Hazard Map. The Geological Survey of the Province of Neuquen, Argentina.

Bernard, A., & Mazot, A. (2004). Geochemical evolution of the young crater lake of Kelud volcano in Indonesia. Dams and Appurtenant Hydraulic Structures, 87.

Bernard, A., Escobar, C. D., Mazot, A., & Gutiérrez, R. E. (2004). The acid volcanic lake of Santa Ana volcano, El Salvador. Special Papers-Geological Society of America, 121-134.

Bernard, A., Maussen, K., Villacorte, O., Reniva, P., Campita, N., & Bornas, M. (2013, July). High CO_2 enrichment in surface waters of MCL lake at Taal volcano, Philippines. In IAVCEI 2013 Scientific Assembly.

Boudon, G., Rancon, J. P., Kieffer, G., Soto-Bonilla, G. J., Traineau, H., & Rossignol, J. C. (1996). Les éruptions de 1966-1970 et 1991-1992 du volcán Rincón de la Vieja, Costa Rica: exemple d'activité recurrente d'un système hydromagmatique. Erupciones del Volcán Rincón de la Vieja en 1966-1970 y 1991-1992: Ejemplo de la actividad recurrente de un sistema hidromagmático. Comptes Rendus de l'Academie des Sciences. Serie 2. Sciences de la Terre et des Planetes., 322(2), 101-108.

Bourdier, J. L. (1994). Le volcanisme (Vol. 25). BRGM (Editions).

Brantley, S. L., Borgiatt, A., Rowe, G., Fernandez, J. F., & Reynolds, J. R. (1987). Poás volcano crater lake acts as a condenser for acid metal-rich brine. Nature, 330(6147), 470.

Brown, G. C., Rymer, H., Dowden, J., Kapadia, P., Stevenson, D., Barquero, J., & Morales, L. D. (1989). Energy budget analysis for Poás crater lake: implications for predicting volcanic activity. Nature, 339(6223), 370.

Brown, G. C., Rymer, H., & Stevenson, D. (1991). Volcano monitoring by microgravity and energy budget analysis. Journal of the Geological Society, 148(3), 585-593.

Browne, P. R. L., & Lawless, J. V. (2001). Characteristics of hydrothermal eruptions, with examples from New Zealand and elsewhere. Earth-Science Reviews, 52(4), 299-331.

Cabassi, J., Tassi, F., Vaselli, O., Fiebig, J., Nocentini, M., Capecchiacci, F., ... & Bicocchi, G. (2013). Biogeochemical processes involving dissolved CO_2 and CH_4 at Albano, Averno, and Monticchio meromictic volcanic lakes (Central–Southern Italy). Bulletin of Volcanology, 75(1), 683.

Cabassi, J., Tassi, F., Mapelli, F., Borin, S., Calabrese, S., Rouwet, D., ... & Vaselli, O. (2014). Geosphere-biosphere interactions in bio-activity volcanic lakes: evidences from Hule and Rìo Cuarto (Costa Rica). PLoS one, 9(7), e102456.

Caliro, S., Chiodini, G., Izzo, G., Minopoli, C., Signorini, A., Avino, R., & Granieri, D. (2008). Geochemical and biochemical evidence of lake overturn and fish kill at Lake Averno, Italy. Journal of Volcanology and Geothermal Research, 178(2), 305-316.

Calvari, S., Spampinato, L., Lodato, L., Harris, A. J., Patrick, M. R., Dehn, J., ... & Andronico, D. (2005). Chronology and complex volcanic processes during the 2002–2003 flank eruption at Stromboli volcano (Italy) reconstructed from direct observations and surveys with a handheld thermal camera. Journal of Geophysical Research: Solid Earth, 110(B2).

Capaccioni, B., Tassi, F., & Vaselli, O. (2001). Organic and inorganic geochemistry of low temperature gas discharges at the Baia di Levante beach, Vulcano Island, Italy. Journal of Volcanology and Geothermal Research, 108(1-4), 173-185.

Capaccioni, B., Rouwet, D., & Tassi, F. (2017). HCl degassing from extremely acidic crater lakes: preliminary results from experimental determinations and implications for geochemical monitoring. In: Ohba, T., Capaccioni, B. & Caudron, C. (eds) Geochemistry and geophysics of Active Volcanic Lakes. Geological Society, London, Special Publications, 437, 97-106. First published online March 24, 2016.

Capasso, G., & Inguaggiato, S. (1998). A simple method for the determination of dissolved gases in natural waters. An application to thermal waters from Vulcano Island. Applied Geochemistry, 13(5), 631-642.

Caponi, C., Tassi, F., Stefánsson A., Fusi, L., Buccianti, A., Vaselli, O., Rosso, F., Bonini, N. , Kjartansdóttir, R., Robin, J. G.. (2018). Behaviour of S-bearing compounds (H_2S and SO_2) emitted in air from the main hydrothermal-volcanic systems of Iceland. Cities on Volcanoes 10 (Naples, Italy)

Caracausi, A., Nicolosi, M., Nuccio, P. M., Favara, R., Paternoster, M., & Rosciglione, A. (2013). Geochemical insight into differences in the physical structures and dynamics of two adjacent maar lakes at Mt. Vulture volcano (southern Italy). Geochemistry, Geophysics, Geosystems, 14(5), 1411-1434.

Carapezza, M. L., Lelli, M., & Tarchini, L. (2008). Geochemistry of the Albano and Nemi crater lakes in the volcanic district of Alban Hills (Rome, Italy). Journal of Volcanology and Geothermal Research, 178(2), 297-304.

Cardwell, R. K., Isaacks, B. L., & Karig, D. E. (1980). The spatial distribution of earthquakes, focal mechanism solutions, and subducted lithosphere in the Philippine and northeastern Indonesian islands. The Tectonic and Geologic Evolution of Southeast Asian Seas and Islands, 23, 1-35.

Carey, R. J., Houghton, B. F., & Thordarson, T. (2009). Abrupt shifts between wet and dry phases of the 1875 eruption of Askja Volcano: microscopic evidence for macroscopic dynamics. Journal of Volcanology and Geothermal Research, 184, 256-270.

Carr, M. J. (1984). Symmetrical and segmented variation of physical and geochemical characteristics of the Central American volcanic front. Journal of Volcanology and Geothermal Research, 20(3-4), 231-252.

Carr, M. J., & Stoiber, R. E. (1977). Geologic setting of some destructive earthquakes in Central America. Geological Society of America Bulletin, 88(1), 151-156.

Carr, M. J., & Pontier, N. K. (1981). Evolution of a young parasitic cone towards a mature central vent; Izalco and Santa Ana volcanoes in El Salvador, Central America. Journal of Volcanology and Geothermal Research, 11(2-4), 277-292.

Carr, M. J., Feigenson, M. D., Patino, L. C., & Walker, J. A. (2003). Volcanism and geochemistry in Central America: Progress and problems. Geophysical Monograph-American Geophysical Union, 138, 153-174.

Carrivick, J. L., Manville, V., & Cronin, S. J. (2009). A fluid dynamics approach to modelling the 18th March 2007 lahar at Mt. Ruapehu, New Zealand. Bulletin of Volcanology, 71(2), 153-169.

Carroll, M. R., & Webster, J. D. (1994). Solubilities of sulfur, noble gases, nitrogen, chlorine, and fluorine in magmas. Reviews in Mineralogy and Geochemistry, 30(1), 231-279.

Casadevall, T. J., De la Cruz-Reyna, S., Rose Jr, W. I., Bagley, S., Finnegan, D. L., & Zoller, W. H. (1984). Crater lake and post-eruption hydrothermal activity, El Chichón Volcano, Mexico. Journal of Volcanology and Geothermal Research, 23(1-2), 169-191.

Casas, A. S., Armienta, M. A., & Ramos, S. (2016). Sulfur speciation with high performance liquid chromatography as a tool for El Chichón volcano, crater lake monitoring. Journal of South American Earth Sciences, 72, 241-249.

Casertano, L., Borgia, A., & Cigolini, C. (1983). El volcán Poás, Costa Rica: cronología y características de la actividad. Geofísica Internacional, 22(3).

Casertano, L., Borgia, A., Cigolini, C., Morales, L. D., Montero, W., Gomez, M., & Fernandez, J. F. (1987). An integrated dynamic model for the volcanic activity at Poás volcano, Costa Rica. Bulletin of volcanology, 49(4), 588-598.

Castillo, R.M. (1984). Geologia de Costa Rica, Editorial de la Universidad de Costa Rica, San Josè, Costa Rica, pp. 188.

Caudron, C., Mazot, A., & Bernard, A. (2012). Carbon dioxide dynamics in Kelud volcanic lake. Journal of Geophysical Research: Solid Earth, 117(B5).

Caudron, C., Lecocq, T., Syahbana, D. K., McCausland, W., Watlet, A., Camelbeeck, T., & Bernard, A. (2015a). Stress and mass changes at a "wet" volcano: Example during the 2011–2012 volcanic unrest at Kawah Ijen volcano (Indonesia). Journal of Geophysical Research: Solid Earth, 120(7), 5117-5134.

Caudron, C., Syahbana, D. K., Lecocq, T., Van Hinsberg, V., McCausland, W., Triantafyllou, A., ... & Bernard, A. (2015b). Kawah Ijen volcanic activity: a review. Bulletin of Volcanology, 77(3), 16.

Caudron, C., Mauri, G., Williams-Jones, G., Lecocq, T., Syahbana, D. K., De Plaen, R., ... & Saracco, G. (2017). New insights into the Kawah Ijen hydrothermal system from geophysical data. In: Ohba, T., Capaccioni, B. & Caudron, C. (eds) Geochemistry and geophysics of Active Volcanic Lakes. Geological Society, London, Special Publications, 437, 57-72. First published online January 22, 2016.

Caudron, C., Bernard, A., Murphy, S., Inguaggiato, S., & Gunawan, H. (2018). Volcano-hydrothermal system and activity of Sirung volcano (Pantar Island, Indonesia). Journal of Volcanology and Geothermal Research, 357, 186-199.

CCVG Newsletter (2010). Newsletter of the IAVCEI Commission on the Chemistry of Volcanic Gases 2010, 21.

Chen, K. Y., & Morris, J. C. (1972). Kinetics of oxidation of aqueous sulfide by oxygen. Environmental Science & Technology, 6(6), 529-537.

Chiodini, G. (1991). Geochemical variations at Fossa Grande crater fumaroles (Volcano Island, Italy) in summer 1988. Acta Volcanol., 1, 179-192.

Chiodini, G., Cioni, R., Raco, B., & Taddeucci, G. (1991). Gas geobarometry applied to evaluate phreatic explosion hazard at Vulcano Island (Sicily, Italy). Acta Vulcanol, 1, 193-197.

Chiodini, G., Cioni, R., Marini, L., & Panichi, C. (1995). Origin of the fumarolic fluids of Vulcano Island, Italy and implications for volcanic surveillance. Bulletin of Volcanology, 57(2), 99-110.

Chiodini, G., Frondini, F., Cardellini, C., Granieri, D., Marini, L., & Ventura, G. (2001). CO_2 degassing and energy release at Solfatara volcano, Campi Flegrei, Italy. Journal of Geophysical Research: Solid Earth, 106(B8), 16213-16221.

Chiodini, G., Tassi, F., Caliro, S., Chiarabba, C., Vaselli, O., & Rouwet, D. (2012). Time-dependent CO_2 variations in Lake Albano associated with seismic activity. Bulletin of Volcanology, 74(4), 861-871.

Christenson, B. W. (2000). Geochemistry of fluids associated with the 1995–1996 eruption of Mt. Ruapehu, New Zealand: signatures and processes in the magmatic-hydrothermal system. Journal of Volcanology and Geothermal Research, 97(1-4), 1-30.

Christenson, B. W., & Wood, C. P. (1993). Evolution of a vent-hosted hydrothermal system beneath Ruapehu Crater Lake, New Zealand. Bulletin of volcanology, 55(8), 547-565.

Christenson, B., & Tassi, F. (2015). Gases in volcanic lake environments. In Volcanic lakes (pp. 125-153). Springer, Berlin, Heidelberg.

Christenson, B. W., Werner, C. A., Reyes, A. G., Sherburn, S., Scott, B. J., Miller, C., ... & Britten, K. A. (2007). Hazards from hydrothermally sealed volcanic conduits. Eos, Transactions American Geophysical Union, 88(5), 53-55.

Christenson, B. W., Reyes, A. G., Young, R., Moebis, A., Sherburn, S., Cole-Baker, J., & Britten, K. (2010). Cyclic processes and factors leading to phreatic eruption events: Insights from the 25

September 2007 eruption through Ruapehu Crater Lake, New Zealand. Journal of Volcanology and Geothermal Research, 191(1-2), 15-32.

Christenson, B., Németh, K., Rouwet, D., Tassi, F., Vandemeulebrouck, J., & Varekamp, J. C. (2015). Volcanic lakes. In Volcanic lakes (pp. 1-20). Springer, Berlin, Heidelberg.

Christenson, B. W., White, S., Britten, K., & Scott, B. J. (2017). Hydrological evolution and chemical structure of a hyper-acidic spring-lake system on Whakaari/White Island, NZ. Journal of Volcanology and Geothermal Research, 346, 180-211.

Cioni, R., & d'Amore, F. (1984). A genetic model for the crater fumaroles of Vulcano Island (Sicily, Italy). Geothermics, 13(4), 375-384.

Clifton, A. E., Pagli, C., Jónsdóttir, J. F., Eythorsdóttir, K., & Vogfjörð, K. (2003). Surface effects of triggered fault slip on Reykjanes Peninsula, SW Iceland. Tectonophysics, 369, 145-154.

Cole, J. W., Deering, C. D., Burt, R. M., Sewell, S., Shane, P. A. R., & Matthews, N. E. (2014). Okataina Volcanic Centre, Taupo Volcanic Zone, New Zealand: A review of volcanism and synchronous pluton development in an active, dominantly silicic caldera system. Earth-Science Reviews, 128, 1-17.

Colvin, A. S. (2008). Crater lake evolution during volcanic unrest: case study of the 2005 phreatic eruption at Santa Ana volcano, El Salvador, 195 pp (MS thesis, Mich. Technol. Univ., Houghton).

Colvin, A., Rose, W. I., Varekamp, J. C., Palma, J. L., Escobar, D., Gutierrez, E., ... & Maclean, A. (2013). Crater lake evolution at Santa Ana Volcano (El Salvador) following the 2005 eruption. Understanding Open-Vent Volcanism and Related Hazards. Geological Society of America, Special Papers, 498, 23-44.

Cornen, G., Bande, Y., Giresse, P., & Maley, J. (1992). The nature and chronostratigraphy of Quaternary pyroclastic accumulations from Lake Barombi Mbo (West-Cameroon). Journal of Volcanology and Geothermal Research, 51(4), 357-374.

Costa, A., & Chiodini, G. (2015). Modelling air dispersion of CO_2 from limnic eruptions. In Volcanic Lakes (pp. 451-465). Springer, Berlin, Heidelberg.

Cronin, S. J., Neall, V. E., Lecointre, J. A., & Palmer, A. S. (1997). Changes in Whangaehu River lahar characteristics during the 1995 eruption sequence, Ruapehu volcano, New Zealand. Journal of volcanology and geothermal research, 76(1-2), 47-61.

Davis, R. E. (1958). Displacement reactions at the sulfur atom. I. An interpretation of the decomposition of acidified thiosulfate. Journal of the American Chemical Society, 80(14), 3565-3569.

Defant, M. J., De Boer, J. Z., & Dietmar, O. (1988). The western Central Luzon volcanic arc, the Philippines: two arcs divided by rifting? Tectonophysics, 145(3-4), 305-317.

Dehn, J., Dean, K. G., Engle, K., & Izbekov, P. (2002). Thermal precursors in satellite images of the 1999 eruption of Shishaldin Volcano. Bulletin of Volcanology, 64(8), 525-534.

Dellino, P., Isaia, R., & Orsi, G. (2001). Statistical analysis of textural data from complex pyroclastic sequences: implications for fragmentation processes of the Agnano-Monte Spina Tephra (4.1 ka), Phlegraean Fields, southern Italy. Bulletin of Volcanology, 63(7), 443-461.

Dellino, P., Isaia, R., La Volpe, L., & Orsi, G. (2004). Interaction between particles transported by fallout and surge in the deposits of the Agnano–Monte Spina eruption (Campi Flegrei, Southern Italy). Journal of Volcanology and Geothermal Research, 133(1-4), 193-210.

Delmelle, P., & Bernard, A. (1994). Geochemistry, mineralogy, and chemical modeling of the acid crater lake of Kawah Ijen Volcano, Indonesia. Geochimica et cosmochimica acta, 58(11), 2445-2460.

Delmelle, P., & Bernard, A. (2000). Downstream composition changes of acidic volcanic waters discharged into the Banyupahit stream, Ijen caldera, Indonesia. Journal of Volcanology and Geothermal Research, 97(1-4), 55-75.

Delmelle, P., & Bernard, A. (2015). The remarkable chemistry of sulfur in hyper-acid crater lakes: a scientific tribute to Bokuichiro Takano and Minoru Kusakabe. In Volcanic Lakes (pp. 239-259). Springer, Berlin, Heidelberg.

Delmelle, P., Kusakabe, M., Bernard, A., Fischer, T., De Brouwer, S., & Del Mundo, E. (1998). Geochemical and isotopic evidence for seawater contamination of the hydrothermal system of Taal Volcano, Luzon, the Philippines. Bulletin of volcanology, 59(8), 562-576.

Delmelle, P., Henley, R. W., Opfergelt, S., & Detienne, M. (2015). Summit acid crater lakes and flank instability in composite volcanoes. In Volcanic lakes (pp. 289-305). Springer, Berlin, Heidelberg.

DeMets, C., Gordon, R. G., Argus, D. F., & Stein, S. (1990). Current plate motions. Geophysical journal international, 101(2), 425-478.

DeMets, C., P. E. Jansma, G. S. Mattioli, T. H. Dixon, F. Farina, R. Bilham, E. Calais and P. Mann (2000). GPS geodetic constraints on Caribbean-North America plate motion, Geophys. Res. Lett., 27, 437-440.

DeMets, C. (2001). A new estimate for present-day Cocos-Caribbean plate motion: Implications for slip along the Central American volcanic arc. Geophysical research letters, 28(21), 4043-4046.

de Moor, J. M., Aiuppa, A., Avard, G., Wehrmann, H., Dunbar, N., Muller, C., ... & Conde, V. (2016a). Turmoil at Turrialba Volcano (Costa Rica): Degassing and eruptive processes inferred from high-frequency gas monitoring. Journal of Geophysical Research: Solid Earth, 121(8), 5761-5775.

de Moor, J. M., Aiuppa, A., Pacheco, J., Avard, G., Kern, C., Liuzzo, M., ... & Fischer, T. P. (2016b). Short-period volcanic gas precursors to phreatic eruptions: Insights from Poás Volcano, Costa Rica. Earth and Planetary Science Letters, 442, 218-227.

de Moor, M. J., Aiuppa, A., Avard, G., Diaz, J. A., Corrales, E., Rüdiger, J., ... & Alan, A. (2017, December). A sulfur trigger for the 2017 phreatomagmatic eruption of Poás volcano, Costa Rica? Insights from MultiGAS and drone-based gas monitoring. In AGU Fall Meeting Abstracts.

De Vita, S., Orsi, G., Civetta, L., Carandente, A., D'Antonio, M., Deino, A., ... & Marotta, E. (1999). The Agnano–Monte Spina eruption (4100 years BP) in the restless Campi Flegrei caldera (Italy). Journal of Volcanology and Geothermal Research, 91(2), 269-301.

Dibble, R. R. (1974). Volcanic seismology and accompanying activity of Ruapehu Volcano, New Zealand. In Developments in Solid Earth Geophysics (Vol. 6, pp. 49-85). Elsevier.

Di Napoli, R., Aiuppa, A., & Allard, P. (2013). First multi-gas based characterisation of the Boiling Lake volcanic gas (Dominica, Lesser Antilles). Annals of Geophysics, 56(5), 0559.

Di Vito, M., Lirer, L., Mastrolorenzo, G., & Rolandi, G. (1987). The 1538 Monte Nuovo eruption (Campi Flegrei, Italy). Bulletin of Volcanology, 49(4), 608-615.

Di Vito, M. A., Arienzo, I., Braia, G., Civetta, L., D'Antonio, M., Di Renzo, V., & Orsi, G. (2011). The Averno 2 fissure eruption: a recent small-size explosive event at the Campi Flegrei Caldera (Italy). Bulletin of Volcanology, 73(3), 295-320.

Dixon, T. H., F. Farina, C. DeMets, P. Jansma, P. Mann and E. Calais (1998). Relative motion between the Caribbean and North American plates and related boundary zone deformation from a decade of GPS observations, J. Geophys. Res., 103, 15157-15183.

Dominey, W. J., & Snyder, A. M. (1988). Kleptoparasitism of freshwater crabs by cichlid fishes endemic to Lake Barombi Mbo, Cameroon, West Africa. Environmental Biology of Fishes, 22(2), 155.

Dumort J.-C., Geologic map and explicative note on the Douala-west and 1/500000 map of geologic recognisance. Dir. Min. Géol. Cam. BRGM Paris, 1968. (In French)

Ehhalt, D. H., & Rohrer, F. (2009). The tropospheric cycle of H_2: a critical review. Tellus B: Chemical and Physical Meteorology, 61(3), 500-535.

Elliot, E.C. (1938). Boiling Lake – the 1900 Story, In: G. Bless (ed.), Broken Atoms.

Ellis, A. J., & Mahon, W. A. J. (1977). Chemistry and geothermanl systems (No. 553.79 E4).

Evans, W. C., Kling, G. W., Tuttle, M. L., Tanyileke, G., & White, L. D. (1993). Gas buildup in Lake Nyos, Cameroon: the recharge process and its consequences.

Fiedler, B., Fietzek, P., Vieira, N., Silva, P., Bittig, H. C., & Körtzinger, A. (2013). In situ CO_2 and O_2 measurements on a profiling float. Journal of Atmospheric and Oceanic Technology, 30(1), 112-126.

Fietzek, P. (2011). Underwater pCO_2 measurements by means of a membrane based NDIR sensor–The HydroC™/CO_2.

Fietzek, P., Kramer, S., & Esser, D. (2011a, September). Deployments of the HydroC™(CO_2/CH_4) on stationary and mobile platforms-Merging trends in the field of platform and sensor development. In OCEANS 2011 (pp. 1-9). IEEE.

Fietzek, P., Kramer, S., & Esser, D. (2011b). Measuring dissolved carbon dioxide and methane on modern platforms. International Ocean Systems, 15(2), 10-12.

Fietzek, P., Thomsen, J., & Esser, D. (2013). Ocean acidification investigations in the Kiel Fjord. International Ocean Systems, 17(2), 11-14.

Fietzek, P., Fiedler, B., Steinhoff, T., & Körtzinger, A. (2014). In situ quality assessment of a novel underwater pCO_2 sensor based on membrane equilibration and NDIR spectrometry. Journal of Atmospheric and Oceanic Technology, 31(1), 181-196.

Fischer, T. P., Ramírez, C., Mora-Amador, R. A., Hilton, D. R., Barnes, J. D., Sharp, Z. D., ... & Shaw, A. M. (2015). Temporal variations in fumarole gas chemistry at Poás volcano, Costa Rica. Journal of Volcanology and Geothermal Research, 294, 56-70.

Fitton, J. G., & Dunlop, H. M. (1985). The Cameroon line, West Africa, and its bearing on the origin of oceanic and continental alkali basalt. Earth and Planetary Science Letters, 72(1), 23-38.

Folguera, A., & Ramos, V. (2000). Control estructural del volcán Copahue (38S-71O): implicancias tectónicas para el arco volcánico cuaternario (36-39). Revista de la Asociación Geológica Argentina, 53(3), 229-244.

Forcella, L. S. (1982). Geochemistry of thermal and mineral waters in the Cascade Mountains of western North America. Groundwater, 20(1), 39-47.

Förster, H., Oles, D., Knittel, U., Defant, M. J., & Torres, R. C. (1990). The Macolod Corridor: a rift crossing the Philippine island arc. Tectonophysics, 183(1-4), 265-271.

Fournier, T., Freymueller, J., & Cervelli, P. (2009). Tracking magma volume recovery at Okmok volcano using GPS and an unscented Kalman filter. Journal of Geophysical Research: Solid Earth, 114(B2).

Frank, C., Fietzek, P., & Sobin, J. (2014). Determination of carbonate parameters in seawater. International Ocean Systems, 18(2).

Freeth, S. J., & Kay, R. L. F. (1991). How much water swept over the Lake Nyos dam during the 1986 gas disaster?. Bulletin of Volcanology, 53(2), 147-150.

Freeth, S. J., Kay, R. L. F., & Baxter, P. J. (1987). Reports by the British scientific mission sent to investigate the Lake Nyos disaster. Report to the Disaster Unit of the Overseas Development Administration, Foreign and Commonwealth Office (London). 86pp.

Friðriksson, Á. (2014). What is below the water masses? Multibeam studies of Öskjuvatn, Thingvallavatn and Kleifarvatn (Master's thesis). Retrieved from Skemman. (http://hdl.handle.net/1946/18548). Reykjavik, Iceland: University of Iceland.

Gaillard, F., Scaillet, B., & Arndt, N. T. (2011). Atmospheric oxygenation caused by a change in volcanic degassing pressure. Nature, 478(7368), 229.

Gemmell, J. B. (1987). Geochemistry of metallic trace elements in fumarolic condensates from Nicaraguan and Costa Rican volcanoes. Journal of Volcanology and Geothermal Research, 33(1-3), 161-181.

Giggenbach, W. (1974). The chemistry of Crater Lake, Mt. Ruapehu (New Zealand) during and after the 1971 active period. NZJ Sci., 17, 33-45.

Giggenbach, W. F. (1975). Variations in the carbon, sulfur and chlorine contents of volcanic gas discharges from White Island, New Zealand. Bulletin Volcanologique, 39(1), 15-27.

Giggenbach, W. F. (1983). Chemical surveillance of active volcanoes in New Zealand. In. Forecasting volcanic events, 311-322.

Giggenbach, W. F. (1987). Redox processes governing the chemistry of fumarolic gas discharges from White Island, New Zealand. Applied Geochemistry, 2(2), 143-161.

Giggenbach, W. F. (1990). The chemistry of fumarolic vapor and thermal-spring discharges from the Nevado del Ruiz volcanic-magmatic-hydrothermal system, Colombia. Journal of Volcanology and Geothermal Research, 42(1-2), 13-39.

Giggenbach, W. F. (1996). Chemical composition of volcanic gases. In Monitoring and mitigation of volcano hazards (pp. 221-256). Springer, Berlin, Heidelberg.

Giggenbach, W. F., & Glover, R. B. (1975). The use of chemical indicators in the surveillance of volcanic activity affecting the crater lake on Mt Ruapehu, New Zealand. Bulletin volcanologique, 39(1), 70-81.

Giresse, P., Maley, J., & Kelts, K. (1991). Sedimentation and palaeoenvironment in crater lake Barombi Mbo, Cameroon, during the last 25,000 years. Sedimentary Geology, 71(3-4), 151-175.

Glover, R. B. (1968). A brief account of the chemistry of the Waimangu Springs. File CD 118/12 NZDSIR.

Glover, R. B., Stewart, M. K., Crump, M. E., Klyen, L. E., & Simmons, S. F. (1994). The relationship of chemical parameters to the cyclic behaviour of Inferno Crater Lake, Waimangu, New Zealand. Geothermics, 23(5-6), 583-597.

González, G., Mora-Amador, R. A., Ramírez, C. J., & Rouwet, D. (2013). Variations in physicochemical features and seismicity related to phreatic activity for the two active crater lakes in Costa Rica: Poás and Rincón de la Vieja volcanoes. In 8th Workshop on Volcanic Lakes. IAVCEI Commission on Volcanic Lakes, Japan (p. 36).

Green, J., Corbet, S. A., & Betney, E. (1973). Ecological studies on crater lakes in West Cameroon The blood of endemic cichlids in Barombi Mbo in relation to stratification and their feeding habits. Journal of Zoology, 170(3), 299-308.

Grinenko, V. A., & Thode, H. G. (1970). Sulfur isotope effects in volcanic gas mixtures. Canadian Journal of Earth Sciences, 7(6), 1402-1409.

Grüger, E., & Thulin, B. (1998). First results of biostratigraphical investigations of Lago d'Averno near Naples relating to the period 800 BC–800 AD. Quaternary International, 47, 35-40.

Gunawan, H., Caudron, C., Pallister, J., Primulyana, S., Christenson, B., McCausland, W.,..., Hendrasto, M. (2016). New insights into Kawah Ijens volcanic system from the wet volcano workshop experiment. Geological Society, London, Special Publications, 437, 35-56.

Gutiérrez, R.E., & Escobar, C.D. (1994). Crisis en la actividad del volcán de Santa ana (Ilamatepec), del 22 de Julio al 21 de Agosto 1992, El Salvador, America Central: Centro de Investigaciones Geotecnicas, unpublished report, 14pp.

GVP (Global Volcanism Program), Smithsonian Institution (2018). https://volcano.si.edu/

Halbwachs, M., Sabroux, J. C., Grangeon, J., Kayser, G., Tochon-Danguy, J. C., Felix, A., ... & Hell, J. (2004). Degassing the "killer lakes" Nyos and Monoun, Cameroon. Eos, Transactions American Geophysical Union, 85(30), 281-285.

Hall, R., Cottam, M. A., & Wilson, M. E. (2011). The SE Asian gateway: history and tectonics of the Australia–Asia collision. Geological Society, London, Special Publications, 355(1), 1-6.

Halsor, S. P., & Rose, W. I. (1988). Common characteristics of paired volcanoes in northern Central America. Journal of Geophysical Research: Solid Earth, 93(B5), 4467-4476.

Hamburger, M. W., Cardwell, R. K., & Isacks, B. L. (1983). Seismotectonics of the northern Philippine island arc. The Tectonic and Geologic Evolution of Southeast Asian Seas and Islands: Part 2, 27, 1-22.

Handley, H. K., Macpherson, C. G., Davidson, J. P., Berlo, K., & Lowry, D. (2007). Constraining fluid and sediment contributions to subduction-related magmatism in Indonesia: Ijen Volcanic Complex. Journal of Petrology, 48(6), 1155-1183.

Harris, A. J., Blake, S., Rothery, D. A., & Stevens, N. F. (1997). A chronology of the 1991 to 1993 Mount Etna eruption using advanced very high resolution radiometer data: Implications for real-time thermal volcano monitoring. Journal of Geophysical Research: Solid Earth, 102(B4), 7985-8003.

Harris, A. J., Carniel, R., & Jones, J. (2005). Identification of variable convective regimes at Erta Ale Lava Lake. Journal of Volcanology and Geothermal Research, 142(3-4), 207-223.

Hasselle, N., Rouwet, D., Aiuppa, A., Jácome-Paz, M. P., Pfeffer, M., Taran, Y., ... & Bergsson, B. (2018). Sulfur degassing from steam-heated crater lakes: El Chichón (Chiapas, Mexico) and Víti (Iceland). Geophysical Research Letters, 45(15), 7504-7513.

Hedenquist, J. W. (1983). Waiotapu, New Zealand: the geochemical evolution and mineralization of an active hydrothermal system (Doctoral dissertation, ResearchSpace@ Auckland).

Hernández, P. A., Notsu, K., Salazar, J. M., Mori, T., Natale, G., Okada, H., ... & Pérez, N. M. (2001). Carbon dioxide degassing by advective flow from Usu volcano, Japan. Science, 292(5514), 83-86.

Hernández, P. A., Pérez, N. M., Varekamp, J. C., Henriquez, B., Hernández, A., Barrancos, J., ... & Melián, G. (2007). Crater lake temperature changes of the 2005 eruption of Santa Ana volcano, El Salvador, Central America. Pure and Applied Geophysics, 164(12), 2507-2522.

Hernández, P. A., Melián, G. V., Somoza, L., Arpa, M. C., Pérez, N. M., Bariso, E., ... & Solidum, R. (2017). The acid crater lake of Taal Volcano, Philippines: hydrogeochemical and hydroacoustic data related to the 2010–11 volcanic unrest. In: Ohba, T., Capaccioni, B. & Caudron, C. (eds) Geochemistry and geophysics of Active Volcanic Lakes. Geological Society, London, Special Publications, 437, 131-152. First published online February 2, 2017.

Hunt, T. M., Glover, R. B., & Wood, C. P. (1994). Waimangu, Waiotapu, and Waikite geothermal systems, New Zealand: background and history. Geothermics, 23(5-6), 379-400.

Hurst, A. W., & Dibble, R. R. (1981). Bathymetry, heat output and convection in Ruapehu crater lake, New Zealand. Journal of Volcanology and Geothermal Research, 9(2-3), 215-236.

Hurst, A. W., & Sherburn, S. (1993). Volcanic tremor at Ruapehu: characteristics and implications for the resonant source. New Zealand journal of geology and geophysics, 36(4), 475-485.

Hurst, A. W., & Vandemeulebrouck, J. (1996). Acoustic noise and temperature monitoring of the Crater Lake of Mount Ruapehu Volcano. Journal of volcanology and geothermal research, 71(1), 45-51.

Hurst, A. W., Bibby, H. M., Scott, B. J., & McGuinness, M. J. (1991). The heat source of Ruapehu Crater Lake; deductions from the energy and mass balances. Journal of volcanology and geothermal research, 46(1-2), 1-20.

Husen, S., Quintero, R., Kissling, E., & Hacker, B. (2003). Subduction-zone structure and magmatic processes beneath Costa Rica constrained by local earthquake tomography and petrological modelling. Geophysical Journal International, 155(1), 11-32.

Improta, C., Andini, S., & Ferrara, L. (2004). Chemical and ecotoxicological characterization of Averno Lake. Bulletin of environmental contamination and toxicology, 72(3), 472-481.

Ingebritsen, S. E., Randolph-Flagg, N. G., Gelwick, K. D., Lundstrom, E. A., Crankshaw, I. M., Murveit, A. M., ... & Mariner, R. H. (2014). Hydrothermal monitoring in a quiescent volcanic arc: Cascade Range, northwestern United States. Geofluids, 14(3), 326-346.

Iwasaki, I., & Ozawa, T. (1960). Genesis of sulfate in acid hot spring. Bulletin of the Chemical Society of Japan, 33(7), 1018b-1019.

Jácome Paz, M. P., Taran, Y., Inguaggiato, S., & Collard, N. (2016). CO_2 flux and chemistry of El Chichón crater lake (México) in the period 2013-2015: Evidence for the enhanced volcano activity. Geophysical Research Letters, 43, 127-134. https://doi.org/10.1002/2015gl066354

Johnston, S. T., & Thorkelson, D. J. (1997). Cocos-Nazca slab window beneath central America. Earth and Planetary Science Letters, 146(3-4), 465-474.

Jolly, A. D., Sherburn, S., Jousset, P., & Kilgour, G. (2010). Eruption source processes derived from seismic and acoustic observations of the 25 September 2007 Ruapehu eruption—North Island, New Zealand. Journal of Volcanology and Geothermal Research, 191(1-2), 33-45.

Joseph, E. P., N. Fournier, J. M. Lindsay and T. P. Fischer (2011). Gas and water geochemistry of geothermal systems in Dominica, Lesser Antilles island arc, J. Volcanol. Geoth. Res., 206, 1-14

Kaasalainen, H., & Stefánsson, A. (2011). Sulfur speciation in natural hydrothermal waters, Iceland. Geochimica et Cosmochimica Acta, 75, 2777-2791.

Kalacheva, E., Taran, Y., Kotenko, T., Hattori, K., Kotenko, L., & Solis-Pichardo, G. (2016). Volcano-hydrothermal system of Ebeko volcano, Paramushir, Kuril Islands: Geochemistry and solute fluxes of magmatic chlorine and sulfur. Journal of Volcanology and Geothermal Research, 310, 118-131.

Kamata, H., & Kodama, K. (1999). Volcanic history and tectonics of the Southwest Japan Arc. Island Arc, 8(3), 393-403.

Kanda, W., Tanaka, Y., Utsugi, M., Takakura, S., Hashimoto, T., & Inoue, H. (2008). A preparation zone for volcanic explosions beneath Naka-dake crater, Aso volcano, as inferred from magnetotelluric surveys. Journal of Volcanology and Geothermal Research, 178(1), 32-45.

Kelly, D. P. (1982). Biochemistry of the chemolithotrophic oxidation of inorganic sulphur. Phil. Trans. R. Soc. Lond. B, 298(1093), 499-528.

Kemmerling, G. L. L. (1921). De uitbarsting van den G. Keloet in den nacht van den 19den op den 20sten mei 1919: Hauptbd. Landsdr.

Kempter, K. A., Benner, S. G., & Williams, S. N. (1996). Rincón de la Vieja volcano, Guanacaste province, Costa Rica: geology of the southwestern flank and hazards implications. Journal of volcanology and geothermal research, 71(2-4), 109-127.

Kempter, K. A., & Rowe, G. L. (2000). Leakage of Active Crater lake brine through the north flank at Rincón de la Vieja volcano, northwest Costa Rica, and implications for crater collapse. Journal of Volcanology and Geothermal Research, 97(1-4), 143-159.

Keywood, M., & Nicholson, K. (1990). Cyclic and temporal changes in water chemistry of Inferno Crater Lake, Waimangu geothermal valley, New Zealand. In Proceedings of the 12th New Zealand Geothermal Workshop, Auckland. Geothermal Institute (pp. 103-110).

Kilgour, G., Manville, V., Della Pasqua, F., Graettinger, A., Hodgson, K. A., & Jolly, G. E. (2010). The 25 September 2007 eruption of Mount Ruapehu, New Zealand: directed ballistics, surtseyan jets, and ice-slurry lahars. Journal of Volcanology and Geothermal Research, 191(1-2), 1-14.

Kling, G. W. (1987). Seasonal mixing and catastrophic degassing in tropical lakes, Cameroon, West Africa. Science, 237(4818), 1022-1024.

Kling, G. W. (1988). Comparative transparency, depth of mixing, and stability of stratification in lakes of Cameroon, West Africa1. Limnology and Oceanography, 33(1), 27-40.

Kling, G. W., Tuttle, M. L., & Evans, W. C. (1989). The evolution of thermal structure and water chemistry in Lake Nyos. Journal of Volcanology and Geothermal Research, 39(2-3), 151-165.

Kling, G. W., Evans, W. C., Tanyileke, G., Kusakabe, M., Ohba, T., Yoshida, Y., & Hell, J. V. (2005). Degassing Lakes Nyos and Monoun: defusing certain disaster. Proceedings of the National Academy of Sciences, 102(40), 14185-14190.

Krushensky, R. D., & Escalante, G. (1967). Activity of Irazú and Poás volcanoes, Costa Rica, November 1964–July 1965. Bulletin Volcanologique, 31(1), 75.

Kusakabe, M. (1996). Hazardous crater lakes. In Monitoring and mitigation of volcano hazards (pp. 573-598). Springer, Berlin, Heidelberg.

Kusakabe, M. (2015). Evolution of CO_2 content in Lakes Nyos and Monoun, and sub-lacustrine CO_2-recharge system at Lake Nyos as envisaged from $CO_2/^3He$ ratios and noble gas signatures. In Volcanic Lakes (pp. 427-450). Springer, Berlin, Heidelberg.

Kusakabe, M. (2017). Lakes Nyos and Monoun gas disasters (Cameroon)–Limnic eruptions caused by excessive accumulation of magmatic CO_2 in crater lakes. Geochemistry, 1-50.

Kusakabe, M., Ohsumi, T., & Aramaki, S. (1989). The Lake Nyos gas disaster: chemical and isotopic evidence in waters and dissolved gases from three Cameroonian crater lakes, Nyos, Monoun and Wum. Journal of volcanology and geothermal research, 39(2-3), 167-185.

Kusakabe, M., Komoda, Y., Takano, B., & Abiko, T. (2000a). Sulfur isotopic effects in the disproportionation reaction of sulfur dioxide in hydrothermal fluids: implications for the δ^{34}S variations of dissolved bisulfate and elemental sulfur from active crater lakes. Journal of Volcanology and Geothermal Research, 97(1-4), 287-307.

Kusakabe, M., Tanyileke, G. Z., McCord, S. A., & Schladow, S. G. (2000b). Recent pH and CO_2 profiles at Lakes Nyos and Monoun, Cameroon: implications for the degassing strategy and its numerical simulation. Journal of Volcanology and Geothermal Research, 97(1-4), 241-260.

Kusakabe, M., Ohba, T., Yoshida, Y., Satake, H., Ohizumi, T., Evans, W. C., ... & Kling, G. W. (2008). Evolution of CO2 in Lakes Monoun and Nyos, Cameroon, before and during controlled degassing. Geochemical Journal, 42(1), 93-118.

Laiolo, M., Coppola, D., Barahona, F., Benítez, J. E., Cigolini, C., Escobar, D., ... & Montalvo, F. (2017). Evidences of volcanic unrest on high-temperature fumaroles by satellite thermal monitoring: The case of Santa Ana volcano, El Salvador. Journal of Volcanology and Geothermal Research, 340, 170-179.

Lebamba, J., Vincens, A., & Maley, J. (2012). Pollen, vegetation change and climate at Lake Barombi Mbo (Cameroon) during the last ca. 33 000 cal yr BP: a numerical approach. Climate of the Past, 8(1), 59-78.

Lefkowitz, J., Varekamp, J. C., & Ku, T. C. W. (2012, March). A tale of two lakes: natural contamination in the Newberry Caldera, OR. In Abstr. Programs Geol. Soc. Am (Vol. 44, No. 2, p. 91).

Lefkowitz, J. N., Varekamp, J. C., Reynolds, R. W., & Thomas, E. (2017). A tale of two lakes: the Newberry Volcano twin crater lakes, Oregon, USA. In: Ohba, T., Capaccioni, B. & Caudron, C. (eds) Geochemistry and geophysics of Active Volcanic Lakes. Geological Society, London, Special Publications, 437, 253-288. First published online November 25, 2016.

Lloyd, E. F. (1974). Waimangu hydrology and temperature measurements–1972. NZ volcanol. Rec, 2, 55-57.

Lowenstern, J. B. (2001). Carbon dioxide in magmas and implications for hydrothermal systems. Mineralium Deposita, 36(6), 490-502.

Macdonald, B. C., Denmead, O. T., White, I., & Melville, M. D. (2004). Natural sulfur dioxide emissions from sulfuric soils. Atmospheric Environment, 38, 1473-1480. https://doi.org/10.1016/j.atmosenv.2003.12.005

MacLeod, N. S., & Sherrod, D. R. (1988). Geologic evidence for a magma chamber beneath Newberry Volcano, Oregon. Journal of Geophysical Research: Solid Earth, 93(B9), 10067-10079.

Maeda, Y., Kumagai, H., Lacson Jr, R., Figueroa, M. S., Yamashina, T., Ohkura, T., & Baloloy, A. V. (2015). A phreatic explosion model inferred from a very long period seismic event at Mayon Volcano, Philippines. Journal of Geophysical Research: Solid Earth, 120(1), 226-242.

Mahon, W. A. J. (1965). Waimangu geochemistry. NZ Dept. Sci. Indust. Res., Volcanol. Inform. Ser, 50, 46-48.

Maley, J., Livingstone, D. A., Giresse, P., Thouveny, N., Brenac, P., Kelts, K., ... & Bandet, Y. (1990). Lithostratigraphy, volcanism, paleomagnetism and palynology of Quaternary lacustrine deposits from Barombi Mbo (West Cameroon): preliminary results. Journal of Volcanology and Geothermal Research, 42(4), 319-335.

Manville, V. (2015). Volcano-hydrologic hazards from volcanic lakes. In Volcanic Lakes (pp. 21-71). Springer, Berlin, Heidelberg.

Marini, L., Zuccolini, M. V., & Saldi, G. (2003). The bimodal pH distribution of volcanic lake waters. Journal of Volcanology and Geothermal Research, 121(1-2), 83-98.

Marini, L., Moretti, R., & Accornero, M. (2011). Sulfur isotopes in magmatic-hydrothermal systems, melts, and magmas. Reviews in Mineralogy and Geochemistry, 73(1), 423-492.

Martınez, M., Fernández, E., Valdés, J., Barboza, V., Van der Laat, R., Duarte, E., ... & Marino, T. (2000). Chemical evolution and volcanic activity of the active crater lake of Poás volcano, Costa Rica, 1993–1997. Journal of Volcanology and Geothermal Research, 97(1-4), 127-141.

Martini, M., Piccardi, G., & Legittimo, P. C. (1980). Geochemical surveillance of active volcanoes: data on the fumaroles of Vulcano (Aeolian Islands, Italy). Bulletin of Volcanology, 43(1), 255-263.

Martini, F., Tassi, F., Vaselli, O., Del Potro, R., Martinez, M., Van del Laat, R., & Fernandez, E. (2010). Geophysical, geochemical and geodetical signals of reawakening at Turrialba volcano (Costa Rica) after almost 150 years of quiescence. Journal of volcanology and Geothermal research, 198(3-4), 416-432.

Mas, G. R., Mas, L. C., Bengochea, L., & del Neuqukn, E. P. D. E. (1996, January). Hydrothermal surface alteration in the Copahue geothermal field (Argentina). In Proceedings, 21st Workshop on Geothermal Reservoir Engineering, Stanford University, Palo Alto California, January (Vol. 2224).

Mas, L. C., Mas, G. R., & Bengochea, L. (2000, June). Heatflow of Copahue geothermal field, its relation with tectonic scheme. In Proceedings of world geothermal congress, Tohoku, Japan (pp. 1419-1424).

Mastin, L. G., & Witter, J. B. (2000). The hazards of eruptions through lakes and seawater. Journal of Volcanology and Geothermal Research, 97(1-4), 195-214.

Maury, R. C., Westbrook, G. K., Baker, P. E., Bouysse, P., & Westercamp, D. (1990). The Geology of North America Vol. H, The Caribbean Region The Geological Society of America, 1990. The Caribbean region, (1), 141.

Maussen, K., Villacorte, E., Rebadulla, R. R., Maximo, R. P., Debaille, V., Bornas, M. A., & Bernard, A. (2018). Geochemical characterisation of Taal volcano-hydrothermal system and temporal evolution during continued phases of unrest (1991–2017). Journal of volcanology and geothermal research, 352, 38-54.

Mazor, E., Cioni, R., Corazza, E., Fratta, M., Magro, G., Matsuo, S., ... & Cellini-Legittimo, P. (1988). Evolution of fumarolic gases—boundary conditions set by measured parameters: case study at Vulcano, Italy. Bulletin of Volcanology, 50(2), 71-85.

Mazot, A., & Taran, Y. (2009). CO_2 flux from the volcanic lake of El Chichón (Mexico). Geofísica internacional, 48(1), 73-83.

Mazot, A., Bernard, A., Fischer, T., Inguaggiato, S., & Sutawidjaja, I. S. (2008). Chemical evolution of thermal waters and changes in the hydrothermal system of Papandayan volcano (West Java, Indonesia) after the November 2002 eruption. Journal of Volcanology and Geothermal Research, 178(2), 276-286.

Mazot, A., Rouwet, D., Taran, Y., Inguaggiato, S., & Varley, N. (2011). CO_2 and He degassing at El Chichón volcano, Chiapas, Mexico: gas flux, origin and relationship with local and regional tectonics. Bulletin of volcanology, 73(4), 423-441.

Mazza, R., Taviani, S., Capelli, G., De Benedetti, A. A., & Giordano, G. (2015). Quantitative hydrogeology of volcanic lakes: examples from the Central Italy Volcanic Lake District. In Volcanic Lakes (pp. 355-377). Springer, Berlin, Heidelberg.

Melián, G., Somoza, L., Padrón, E., Pérez, N. M., Hernández, P. A., Sumino, H., ... & França, Z. (2017). Surface CO_2 emission and rising bubble plumes from degassing of crater lakes in Sao Miguel Island, Azores. In: Ohba, T., Capaccioni, B. & Caudron, C. (eds) Geochemistry and geophysics of Active Volcanic Lakes. Geological Society, London, Special Publications, 437, 233-252. First published online August 12, 2016.

Melnick, D., Folguera, A., & Ramos, V. A. (2006). Structural control on arc volcanism: The Caviahue–Copahue complex, Central to Patagonian Andes transition (38 S). Journal of South American Earth Sciences, 22(1-2), 66-88.

Melnikov, D., & Ushakov, S. (2011). SO_2 gas emission of Mutnovsky and Gorely volcanoes (Kamchatka): satellite data and ground-based observations. In Abstract CCVG11 Workshop on Volcanic Gases. Kamchatka, Russia (p. 33).

Mendoza-Rosas, A. T., & De la Cruz-Reyna, S. (2008). A statistical method linking geological and historical eruption time series for volcanic hazard estimations: applications to active polygenetic volcanoes. Journal of Volcanology and Geothermal Research, 176(2), 277-290.

Mercalli, G., & Silvestri, O. (1888). Le eruzioni dell'isola di Vulcano incominciate il 3 Agosto 1888. Ann. Uff. Centr. Meteor. Geodin. X.

Meyer-Abich, H. (1956). Los Volcanes Activos De Guatemala Y El Salvador,(America Central). Ministerio de Obras Públicas, República de El Salvador.

Miloshevich, L. M., Paukkunen, A., Vömel, H., & Oltmans, S. J. (2004). Development and validation of a time-lag correction for Vaisala radiosonde humidity measurements. Journal of Atmospheric and Oceanic Technology, 21(9), 1305-1327.

Minakami, T., Matsuita, K., & Utibori, S. (1943). 36. Explosive Activities of Volcano Kusatu-Sirane during 1938 and 1942.(Part II). Bull. Earthq. Res. Inst, 20(4), 505-526.

Miyabuchi, Y., & Terada, A. (2009). Subaqueous geothermal activity revealed by lacustrine sediments of the acidic Nakadake crater lake, Aso Volcano, Japan. Journal of Volcanology and Geothermal Research, 187(1-2), 140-145.

Mizutani, Y., & Sugiura, T. (1966). The chemical equilibrium of the $2H_2S + SO_2 = 3S + 2H_2O$ reaction in solfataras of the Nasudake Volcano. Bulletin of the Chemical Society of Japan, 39(11), 2411-2414.

Molnar, P., & Sykes, L. R. (1969). Tectonics of the Caribbean and Middle America regions from focal mechanisms and seismicity. Geological Society of America Bulletin, 80(9), 1639-1684.

Mooser, F., Meyer-Abich, H., & McBirney, A. R. (1958). Catalogue of the Active Volcanoes and Solfatara Fields of Central America. International Volcanological Association.

Morgan, D. S., Tanner, D. Q., & Crumrine, M. D. (1997). Hydrologic and Water-quality Conditions at Newberry Volcano Deschutes County, Oregon, 1991-95. US Department of the Interior, US Geological Survey.

Morse, J. W., Millero, F. J., Cornwell, J. C., & Rickard, D. (1987). The chemistry of the hydrogen sulfide and iron sulfide systems in natural waters. Earth-Science Reviews, 24, 1-42.

Moussallam, Y., Tamburello, G., Peters, N., Apaza, F., Schipper, C. I., Curtis, A., ... & Barnie, T. (2017). Volcanic gas emissions and degassing dynamics at Ubinas and Sabancaya volcanoes; implications for the volatile budget of the central volcanic zone. Journal of Volcanology and Geothermal Research, 343, 181-191.

Murphy, S., Wright, R., & Rouwet, D. (2018). Color and temperature of the crater lakes at Kelimutu volcano through time. Bulletin of Volcanology, 80(1), 2.

Nairn, I. A., Scott, B. J., Otway, P. M., & Cody, A. D. (1982). Depth measurement in Ruapehu Crater Lake. Volcano News, 12(3).

Nakai, N., & Jensen, M. L. (1964). The kinetic isotope effect in the bacterial reduction and oxidation of sulfur. Geochimica et Cosmochimica Acta, 28(12), 1893-1912.

Ngwa, C. N., Suh, C. E., & Devey, C. W. (2010). Phreatomagmatic deposits and stratigraphic reconstruction at Debunscha Maar (Mt Cameroon volcano). Journal of Volcanology and Geothermal Research, 192(3-4), 201-211.

Nicholls, H. A. A. (1880a). The volcanic eruption in Dominica, Nature, 21, 372-373.

Nicholls, H. A. A. (1880b). Visit to the scene of the late volcanic eruption, The Dominican, 17 January 1880.

Ohba, T., Fantong, W., Fouepe, A., Tchamabe, B. C., Yoshida, Y., Kusakabe, M., ... & Satake, H. (2013). Contribution of methane to total gas pressure in deep waters at lakes Nyos and Monoun (Cameroon, West Africa). Geochemical Journal, 47(3), 349-362.

Ohba, T., Hirabayashi, J. I., & Nogami, K. (1994). Water, heat and chloride budgets of the crater lake, Yugama at Kusatsu-Shirane volcano, Japan. Geochemical Journal, 28(3), 217-231.

Ohba, T., Hirabayashi, J., & Nogami, K. (2000). D/H and $^{18}O/^{16}O$ ratios of water in the crater lake at Kusatsu-Shirane volcano, Japan. Journal of volcanology and geothermal research, 97(1-4), 329-346.

Ohba, T., Hirabayashi, J. I., & Nogami, K. (2008). Temporal changes in the chemistry of lake water within Yugama Crater, Kusatsu-Shirane Volcano, Japan: Implications for the evolution of the magmatic hydrothermal system. Journal of Volcanology and Geothermal Research, 178(2), 131-144.

Ohba, T., Tchamabé, B. C., Padrón, E., Hernández, P., Takem, E. E., Barrancos, J., ... & Yoshida, Y. (2014). Gas emission from diffuse degassing structures (DDS) of the Cameroon volcanic line (CVL):

Implications for the prevention of CO_2-related hazards. Journal of Volcanology and Geothermal Research, 283, 82-93.

Ohba, T., Ooki, S., Oginuma, Y., Kusakabe, M., Yoshida, Y., Ueda, A., ... & Aka, F. (2017). Decreasing removal rate of the dissolved CO_2 in Lake Nyos, Cameroon, after the installation of additional degassing pipes. In: Ohba, T., Capaccioni, B. & Caudron, C. (eds) Geochemistry and geophysics of Active Volcanic Lakes. Geological Society, London, Special Publications, 437, 177-184. First published online December 23, 2015.

Ohmoto, H., & Rye, R. (1972). 0.(1979) Isotopes of sulfur and carbon. Geochemistry of hydrothermal ore deposits, 509-567.

Ohsawa, S. (2003). Some geochemical features of Yudamari crater lake, Aso Volcano, Japan. Geotherm. Res. Rep. Kyusyu Univ., 12, 62-65.

Ohsawa, S., Takano, B., Kusakabe, M., & Watanuki, K. (1993). Variation in volcanic activity of Kusatsu-Shirane volcano as inferred from $\delta^{34}S$ in sulfate from the Yugama crater lake. Bulletin of the Volcanological Society of Japan, 38(3), 95-99

Ohsawa, S., Saito, T., Yoshikawa, S., Mawatari, H., Yamada, M., Amita, K., ... & Kagiyama, T. (2010). Color change of lake water at the active crater lake of Aso volcano, Yudamari, Japan: is it in response to change in water quality induced by volcanic activity?. Limnology, 11(3), 207-215.

Olmos, R., Barrancos, J., Rivera, C., Barahona, F., López, D. L., Henriquez, B., ... & Galle, B. O. (2007). Anomalous emissions of SO_2 during the recent eruption of Santa Ana volcano, El Salvador, Central America. Pure and Applied Geophysics, 164(12), 2489-2506.

Ono, K., Watanabe, K., Hoshizumi, H., & Ikebe, S. I. (1995). Ash eruption of the Naka-dake crater, Aso volcano, southwestern Japan. Journal of volcanology and geothermal research, 66(1-4), 137-148.

Oppenheimer, C. (1997). Ramifications of the skin effect for crater lake heat budget analysis. Journal of Volcanology and Geothermal Research, 75(1-2), 159-165.

Oppenheimer, C., Francis, P. W., Rothery, D. A., Carlton, R. W., & Glaze, L. S. (1993). Infrared image analysis of volcanic thermal features: Lascar Volcano, Chile, 1984–1992. Journal of Geophysical Research: Solid Earth, 98(B3), 4269-4286.

Oppenheimer, C., Scaillet, B., & Martin, R. S. (2011). Sulfur degassing from volcanoes: source conditions, surveillance, plume chemistry and earth system impacts. Reviews in Mineralogy and Geochemistry, 73(1), 363-421.

Orsi, G., De Vita, S., & Di Vito, M. (1996). The restless, resurgent Campi Flegrei nested caldera (Italy): constraints on its evolution and configuration. Journal of Volcanology and Geothermal Research, 74(3-4), 179-214.

Orsi, G., Di Vito, M. A., & Isaia, R. (2004). Volcanic hazard assessment at the restless Campi Flegrei caldera. Bulletin of Volcanology, 66(6), 514-530.

Ossaka, J., Ozawa, T., Nomara, T., Ossaka, T., Hirabayashi, J., Takaesu, A., & Hayashi, T. (1980). Variation of chemical compositions in volcanic gases and water at Kusatsu-Shirane Volcano and its activity in 1976. Bulletin Volcanologique, 43(1), 207-216.

Ossaka, J., Ossaka, T., Hirabayashi, J., Oi, T., Ohba, T., Nogami, K., ... & Fukuhara, H. (1997). Volcanic activity of Kusatsu-Shirane volcano, Gunma, and secular change in water quality of crater lake Yugama. Chikyukagaku, 31, 119-128.

Paganin, P., Chiarini, L., Bevivino, A., Dalmastri, C., Farcomeni, A., Izzo, G., ... & Tabacchioni, S. (2013). Vertical distribution of bacterioplankton in Lake Averno in relation to water chemistry. FEMS microbiology ecology, 84(1), 176-188.

Paonita, A., Federico, C., Bonfanti, P., Capasso, G., Inguaggiato, S., Italiano, F., ... & Sortino, F. (2013). The episodic and abrupt geochemical changes at La Fossa fumaroles (Vulcano Island, Italy) and related constraints on the dynamics, structure, and compositions of the magmatic system. Geochimica et cosmochimica acta, 120, 158-178.

Pardyanto, L. (1990). Progress of volcano monitoring system in Indonesia. Bulletin of the International Institute of Seismology and Earthquake Engineering, 24, 59-70.

Pasternack, G. B., & Varekamp, J. C. (1994). The geochemistry of the Keli Mutu crater lakes, Flores, Indonesia. Geochemical journal, 28(3), 243-262.

Pasternack, G. B., & Varekamp, J. C. (1997). Volcanic lake systematics I. Physical constraints. Bulletin of volcanology, 58(7), 528-538.

Pedroni, A., Hammerschmidt, K., & Friedrichsen, H. (1999). He, Ne, Ar, and C isotope systematics of geothermal emanations in the Lesser Antilles Islands Arc. Geochimica et Cosmochimica Acta, 63(3-4), 515-532.

Peiffer, L., Taran, Y. A., Lounejeva, E., Solís-Pichardo, G., Rouwet, D., & Bernard-Romero, R. A. (2011). Tracing thermal aquifers of El Chichón volcano–hydrothermal system (México) with $^{87}Sr/^{86}Sr$, Ca/Sr and REE. Journal of Volcanology and Geothermal Research, 205(3-4), 55-66.

Peiffer, L., Rouwet, D., & Taran, Y. (2015). Fluid geochemistry of El Chichón volcano-hydrothermal system. In Active Volcanoes of Chiapas (Mexico): El Chichón and Tacaná (pp. 77-95). Springer, Berlin, Heidelberg.

Pérez, N. M., Hernández, P. A., Padilla, G., Nolasco, D., Barrancos, J., Melían, G., ... & Notsu, K. (2011). Global CO_2 emission from volcanic lakes. Geology, 39(3), 235-238.

Pope, J., & Brown, K. L. (2014). Geochemistry of discharge at Waiotapu geothermal area, New Zealand–trace elements and temporal changes. Geothermics, 51, 253-269.

Pullinger, C. R. (1998). Evolution of the Santa Ana volcanic complex, El Salvador, 145 pp (MS thesis, Mich. Technol. Univ., Houghton).

Ramírez, C.J., Mora-Amador, R.A., González, G., Alpizar, Y., 2013. Applications of infrared cameras at Costa Rican volcanoes, crater lakes and thermal features. 8th Workshop on Volcanic Lakes. IAVCEI Commission on Volcanic Lakes, Japan, p. 6.

Reyes, P. J. D., Bornas, M. A. V., Dominey-Howes, D., Pidlaoan, A. C., Magill, C. R., & Solidum, R. U. (2017). A synthesis and review of historical eruptions at Taal Volcano, Southern Luzon, Philippines. Earth-Science Reviews.

Rodríguez, A., Bergen, M. J., & Eggenkamp, H. G. (2017). Experimental evaporation of hyperacid brines: Effects on chemical composition and chlorine isotope fractionation. Geochimica et Cosmochimica Acta.

Roobol, M.J., and A.L. Smith (2005). Geological Map of Dominica, scale 1:100,000, In: J. M. Lindsay, R. E. A. Robertson, J. B. Sheph erd and S. Ali (eds.), Volcanic Hazard Atlas of the Lesser Antilles, University of the West Indies.

Rosi, M., & Sbrana, A. (Eds.). (1987). Phlegrean fields (Vol. 9). Consiglio nazionale delle ricerche.

Rouwet, D., & Morrissey, M. M. (2015). Mechanisms of crater lake breaching eruptions. In Volcanic Lakes (pp. 73-91). Springer, Berlin, Heidelberg.

Rouwet, D., & Ohba, T. (2015). Isotope fractionation and HCl partitioning during evaporative degassing from active crater lakes. In Volcanic Lakes (pp. 179-200). Springer, Berlin, Heidelberg.

Rouwet, D., & Tassi, F. (2011). Geochemical monitoring of volcanic lakes. A generalized box model for active crater lakes. Annals of Geophysics, 54(2).

Rouwet, D., Taran, Y. A., & Varley, N. R. (2004). Dynamics and mass balance of El Chichón crater lake, Mexico. Geofísica Internacional, 43, 427-434.

Rouwet, D., Taran, Y., Inguaggiato, S., Varley, N., & Santiago, J. S. (2008). Hydrochemical dynamics of the "lake–spring" system in the crater of El Chichón volcano (Chiapas, Mexico). Journal of Volcanology and Geothermal Research, 178(2), 237-248.

Rouwet, D., Bellomo, S., Brusca, L., Inguaggiato, S., Jutzeler, M., Mora, R., . . . Taran, Y. (2009). Major and trace element geochemistry of El Chichón volcano-hydrothermal system (Chiapas, Mexico) in 2006-2007: Implications for future geochemical monitoring. Geofísica internacional, 48, 55-72.

Rouwet, D., Sandri, L., Marzocchi, W., Gottsmann, J., Selva, J., Tonini, R., & Papale, P. (2014a). Recognizing and tracking volcanic hazards related to non-magmatic unrest: a review. Journal of Applied Volcanology, 3(1), 17.

Rouwet, D., Tassi, F., Mora-Amador, R., Sandri, L., & Chiarini, V. (2014b). Past, present and future of volcanic lake monitoring. Journal of volcanology and geothermal research, 272, 78-97.

Rouwet, D., Christenson, B. W., Tassi, F., & Vandemeulebrouck, J. (2015). Volcanic Lakes. Springer.

Rouwet, D., Sandri, L., Todesco, M., Tonini, R., Pecoraino, G., & Diliberto, I. S. (2016, April). Recurrent patterns in fluid geochemistry data prior to phreatic eruptions. In EGU General Assembly Conference Abstracts (Vol. 18, p. 7755).

Rouwet, D., Mora-Amaña, R., Ramírez-Umaña, C. J., González, G., & Inguaggiato, S. (2017). Dynamic fluid recycling at Laguna Caliente (Poás, Costa Rica) before and during the 2006–ongoing phreatic eruption cycle (2005–10). In: Ohba, T., Capaccioni, B. & Caudron, C. (eds) Geochemistry and geophysics of Active Volcanic Lakes. Geological Society, London, Special Publications, 437, 73-96. First published online March 24, 2016.

Rowe Jr, G. L. (1994). Oxygen, hydrogen, and sulfur isotope systematics of the crater lake system of Poas volcano, Costa Rica. Geochemical Journal, 28(3), 263-287.

Rowe Jr, G. L., Brantley, S. L., Fernandez, M., Fernandez, J. F., Borgia, A., & Barquero, J. (1992a). Fluid-volcano interaction in an active stratovolcano: the crater lake system of Poás volcano, Costa Rica. Journal of Volcanology and Geothermal Research, 49(1-2), 23-51.

Rowe, G. L., Ohsawa, S., Takano, B., Brantley, S. L., Fernandez, J. F., & Barquero, J. (1992b). Using crater lake chemistry to predict volcanic activity at Poás volcano, Costa Rica. Bulletin of volcanology, 54(6), 494-503.

Rowe Jr, G. L., Brantley, S. L., Fernandez, J. F., & Borgia, A. (1995). The chemical and hydrologic structure of Poa s volcano, Costa Rica. Journal of Volcanology and Geothermal Research, 64(3-4), 233-267.

Rye, R. O. (2005). A review of the stable-isotope geochemistry of sulfate minerals in selected igneous environments and related hydrothermal systems. Chemical Geology, 215(1-4), 5-36.

Rye, R. O., Bethke, P. M., & Wasserman, M. D. (1992). The stable isotope geochemistry of acid sulfate alteration. Economic Geology, 87(2), 225-262.

Rymer, H., Cassidy, J., Locke, C. A., Barboza, M. V., Barquero, J., Brenes, J., & Van der Laat, R. (2000). Geophysical studies of the recent 15-year eruptive cycle at Poas Volcano, Costa Rica. Journal of Volcanology and Geothermal Research, 97(1-4), 425-442.

Rymer, H., Locke, C. A., Borgia, A., Martinez, M., Brenes, J., Van der Laat, R., & Williams-Jones, G. (2009). Long-term fluctuations in volcanic activity: implications for future environmental impact. Terra Nova, 21(4), 304-309.

Sabroux, J. C., Dubois, E., & Doyotte, C. (1987, March). The limnic eruption: a new geological hazard. In International Scientific Congress on Lake Nyos Disaster (Vol. 16, p. 20).

Saito, T., Ouhsawa, S., Hashimoto, T., Terada, A., Yoshikawa, S., & Ohkuba, T. (2008). Water, heat and chloride balances of the crater lake at Aso volcano, Japan. Journal of the Geothermal Research Society of Japan, 30(2), 107-120.

Sakai, H. (1968). Isotopic properties of sulfur compounds in hydrothermal processes. Geochemical Journal, 2(1), 29-49.

Sander, R. (1999). Compilation of Henry's law constants for inorganic and organic species of potential importance in environmental chemistry.

Sander, R. (2015). Compilation of Henry's law constants (version 4.0) for water as solvent. Atmospheric Chemistry & Physics, 15(8).

Sandri, L., Marzocchi, W., & Zaccarelli, L. (2004). A new perspective in identifying the precursory patterns of eruptions. Bulletin of Volcanology, 66(3), 263-275.

Sandri, L., Marzocchi, W., & Gasperini, P. (2005). Some insights on the occurrence of recent volcanic eruptions of Mount Etna volcano (Sicily, Italy). Geophysical Journal International, 163(3), 1203-1218.

Sato, H., Aramaki, S., Kusakabe, M., Hirabayashi, J. I., Sano, Y., Nojiri, Y., & Tchoua, F. (1990). Geochemical difference of basalts between polygenetic and monogenetic volcanoes in the central part of the Cameroon volcanic line. Geochemical Journal, 24(6), 357-370.

Schaefer, J. R., Scott, W. E., Evans, W. C., Jorgenson, J., McGimsey, R. G., & Wang, B. (2008). The 2005 catastrophic acid crater lake drainage, lahar, and acidic aerosol formation at Mount Chiginagak volcano, Alaska, USA: field observations and preliminary water and vegetation chemistry results. Geochemistry, Geophysics, Geosystems, 9(7).

Schmid, M., Halbwachs, M., Wehrli, B., & Wüest, A. (2005). Weak mixing in Lake Kivu: new insights indicate increasing risk of uncontrolled gas eruption. Geochemistry, Geophysics, Geosystems, 6(7).

Schmincke, H. U. (2004). Volcanism (Vol. 28). Springer Science & Business Media.

Schoell, M., Tietze, K., & Schoberth, S. M. (1988). Origin of methane in Lake Kivu (east-central Africa). Chemical Geology, 71(1-3), 257-265.

Schulte, M. D., Shock, E. L., & Wood, R. H. (2001). The temperature dependence of the standard-state thermodynamic properties of aqueous nonelectrolytes. Geochimica et Cosmochimica Acta, 65(21), 3919-3930.

Scolamacchia, T., & Cronin, S. J. (2016). Idiosyncrasies of volcanic sulfur viscosity and the triggering of unheralded volcanic eruptions. Frontiers in Earth Science, 4, 24.

Scolamacchia, T., Pullinger, C., Caballero, L., Montalvo, F., Orosco, L. E. B., & Hernández, G. G. (2010). The 2005 eruption of Ilamatepec (Santa Ana) volcano, El Salvador. Journal of Volcanology and Geothermal Research, 189(3), 291-318.

Sheppard, D. S. (1986). Fluid chemistry of the Waimangu geothermal system. Geothermics, 15(3), 309-328.

Sherrod, D. R., Mastin, L. G., Scott, W. E., & Schilling, S. P. (1997). Volcano hazards at Newberry Volcano, Oregon. Open-file report 97–0513. US Geological Survey.

Shinohara, H. (2005). A new technique to estimate volcanic gas composition: plume measurements with a portable multi-sensor system. Journal of Volcanology and Geothermal Research, 143(4), 319-333.

Shinohara, H., Yoshikawa, S., & Miyabuchi, Y. (2010). Degassing of Aso Volcano, Japan through an acid crater lake: differentiation of volcanic gas-hydrothermal fluids deduced from volcanic plume chemistry. AGU Fall Meeting Abstracts.

Shinohara, H., Yoshikawa, S., & Miyabuchi, Y. (2015). Degassing activity of a volcanic crater lake: volcanic plume measurements at the Yudamari crater lake, Aso volcano, Japan. In Volcanic lakes (pp. 201-217). Springer, Berlin, Heidelberg.

Shinohara, H., Yokoo, A., & Kazahaya, R. (2018). Variation of volcanic gas composition during the eruptive period in 2014–2015 at Nakadake crater, Aso volcano, Japan. Earth, Planets and Space, 70(1), 151.

Siebert, L., Simkin, T., & Kimberly, P. (2010). Volcanoes of the World. Univ of California Press.

Sigurdsson, H. (1977). Chemistry of the crater lake during the 1971–1972 Soufrière eruption. Journal of Volcanology and Geothermal Research, 2(2), 165-186.

Sigurdsson, H. (1987). Lethal gas bursts from Cameroon crater lakes. Eos, Transactions American Geophysical Union, 68(23), 570-573.

Sigurdsson, H., Carey, S. N., & Espindola, J. M. (1984). The 1982 eruptions of El Chichón volcano, Mexico: stratigraphy of pyroclastic deposits. Journal of Volcanology and Geothermal Research, 23, 11-37. https://doi.org/10.1016/0377-0273(84)90055-6

Sigurdsson, H., Devine, J. D., Tchua, F. M., Presser, F. M., Pringle, M. K. W., & Evans, W. C. (1987). Origin of the lethal gas burst from Lake Monoun, Cameroun. Journal of Volcanology and Geothermal Research, 31(1-2), 1-16.

Sigvaldason, G. E. (1979). Rifting, magmatic activity and interaction between acid and basic liquids. Nord Volcanol Inst Rep, 7903.

Sigvaldason, G. E. (1989). International conference on Lake Nyos disaster, Yaoundé, Cameroon 16-20 March, 1987: Conclusions and recommendations. Journal of Volcanology and Geothermal Research, 39, 97-107.

Silvestri, O., Mercalli, G., Grablowitz, G., & Clerici, V. (1891). Le eruzioni dell'isola di Vulcano, incominciate il 3 Agosto 1888 e terminate il 22 Marzo 1890. Ann Uff Centr Meteor Geod, 10, 212.

Simkin, T., & Siebert, L. (1994). Volcanoes of the World, 349 pp. Geoscience, Tucson, Ariz.

SNET monthly reports. http://www.snet.gob.sv/ver/vulcanologia/monitoreo/informe+mensual/?id_volcan=6

Spampinato, L., Oppenheimer, C., Cannata, A., Montalto, P., Salerno, G. G., & Calvari, S. (2012). On the time-scale of thermal cycles associated with open-vent degassing. Bulletin of volcanology, 74(6), 1281-1292.

Sriwana, T., Van Bergen, M. J., Sumarti, S., De Hoog, J. C. M., Van Os, B. J. H., Wahyuningsih, R., & Dam, M. A. C. (1998). Volcanogenic pollution by acid water discharges along Ciwidey River, West Java (Indonesia). Journal of Geochemical Exploration, 62(1-3), 161-182.

Sriwana, T., Van Bergen, M. J., Varekamp, J. C., Sumarti, S., Takano, B., Van Os, B. J. H., & Leng, M. J. (2000). Geochemistry of the acid Kawah Putih lake, Patuha volcano, west Java, Indonesia. Journal of Volcanology and Geothermal Research, 97(1-4), 77-104.

Sruoga, P., & Consoli, V. (2011, May). Volcán Copahue. In Relatorio XVIII Congreso Geológico Argentino (Vol. 2, No. 6).

Stern, C. R. (2004). Active Andean volcanism: its geologic and tectonic setting. Revista geológica de Chile, 31(2), 161-206.

Stimac, J. A., Goff, F., Counce, D., Larocque, A. C., Hilton, D. R., & Morgenstern, U. (2004). The crater lake and hydrothermal system of Mount Pinatubo, Philippines: evolution in the decade after eruption. Bulletin of Volcanology, 66(2), 149-167.

Stix, J., & de Moor, J. M. (2018). Understanding and forecasting phreatic eruptions driven by magmatic degassing. Earth, Planets and Space, 70(1), 83.

Strehlow, K., Gottsmann, J., Rust, A., Hemmings, B., & Hautmann, S. (2017). Hydrological responses to volcanic strain and the arising capabilities for volcano monitoring.

Stumm, W., & Morgan, J. J. (1981). Aquatic Chemistry, 780 pp.

Sudo, Y., Tsutsui, T., Nakaboh, M., Yoshikawa, M., Yoshikawa, S., & Inoue, H. (2006). Ground deformation and magma reservoir at Aso Volcano: location of deflation source derived from long-term geodetic surveys. Bull Volcanol Soc Jpn, 51, 291-309.

Sugimura, A. (1960). Zonal arrangement of some geophysical and petrological features in Japan and its environs. J. Fac. Sci., Univ. Tokyo, SecII, 133-153.

Symonds, R. B., Rose, W. I., Reed, M. H., Lichte, F. E., & Finnegan, D. L. (1987). Volatilization, transport and sublimation of metallic and non-metallic elements in high temperature gases at Merapi Volcano, Indonesia. Geochimica et Cosmochimica Acta, 51(8), 2083-2101.

Symonds, R. B., Rose, W. I., Bluth, G. J., & Gerlach, T. M. (1994). Volcanic-gas studies; methods, results, and applications. Reviews in Mineralogy and Geochemistry, 30(1), 1-66.

Symonds, R. B., Gerlach, T. M., & Reed, M. H. (2001). Magmatic gas scrubbing: implications for volcano monitoring. Journal of Volcanology and Geothermal Research, 108(1-4), 303-341.

Takano, B. (1987). Correlation of volcanic activity with sulfur oxyanion speciation in a crater lake. Science, 235(4796), 1633-1635.

Takano, B., & Watanuki, K. (1990). Monitoring of volcanic eruptions at Yugama crater lake by aqueous sulfur oxyanions. Journal of Volcanology and Geothermal Research, 40(1), 71-87.

Takano, B., Ohsawa, S., & Glover, R. B. (1994). Surveillance of Ruapehu crater lake, New Zealand, by aqueous polythionates. Journal of Volcanology and Geothermal Research, 60(1), 29-57.

Takano, B., Suzuki, K., Sugimori, K., Ohba, T., Fazlullin, S. M., Bernard, A., ... & Hirabayashi, M. (2004). Bathymetric and geochemical investigation of Kawah Ijen crater lake, East Java, Indonesia. Journal of Volcanology and Geothermal Research, 135(4), 299-329.

Tamburello, G. (2015). Ratiocalc: software for processing data from multicomponent volcanic gas analyzers. Computers & Geosciences, 82, 63-67.

Tamburello, G., Agusto, M., Caselli, A., Tassi, F., Vaselli, O., Calabrese, S., ... & Chiodini, G. (2015). Intense magmatic degassing through the lake of Copahue volcano, 2013–2014. Journal of Geophysical Research: Solid Earth, 120(9), 6071-6084.

Taran, Y., & Rouwet, D. (2008). Estimating thermal inflow to El Chichón crater lake using the energy-budget, chemical and isotope balance approaches. Journal of Volcanology and Geothermal Research, 175(4), 472-481.

Taran, Y. A., & Peiffer, L. (2009). Hydrology, hydrochemistry and geothermal potential of El Chichón volcano-hydrothermal system, Mexico. Geothermics, 38(4), 370-378.

Taran, Y. A., Znamenskiy, V. S., & Yurova, L. M. (1996). Geochemical model of the hydrothermal system of Baransky volcano, Iturup, Kuril islands. Volcanol. Seismol, 17, 471-496.

Taran, Y., Fischer, T. P., Pokrovsky, B., Sano, Y., Armienta, M. A., & Macias, J. L. (1998). Geochemistry of the volcano-hydrothermal system of El Chichón Volcano, Chiapas, Mexico. Bulletin of Volcanology, 59(6), 436-449.

Taran, Y., Gavilanes, J. C., Cortés, A., & Armienta, M. A. (2000). Chemical precursors to the 1998-1999 eruption of Colima volcano, Mexico. Revista mexicana de ciencias geológicas, 17(2), 112-126.

Taran, Y., Inguaggiato, S., Cardellini, C., & Karpov, G. (2013). Posteruption chemical evolution of a volcanic caldera lake: Karymsky Lake, Kamchatka. Geophysical research letters, 40(19), 5142-5146.

Tassi, F., & Rouwet, D. (2014). An overview of the structure, hazards, and methods of investigation of Nyos-type lakes from the geochemical perspective. Journal of limnology, 73(1).

Tassi, F., Vaselli, O., Capaccioni, B., Macias, J. L., Nencetti, A., Montegrossi, G., & Magro, G. (2003). Chemical composition of fumarolic gases and spring discharges from El Chichón volcano, Mexico: causes and implications of the changes detected over the period 1998-2000. Journal of Volcanology and Geothermal Research, 123, 105-121.

Tassi, F., Vaselli, O., Capaccioni, B., Giolito, C., Duarte, E., Fernandez, E., ... & Magro, G. (2005). The hydrothermal-volcanic system of Rincon de la Vieja volcano (Costa Rica): a combined (inorganic and organic) geochemical approach to understanding the origin of the fluid discharges and its possible application to volcanic surveillance. Journal of Volcanology and Geothermal Research, 148(3-4), 315-333.

Tassi, F., Vaselli, O., Tedesco, D., Montegrossi, G., Darrah, T., Cuoco, E., ... & Delgado Huertas, A. (2009). Water and gas chemistry at Lake Kivu (DRC): geochemical evidence of vertical and horizontal heterogeneities in a multibasin structure. Geochemistry, Geophysics, Geosystems, 10(2).

Tassi, F., Fazi, S., Rossetti, S., Pratesi, P., Ceccotti, M., Cabassi, J., ... & Vaselli, O. (2018). The biogeochemical vertical structure renders a meromictic volcanic lake a trap for geogenic CO_2 (Lake Averno, Italy). PloS one, 13(3), e0193914.

Tchamabé, B. C., Ohba, T., Issa, I., Youmen, D., Owona, S., Aka, F. T., ... & Hell, J. V. (2013). Eruptive history of the barombi mbo maar, southwest cameroon, central Africa: constraints from tephrostratigraphic analysis of phreatomagmatic deposits.

Tchamabé, B. C., Ohba, T., Kereszturi, G., Németh, K., Aka, F. T., Youmen, D., ... & Hell, J. V. (2015). Towards the reconstruction of the shallow plumbing system of the Barombi Mbo Maar (Cameroon) Implications for diatreme growth processes of a polygenetic maar volcano. Journal of Volcanology and Geothermal Research, 301, 293-313.

Terada, A., & Hashimoto, T. (2017). Variety and sustainability of volcanic lakes: Response to subaqueous thermal activity predicted by a numerical model. Journal of Geophysical Research: Solid Earth, 122(8), 6108-6130.

Terada, A., Hashimoto, T., Kagiyama, T., & Sasaki, H. (2008). Precise remote-monitoring technique of water volume and temperature of a crater lake in Aso volcano, Japan: implications for a sensitive window of a volcanic hydrothermal system. Earth, planets and space, 60(6), 705-710.

Terada, A., Morita, Y., Hashimoto, T., Mori, T., Ohba, T., Yaguchi, M., & Kanda, W. (2018). Water sampling using a drone at Yugama crater lake, Kusatsu-Shirane volcano, Japan. Earth, Planets and Space, 70(1), 64.

Tietze, K., Geyh, M., Müller, H., Schröder, L., Stahl, W., & Wehner, H. (1980). The genesis of the methane in Lake Kivu (Central Africa). Geologische Rundschau, 69(2), 452-472.

Todesco, M., Rouwet, D., Nespoli, M., & Bonafede, M. (2015). How steep is my seep? Seepage in volcanic lakes, hints from numerical simulations. In Volcanic Lakes (pp. 323-339). Springer, Berlin, Heidelberg.

Tongwa, F. A., Mouliom, A. G., Rouwet, D., Fantong, W. Y., Tchamabé, B. C., Ohba, T., ... & Kusakabe, M. (2014). δ^{18}O and δD variations in some volcanic lakes on the Cameroon Volcanic Line (West-Africa): generating isotopic baseline data for volcano monitoring and surveillance in Cameroon. Journal of Limnology, 74(1).

Tonini, R., Sandri, L., Rouwet, D., Caudron, C., & Marzocchi, W. (2016). A new Bayesian Event Tree tool to track and quantify volcanic unrest and its application to Kawah Ijen volcano. Geochemistry, Geophysics, Geosystems, 17(7), 2539-2555.

Torres, R. C., Self, S., & Punongbayan, R. S. (1995). Attention focuses on Taal: Decade volcano of the Philippines. Eos, Transactions American Geophysical Union, 76(24), 241-247.

Truesdell, A. H., Haizlip, J. R., Armannsson, H., & d'Amore, F. (1989). Origin and transport of chloride in superheated geothermal steam. Geothermics, 18(1-2), 295-304.

Trunk, L., & Bernard, A. (2008). Investigating crater lake warming using ASTER thermal imagery: Case studies at Ruapehu, Poás, Kawah Ijen, and Copahué Volcanoes. Journal of volcanology and geothermal research, 178(2), 259-270.

Tsafack, J. P. F., Wandji, P., Bardintzeff, J. M., Bellon, H., & Guillou, H. (2009). The Mount Cameroon stratovolcano (Cameroon volcanic line, Central Africa): petrology, geochemistry, isotope and age data. Geochemistry, Mineralogy and Petrology, 47, 65-78.

Vandemeulebrouck, J., Hurst, A. W., & Poussielgue, N. (1994). Implications for the thermal regime of acoustic noise measurements in Crater Lake, Mount Ruapehu, New Zealand. Bulletin of volcanology, 56(6-7), 493-501.

Vandemeulebrouck, J., Sabroux, J. C., Halbwachs, M., Poussielgue, N., Grangeon, J., & Tabbagh, J. (2000). Hydroacoustic noise precursors of the 1990 eruption of Kelut Volcano, Indonesia. Journal of Volcanology and Geothermal Research, 97(1-4), 443-456.

Vandemeulebrouck, J., Stemmelen, D., Hurst, T., & Grangeon, J. (2005). Analogue modeling of instabilities in crater lake hydrothermal systems. Journal of Geophysical Research: Solid Earth, 110(B2).

Vandemeulebrouck, J., Hurst, A. W., & Scott, B. J. (2008). The effects of hydrothermal eruptions and a tectonic earthquake on a cycling crater lake (Inferno Crater Lake, Waimangu, New Zealand). Journal of Volcanology and Geothermal Research, 178(2), 271-275.

van Hinsberg, V., Berlo, K., Sumarti, S., Van Bergen, M., & Williams-Jones, A. (2010). Extreme alteration by hyperacidic brines at Kawah Ijen volcano, East Java, Indonesia: II: metasomatic imprint and element fluxes. Journal of Volcanology and Geothermal Research, 196(3), 169-184.

van Hinsberg, V., Vigouroux, N., Palmer, S., Berlo, K., Mauri, G., Williams-Jones, A., ... & Fischer, T. (2017). Element flux to the environment of the passively degassing crater lake-hosting Kawah Ijen

volcano, Indonesia, and implications for estimates of the global volcanic flux. In: Ohba, T., Capaccioni, B. & Caudron, C. (eds) Geochemistry and geophysics of Active Volcanic Lakes. Geological Society, London, Special Publications, 437, 9-34. First published online December 17, 2015.

van Rotterdam-Los, A. M. D., Vriend, S. P., van Bergen, M. J., & van Gaans, P. F. M. (2008). The effect of naturally acidified irrigation water on agricultural volcanic soils. The case of Asembagus, Java, Indonesia. Journal of Geochemical Exploration, 96(1), 53-68.

Varekamp, J. C. (2003). Lake contamination models for evolution towards steady state. Journal of Limnology, 62(1s), 67-72.

Varekamp, J. C. (2004). Copahue volcano: a modern terrestrial analog for the opportunity landing site? Eos, Transactions American Geophysical Union, 85(41), 401-407.

Varekamp, J. C. (2015). The chemical composition and evolution of volcanic lakes. In volcanic lakes (pp. 93-123). Springer, Berlin, Heidelberg.

Varekamp, J. C., & Kreulen, R. (2000). The stable isotope geochemistry of volcanic lakes, with examples from Indonesia. Journal of Volcanology and Geothermal Research, 97(1-4), 309-327.

Varekamp, J. C., Luhr, J. F., & Prestegaard, K. L. (1984). The 1982 eruptions of El Chichón Volcano (Chiapas, Mexico): character of the eruptions, ash-fall deposits, and gas phase. Journal of Volcanology and Geothermal Research, 23, 39-68. https://doi.org/10.1016/0377-0273(84)90056-8

Varekamp, J. C., Pasternack, G. B., & Rowe Jr, G. L. (2000). Volcanic lake systematics II. Chemical constraints. Journal of Volcanology and Geothermal Research, 97(1-4), 161-179.

Varekamp, J. C., Ouimette, A. P., Herman, S. W., Bermúdez, A., & Delpino, D. (2001). Hydrothermal element fluxes from Copahue, Argentina: a "beehive" volcano in turmoil. Geology, 29(11), 1059-1062.

Varekamp, J. C., de Moor, J. M., Merrill, M. D., Colvin, A. S., Goss, A. R., Vroon, P. Z., & Hilton, D. R. (2006). Geochemistry and isotopic characteristics of the Caviahue-Copahue volcanic complex, Province of Neuquén, Argentina. Special papers-Geological Society of America, 407, 317.

Vaselli, O., Tassi, F., Minissale, A., Montegrossi, G., Duarte, E., Fernandez, E., & Bergamaschi, F. (2003). Fumarole migration and fluid geochemistry at Poás volcano (Costa Rica) from 1998 to 2001. Geological Society, London, Special Publications, 213(1), 247-262.

Velez, M. L., Euillades, P., Caselli, A., Blanco, M., & Díaz, J. M. (2011). Deformation of Copahue volcano: inversion of InSAR data using a genetic algorithm. Journal of Volcanology and Geothermal Research, 202(1-2), 117-126.

Vera, E. A. R., Folguera, A., Valcarce, G. Z., Giménez, M., Ruiz, F., Martínez, P., ... & Ramos, V. A. (2010). Neogene to Quaternary extensional reactivation of a fold and thrust belt: the Agrio belt in the Southern Central Andes and its relation to the Loncopué trough (38–39 S). Tectonophysics, 492(1-4), 279-294.

Vigouroux, N., Wallace, P. J., Williams-Jones, G., Kelley, K., Kent, A. J., & Williams-Jones, A. E. (2012). The sources of volatile and fluid-mobile elements in the Sunda arc: A melt inclusion study from Kawah Ijen and Tambora volcanoes, Indonesia. Geochemistry, Geophysics, Geosystems, 13(9).

Vroon, P. Z., Bergen, M. V., White, W. M., & Varekamp, J. C. (1993). Sr-Nd-Pb isotope systematics of the Banda Arc, Indonesia: Combined subduction and assimilation of continental material. Journal of Geophysical Research: Solid Earth, 98(B12), 22349-22366.

Wadge, G. (1984). A preliminary volcanic hazards study of Dominica, West Indies. Special publication, 5.

Wagner, T. P., McKee, C. O., Kuduon, J., & Kombua, R. (2003). Landslide-induced wave in a small volcanic lake: Kasu Tephra Cone, Papua New Guinea. International Journal of Earth Sciences, 92(3), 405-406.

Wallace, P. J. (2005). Volatiles in subduction zone magmas: concentrations and fluxes based on melt inclusion and volcanic gas data. Journal of Volcanology and Geothermal Research, 140(1-3), 217-240.

Webster, J. D., & Mandeville, C. W. (2007). Fluid immiscibility in volcanic environments. Reviews in Mineralogy and Geochemistry, 65(1), 313-362.

Werner, C., Christenson, B. W., Hagerty, M., & Britten, K. (2006). Variability of volcanic gas emissions during a crater lake heating cycle at Ruapehu Volcano, New Zealand. Journal of volcanology and geothermal research, 154, 291-302. https://doi.org/10.1016/j.jvolgeores.2006.03.017

West System (2012). Portable diffuse flux meter with LI-COR CO_2 detector, Handbook, West Systems srl, Italy

White, D. E. (1957). Thermal waters of volcanic origin. Geological Society of America Bulletin, 68(12), 1637-1658.

Wiesemann, G. (1975). Remarks on the geologic structure of the Republic of El Salvador, Central America.

Williams, H., & Meyer-Abich, H. (1955). Volcanism in the Southern Part of El Salvador: With Particular Reference to the Collapse Basins of Lakes Coatepeque and Ilopango (Vol. 32, No. 1). University of California Press.

Witter, J. B., Hernandez, P., Harris, A. J., & Pérez, N. (2012). Quantification of the mass flux of H 2 O gas (steam) at three active volcanoes using thermal infrared imagery. Pure and applied geophysics, 169(10), 1875-1889.

Wolery, T. J. (1992). EQ3NR, a computer program for geochemical aqueous speciation-solubility calculations: Theoretical manual, users guide, and related documentation (Version 7.0); Part 3. Tech. rep., Lawrence Livermore National Lab., CA (United States).

Xu, Y., Schoonen, M. A. A., Nordstrom, D. K., Cunningham, K. M., & Ball, J. W. (1998). Sulfur geochemistry of hydrothermal waters in Yellowstone National Park: I. The origin of thiosulfate in hot spring waters. Geochimica et Cosmochimica Acta, 62(23-24), 3729-3743.

Xu, Y., Schoonen, M. A. A., Nordstrom, D. K., Cunningham, K. M., & Ball, J. W. (2000). Sulfur geochemistry of hydrothermal waters in Yellowstone National Park, Wyoming, USA. II. Formation and decomposition of thiosulfate and polythionate in Cinder Pool. Journal of Volcanology and Geothermal Research, 97(1-4), 407-423.

Zhang, Y., & Kling, G. W. (2006). Dynamics of lake eruptions and possible ocean eruptions. Annu. Rev. Earth Planet. Sci., 34, 293-324.

Zimanowski, B., Wohletz, K., Dellino, P., & Büttner, R. (2003). The volcanic ash problem. Journal of Volcanology and Geothermal Research, 122(1-2), 1-5.

Zimmer, M., Walter, T. R., Kujawa, C., Gaete, A., & Franco-Marin, L. (2017). Thermal and gas dynamic investigations at Lastarria volcano, Northern Chile. The influence of precipitation and atmospheric pressure on the fumarole temperature and the gas velocity. Journal of Volcanology and Geothermal Research, 346, 134-140.

Zlotnicki, J., Sasai, Y., Toutain, J. P., Villacorte, E. U., Bernard, A., Sabit, J. P., ... & Hase, H. (2009). Combined electromagnetic, geochemical and thermal surveys of Taal volcano (Philippines) during the period 2005–2006. Bulletin of Volcanology, 71(1), 29-47.

APPENDIX

Table S1 - Santa Ana lake gas ratios

Date	Location	SO$_2$ MAX (ppm)	CO$_2$/SO$_2$	r^2	H$_2$/SO$_2$	r^2	H$_2$O/SO$_2$	r^2	H$_2$S/SO$_2$	r^2
06-03-17	Rim	1.15					352.66	0.66	0.10	
06-03-17	Rim	1.9					525.91	0.70		
06-03-17	Rim	1.47					615.42	0.66		
06-03-17	Rim	1.47					698.88	0.80		
07-03-17	Plateau	4.05	26.64	0.84	2.44	0.98	64.7352			
07-03-17	Plateau	4.59	23.15	0.82	1.59	0.94	65.0515			
07-03-17	Plateau	8.2	37.17	0.81	2.39	0.96				
07-03-17	Shore	13.9	40.73	0.83	0.49	0.66				
07-03-17	Shore	16.53	21.34	0.58	0.34	0.89				
08-03-17	Shore	18.7	39.14	0.66					0.034	
08-03-17	Shore	23.14	25.2	0.84	0.47	0.75			0.025	
08-03-17	Shore	23.14							0.02538715	
08-03-17	Shore	26.6	55.41	0.71	0.57	0.70				
08-03-17	Shore	25.07	57.05	0.93						
08-03-17	Shore	26.56	51.34	0.80	0.5	0.62				
08-03-17	Shore	25.26	99.03	0.84	0.6	0.74				
04-06-17	Rim	0.7	35.4	0.59	1.15	0.51	1091.78	0.53		
04-06-17	Rim	1.6	9.63	0.52			423.59	0.51		
04-06-17	Plateau	4.2			0.35	0.63	128	0.58	0.04	0.47
04-06-17	Plateau	1.27					563.71	0.74		
04-06-17	Plateau	6.22			0.61	0.81				
04-06-17	Plateau	3.8	4.96	0.58	0.4	0.74	153.76	0.56		
04-06-17	Plateau	1.92			0.43	0.55				
05-06-17	Plateau	4.81			0.76	0.61				
05-06-17	Plateau	7.7	6.71	0.78						
05-06-17	Plateau	7.54	4.42	0.60	0.68	0.93				
05-06-17	Plateau	10.31	2.98	0.70	0.24	0.83			0.03	0.56
05-06-17	Plateau	3.4			0.77	0.91				
05-06-17	Plateau	1.53			0.96	0.68				
06-06-17	Plateau	1.57					189.47	0.81		
06-06-17	Plateau	1.6			0.66	0.68	91.52	0.66		
06-06-17	Plateau	2.45			0.98	0.79				
06-06-17	Plateau	2.25			1	0.57				
06-06-17	Plateau	1.9	14.22	0.59	0.67	0.58				
06-06-17	Plateau	0.77					3651.43	0.77		
06-06-17	Plateau	2			0.51	0.65	411.5	0.98		
06-06-17	Plateau	1.91			0.44	0.55				
06-06-17	Plateau	0.649					1758.24	0.65		
06-06-17	Plateau	0.566					1958.19	0.57		

Table S1 – Continued

Date	Location	SO$_2$ MAX (ppm)	CO$_2$/SO$_2$	r²	H$_2$/SO$_2$	r²	H$_2$O/SO$_2$	r²	H$_2$S/SO$_2$	r²
07-06-17	Plateau	0.2			1.79	0.53				
07-06-17	Plateau	0.2			2.53	0.59				
07-06-17	Plateau	0.37			2.56	0.81				
07-06-17	Plateau	1.01			1.52	0.73				
07-06-17	Plateau	2.3	4.88	0.54						
07-06-17	Plateau	1.38					687.46	0.85		
07-06-17	Plateau	0.754					2471.31	0.75		
07-06-17	Plateau	0.948					2853.74	0.95		
08-06-17	Plateau	3	11	0.79	0.49	0.63			0.1	0.95
08-06-17	Plateau	3.96							0.04	0.38
08-06-17	Plateau	1.08	32.58	0.57	0.91	0.55				
08-06-17	Plateau	1.09			0.98	0.57				
08-06-17	Plateau	2.84	8.38	0.67	0.44	0.68				
08-06-17	Plateau	2.06	7.04	0.51	0.35	0.53				
08-06-17	Plateau	1.34			1.03	0.66				
08-06-17	Plateau	1.93	8.92	0.82						
08-06-17	Plateau	3.83	5.64	0.55	0.64	0.77				
08-06-17	Plateau	4.15	8.28	0.81	0.31	0.54				
08-06-17	Plateau	2.51	56.57	0.75						
08-06-17	Plateau	3.21	32.64	0.65						
08-06-17	Plateau	3.22			1.32	0.92				
09-06-17	Plateau	1			1.01	0.66				
09-06-17	Plateau	0.4			2.13	0.52				
09-06-17	Plateau	0.58			1.86	0.50				
09-06-17	Plateau	0.786			1.17	0.67	307.34	0.79		
10-06-17	Plateau	1.09			1.74	0.80				
10-06-17	Plateau	2.48	11.95	0.57	0.44	0.69				
10-06-17	Plateau	2.65	16.14	0.71	0.63	0.65				
10-06-17	Plateau	3.21	36.32	0.59	0.44	0.52				
10-06-17	Plateau	3.65	10.34	0.58	0.34	0.52				
10-06-17	Plateau	2.48							0.13	0.66
11-06-17	Plateau	0.97			1.98	0.61				
11-06-17	Plateau	0.42			2.85	0.66				
11-06-17	Plateau	0.46			2.81	0.78				
11-06-17	Plateau	0.96			2.53	0.85				
11-06-17	Plateau	0.49			4.09	0.73				
11-06-17	Plateau	0.91			2.24	0.68				
11-06-17	Plateau	0.38			2.71	0.70				
11-06-17	Plateau	0.887					343.05	0.89		
12-06-17	Plateau	1.1			3.42	0.66				
12-06-17	Plateau	1.7	21.23	0.60	0.975					
12-06-17	Plateau	1.6			0.83	0.57			0.05	0.53
12-06-17	Plateau	1.19					2518.21	0.54		
12-06-17	Plateau	1.61			1.2	0.71				
13-06-17	Plateau	3.11	13.545		1.96	0.72	86.54	0.50	0.09	0.64

Table S1 – Continued

Date	Location	SO$_2$ MAX (ppm)	CO$_2$/SO$_2$	r²	H$_2$/SO$_2$	r²	H$_2$O/SO$_2$	r²	H$_2$S/SO$_2$	r²
13-06-17	Plateau	2.28			1.15	0.67				
13-06-17	Plateau	15.6	3.95	0.92	0.15	0.83	25.45	0.56		
13-06-17	Plateau	7.26	6.23	0.66	1.69	0.92				
13-06-17	Plateau	13.87	2.29	0.60	0.28	0.66	121.59	0.88	0.08	0.65
13-06-17	Plateau	6.51	13.41	0.74	1.6	0.80				
13-06-17	Plateau	14.21	4.63	0.80	1.25	0.94	80.36	0.66	0.04	0.57
13-06-17	Plateau	14.21	3.68	0.64						
13-06-17	Shore	20	5.29	0.62			74.64	0.69		
13-06-17	Shore	11.39	5.43	0.74	0.06	0.55	80.19	0.77		
06-04-18	Plateau	14.7	5.26	0.84	0.92	0.92	169.51	0.87	0.06	0.62
06-04-18	Plateau	12.97	2.98	0.63	0.11	0.66	184.81	0.88	0.09	0.87
12-04-18	Plateau	3.56							0.1	0.87
12-04-18	Plateau	8.7	6.43	0.84	0.9	0.93	93.35	0.62	0.05	0.58
12-04-18	Plateau	9.56	6.56	0.82	0.99	0.88	77.59	0.79	0.02	0.69
12-04-18	Plateau	9.43	4.63	0.66	0.5225		123.246		0.084	
12-04-18	Plateau	14.79	3.65	0.84	0.6	0.73				
12-04-18	Plateau	13.27	3.86	0.86	0.4	0.90				
12-04-18	Plateau	19.96	3.56	0.90	0.37	0.84	81.31	0.89		
12-04-18	Plateau	23.64	2.64	0.76			111.54	0.85		
12-04-18	Plateau	20.72	4.49	0.94	0.72	0.93	106.89	0.60	0.18	0.96
12-04-18	Plateau	5.33					261.97	0.81		
12-04-18	Plateau	10.13	6.77	0.90	1.15	0.94	173.79	0.65	0.085	
12-04-18	Plateau	23.74	3.32	0.79	0.55	0.83	106.85	0.74		
12-04-18	Plateau	19.64	2.38	0.51			98.24	0.59		
12-04-18	Plateau	26.68	2.53	0.82			73.68	0.85		
12-04-18	Plateau	26.68	3.07	0.77	0.43	0.85	86.56	0.87		
12-04-18	Plateau	15.15					83.24	0.60		
12-04-18	Plateau	19.5	2.24	0.74	0.14	0.50	72.3	0.67		
12-04-18	Plateau	22.69					90.84	0.71		
12-04-18	Plateau	10.94	3.09	0.69	0.28	0.86	41.76	0.75		
12-04-18	Plateau	24.3	2.32	0.74	0.28	0.64	63.04	0.79		
12-04-18	Plateau	24.3	2.32	0.74	0.2	0.60	38.68	0.72		
12-04-18	Plateau	17.01	3.17	0.63	0.39	0.67				
12-04-18	Plateau	24.3	2.76	0.91	0.21	0.77	47.24	0.82		
12-04-18	Plateau	18.91					42.56	0.68	0.05	0.83
13-04-18	Plateau	15.85					54.23	0.76		
13-04-18	Plateau	22.7	2.9	0.81	0.28	0.87	54.08	0.77		
13-04-18	Plateau	14.76	2.85	0.74	0.15	0.54	31.61	0.56		
13-04-18	Plateau	19.21	2.2	0.54	0.49	0.95	49.28	0.72		
13-04-18	Plateau	21.48	2.28	0.76	0.29		50.45	0.61		
13-04-18	Plateau	6.2			0.53	0.70				
13-04-18	Plateau	9.05	2.3	0.58					0.1	0.61
13-04-18	Plateau	10.85	3	0.91	0.15	0.53				
13-04-18	Plateau	10.58	3.5	0.62	0.19	0.50				
13-04-18	Plateau	19.84	2.85	0.90	0.32	0.79				

Table S1 – Continued

Date	Location	SO₂ MAX (ppm)	CO₂/SO₂	r²	H₂/SO₂	r²	H₂O/SO₂	r²	H₂S/SO₂	r²
13-04-18	Plateau	11.4	2.07	0.69						
13-04-18	Plateau	12.05	2.36	0.61	0.19	0.71				
13-04-18	Plateau	10.68	4.11	0.82	0.8	0.77				
13-04-18	Plateau	4.88							0.13	0.80
13-04-18	Plateau	11.3	3.12	0.64						
13-04-18	Plateau	4.15	5.95	0.67	0.92	0.85			0.07	0.72
13-04-18	Plateau	3.49			0.44	0.67			0.09	0.62
13-04-18	Plateau	3.94	7.07	0.60	0.72	0.67			0.07	0.69
13-04-18	Plateau	7.43	7.1	0.88	0.49	0.88				
13-04-18	Plateau	10.79	4.32	0.88	0.48	0.92			0.03	0.51
13-04-18	Plateau	5.6	7.32	0.80	0.67	0.84			0.06	0.95
13-04-18	Plateau	7.36	4.25	0.56	0.73					
13-04-18	Plateau	3.76							0.25	0.94
13-04-18	Plateau	2.55							0.32	0.67
13-04-18	Plateau	2.61							0.27	0.66
13-04-18	Plateau	6.67	3.21	0.58	0.23	0.63				
13-04-18	Plateau	4.62	5.34	0.70	0.18	0.95				
13-04-18	Plateau	13.88	4.48	0.97	0.59	0.98				
13-04-18	Plateau	3.28	5.59	0.60					0.2	0.98
13-04-18	Plateau	5.32	7.67	0.89	0.59	0.91				
13-04-18	Plateau	6.79	5.28	0.82	0.46	0.71			0.07	0.66
13-04-18	Plateau	7.54	3.75	0.57	0.5				0.08	
13-04-18	Plateau	5.35			0.55	0.71				
13-04-18	Plateau	3.68							0.05	0.88
13-04-18	Plateau	5.5	8.46	0.86	1.43	0.94				
13-04-18	Plateau	4.76	6.52	0.75	0.8	0.90	12.27	0.67		
13-04-18	Plateau	3.07			0.54	0.64	36.93	0.79		
13-04-18	Plateau	3.01	13.5	0.57						
13-04-18	Plateau	3.16					74.55	0.85		
13-04-18	Plateau	3.35			0.76	0.61	48.68	0.50		
13-04-18	Plateau	3.13			0.62	0.59				
13-04-18	Plateau	4.38			0.48	0.58				
13-04-18	Plateau	4.78	4.74	0.57	0.59	0.84				
13-04-18	Plateau	3.08	11.4	0.69						
13-04-18	Plateau	3.5					37.25	0.65		
13-04-18	Plateau	7.5	3.98	0.76	0.38	0.90			0.07	0.95
13-04-18	Plateau	6.18	8.05	0.83	0.99	0.96	18	0.54	0.03	0.65
13-04-18	Plateau	3.79							0.1	0.59
13-04-18	Plateau	12.52	4.58	0.84	0.59				0.13	0.76
13-04-18	Plateau	4.52							0.22	0.85
13-04-18	Plateau	3.94			0.89	0.68				
13-04-18	Plateau	10.77	4.19	0.74	0.56	0.73				
13-04-18	Plateau	6.94			0.31	0.56			0.08	0.63
13-04-18	Plateau	20.17	3.21	0.92	0.275					
13-04-18	Plateau	9.37	4.21	0.75	0.51	0.73				

Table S1 – Continued

Date	Location	SO₂ MAX (ppm)	CO₂/SO₂	r²	H₂/SO₂	r²	H₂O/SO₂	r²	H₂S/SO₂	r²
13-04-18	Plateau	5.49							0.13	0.84
13-04-18	Plateau	4.84	3.42	0.50	0.96	0.77	80.09	0.63	0.16	0.88
13-04-18	Plateau	3.88	6.2	0.71			14.43	0.56		
13-04-18	Plateau	4.21	6.87	0.54					0.15	0.94
13-04-18	Plateau	3.34	9.02	0.65	0.52	0.71				
13-04-18	Plateau	3.39					23.85	0.50	0.18	0.78
13-04-18	Plateau	3.83							0.11	0.65
13-04-18	Plateau	3.96							0.06	0.95
13-04-18	Plateau	4.8	2.73	0.69	0.16	0.63			0.05	0.51
13-04-18	Plateau	3.97	5.09	0.61			49.36	0.52	0.14	0.92
13-04-18	Plateau	5.24			0.18	0.61			0.12	0.71
13-04-18	Plateau	3.6							0.22	0.93
13-04-18	Plateau	5.61	6.44	0.61	0.6	0.66	360.66	0.52	0.14	0.82
13-04-18	Plateau	3.87					346.99	0.50	0.04	0.71
13-04-18	Plateau	4.74					293.18	0.64		
13-04-18	Plateau	7.4	4.71	0.52	0.89	0.80				
13-04-18	Plateau	5.67					192.91	0.91		
13-04-18	Plateau	11.92	3	0.85	0.28	0.73				
13-04-18	Plateau	5.54					238.62	0.76		
13-04-18	Plateau	4.41					337.65	0.83		
13-04-18	Plateau	15.15	3.28	0.96	0.3	0.93	57.66	0.76		
13-04-18	Plateau	8.08	4.22	0.82	0.49	0.81	56.87	0.72		
13-04-18	Plateau	8.72	3.14	0.50						
13-04-18	Plateau	15.49	3.28	0.69	0.34	0.85				
13-04-18	Plateau	17.62	2.79	0.73	0.34	0.76	26.19	0.57		
13-04-18	Plateau	24.76	2.86	0.92	0.27	0.77	59	0.72		
13-04-18	Plateau	18.13	3.31	0.90	0.41	0.95				
13-04-18	Plateau	16.37	4.23	0.86	0.71	0.93	84.58	0.55		
13-04-18	Plateau	7.83	3.04	0.68			137.33	0.75		
13-04-18	Plateau	9.93	4.45	0.88						
13-04-18	Plateau	7.98	5.3	0.61	0.47	0.90			0.13	0.51
13-04-18	Plateau	7.57	5.66	0.81	0.21	0.61			0.09	0.77
13-04-18	Plateau	7.74			0.37	0.61	40.32	0.80	0.12	0.80
13-04-18	Plateau	17.61	2.82	0.69	0.39	0.79	52.34	0.55		
13-04-18	Plateau	10.72	3.84	0.58						
13-04-18	Plateau	13.79	2.47	0.70			164.96	0.67		
13-04-18	Plateau	7.92	4.24	0.85			101.7	0.52		
13-04-18	Plateau	19.83	3.3	0.92	0.4	0.94				
13-04-18	Plateau	14.33	2.35	0.74						
13-04-18	Plateau	14.18	2.99	0.82						
13-04-18	Plateau	17.23	3.8	0.79	0.45	0.81				
13-04-18	Plateau	3.56			0.5	0.68				
13-04-18	Plateau	6.57	7.87	0.77						
13-04-18	Plateau	5.28	5.67	0.68	0.52	0.62				

Table S1 – Continued

Date	Location	SO$_2$ MAX (ppm)	CO$_2$/SO$_2$	r²	H$_2$/SO$_2$	r²	H$_2$O/SO$_2$	r²	H$_2$S/SO$_2$	r²
13-04-18	Plateau	5.24	7.51	0.72						
13-04-18	Plateau	5.73			0.42	0.67			0.18	0.83
13-04-18	Plateau	4.87					81.83	0.62	0.11	0.87
13-04-18	Plateau	6.94	4.27	0.66	0.44	0.65				
13-04-18	Plateau	5.41	8.2	0.83					0.18	0.77
13-04-18	Plateau	6.75	4.97	0.73			88.1	0.73		
13-04-18	Plateau	5.79							0.12	0.76
13-04-18	Plateau	4.67							0.17	0.94
13-04-18	Plateau	5.02			0.81	0.79				
13-04-18	Plateau	5.43					124.77	0.89		
13-04-18	Plateau	3.45					116.67	0.92		
13-04-18	Plateau	3.34					77.14	0.62		
13-04-18	Plateau	4.67					83.14	0.50		
13-04-18	Plateau	4.83					77.04	0.53		
13-04-18	Plateau	2.22							0.14	0.69
13-04-18	Plateau	1.66							0.32	0.87
13-04-18	Plateau	2.01							0.15	0.83
13-04-18	Plateau	1.91							0.26	0.96
13-04-18	Plateau	1.76							0.24	0.68
13-04-18	Plateau	1.24							0.17	0.82
13-04-18	Plateau	2.66							0.12	0.88
13-04-18	Plateau	2.96							0.25	0.93
13-04-18	Plateau	2.35			1.29	0.68			0.18	0.66
13-04-18	Plateau	2.73							0.23	0.89
13-04-18	Plateau	1.81							0.34	0.71
13-04-18	Plateau	2.12							0.16	0.96
13-04-18	Plateau	2.79							0.35	0.91
13-04-18	Plateau	2.76							0.09	0.87
13-04-18	Plateau	2.24			0.58	0.61				
13-04-18	Plateau	2.49	8.48	0.65	0.78	0.82				
13-04-18	Plateau	1.93			0.97	0.54				
13-04-18	Plateau	2.08							0.17	0.90
13-04-18	Plateau	2.04			0.66	0.69				
13-04-18	Plateau	2.4	9.68	0.64					0.13	0.75
13-04-18	Plateau	2.4			1.53	0.86			0.06	0.81
13-04-18	Plateau	2.53			0.87	0.76	22.34	0.75		
13-04-18	Plateau	2.67			0.47	0.68			0.1	0.93
13-04-18	Plateau	1.64					25.49	0.54	0.17	0.63
13-04-18	Plateau	1.94							0.22	0.84
13-04-18	Plateau	1.75							0.12	0.88
13-04-18	Plateau	2.64							0.22	0.98
13-04-18	Plateau	1.96							0.23	0.92
13-04-18	Plateau	2.32							0.22	0.90
13-04-18	Plateau	1.55					92.59	0.84		

Table S1 – Continued

Date	Location	SO$_2$ MAX (ppm)	CO$_2$/SO$_2$	r²	H$_2$/SO$_2$	r²	H$_2$O/SO$_2$	r²	H$_2$S/SO$_2$	r²
13-04-18	Plateau	2.32	7.32	0.52	0.73	0.68	33.6	0.57		
13-04-18	Plateau	2.65							0.19	0.94
13-04-18	Plateau	2.87					55.63	0.65		
13-04-18	Plateau	3.62			0.49	0.66	66.58	0.65		
13-04-18	Plateau	2.69					81.21	0.61		
13-04-18	Plateau	2.1					77.29	0.81		
13-04-18	Plateau	1.52					51.92	0.73		
13-04-18	Plateau	2.9	7.56	0.58	0.6	0.82				
13-04-18	Plateau	0.29					43.7	0.57		
13-04-18	Plateau	1.46			0.66	0.55				
13-04-18	Plateau	2.7	5.8	0.52					0.12	0.91
13-04-18	Plateau	2.55	10.67	0.54					0.15	0.69
13-04-18	Plateau	1.71					581.2	0.74		
13-04-18	Plateau	2.81							0.42	0.92
13-04-18	Plateau	1.73							0.24	0.97
13-04-18	Plateau	2.6							0.23	0.95
13-04-18	Plateau	0.84					620.09	0.91		
13-04-18	Plateau	2.19			1.7	0.67	476.86	0.87		
13-04-18	Plateau	2.53	13.83	0.51					0.08	0.69
13-04-18	Plateau	2.78	8.03	0.65	0.6	0.74				
13-04-18	Plateau	1.48					165.46	0.53		
14-04-18	Plateau	14.1	3.36	0.84	0.13	0.70	13.73	0.72		
14-04-18	Plateau	12.56	2.56	0.48	0.36	0.68	55.4	0.59		
14-04-18	Plateau	10.57	3.12	0.86	0.52	0.90	31.18	0.87		
14-04-18	Plateau	12.34	3.6	0.84	0.69	0.87				
14-04-18	Plateau	10.79					45.37	0.74		
14-04-18	Plateau	17.62	4	0.91	0.5	0.91	14.46	0.70		
14-04-18	Plateau	4.1			0.46	0.51				
14-04-18	Plateau	5.88			0.48	0.81	42.73	0.77		
14-04-18	Plateau	3.62							0.09	0.55
14-04-18	Plateau	4.34	4.84	0.67	0.42	0.60				
14-04-18	Plateau	3.03					69.61	0.69		
14-04-18	Plateau	4.47			0.27	0.69	75.53	0.87		
14-04-18	Plateau	3.33			0.44	0.63	52.23	0.86		
14-04-18	Plateau	3.73					103.03	0.88		
14-04-18	Plateau	4.05			0.42	0.64	66.7	0.82		
14-04-18	Plateau	4.94	8.41	0.80	0.43	0.74				
14-04-18	Plateau	3.43			0.33	0.59				
14-04-18	Plateau	3.66			0.34	0.63	69.36	0.93		
14-04-18	Plateau	4.73			0.73	0.74				
14-04-18	Plateau	3.58	8.86	0.70	0.39	0.73				
14-04-18	Plateau	3.34					316.93	0.62		
14-04-18	Plateau	6.83	5.74	0.60						
14-04-18	Plateau	2.58					36.34	0.57		
14-04-18	Plateau	2.45	11.27	0.77	0.32	0.57				

Table S1 – Continued

Date	Location	SO$_2$ MAX (ppm)	CO$_2$/SO$_2$	r²	H$_2$/SO$_2$	r²	H$_2$O/SO$_2$	r²	H$_2$S/SO$_2$	r²
14-04-18	Plateau	2.9	3.99	0.43						
14-04-18	Plateau	2.53			0.53	0.66				
14-04-18	Plateau	2.02	9.07	0.54	0.9	0.66				
14-04-18	Plateau	2.62			0.51	0.60				
14-04-18	Plateau	2.76			0.37	0.54				
03-05-18	Plateau	14.9	2.99	0.67						
03-05-18	Plateau	14.64					105.38	0.93		
03-05-18	Plateau	28.78	2.94	0.77	0.42	0.67	51.75	0.75		
03-05-18	Plateau	17.31	2.47	0.79						
03-05-18	Plateau	16.17	2.08	0.81	0.18	0.78	87.56	0.69		
03-05-18	Plateau	17.74	2.41	0.57	0.35	0.69	69.27	0.67		
03-05-18	Plateau	15.51	3.47	0.86	0.38	0.82	66.25	0.83		
03-05-18	Plateau	16.78	2.08	0.54			119.33	0.57		
03-05-18	Plateau	14.45	4.53	0.71	0.3	0.64				
03-05-18	Plateau	15.95	2.88	0.67	0.25	0.62				
03-05-18	Plateau	12.73	2.83	0.74	0.43	0.66				
03-05-18	Plateau	12.09	2.73	0.59	0.62	0.80	102.98	0.54		
03-05-18	Plateau	20.73	3.74	0.91	0.57	0.82	29.33	0.65		
03-05-18	Plateau	23.88	1.16	0.64			61.25	0.67		
03-05-18	Plateau	9.82			0.61	0.74				
03-05-18	Plateau	13.17	3.29	0.83	0.21	0.62				
03-05-18	Plateau	29.47	3.58	0.93	0.44	0.80	60.75	0.76		
03-05-18	Plateau	23.27	3.31	0.96	0.27	0.90	66.85	0.91		
28-06-18	Plateau	14.8	3.29	0.95	0.41	0.90	139.29	0.75		
28-06-18	Plateau	25.83	2.41	0.97	0.4	0.96	82.8	0.95		
28-06-18	Plateau	11.57	2.79	0.71	0.67	0.94	90.46	0.91		
28-06-18	Plateau	21.41	2.55	0.86	0.22	0.57	101.14	0.79		
28-06-18	Plateau	12.35	2.26	0.78	0.42	0.66	116.68	0.90		
28-06-18	Plateau	12.4	2.5	0.80	0.19	0.83	124.07	0.55		
28-06-18	Plateau	9.41	2.96	0.89	0.38	0.70				
28-06-18	Plateau	21.4	1.39				107.86	0.85		
28-06-18	Plateau	12.35	2.26	0.78	0.42	0.66	116.68	0.90		
28-06-18	Plateau	22.06	2.1	0.91	0.28	0.58				
28-06-18	Plateau	6.15	3.9	0.58	0.46	0.76				
28-06-18	Plateau	2.1	36.2	0.89	1.63	0.64	376.31	0.76	0.07	0.72
28-06-18	Plateau	1.06							0.7	0.77
28-06-18	Plateau	1.44							0.06	0.81

Table S2 - Gas ratios (SO_2/H_2S, H_2S/SO_2, CO_2/X, where $X=H_2S$, SO_2 or Stot ($=H_2S+SO_2$) presented in the Chapter 6.

Location	Sample type	Date	SO_2/H_2S	σ	H_2S/SO_2	σ	CO_2/H_2S	σ	CO_2/SO_2	σ	$CO_2/Stot$	σ	References
Boiling Lake	Lake	26-02-12	-	-	-	-	5.2	0.4	-	-	5.2	0.4	Di Napoli et al. (2013)
Boiling Lake	Lake	18-05-16	-	-	-	-	4.8	0.6	-	-	4.8	0.6	Tamburello pers.comm.
Valley of Desolation	Fumaroles	26/02/1012	0.0002	-	5000.0	-	5.7	-	28500.0	-	5.7	-	Di Napoli et al. (2013)
El Chichón	Diffuse lake gas	03-03-16	0.47	0.07	2.1	0.3	2042.0	1512.7	4339.2	3232.0	1387.8	1029.5	Hasselle et al. (2018)
El Chichón	Bubbling lake gas	03-03-16	0.07	0.04	17.9	9.6	2637.0	1452.9	39546.0	18722.3	2453.4	1337.8	Hasselle et al. (2018)
El Chichón	Hot pools	03-03-16	0.02	0.01	69.3	29.5	256.0	122.0	21729.6	10333.7	252.5	119.8	Hasselle et al. (2018)
El Chichón	Fumaroles	03 and 04-03-2016	0.00	0.002	505.3	211.0	23.0	4.8	7666.7	2952.7	22.9	6.8	Hasselle et al. (2018)
El Chichón	Fumaroles	November 2008	0.01	0.004	229.9	166.3	23.5	5.5	5404.8	2581.6	23.4	8.3	CCVG Newsletter (2010)
El Chichón	Fumaroles	1983	7.08	-	0.1	-	291.0	-	41.1	-	36.0	-	Casadevall et al. (1984)
Víti	Diffuse lake gas	16-17/08/2016	0.0007	0.00052	2136.0	1661.5	101.0	34.4	102312.2	34264.8	100.8	34.4	Hasselle et al. (2018)
Víti	Bubbling lake gas	16-17/08/2016	0.0016	0.00018	1050.8	111.6	61.0	36.2	57258.7	37580.7	60.8	36.2	Hasselle et al. (2018)
Víti	Fumaroles	16-17/08/2016	0.0003	0.00003	3293.1	317.3	22.0	6.1	72440.5	24798.6	21.7	6.1	Hasselle et al. (2018)
Vasca degli ippopotami	Whole Pond	07-06-18	-	-	-	-	45.3	7.5	-	-	-	-	This study (sigma)
Vasca degli ippopotami	Pond	21-04-16	0.02	0.01	67.7	34.0	57.7	1.5	3846.8	1817.0	57.1	1.6	This study
Vasca degli ippopotami	Pond	May 1995	-	-	-	-	39.3	-	-	-	-	-	Capaccioni et al., 2001
Vasca degli ippopotami	Pond	November 1995	-	-	-	-	52.2	-	-	-	-	-	Capaccioni et al., 2001
Vasca degli ippopotami	Pond	01-09-82	-	-	-	-	56.7	-	-	-	-	-	H. in Mazor et al.1988
Vasca degli ippopotami	Pond	01-09-82	-	-	-	-	49.9	-	-	-	-	-	M.C.P.G. in Mazor et al.1989
Vasca degli ippopotami	Bubbling gas	07-06-18	0.001	0.0001	1791.0	317.3	46.3	3.8	82834.2	10776.8	46.2	4.9	This study (error)
Baia di Levante	Fumaroles	07-08/06 2018	0.01	0.01	125.5	82.1	33.6	9.9	4210.4	1999.0	33.3	12.8	This study
Vasca degli ippopotami	Fumarole	21-04-16	0.01	0.0010	113.8	13.1	33.4	1.5	3796.7	304.4	33.1	2.1	This study
Vulcano crater	Fumarole field	05-06-18	4.80	1.60	0.2	0.1	458.1	345.8	95.4	51.9	79.0	51.3	This study
Vulcano crater	Fumarole	01-09-82	2.18	-	0.5	-	32.9	-	15.1	-	10.4	-	H. in Mazor et al.1988
Vulcano crater	Fumarole	01-09-82	0.97	-	1.0	-	22.8	-	23.6	-	11.6	-	M.C.P.G. in Mazor et al.1989
Frying Pan Lake	Pond + FUM?	02-12-15	0.03	0.02	33.3	17.9	161.1	8.0	5371.3	1574.4	156.4	26.8	G. Giudice & M.Liuzzo pers.comm.
Inferno Crater Lake	Pond + FUM?	02-12-15	-	-	-	-	1103.3	288.8	-	-	1103.3	288.8	G. Giudice & M.Liuzzo pers.comm.
Champagne Pool	Pond + FUM?	28-11-15	0.01	0.0016	100.0	16.0	15.7	0.8	1569.0	163.6	15.5	1.2	G. Giudice & M.Liuzzo pers.comm.
Oyster Pool	Pond + FUM?	28-11-15	0.001	0.0004	1000.0	400.0	13.9	1.4	13900.0	3479.8	13.9	2.4	G. Giudice & M.Liuzzo pers.comm.

Location	Sample type	Date	SO_2/H_2S	σ	H_2S/SO_2	σ	CO_2/H_2S	σ	CO_2/SO_2	σ	$CO_2/Stot$	σ	References
Taal	Lake	25-07-16	-	-	-	-	9623.7	3348.0	-	-	-	-	This study
Taal	Lake	25-07-16	-	-	-	-	8191.5	3420.0	-	-	-	-	This study
Taal	Lake (bubbling+ fumaroles?)	22-07-16	-	-	-	-	129.5	41.3	-	-	-	-	This study
Taal	Lake (bubbling)	23-07-16	-	-	-	-	4792.4	347.0	-	-	-	-	This study
Taal	Mud pool	25-07-16	0.03	0.02	37.6	34.4	155.5	35.0	5849.2	3335.2	151.5	60.2	This study
Taal	Geyser	25-07-16	-	-	-	-	206.5	53.1	-	-	-	-	This study
Taal	Fumaroles	25-07-16	0.003	0.001	368.5	176.5	247.8	113.5	68474.6	24704.5	246.9	101.1	This study
Taal	Fumaroles	March 2011	5.14	-	0.19	-	478.0	-	93.0	-	77.9	-	Arpa et al. 2013
Taal	Fumaroles	March 2010	4.50	-	0.22	-	445.5	-	99.0	-	81.0	-	Arpa et al. 2013
Taal	Fumaroles	February 2009	0.45	-	2.22	-	310.1	-	689.0	-	213.8	-	Arpa et al. 2013
East Lake	Bubbling lake gas	20-08-17	-	-	-	-	166.9	-	-	-	-	-	This study
East Lake	Fumaroles	20-08-17	0.01	0.001	148.2	27.1	236.7	47.6	35077.5	6736.7	235.1	46.2	This study
Yugama	Lake	28-10-16	0.15	0.08	6.7	3.6	220.2	130.9	1468.1	836.2	191.5	111.5	This study (Ohba pers.comm.)
Yugama	Fumaroles	28-10-16	0.00	0.0004	660.9	171.4	6.1	1.5	4015.3	952.9	6.1	1.5	This study (Ohba pers.comm.)
Sirung	Crater lake	August 2015	2.50	0.63	0.40	0.1	20.0	5.4	8.0	2.3	5.7	1.6	Bani et al., 2017
Sirung	Fumaroles	August 2015	3.33	0.11	0.30	0.01	19.0	2.0	5.7	1.0	4.4	0.6	Bani et al., 2017
Sirung	pools	August 2015	0.83	0.01	1.20	0.01	1.1	0.3	1.3	0.8	0.6	0.3	Bani et al., 2017
Sirung	Fumaroles Z4	August 2015	3.45	0.83	0.29	0.1	5.9	2.3	1.7	0.9	1.3	0.6	Bani et al., 2017
Sirung	Sub-craters B	August 2015	2.00	0.40	0.50	0.1	2.4	0.8	1.2	0.6	0.8	0.3	Bani et al., 2017
Rincon	Gas discharge in active crater	April 2002	0.23	-	4.44	-	70.0	-	310.7	-	57.1	-	Tassi et al., 2005
Rincon	Lake (+fum)	08-04-13	1.12	0.17	0.89	0.1	30.2	11.4	27.0	16.3	14.3	7.0	rsn.ucr
Rincon	Lake (+fum)	03-10-14	20.00	6.93	0.05	0.02	85.1	30.0	4.3	1.5	4.1	1.4	rsn.ucr
Rincon	Lake (+fum)	14-04-14	2.78	1.66	0.36	0.2	19.1	11.1	6.9	3.9	5.0	2.9	rsn.ucr
Rincon	Lake (background)	Feb-May 2017	1.75	0.62	0.57	0.2	112.3	71.5	64.0	59.0	40.8	31.8	Battaglia et al., 2018 (in prep)
Rincon	Lake (phreatic eruption)	20-02-17	12.5	-	0.08	-	1237.5	-	99.0	-	91.7	-	Battaglia et al., 2018 (in prep)
Rincon	Lake (phreatic eruption)	27-02-17	100.0	-	0.01	-	23100.0	-	231.0	-	228.7	-	Battaglia et al., 2018 (in prep)
Rincon	Lake (phreatic eruption)	02-03-17	5.0	-	0.20	-	655.0	-	131.0	-	109.2	-	Battaglia et al., 2018 (in prep)
Rincon	Lake (phreatic eruption)	12-04-17	33.3	-	0.03	-	2833.3	-	85.0	-	82.5	-	Battaglia et al., 2018 (in prep)
Ijen	Lake	15-18/09/2014	-	-	-	-	-	-	89.5	10.1	-	-	Gunawan et al., 2016

Table S2 - Continued

Location	Sample type	Date	SO$_2$/H$_2$S	σ	H$_2$S/SO$_2$	σ	CO$_2$/H$_2$S	σ	CO$_2$/SO$_2$	σ	CO$_2$/Stot	σ	References
Ijen	Fumarole	15-18/09/2014	2.0	0.20	0.501	0.1	6.8	0.6	3.4	0.3	2.3	0.2	Gunawan et al., 2016
Ijen	Lake (+Fum?)	19-09-14	4.3	1.28	0.240	0.1	5.1	1.5	1.2	0.4	1.0	0.3	Aiuppa pers. comm.
Yudamari	Lake	19-10-03	–	-	-	-	-	-	0.8	-	-	-	Shinohara et al., 2015
Yudamari	Lake	04-10-04	70.0	-	0.014	-	133.0	-	1.9	-	1.9	-	Shinohara et al., 2015
Yudamari	Lake	25-04-05	6.5	-	0.154	-	7.8	-	1.2	-	1.0	-	Shinohara et al., 2015
Yudamari	Lake	19-11-05	59.0	-	0.017	-	135.7	-	2.3	-	2.3	-	Shinohara et al., 2015
Yudamari	Lake	26-10-06	50.0	-	0.020	-	110.0	-	2.2	-	2.2	-	Shinohara et al., 2015
Yudamari	Lake	27-10-06	60.0	-	0.017	-	156.0	-	2.6	-	2.6	-	Shinohara et al., 2015
Yudamari	Lake	17-09-07	140.0	-	0.007	-	238.0	-	1.7	-	1.7	-	Shinohara et al., 2015
Yudamari	Lake	18-09-07	85.0	-	0.012	-	170.0	-	2.0	-	2.0	-	Shinohara et al., 2015
Yudamari	Lake	28-02-08	170.0	-	0.006	-	238.0	-	1.4	-	1.4	-	Shinohara et al., 2015
Yudamari	Lake	10-07-08	–	-	-	-	-	-	1.3	-	-	-	Shinohara et al., 2018
Yudamari	Lake	11-07-08	100.0	-	0.010	-	80.0	-	0.8	-	0.8	-	Shinohara et al., 2015
Yudamari	Lake	28-10-08	300.0	-	0.003	-	510.0	-	1.7	-	1.7	-	Shinohara et al., 2015
Yudamari	Lake	23-03-09	2000.0	-	0.001	-	2000.0	-	1.0	-	1.0	-	Shinohara et al., 2015
Yudamari	Lake	24-03-09	2000.0	-	0.001	-	2000.0	-	1.0	-	1.0	-	Shinohara et al., 2015
Yudamari	Lake	06-07-10	100.0	-	0.010	-	50.0	-	0.5	-	0.5	-	Shinohara et al., 2018
Yudamari	Lake	19-08-10	1000.0	-	0.001	-	700.0	-	0.7	-	0.7	-	Shinohara et al., 2018
Yudamari	Lake	28-04-11	4.5	-	0.222	-	3.2	-	0.7	-	0.6	-	Shinohara et al., 2018
Yudamari	Lake	19-05-11	10.0	-	0.100	-	5.0	-	0.5	-	0.5	-	Shinohara et al., 2018
Yudamari	Lake	19-05-11	7.0	-	0.143	-	7.0	-	1.0	-	0.9	-	Shinohara et al., 2018
Yudamari	Lake	27-03-12	200.0	-	0.005	-	68.0	-	0.3	-	0.3	-	Shinohara et al., 2018
Yudamari	Lake	27-03-12	20.0	-	0.050	-	17.4	-	0.9	-	0.8	-	Shinohara et al., 2018
Yudamari	Lake	15-03-13	150.0	-	0.007	-	52.5	-	0.4	-	0.3	-	Shinohara et al., 2018
Yudamari	Lake	06-08-13	40.0	-	0.025	-	28.0	-	0.7	-	0.7	-	Shinohara et al., 2018
Yudamari	Lake	07-10-13	40.0	-	0.025	-	28.0	-	0.7	-	0.7	-	Shinohara et al., 2018
Yudamari	Lake	28-02-14	10.0	-	0.100	-	8.0	-	0.8	-	0.7	-	Shinohara et al., 2018
Yudamari	Lake	06-06-14	60.0	-	0.017	-	36.0	-	0.6	-	0.6	-	Shinohara et al., 2018

Table S2 - Continued

Location	Sample type	Date	SO_2/H_2S	σ	H_2S/SO_2	σ	CO_2/H_2S	σ	CO_2/SO_2	σ	$CO_2/Stot$	σ	References
Yudamari	Lake	18-11-14	500.0	-	0.002	-	500.0	-	1.0	-	1.0	-	Shinohara et al., 2018
Yudamari	Fumaroles	15-10-03	–	-	-	-	-	-	5.0	-	-	-	Shinohara et al., 2015
Yudamari	Fumaroles	04-10-04	6.0	-	0.167	-	10.8	-	1.8	-	1.5	-	Shinohara et al., 2015
Yudamari	Fumaroles	26-10-06	6.0	-	0.167	-	21.6	-	3.6	-	3.1	-	Shinohara et al., 2015
Yudamari	Fumaroles	19-09-07	13.0	-	0.077	-	62.4	-	4.8	-	4.5	-	Shinohara et al., 2015
Yudamari	Fumaroles	28-02-08	20.0	-	0.050	-	44.0	-	2.2	-	2.1	-	Shinohara et al., 2015
Yudamari	Fumaroles	29-02-08	20.0	-	0.050	-	42.0	-	2.1	-	2.0	-	Shinohara et al., 2015
Yudamari	Fumaroles	10-07-08	29.0	-	0.034	-	104.4	-	3.6	-	3.5	-	Shinohara et al., 2015
Yudamari	Fumaroles	10-07-08	23.0	-	0.043	-	50.6	-	2.2	-	2.1	-	Shinohara et al., 2015
Yudamari	Fumaroles	11-07-08	25.0	-	0.040	-	75.0	-	3.0	-	2.9	-	Shinohara et al., 2015
Yudamari	Fumaroles	11-07-08	32.0	-	0.031	-	96.0	-	3.0	-	2.9	-	Shinohara et al., 2015
Yudamari	Fumaroles	28-10-08	31.0	-	0.032	-	52.7	-	1.7	-	1.6	-	Shinohara et al., 2015
Yudamari	Fumaroles	23-03-09	19.0	-	0.053	-	76.0	-	4.0	-	3.8	-	Shinohara et al., 2015
Yudamari	Fumaroles	23-03-09	23.0	-	0.043	-	62.1	-	2.7	-	2.6	-	Shinohara et al., 2015
Yudamari	Fumaroles	19-11-09	12.0	-	0.083	-	51.6	-	4.3	-	4.0	-	Shinohara et al., 2015
Yudamari	Fumaroles	19-11-09	17.0	-	0.059	-	51.0	-	3.0	-	2.8	-	Shinohara et al., 2015
Yudamari	Fumaroles	19-11-09	17.0	-	0.059	-	49.3	-	2.9	-	2.7	-	Shinohara et al., 2015
Yudamari	Fumaroles	19-11-09	15.0	-	0.067	-	51.0	-	3.4	-	3.2	-	Shinohara et al., 2015
Yudamari	Fumaroles	06-07-10	8.6	-	0.116	-	27.5	-	3.2	-	2.9	-	Shinohara et al., 2018
Yudamari	Fumaroles	19-08-10	7.0	-	0.143	-	31.5	-	4.5	-	3.9	-	Shinohara et al., 2018
Yudamari	Fumaroles	01-10-10	6.5	-	0.154	-	30.6	-	4.7	-	4.1	-	Shinohara et al., 2018
Yudamari	Fumaroles	28-04-11	5.0	-	0.200	-	50.0	-	10.0	-	8.3	-	Shinohara et al., 2018
Yudamari	Fumaroles	05-12-11	13.0	-	0.077	-	59.8	-	4.6	-	4.3	-	Shinohara et al., 2018
Yudamari	Fumaroles	27-03-12	5.0	-	0.200	-	22.5	-	4.5	-	3.8	-	Shinohara et al., 2018
Yudamari	Fumaroles	15-03-13	6.0	-	0.167	-	31.8	-	5.3	-	4.5	-	Shinohara et al., 2018
Yudamari	Fumaroles	06-08-13	7.0	-	0.143	-	26.6	-	3.8	-	3.3	-	Shinohara et al., 2018
Yudamari	Fumaroles	07-10-13	6.5	-	0.154	-	40.3	-	6.2	-	5.4	-	Shinohara et al., 2018
Yudamari	Fumaroles	28-02-14	6.0	-	0.167	-	21.0	-	3.5	-	3.0	-	Shinohara et al., 2018
Yudamari	Fumaroles	28-02-14	5.0	-	0.200	-	30.0	-	6.0	-	5.0	-	Shinohara et al., 2018

Table S2 - Continued

Location	Sample type	Date	SO$_2$/H$_2$S	σ	H$_2$S/SO$_2$	σ	CO$_2$/H$_2$S	σ	CO$_2$/SO$_2$	σ	CO$_2$/Stot	σ	References
Yudamari	Fumaroles	06-06-14	9.0	-	0.111	-	52.2	-	5.8	-	5.2	-	Shinohara et al., 2018
Yudamari	Fumaroles	18-11-14	6.0	-	0.167	-	18.6	-	3.1	-	2.7	-	Shinohara et al., 2018
Yudamari	Eruption	12-01-15	3.0	-	0.333	-	24.0	-	8.0	-	6.0	-	Shinohara et al., 2018
Yudamari	Eruption	12-01-15	40.0	-	0.025	-	64.0	-	1.6	-	1.6	-	Shinohara et al., 2018
Yudamari	Eruption	12-01-15	300.0	-	0.003	-	480.0	-	1.6	-	1.6	-	Shinohara et al., 2018
Yudamari	Eruption	25-02-15	24.0	-	0.042	-	40.8	-	1.7	-	1.6	-	Shinohara et al., 2018
Yudamari	Eruption	17-03-15	3.0	-	0.333	-	12.0	-	4.0	-	3.0	-	Shinohara et al., 2018
Yudamari	Eruption	17-03-15	30.0	-	0.033	-	48.0	-	1.6	-	1.5	-	Shinohara et al., 2018
Yudamari	Eruption	17-03-15	300.0	-	0.003	-	480.0	-	1.6	-	1.6	-	Shinohara et al., 2018
Yudamari	Eruption	19-05-15	6.5	-	0.154	-	20.8	-	3.2	-	2.8	-	Shinohara et al., 2018
Yudamari	Eruption	20-05-15	4.6	-	0.217	-	11.0	-	2.4	-	2.0	-	Shinohara et al., 2018
Yudamari	Eruption	20-05-15	3.4	-	0.294	-	11.9	-	3.5	-	2.7	-	Shinohara et al., 2018
Yudamari	Eruption	20-05-15	5.7	-	0.175	-	13.7	-	2.4	-	2.0	-	Shinohara et al., 2018
Copahue	Lake	06-10 March 2014	>1000	-	<0.001	-	970.0	-	1.0	0.3	1.0	-	Tamburello et al., 2015
Copahue	Fumarole	01-03-13	18.9	-	0.053	-	85.0	-	4.5	-	4.3	-	Tamburello et al., 2015
Copahue	Fumarole	01-03-13	13.5	-	0.074	-	92.1	-	6.8	-	6.4	-	Tamburello et al., 2015
Poás	Lake (non eruptive)	29-04-14	2777.5	2722.50	0.00036	0.00035	4553.3	2380.8	1.6	0.1	1.6	0.5	de Moor et al., 2016b
Poás	Lake (non eruptive)	16-10-14	2777.5	2722.50	0.00036	0.00035	2923.7	1679.1	1.1	0.2	1.1	0.4	de Moor et al., 2016b
Poás	Lake (non eruptive)	29-10-14	2777.5	2722.50	0.00036	0.00035	2571.8	1331.9	0.9	0.1	0.9	0.3	de Moor et al., 2016b
Poás	Lake (non eruptive)	29-11-14	2777.5	2722.50	0.00036	0.00035	3120.8	1897.7	1.1	0.3	1.1	0.5	de Moor et al., 2016b
Poás	Lake (eruptive)	19-03-14	2272.5	2227.50	0.00044	0.00043	2582.4	1339.0	1.1	0.1	1.1	0.3	de Moor et al., 2016b
Poás	Lake (eruptive)	16-05-14	2272.5	2227.50	0.00044	0.00043	1097.8	564.6	0.5	0.0	0.5	0.1	de Moor et al., 2016b
Poás	Lake (eruptive)	28-08-14	2272.5	2227.50	0.00044	0.00043	1385.7	890.3	0.6	0.2	0.6	0.3	de Moor et al., 2016b
Poás	Lake (eruptive)	30-09-14	2272.5	2227.50	0.00044	0.00043	1734.7	982.6	0.8	0.1	0.8	0.3	de Moor et al., 2016b
Poás	Fumaroles (non eruptive)	29-04-14	10.8	-	0.093	-	4.6	-	0.4	-	0.4	-	de Moor et al., 2016b
Poás	Fumaroles (non eruptive)	16-10-14	3.8	-	0.264	-	1.4	-	0.4	-	0.3	-	de Moor et al., 2016b
Poás	Fumaroles (non eruptive)	29-10-14	3.8	-	0.264	-	1.4	-	0.4	-	0.3	-	de Moor et al., 2016b
Poás	Fumaroles (non eruptive)	29-11-14	8.7	-	0.114	-	6.0	-	0.7	-	0.6	-	de Moor et al., 2016b
Poás	Fumaroles (eruptive)	19-03-14	13.5	-	0.074	-	6.2	-	0.5	-	0.4	-	de Moor et al., 2016b

Table S2 - Continued

Location	Sample type	Date	SO$_2$/H$_2$S	σ	H$_2$S/SO$_2$	σ	CO$_2$/H$_2$S	σ	CO$_2$/SO$_2$	σ	CO$_2$/Stot	σ	References
Poás	Fumaroles (eruptive)	16-05-14	9.9	-	0.101	-	4.1	-	0.4	-	0.4	-	de Moor et al., 2016b
Poás	Fumaroles (eruptive)	28-08-14	9.1	-	0.110	-	3.1	-	0.3	-	0.3	-	de Moor et al., 2016b
Poás	Fumaroles (eruptive)	30-09-14	11.3	-	0.089	-	5.6	-	0.5	-	0.5	-	de Moor et al., 2016b
Ruapehu	Lake	10-07-08	44.5	4.16	0.022	0.0021	635.0	57.8	14.3	1.3	14.0	1.3	Christenson et al. 2010
Ruapehu	Lake	12-06-08	230.7	8.07	0.004	0.0002	1534.4	53.0	6.7	0.2	6.6	0.2	Christenson et al. 2010
Ruapehu	Lake	13-05-08	-	-	-	-	-	-	3.8	0.2	-	-	Christenson et al. 2010
Ruapehu	Lake	07-05-08	-	-	-	-	-	-	5.9	0.4	-	-	Christenson et al. 2010
Ruapehu	Lake	03-04-08	-	-	-	-	-	-	-		-	-	Christenson et al. 2010
Ruapehu	Lake	11-01-08	-	-	-	-	-	-	3.3	0.5	-	-	Christenson et al. 2010
Ruapehu	Lake	21-11-07	-	-	-	-	-	-	3.8	0.5	-	-	Christenson et al. 2010
Ruapehu	Lake	29-10-07	-	-	-	-	-	-	2.9	0.0	-	-	Christenson et al. 2010
Ruapehu	Lake	09-10-07	-	-	-	-	-	-	21.0	2.8	-	-	Christenson et al. 2010
Ruapehu	Lake	23-08-07	-	-	-	-	-	-	19.9	2.8	-	-	Christenson et al. 2010
Ruapehu	Lake	18-06-07	-	-	-	-	-	-	12.5	1.0	-	-	Christenson et al. 2010
Ruapehu	Lake	20-04-07	-	-	-	-	-	-	4.9	0.3	-	-	Christenson et al. 2010
Ruapehu	Lake	09-03-07	-	-	-	-	-	-	15.8	3.5	-	-	Christenson et al. 2010
Ruapehu	Lake	05-01-07	-	-	-	-	-	-	21.7	5.0	-	-	Christenson et al. 2010
Ruapehu	Lake	07-12-06	11.0	1.70	0.091	0.014	625.2	95.7	56.7	8.6	52.0	7.9	Christenson et al. 2010
Ruapehu	Lake	26-10-06	-	-	-	-	-	-	51.7	5.9	-	-	Christenson et al. 2010
Ruapehu	Lake	01-06-06	-	-	-	-	-	-	60.7	8.1	-	-	Christenson et al. 2010
Ruapehu	Lake	11-01-06	-	-	-	-	-	-	39.9	9.1	-	-	Christenson et al. 2010
Ruapehu	Lake	11-11-05	-	-	-	-	-	-	39.8	2.4	-	-	Christenson et al. 2010
Ruapehu	Lake	18-10-05	-	-	-	-	-	-	44.8	7.8	-	-	Christenson et al. 2010
Ruapehu	Lake	04-08-05	-	-	-	-	-	-	179.1	6.7	-	-	Christenson et al. 2010
Ruapehu	Lake	09-06-05	-	-	-	-	-	-	33.0	2.8	-	-	Christenson et al. 2010
Ruapehu	Lake	15-04-05	-	-	-	-	-	-	49.4	9.2	-	-	Christenson et al. 2010
Ruapehu	Lake	02-03-05	-	-	-	-	-	-	72.1	14.1	-	-	Christenson et al. 2010
Ruapehu	Lake	13-01-05	-	-	-	-	-	-	84.8	6.6	-	-	Christenson et al. 2010
Ruapehu	Lake	08-07-04	-	-	-	-	-	-	-		-	-	Christenson et al. 2010

Table S2 - Continued

Location	Sample type	Date	SO$_2$/H$_2$S	σ	H$_2$S/SO$_2$	σ	CO$_2$/H$_2$S	σ	CO$_2$/SO$_2$	σ	CO$_2$/Stot	σ	References
Ruapehu	Lake	21-05-04	50.8	6.61	0.020	0.003	1429.2	190.0	28.1	3.8	27.6	3.7	Christenson et al. 2010
Ruapehu	Lake	21-04-04	62.9	3.85	0.016	0.001	1893.8	122.5	30.1	2.1	29.7	2.0	Christenson et al. 2010
Ruapehu	Lake	25-03-04	-	-	-	-	-	-	24.6	3.0	-	-	Christenson et al. 2010
Ruapehu	Lake	09-05-16	-	-	-	-	-	-	6.1	0.1	-	-	Christenson pers.com.
Ruapehu	Lake	02-06-16	9.1	6.97	0.11	0.1	95.2	39.3	10.5	0.6	9.4	2.2	Christenson pers.com.
Santa Ana	Lake shore	07-03-17	-	-	-	-	-	-	31.0	13.7	-	-	This study
Santa Ana	Lake plateau	07-03-17	-	-	-	-	-	-	37.2	9.7	-	-	This study
Santa Ana	Lake shore	08-03-17	33.3	11.11	0.03	0.01	1816.7	717.8	54.5	24.9	52.9	22.5	This study
Santa Ana	Lake plateau	05-06-17	33.3	22.22	0.03	0.02	156.7	83.9	4.7	1.9	4.6	2.1	This study
Santa Ana	Lake shore	13-06-17	-	-	-	-	-	-	5.4	0.1	-	-	This study
Santa Ana	Lake plateau	13-06-17	16.7	8.33	0.06	0.03	70.0	29.2	4.2	1.4	4.0	1.5	This study
Santa Ana	Lake plateau	06-04-18	12.5	3.13	0.08	0.02	51.3	16.4	4.1	1.6	3.8	1.3	This study
Santa Ana	Lake plateau	12-04-18	9.1	5.79	0.11	0.1	30.0	14.5	3.3	1.1	3.0	1.2	This study
Santa Ana	Lake plateau	13-04-18	12.5	10.94	0.08	0.1	40.0	21.9	3.2	0.7	3.0	1.1	This study
Santa Ana	Lake plateau	14-04-18	-	-	-	-	-	-	3.3	0.5	-	-	This study
Santa Ana	Lake plateau	03-05-18	-	-	-	-	-	-	2.9	0.8	-	-	This study
Santa Ana	Lake plateau	28-06-18	-	-	-	-	-	-	2.4	0.5	-	-	This study
Santa Ana	Fumaroles	27-06-05	44.1	-	0.023	-	573.1	-	13.0	-	12.7	-	Fischer pers. comm.
Santa Ana	Fumaroles	27-06-05	26.7	-	0.038	-	28.7	-	1.1	-	1.0	-	Fischer pers. comm.
Kaba	Lake	2014	12.6	2.97	0.079	0.019	13.6	7.1	1.1	0.4	1.0	0.5	Aiuppa pers. comm.

Table S3 - Gas ratios (H_2O/X, H_2/X and H_2O/CO_2, $X=H_2S$, SO_2 or Stot (H_2S+SO_2) presented in the Chapter 6.

Location	Sample type	Date	H_2O/H_2S	σ	H_2O/SO_2	σ	$H_2O/Stot$	σ	H_2/H_2S	σ	H_2/SO_2	σ	$H_2/Stot$	σ	H_2O/CO_2	σ	References
Boiling Lake	Lake	26-02-12	161.2	21.8	-	-	161.2	21.8	-	-	-	-	-	-	31.0	6.0	Di Napoli et al. (2013)
Boiling Lake	Lake	18-05-16	-	-	-	-	-	-	0.1	0.02	-	-	0.14	0.02	-	-	Tamburello pers.comm.
Valley of Desolation	Fumaroles	26/02/1012	114.0	-	570000.0	-	114.0	-	-	-	-	-	-	-	20.0	-	Di Napoli et al. (2013)
El Chichón	Diffuse lake gas	03-03-16	15342.2	6484.6	32344.0	13756.8	10401.9	4407.7	5.3	5.08	11.6	12.9	3.64	3.64	11.6	9.3	Hasselle et al. (2018)
El Chichón	Bubbling lake gas	03-03-16	7116.6	6613.1	95755.5	90658.3	6595.6	6174.9	14.8	9.63	249.0	186.3	13.76	8.88	2.2	1.2	Hasselle et al. (2018)
El Chichón	Hot pools	03-03-16	241.0	410.8	14304.8	18233.2	235.5	400.9	1.6	1.48	168.4	153.9	1.56	1.47	1.0	1.7	Hasselle et al. (2018)
El Chichón	Fumaroles	03 and 04-03-2016	18.2	27.6	9212.7	8885.1	18.2	22.5	0.3	0.08	126.3	46.4	0.25	0.09	0.5	0.8	Hasselle et al. (2018)
El Chichón	Fumaroles	November 2008	11.5	2.8	2650.9	1278.8	11.5	4.2	0.2	0.02	37.1	15.5	0.16	0.04	0.5	0.1	CCVG Newsletter (2010)
El Chichón	Fumaroles	1983	41350.0	-	5837.6	-	5115.5	-	5.7	-	0.8	-	0.71	-	142.1	-	Casadevall et al. (1984)
Víti	Diffuse lake gas	16-17/08/2016	-	-	-	-	-	-	1.7	0.94	1751.9	866.7	1.74	0.94	-	-	Hasselle et al. (2018)
Víti	Bubbling lake gas	16-17/08/2016	6.5	4.9	5895.7	4875.0	6.5	4.9	0.7	0.66	688.8	665.4	0.74	0.66	0.2	0.1	Hasselle et al. (2018)
Víti	Fumaroles	16-17/08/2016	73.5	35.4	216769.9	62645.8	73.5	34.0	0.4	0.14	1319.8	577.2	0.39	0.14	5.0	-	Hasselle et al. (2018)
Vasca degli ippopotami	Whole Pond	07-06-18	100.6	58.5	-	-	-	-	0.3	0.06	-	-	-	-	2.2	0.8	This study (sigma)
Vasca degli ippopotami	Pond	21-04-16	146.4	135.2	3986.1	774.8	145.4	135.8	0.7	0.20	40.5	29.6	0.65	0.20	2.5	2.3	This study
Vasca degli ippopotami	Pond	May 1995	-	-	-	-	-	-	0.02	-	-	-	-	-	-	-	Capaccioni et al., 2001
Vasca degli ippopotami	Pond	November 1995	-	-	-	-	-	-	0.03	-	-	-	-	-	-	-	Capaccioni et al., 2001
Vasca degli ippopotami	Pond	01-09-82	-	-	-	-	-	-	0.7	-	-	-	-	-	-	-	H. in Mazor et al.1988
Vasca degli ippopotami	Pond	01-09-82	-	-	-	-	-	-	0.4	-	-	-	-	-	-	-	M.C.P.G. in Mazor et al.1989
Vasca degli ippopotami	Bubbling gas	07-06-18	26.7	5.7	47802.1	9304.6	26.7	5.4	0.5	0.12	967.1	193.0	0.54	0.11	0.6	0.1	This study (error)
Baia di Levante	Fumaroles	07-08/06 2018	192.5	86.3	24159.1	13318.8	191.0	95.5	0.15	0.04	18.2	8.2	0.14	0.05	6.1	3.5	This study
Vasca degli ippopotami	Fumarole	21-04-16	-	-	-	-	-	-	0.16	0.02	18.2	2.0	0.16	0.02	-	-	This study
Vulcano crater	Fumarole field	05-06-18	768.0	329.2	160.0	61.0	132.4	53.6	0.08	0.02	0.02	0.005	0.013	0.004	2.2	0.5	This study
Vulcano crater	Fumarole	01-09-82	547.6	-	251.6	-	172.4	-	0.004	-	0.002	-	0.001	-	16.6	-	H. in Mazor et al.1988
Vulcano crater	Fumarole	01-09-82	317.2	-	328.6	-	161.4	-	0.003	-	0.004	-	0.002	-	13.9	-	M.C.P.G. in Mazor et al.1989
Frying Pan Lake	Pond + FUM?	02-12-15	557.8	380.0	18593.4	11321.0	541.6	349.3	0.10	0.01	3.3	1.1	0.10	0.02	3.5	1.3	G. Giudice & M.Liuzzo pers.comm.
Inferno Crater Lake	Pond + FUM?	02-12-15	14078.7	5671.6	-	-	14078.7	5671.6	-	-	-	-	-	-	12.8	4.2	G. Giudice & M.Liuzzo pers.comm.
Champagne Pool	Pond + FUM?	28-11-15	610.6	117.0	61055.0	10733.0	604.5	111.0	0.04	0.01	4.0	0.8	0.04	0.01	38.9	4.7	G. Giudice & M.Liuzzo pers.comm.

Table S3 - Continued

Location	Sample type	Date	H_2O/H_2S	σ	H_2O/SO_2	σ	$H_2O/Stot$	σ	H_2/H_2S	σ	H_2/SO_2	σ	$H_2/Stot$	σ	H_2O/CO_2	σ	References
Oyster Pool	Pond + FUM?	28-11-15	30.0	14.5	30010.0	13270.0	30.0	13.9	0.1	0.02	110.0	30.7	0.11	0.02	2.2	0.6	G. Giudice & M.Liuzzo pers.comm.
Taal	Lake	25-07-16	-	-	-	-	-	-	80.1	21.6	-	-	-	-	-	-	This study
Taal	Lake (bubbling+ fumaroles?)	22-07-16	21527.0	2591.4	-	-	-	-	9.5	6.68	-	-	-	-	166.9	66.6	This study
Taal	Lake (bubbling)	23-07-16	-	-	-	-	-	-	170.8	-	-	-	-	-	-	-	This study
Taal	Mud pool	25-07-16	2972.9	607.4	111838.6	62606.5	2895.9	1106.4	0.3	0.10	10.2	6.5	0.26	0.13	19.1	4.1	This study
Taal	Geyser	25-07-16	-	-	-	-	-	-	0.4	0.15	-	-	-		-	-	This study
Taal	Fumaroles	25-07-16	-	-	-	-	-	-	0.5	0.23	195.3	89.0	0.53	0.23	-	-	This study
Taal	Fumaroles	March 2011	8241.7	-	1603.4	-	1342.3	-	-	-	-	-	-	-	17.2	-	Arpa et al. 2013
Taal	Fumaroles	March 2010	1310.3	-	291.2	-	238.2	-	-	-	-	-	-	-	2.9	-	Arpa et al. 2013
Taal	Fumaroles	February 2009	25837.5	-	57416.7	-	17819.0	-	-	-	-	-	-	-	83.3	-	Arpa et al. 2013
East Lake	Bubbling lake gas	20-08-17	-	-	-	-	-	-	-	-	-	-	-	-	-	-	This study (error)
East Lake	Fumaroles	20-08-17	222.8	57.6	33019.0	7288.4	221.3	53.0	-	-	-	-	-	-	0.9	0.2	This study (error)
Yugama	Lake	28-10-16	304.9	114.2	2032.9	934.4	265.2	76.8	12.4	4.25	82.87		10.81	4.24	1.4	0.7	This study (Ohba pers.comm.)
Yugama	Fumaroles	28-10-16	25.5	7.4	16868.9	4618.3	25.5	7.7	0.02	0.01	11.62		0.02	0.01	4.2	1.1	This study (Ohba pers.comm.)
Sirung	Crater lake	August 2015	-	-	-	-	-	-	-	-	-	-	-	-	-	-	Bani et al., 2017
Sirung	Fumaroles Z1	August 2015	1606.7	326.5	482.0	180.0	370.8	106.9	-	-	-	-	-	-	84.6	23.2	Bani et al., 2017
Sirung	Sub-craters;Fumaroles Z2, mud pools	August 2015	141.7	18.1	170.0	42.0	77.3	14.5	-	-	-	-	-	-	130.8	56.4	Bani et al., 2017
Sirung	Fumaroles Z4	August 2015	493.1	118.1	143.0	34.0	110.9	26.5	-	-	-	-	-	-	84.1	32.3	Bani et al., 2017
Sirung	Sub-craters B	August 2015	-	-	-	-	-	-	-	-	-	-	-	-	-	-	Bani et al., 2017
Rincon	Gas discharge in active crater	April 2002	-	-	-	-	-	-	0.01	-	0.07	-	0.01	-	-	-	Tassi et al., 2005
Rincon	Lake (+fum)	08-04-13	6074.0	2162.2	5423.2	3059.5	2865.1	1318.1	-	-	-	-	-	-	201.0	105.5	rsn.ucr
Rincon	Lake (+fum)	03-10-14	2887.6	688.4	144.4	18.8	137.5	25.4	0.00	0.00	0.10	0.03	0.005	0.001	34.0	8.3	rsn.ucr
Rincon	Lake (+fum)	14-04-14	-	-	-	-	-	-	0.38	0.20	1.05	0.5	0.28	0.14	-	-	rsn.ucr
Rincon	Lake (background)	Feb-May 2017	-	-	-	-	-	-	-	-	-	-	-	-	-	-	Battaglia et al., 2018 (in prep)
Rincon	Lake (phreatic eruption)	20-02-17	-	-	-	-	-	-	-	-	-	-	-	-	-	-	Battaglia et al., 2018 (in prep)
Rincon	Lake (phreatic eruption)	27-02-17	-	-	-	-	-	-	-	-	-	-	-	-	-	-	Battaglia et al., 2018 (in prep)
Rincon	Lake (phreatic eruption)	02-03-17	-	-	-	-	-	-	-	-	-	-	-	-	-	-	Battaglia et al., 2018 (in prep)

Table S3 - Continued

Location	Sample type	Date	H_2O/H_2S	σ	H_2O/SO_2	σ	$H_2O/Stot$	σ	H_2/H_2S	σ	H_2/SO_2	σ	$H_2/Stot$	σ	H_2O/CO_2	σ	References
Rincon	Lake (phreatic eruption)	12-04-17	-	-	-	-	-	-	-	-	-	-	-	-	-	-	Battaglia et al., 2018 (in prep)
Ijen	Lake (+Fum?)	19-09-14	40.2	19.9	9.5	6.5	7.7	4.5	0.0048	0.002	0.02	0.01	0.004	0.002	7.9	4.0	Aiuppa pers. comm.
Yudamari	Lake	19-10-03	-	-	–	-	-	-	-	-	-	-	-	-	-	-	Shinohara et al., 2015
Yudamari	Lake	04-10-04	4620.0	-	66.0	-	65.1	-	-	-	-	-	-	-	34.7	-	Shinohara et al., 2015
Yudamari	Lake	25-04-05	221.0	-	34.0	-	29.5	-	0.0092	-	0.06	-	0.0080	-	28.3	-	Shinohara et al., 2015
Yudamari	Lake	19-11-05	3304.0	-	56.0	-	55.1	-	0.0008	-	0.05	-	0.0008	-	24.3	-	Shinohara et al., 2015
Yudamari	Lake	26-10-06	2500.0	-	50.0	-	49.0	-	0.0004	-	0.02	-	0.0004	-	22.7	-	Shinohara et al., 2015
Yudamari	Lake	27-10-06	-	-	–	-		-	0.0002	-	0.01	-	0.0002	-	-	-	Shinohara et al., 2015
Yudamari	Lake	17-09-07	26600.0	-	190.0	-	188.7	-	0.0004	-	0.06	-	0.0004	-	111.8	-	Shinohara et al., 2015
Yudamari	Lake	18-09-07	10200.0	-	120.0	-	118.6	-	0.0006	-	0.05	-	0.0006	-	60.0	-	Shinohara et al., 2015
Yudamari	Lake	28-02-08	13600.0	-	80.0	-	79.5	-	0.0004	-	0.06	-	0.0004	-	57.1	-	Shinohara et al., 2015
Yudamari	Lake	10-07-08	-	-	-	-	-	-	-	-	-	-	-	-	-	-	Shinohara et al., 2018
Yudamari	Lake	11-07-08	7000.0	-	70.0	-	69.3	-	0.0005	-	0.05	-	0.0005	-	87.5	-	Shinohara et al., 2015
Yudamari	Lake	28-10-08	54000.0	-	180.0	-	179.4	-	0.0002	-	0.05	-	0.0002	-	105.9	-	Shinohara et al., 2015
Yudamari	Lake	23-03-09	180000.0	-	90.0	-	90.0	-	0.0000	-	0.03	-	0.0000	-	90.0	-	Shinohara et al., 2015
Yudamari	Lake	24-03-09	200000.0	-	100.0	-	100.0	-	0.0000	-	0.01	-	0.0000	-	100.0	-	Shinohara et al., 2015
Yudamari	Lake	06-07-10	4200.0	-	42.0	-	41.6	-	0.0005	-	0.05	-	0.0005	-	84.0	-	Shinohara et al., 2018
Yudamari	Lake	19-08-10	80000.0	-	80.0	-	79.9	-	0.0001	-	0.05	-	0.0000	-	114.3	-	Shinohara et al., 2018
Yudamari	Lake	28-04-11	135.0	-	30.0	-	24.5	-	0.0049	-	0.02	-	0.0040	-	42.9	-	Shinohara et al., 2018
Yudamari	Lake	19-05-11	200.0	-	20.0	-	18.2	-	0.0070	-	0.07	-	0.0064	-	40.0	-	Shinohara et al., 2018
Yudamari	Lake	19-05-11	315.0	-	45.0	-	39.4	-	0.0057	-	0.04	-	0.0050	-	45.0	-	Shinohara et al., 2018
Yudamari	Lake	27-03-12	10800.0	-	54.0	-	53.7	-	0.0004	-	0.08	-	0.0004	-	158.8	-	Shinohara et al., 2018
Yudamari	Lake	27-03-12	1000.0	-	50.0	-	47.6	-	0.0030	-	0.06	-	0.0029	-	57.5	-	Shinohara et al., 2018
Yudamari	Lake	15-03-13	7500.0	-	50.0	-	49.7	-	0.0004	-	0.06	-	0.0004	-	142.9	-	Shinohara et al., 2018
Yudamari	Lake	06-08-13	3200.0	-	80.0	-	78.0	-	0.0020	-	0.08	-	0.0020	-	114.3	-	Shinohara et al., 2018
Yudamari	Lake	07-10-13	3200.0	-	80.0	-	78.0	-	0.0020	-	0.08	-	0.0020	-	114.3	-	Shinohara et al., 2018
Yudamari	Lake	28-02-14	-	-	–	-	-	-	0.0060	-	0.06	-	0.0055	-	-	-	Shinohara et al., 2018
Yudamari	Lake	06-06-14	3000.0	-	50.0	-	49.2	-	0.0033	-	0.20	-	0.0033	-	83.3	-	Shinohara et al., 2018
Yudamari	Lake	18-11-14	20000.0	-	40.0	-	39.9	-	0.0001	-	0.05	-	0.0001	-	40.0	-	Shinohara et al., 2018

Table S3 - Continued

Location	Sample type	Date	H$_2$O/H$_2$S	σ	H$_2$O/SO$_2$	σ	H$_2$O/Stot	σ	H$_2$/H$_2$S	σ	H$_2$/SO$_2$	σ	H$_2$/Stot	σ	H$_2$O/CO$_2$	σ	References
Yudamari	Fumaroles	15-10-03	-	-	26.0	-	-	-	-	-	-	-	-	-	5.2	-	Shinohara et al., 2015
Yudamari	Fumaroles	04-10-04	810.0	-	135.0	-	115.7	-	-	-	-	-	-	-	75.0	-	Shinohara et al., 2015
Yudamari	Fumaroles	26-10-06	360.0	-	60.0	-	51.4	-	0.002	-	0.01	-	0.001	-	16.7	-	Shinohara et al., 2015
Yudamari	Fumaroles	19-09-07	559.0	-	43.0	-	39.9	-	0.022	-	0.28	-	0.02	-	9.0	-	Shinohara et al., 2015
Yudamari	Fumaroles	28-02-08	400.0	-	20.0	-	19.0	-	0.006	-	0.11	-	0.005	-	9.1	-	Shinohara et al., 2015
Yudamari	Fumaroles	29-02-08	700.0	-	35.0	-	33.3	-	0.003	-	0.05	-	0.002	-	16.7	-	Shinohara et al., 2015
Yudamari	Fumaroles	10-07-08	1305.0	-	45.0	-	43.5	-	0.005	-	0.15	-	0.005	-	12.5	-	Shinohara et al., 2015
Yudamari	Fumaroles	10-07-08	1150.0	-	50.0	-	47.9	-	0.003	-	0.07	-	0.003	-	22.7	-	Shinohara et al., 2015
Yudamari	Fumaroles	11-07-08	1625.0	-	65.0	-	62.5	-	0.004	-	0.10	-	0.004	-	21.7	-	Shinohara et al., 2015
Yudamari	Fumaroles	11-07-08	1760.0	-	55.0	-	53.3	-	0.004	-	0.13	-	0.004	-	18.3	-	Shinohara et al., 2015
Yudamari	Fumaroles	28-10-08	1240.0	-	40.0	-	38.8	-	0.005	-	0.15	-	0.005	-	23.5	-	Shinohara et al., 2015
Yudamari	Fumaroles	23-03-09	1330.0	-	70.0	-	66.5	-	0.007	-	0.13	-	0.01	-	17.5	-	Shinohara et al., 2015
Yudamari	Fumaroles	23-03-09	1380.0	-	60.0	-	57.5	-	0.005	-	0.11	-	0.0046	-	22.2	-	Shinohara et al., 2015
Yudamari	Fumaroles	19-11-09	600.0	-	50.0	-	46.2	-	0.028	-	0.33	-	0.03	-	11.6	-	Shinohara et al., 2015
Yudamari	Fumaroles	19-11-09	748.0	-	44.0	-	41.6	-	0.021	-	0.36	-	0.02	-	14.7	-	Shinohara et al., 2015
Yudamari	Fumaroles	19-11-09	765.0	-	45.0	-	42.5	-	0.019	-	0.33	-	0.02	-	15.5	-	Shinohara et al., 2015
Yudamari	Fumaroles	19-11-09	555.0	-	37.0	-	34.7	-	0.025	-	0.38	-	0.02	-	10.9	-	Shinohara et al., 2015
Yudamari	Fumaroles	06-07-10	404.2	σ	47.0	σ	42.1	-	0.001	-	0.01	-	0.001	-	14.7	-	Shinohara et al., 2018
Yudamari	Fumaroles	19-08-10	623.0	-	89.0	-	77.9	-	0.007	-	0.05	-	0.006	-	19.8	-	Shinohara et al., 2018
Yudamari	Fumaroles	01-10-10	455.0	-	70.0	-	60.7	-	0.005	-	0.03	-	0.004	-	14.9	-	Shinohara et al., 2018
Yudamari	Fumaroles	28-04-11	400.0	-	80.0	-	66.7	-	0.002	-	0.01	-	0.002	-	8.0	-	Shinohara et al., 2018
Yudamari	Fumaroles	05-12-11	780.0	-	60.0	-	55.7	-	0.001	-	0.01	-	0.001	-	13.0	-	Shinohara et al., 2018
Yudamari	Fumaroles	27-03-12	200.0	-	40.0	-	33.3	-	0.005	-	0.02	-	0.004	-	8.9	-	Shinohara et al., 2018
Yudamari	Fumaroles	15-03-13	240.0	-	40.0	-	34.3	-	0.012	-	0.07	-	0.010	-	7.5	-	Shinohara et al., 2018
Yudamari	Fumaroles	06-08-13	350.0	-	50.0	-	43.8	-	0.02	-	0.11	-	0.014	-	13.2	-	Shinohara et al., 2018
Yudamari	Fumaroles	07-10-13	325.0	-	50.0	-	43.3	-	0.03	-	0.20	-	0.03	-	8.1	-	Shinohara et al., 2018
Yudamari	Fumaroles	28-02-14	180.0	-	30.0	-	25.7	-	0.012	-	0.07	-	0.010	-	8.6	-	Shinohara et al., 2018
Yudamari	Fumaroles	28-02-14	250.0	-	50.0	-	41.7	-	0.010	-	0.05	-	0.008	-	8.3	-	Shinohara et al., 2018
Yudamari	Fumaroles	06-06-14	270.0	-	30.0	-	27.0	-	0.03	-	0.30	-	0.03	-	5.2	-	Shinohara et al., 2018

Table S3 - Continued

Location	Sample type	Date	H_2O/H_2S	σ	H_2O/SO_2	σ	$H_2O/Stot$	σ	H_2/H_2S	σ	H_2/SO_2	σ	$H_2/Stot$	σ	H_2O/CO_2	σ	References
Yudamari	Fumaroles	18-11-14	384.0	-	64.0	-	54.9	-	0.05	-	0.30	-	0.04	-	20.6	-	Shinohara et al., 2018
Yudamari	Eruption	12-01-15	90.0	-	30.0	-	22.5	-	0.04	-	0.11	-	0.03	-	3.8	-	Shinohara et al., 2018
Yudamari	Eruption	12-01-15	1200.0	-	30.0	-	29.3	-	0.0028	-	0.11	-	0.003	-	18.8	-	Shinohara et al., 2018
Yudamari	Eruption	12-01-15	9000.0	-	30.0	-	29.9	-	0.0004	-	0.11	-	0.0004	-	18.8	-	Shinohara et al., 2018
Yudamari	Eruption	25-02-15	1440.0	-	60.0	-	57.6	-	0.01	-	0.16	-	0.01	-	35.3	-	Shinohara et al., 2018
Yudamari	Eruption	17-03-15	1200.0	-	400.0	-	300.0	-	0.03	-	0.10	-	0.03	-	100.0	-	Shinohara et al., 2018
Yudamari	Eruption	17-03-15	2100.0	-	70.0	-	67.7	-	0.0005	-	0.02	-	0.0005	-	43.8	-	Shinohara et al., 2018
Yudamari	Eruption	17-03-15	21000.0	-	70.0	-	69.8	-	0.000	-	0.008	-	0.00003	-	43.8	-	Shinohara et al., 2018
Yudamari	Eruption	19-05-15	-	-	–	-	-	-	0.0011	-	0.007	-	0.0009	-	-	-	Shinohara et al., 2018
Yudamari	Eruption	20-05-15	-	-	–	-	-	-	0.0013	-	0.006	-	0.0011	-	-	-	Shinohara et al., 2018
Yudamari	Eruption	20-05-15	-	-	–	-	-	-	0.003	-	0.011	-	0.0025	-	-	-	Shinohara et al., 2018
Yudamari	Eruption	20-05-15	-	-	–	-	-	-		-				-	-	-	Shinohara et al., 2018
Copahue	Lake	06-10 March 2014	40870.0	-	40.9	14.7	40.8	-	9090.9	-	9.09	-	9.08	-	42.1	-	Tamburello et al., 2015
Copahue	Fumarole	01-03-13	1088.1	-	57.5	-	54.6	-	0.03	-	0.55	-	0.03	-	12.8	-	Tamburello et al., 2015
Copahue	Fumarole	01-03-13	1683.5	-	124.8	-	116.2	-	0.003	-	0.05	-	0.003	-	18.3	-	Tamburello et al., 2015
Poás	Lake (non eruptive)	29-04-14	-	-	-	-	-	-	-	-	-	-	-	-	-	-	de Moor et al., 2016b
Poás	Lake (non eruptive)	16-10-14	-	-	-	-	-	-	-	-	-	-	-	-	-	-	de Moor et al., 2016b
Poás	Lake (non eruptive)	29-10-14	-	-	-	-	-	-	-	-	-	-	-	-	-	-	de Moor et al., 2016b
Poás	Lake (non eruptive)	29-11-14	-	-	-	-	-	-	-	-	-	-	-	-	-	-	de Moor et al., 2016b
Poás	Lake (eruptive)	19-03-14	-	-	-	-	-	-	-	-	-	-	-	-	-	-	de Moor et al., 2016b
Poás	Lake (eruptive)	16-05-14	-	-	-	-	-	-	-	-	-	-	-	-	-	-	de Moor et al., 2016b
Poás	Lake (eruptive)	28-08-14	-	-	-	-	-	-	-	-	-	-	-	-	-	-	de Moor et al., 2016b
Poás	Lake (eruptive)	30-09-14	-	-	-	-	-	-	-	-	-	-	-	-	-	-	de Moor et al., 2016b
Poás	Fumaroles (non eruptive)	29-04-14	650.9	-	60.3	-	55.2	-	0.01	-	0.15	-	0.01	-	140.4	-	de Moor et al., 2016b
Poás	Fumaroles (non eruptive)	16-10-14	130.7	-	34.6	-	27.3	-	0.03	-	0.12	-	0.03	-	91.6	-	de Moor et al., 2016b
Poás	Fumaroles (non eruptive)	29-10-14	130.7	-	34.6	-	27.3	-	0.03	-	0.12	-	0.03	-	91.6	-	de Moor et al., 2016b
Poás	Fumaroles (non eruptive)	29-11-14	202.0	-	23.1	-	20.7	-	-	-	-	-	-	-	33.7	-	de Moor et al., 2016b
Poás	Fumaroles (eruptive)	19-03-14	814.3	-	60.3	-	56.2	-	-	-	-	-	-	-	130.9	-	de Moor et al., 2016b
Poás	Fumaroles (eruptive)	16-05-14	510.6	-	51.3	-	46.6	-	0.02	-	0.16	-	0.01	-	125.3	-	de Moor et al., 2016b

Table S3 - Continued

Location	Sample type	Date	H$_2$O/H$_2$S	σ	H$_2$O/SO$_2$	σ	H$_2$O/Stot	σ	H$_2$/H$_2$S	σ	H$_2$/SO$_2$	σ	H$_2$/Stot	σ	H$_2$O/CO$_2$	σ	References
Poás	Fumaroles (eruptive)	28-08-14	186.5	-	20.6	-	18.5	-	-	-	-	-	-	-	59.3	-	de Moor et al., 2016b
Poás	Fumaroles (eruptive)	30-09-14	456.6	-	40.5	-	37.2	-	0.02	-	0.23	-	0.02	-	80.9	-	de Moor et al., 2016b
Ruapehu	Lake	10-07-08	-	-	-	-	-	-	-	-	-	-	-	-	-	-	Christenson et al. 2010
Ruapehu	Lake	12-06-08	-	-	-	-	-	-	-	-	-	-	-	-	-	-	Christenson et al. 2010
Ruapehu	Lake	13-05-08	-	-	-	-	-	-	-	-	-	-	-	-	-	-	Christenson et al. 2010
Ruapehu	Lake	07-05-08	-	-	-	-	-	-	-	-	-	-	-	-	-	-	Christenson et al. 2010
Ruapehu	Lake	03-04-08	-	-	-	-	-	-	-	-	-	-	-	-	-	-	Christenson et al. 2010
Ruapehu	Lake	11-01-08	-	-	-	-	-	-	-	-	-	-	-	-	-	-	Christenson et al. 2010
Ruapehu	Lake	21-11-07	-	-	-	-	-	-	-	-	-	-	-	-	-	-	Christenson et al. 2010
Ruapehu	Lake	29-10-07	-	-	-	-	-	-	-	-	-	-	-	-	-	-	Christenson et al. 2010
Ruapehu	Lake	09-10-07	-	-	-	-	-	-	-	-	-	-	-	-	-	-	Christenson et al. 2010
Ruapehu	Lake	23-08-07	-	-	-	-	-	-	-	-	-	-	-	-	-	-	Christenson et al. 2010
Ruapehu	Lake	18-06-07	-	-	-	-	-	-	-	-	-	-	-	-	-	-	Christenson et al. 2010
Ruapehu	Lake	20-04-07	-	-	-	-	-	-	-	-	-	-	-	-	-	-	Christenson et al. 2010
Ruapehu	Lake	09-03-07	-	-	-	-	-	-	-	-	-	-	-	-	-	-	Christenson et al. 2010
Ruapehu	Lake	05-01-07	-	-	-	-	-	-	-	-	-	-	-	-	-	-	Christenson et al. 2010
Ruapehu	Lake	07-12-06	-	-	-	-	-	-	-	-	-	-	-	-	-	-	Christenson et al. 2010
Ruapehu	Lake	26-10-06	-	-	-	-	-	-	-	-	-	-	-	-	-	-	Christenson et al. 2010
Ruapehu	Lake	01-06-06	-	-	-	-	-	-	-	-	-	-	-	-	-	-	Christenson et al. 2010
Ruapehu	Lake	11-01-06	-	-	-	-	-	-	-	-	-	-	-	-	-	-	Christenson et al. 2010
Ruapehu	Lake	11-11-05	-	-	-	-	-	-	-	-	-	-	-	-	-	-	Christenson et al. 2010
Ruapehu	Lake	18-10-05	-	-	-	-	-	-	-	-	-	-	-	-	-	-	Christenson et al. 2010
Ruapehu	Lake	04-08-05	-	-	-	-	-	-	-	-	-	-	-	-	-	-	Christenson et al. 2010
Ruapehu	Lake	09-06-05	-	-	-	-	-	-	-	-	-	-	-	-	-	-	Christenson et al. 2010
Ruapehu	Lake	02-03-05	-	-	-	-	-	-	-	-	-	-	-	-	-	-	Christenson et al. 2010
Ruapehu	Lake	13-01-05	-	-	-	-	-	-	-	-	-	-	-	-	-	-	Christenson et al. 2010
Ruapehu	Lake	08-07-04	-	-	-	-	-	-	-	-	-	-	-	-	-	-	Christenson et al. 2010
Ruapehu	Lake	21-05-04	-	-	-	-	-	-	-	-	-	-	-	-	-	-	Christenson et al. 2010
Ruapehu	Lake	21-04-04	-	-	-	-	-	-	-	-	-	-	-	-	-	-	Christenson et al. 2010

Table S3 - Continued

Location	Sample type	Date	H_2O/H_2S	σ	H_2O/SO_2	σ	$H_2O/Stot$	σ	H_2/H_2S	σ	H_2/SO_2	σ	$H_2/Stot$	σ	H_2O/CO_2	σ	References
Ruapehu	Lake	25-03-04	-	-	-	-	-	-	-	-	-	-	-	-	-	-	Christenson et al. 2010
Ruapehu	Lake	09-05-16	-	-	39.3	29.9	-	-	-	-	-	-	-	-	6.5	2.5	Christenson pers.com.
Ruapehu	Lake	02-06-16	375.6	178.6	41.3	7.6	37.2	12.3	-	-	-	-	-	-	3.9	0.5	Christenson pers.com.
Santa Ana	Lake shore	07-03-17	-	-	-	-	-	-	-	-	0.42	0.1	-	-	-	-	This study
Santa Ana	Lake plateau	07-03-17	-	-	-	-	-	-	-	-	2.39	0.3	-	-	-	-	This study
Santa Ana	Lake shore	08-03-17	-	-	-	-	-	-	0.02	0.004	0.54	0.1	0.02	0.003	-	-	This study
Santa Ana	Lake plateau	05-06-17	-	-	-	-	-	-	0.01	0.009	0.46	0.3	0.01	0.01	-	-	This study
Santa Ana	Lake shore	13-06-17	-	-	77.4	3.9	-	-	-	-	0.06	0.0	-	-	-	-	This study
Santa Ana	Lake plateau	13-06-17	1263.3	717.5	75.8	48.2	71.5	43.0	0.05	0.04	0.84	0.8	0.05	0.04	18.0	8.9	This study
Santa Ana	Lake plateau	06-04-18	2215.0	344.4	177.2	10.8	164.1	17.8	0.04	0.03	0.52	0.6	0.04	0.03	43.2	10.3	This study
Santa Ana	Lake plateau	12-04-18	749.1	394.3	82.4	34.3	74.2	35.0	0.05	0.03	0.44	0.3	0.04	0.03	25.0	12.6	This study
Santa Ana	Lake plateau	13-04-18	777.5	572.7	62.2	37.2	57.6	38.4	0.03	0.02	0.39	0.2	0.03	0.02	19.4	12.5	This study
Santa Ana	Lake plateau	14-04-18	-	-	32.0	18.5	-	-	-	-	0.44	0.2	-	-	-	-	This study
Santa Ana	Lake plateau	03-05-18	-	-	74.6	26.5	-	-	-	-	0.39	0.2	-	-	-	-	This study
Santa Ana	Lake plateau	28-06-18	-	-	107.0	18.9	-	-	-	-	0.37	0.1	-	-	-	-	This study
Santa Ana	Fumaroles	27-06-05	28209.2	-	639.8	-	625.6	-	2.7	-	0.06	-	0.06		49.2		Fischer pers. comm.
Santa Ana	Fumaroles	27-06-05	2600.2	-	97.5	-	94.0	-	11.0	-	0.41	-	0.40		90.6		Fischer pers. comm.
Kaba	Lake	2014	1070.5	299.1	84.7	21.8	78.5	21.1	-	-	-	-	-	-	78.5	31.5	Aiuppa pers. comm.